WARWICK
THE UNIVERSITY OF WARWICK

A Thesis Submitted for the Degree of PhD at the University of Warwick

Permanent WRAP URL:

http://wrap.warwick.ac.uk/164404

Copyright and reuse:
This thesis is made available online and is protected by original copyright.
Please scroll down to view the document itself.
Please refer to the repository record for this item for information to help you to cite it.
Our policy information is available from the repository home page.

For more information, please contact the WRAP Team at: wrap@warwick.ac.uk

warwick.ac.uk/lib-publications

THE OPTICAL EFFECTS OF ELECTRON IRRADIATION IN CRYSTALLINE SODIUM BROMIDE

by

Alan M. Calverd. M.A.

Short Title: Electron Irradiation of NaBr.

A thesis submitted to the University of Warwick for admission to the degree of Doctor of Philosophy.

1971

MEMORANDUM

This thesis is submitted to the University of Warwick in support of my application for admission to the degree of Doctor of Philosophy. It contains an account of my own work performed at the School of Physics of the University of Warwick in the period 1966 - 1971 under the supervision of Dr. M. R. Tubbs.

No part of it has been used previously in a degree thesis submitted to this or any other university.

The work described in this thesis is the result of my own independent research except where specifically acknowledged in the text.

ACKNOWLEDGMENTS

The work described in this thesis was carried out as a research project supported by the Central Electricity Generating Board and the Science Research Council.

I am indebted to Professor A. J. Forty for permission to carry out this work in the stimulating atmosphere of the School of Physics at Warwick.

Gratitude is especially due to Dr. M. R. Tubbs for his enthusiastic supervision, guidance and detailed, constructive criticism at all stages of the work.

The co-operation of Mr. H. G. Ellacott and the staff of the Physics Workshop, in constructing and modifying the experimental equipment is gratefully acknowledged.

I wish to thank the C. E. G. B. for a maintenance award.

Nec rhoncos metues, maligniorum
Nec scombris tunicas, dabis molestas.

Webster

INDEX

Title	Page
Abstract	A/1
Chapter 1 Introduction	
1.1.1. The interaction of radiation with condensed matter	1/1
1.1.2. Phenomenology: the effect of ionising radiation on alkali halides	1/2
1.2.1. Displacement threshold estimation	1/2
1.2.2. Brief review of co-operative energy-transfer processes	1/4
1.2.3. Co-operative momentum-transfer mechanisms	1/5
1.3.1. Comparative studies of alkali halide radiolysis	1/6
1.3.2. Reasons for studying NaBr	1/8
Chapter 2 Experimental methods and equipment	
2.1.1. Aims and conditions of experiments	2/1
2.1.2. The experimental sequence and broad layout of equipment	2/1
2.2.1. The electron beam source: description of basic instrument	2/2
2.2.2. Beam switching system	2/3
2.2.3. Calibration of accelerator beam energy	2/4
2.3.1. Beam dose measurement system	2/5
2.3.2. Sample temperature measurement system	2/8
2.3.3. Electron beam switching pulse generator	2/9
2.3.4. A simple stopclock for calibration purposes	2/10
2.3.5. Optical density measurements: spectrophotometric apparatus	2/11
2.3.6. Power supplies and other instrumentation	2/13
2.4.1. Design criteria for the main cryostat	2/13
2.4.2. Cryostat design and construction techniques	2/14
2.4.3. Cryostat manipulation and lubrication	2/15
2.4.4. Cryostat performance: vacuum, thermal retention: fatigue	2/17
2.4.5. Beam alignment, collimation and measurement	2/18
2.5.1. Apparatus trolley: description	2/19
2.5.2. High-purity glovebox preparations	2/19
2.5.3. Specimen sources and cleavage	2/20
2.5.4. Microscope examination of irradiated material	2/20
Chapter 3 F band growth curves in NaBr	
3.1.1. General description of experiments on F band growth	3/1
3.1.2. Anticipated results and strategy of experiments	3/2
3.2.1. The effect of moisture on the coloration of Harshaw NaBr	3/3
3.2.2. The effect of non-aqueous impurities: comparison of Harshaw and BDH material (NT)	3/4
3.2.3. Qualitative confirmation of "plateau"	3/5
3.3.1. The effect of beam flux on the F band growth curve at NT	3/6
3.3.2. The beam energy dependence of the F band growth curve	3/7

INDEX (Cont.)

Page

3.4.1. The temperature dependence of the coloration growth curve 3/9
3.5.1. Summary of experimental observations 3/10
3.6.1. The saturation concentration of F centres in the irradiated material 3/11
3.6.2. The assumed distribution of F centres in the irradiated material 3/12
3.6.3. The saturation concentration of F centres in NaBr .. 3/13
3.6.4. The plateau concentration of F centres in NaBr .. 3/14
3.7.1. Contingency relations of plateau and saturation concentrations of F centres 3/14

Chapter 4 Optical microscopy of irradiated materials
4.1.1. The necessity for determining colour centre penetration depth 4/1
4.1.2. Surface damage investigations 4/2
4.2.1. A feasibility study: colour penetration in NaCl ... 4/2
4.2.2. Colour penetration in KI: effect of stress 4/3
4.2.3. Bleaching effect of storage and microscope illumination 4/3
4.2.4. Summary of preliminary results 4/3
4.3.1. Coloration penetration in NaBr irradiated at NT... 4/4
4.3.2. Coloration penetration in NaBr irradiated at RT: evaluation of precision 4/5
4.3.3. Projectile penetration and colour penetration: a résumé and discussion of published work 4/7
4.3.4. Comparison of coloration and projectile ranges in NaBr. Limitation of theoretical validity 4/9
4.3.5. Empirical depth/energy relationships 4/9
4.4.1. Background considerations regarding direction dependence of coloration depth in NaCl 4/11
4.4.2. Experimental results: polar penetration plot 4/12
4.4.3. Discussion of penetration/angle of incidence experiments 4/13
4.4.4. Theoretical considerations: extension to NaBr 4/14
4.5.1. Surface damage: techniques and results for NaCl .. 4/16
4.5.2. Revised method of study: NaBr 4/16
4.5.3. Discussion of results in the light of published work .. 4/17

Chapter 5 Cathodoluminescence of NaBr and NaI
5.1.1. The importance of cathodoluminescence as an analytical tool 5/1
5.1.2. Experimental details 5/2
5.2.1. Initial results: Harshaw NaBr, NT 5/3
5.2.2. Detailed experiments at NT: Harshaw NaBr 5/3
5.2.3. Conclusions from cathodoluminescence experiments at NT 5/4
5.2.4. Cathodoluminescence of NaBr irradiated at RT 5/5
5.2.5. Summary: the effect of temperature on NaBr cathodoluminescence 5/6
5.3.1. Cathodoluminescence of NaI: comparison with NaBr .. 5/6
5.4.1. Comparison with other authors' results. Theory of intrinsic cathodoluminescence 5/7
5.4.2. Implications of theory and notes for discussion 5/8

INDEX (Cont.)

	Title	Page
Chapter 6	Optical spectrophotometry of non-F bands in NaBr and the effect of thermal and optical bleaching of the F band	
6.1.1.	Introduction: previously published studies of non-F bands in NaBr	6/1
6.1.2.	Experimental procedures	6/2
6.2.1.	Absorbance of irradiated BDH NaBr (400 keV, NT) and effect of optical bleaching of F band	6/3
6.2.2.	Behaviour of BDH NaBr irradiated at 200 keV, NT	6/4
6.2.3.	Discussion of F band optical bleaching results and UV absorbance measurements	6/5
6.2.4.	"Homology" argument for re-allocation of α band	6/6
6.2.5.	F/α ratio: the relative concentrations of filled and unfilled vacancies created by irradiation	6/6
6.3.1.	A survey of all the absorption bands in irradiated NaBr between 195nm and 750nm	6/8
6.3.2.	Tabulation of location, bahaviour and possible identities of all bands found	6/9
6.4.1.	Thermal bleaching of F centres. Experimental method	6/10
6.4.2.	Detailed results: fast thermal bleaching	6/11
6.4.3.	Detailed results: slow thermal bleaching	6/12
6.4.4.	Discussion of thermal bleaching effects	6/12
6.5.1.	Transient bleaching investigations: interrupted irradiation at NT	6/13
6.5.2.	Analysis of transient bleaching results	6/14
Chapter 7	Kinetics of radiolysis of NaBr and a new mechanism for F centre generation	
7.1.1.	A general review of previous approaches to reaction kinetics of F band formation	7/1
7.1.2.	The materials investigated in previously published literature	7/2
7.1.3.	Single curve parametrisation methods	7/2
7.1.4.	The F-complementary centre	7/3
7.1.5.	Possible anion fates and vacancy creation sequences	7/3
7.1.6.	Available-site saturation as a limiting process	7/6
7.2.1.	Single-curve parameters based on dynamic equilibrium and site-saturation mechanisms. Comparison with experiment	7/7
7.2.2.	Developments of Pooley formalism to variable dose/depth distributions	7/8
7.2.3.	The spatial distribution of colour centres predicted by the foregoing argument	7/9
7.2.4.	The Herrmann-Pinard curve	7/9
7.2.5.	Comparison of the Herrmann-Pinard curve with 7.2.2(b)	7/11
7.3.1.	The need for a two-curve model	7/11
7.3.2.	The work of Mitchell, Wiegand and Smoluchowski: two-curve parametrisation	7/12
7.3.3.	The two-curve approach re-appraised with particular respect to NaBr Stage I	7/14
7.3.4.	The Hayes-Nichols centre: stabilisation of focuson termination	7/15

INDEX (Cont.)

Title	Page
7.3.5. Application of Hayes-Nichols to Stage 1 coloration...	7/16
7.4.1. Stage II coloration. The need for an intrinsic coloration mode and its required functional characteristic.....	7/18
7.4.2. Stage II coloration. General kinetic theory	7/19
7.4.3. A review of previously postulated intrinsic F centre creation processes, referred to NaBr, and the foundation of a new mechanism.....	7/21
7.4.4. Analysis of a possible mechanism having detailed consistency with the experimental results	7/23
7.4.5. Kinetic implications of generalised first-order intrinsic enhancement processes	7/25
7.4.6. Kinetics of Stage II saturation	7/27
7.5.1. A summary of the arguments presented so far and a complete kinetic description of F centre generation in NaBr	7/28

Tables

Certificate of Analysis
3.2.1. Mean plateau optical densities: NT-irradiated dry NaBr
3.2.2. Mean saturation optical densities: NT-irradiated dry NaBr
3.4.1. Saturation optical densities: RT-irradiated dry Harshaw NaBr
3.6.1. Saturation concentration of F centres in NaBr (cm^{-3})
3.6.2. Numerical saturation concentration of F centres in NaBr
3.6.3. Numerical saturation concentration of F centres in NaBr assuming linear penetration/energy relation
3.6.4. Plateau concentration of F centres in NaBr. Linear penetration/energy relation
3.7.1. Concentration ratios for different sources
3.7.2. Concentration ratios for different stages of coloration
4.3.1. Colour penetration and incident electron energy: NaBr
4.3.2. Calculated absorption coefficients for electrons in NaBr
5.3.1. Wavelengths (nm) of observed cathodoluminescence bands at NT and $d\lambda/dt$ between NT and RT: for NaBr and NaI
5.3.2. Results quoted by Kabler and Patterson
6.2.1. Energy differences from first exciton band (eV) after Jacobs and Krishna Menon
6.5.1. Parameters of Figure 6.5.(i)
6.3.1. Bands in NaBr irradiated at NT, and effect of F band optical bleach
7.3.1. L.H.S. of equation 7.3.3.(a)
7.3.2. Values of η from tables 4.3.1., 4.3.2., 7.3.1.

Figures

2.2.(i) Beam switching aperture
2.3.(i) Schematic diagrams of the four types of dose integrator discussed
2.3.(ii) Thermocouple amplifier configurations
2.3.(iii) Pulse generator
2.3.(iv) Time clock
2.3.(v) Integrator, divider and thermocouple indicator panel
2.4.(i) Cryostat section
2.4.(ii) Cryostat case and inner tube
2.4.(iii) Alignment drive and cam switch with thermocouple lead-through

INDEX(Cont.)

Title

Figures(cont.)

2.4.(iv) Sample holder, clamp and Faraday cup
2.4.(v) Beam tube alignment accessories
2.5.(i) Apparatus trolley
2.5.(ii) High-purity glove box
3.1.(i) Continuous measurement - schematic
3.1.(ii) Schematic: "Growth curve" illustrating terms used in the text.
3.2.(i) F band optical density as a function of dose. NaBr
3.2.(ii) Current dependence of F band growth. 300kV
3.2.(iii) F band growth in BDH NaBr
3.2.(iv) F band growth in Harshaw NaBr (NT)
3.2.(v) Differential of continuous F band growth curve
3.3.(i) Current dependence; G30
3.3.(iii) Voltage dependence; G14
3.3.(iv) 100kV growth curve
3.4.(i) Growth of F band at RT: Harshaw NaBr
3.4.(ii) Growth of F band at RT: Harshaw NaBr
3.6.(i) Assumed distributions
4.2.(i) NaCl: colour penetration
4.2.(ii) Microdensitometer trace of 4.2.(i)
4.2.(iii) KI: colour penetration in stressed material
4.2.(iv) KI: bleaching effect of storage
4.3.(i), 4.3.(ii) NaBr colour penetration, 200kV and 400kV: NT
4.3.(iii) Microdensitometer trace (averaged). 400kV, NT
4.3.(iv)(a) and (b), 4.3.(v) (a) and (b) Variation of apparent penetration with sample thickness(NaBr, 400 and 200keV, RT)
4.3.(vi) Microdensitometer traces of 4.3.(iv)
4.3.(vii) Microdensitometer traces of 4.3.(v)
4.3.(viii) Weber practical range vs energy
4.3.(ix) Rate of deposition of energy as a function of depth and incident electron energy (NaBr)
4.4.(i) KI: coloration anisotropy
4.4.(ii) Coloration range vs θ
4.4.(iii) Experimental, 4.4.(iv) Section NaCl: lateral spread of coloration
4.5.(i), 4.5.(ii), 4.5.(iii) NaCl: surface damage
4.5.(iv), 4.5.(v) NaBr: surface damage 200kV
4.5.(vi), 4.5.(vii) NaBr: surface damage 100kV
5.1.(i) Principle of analogue divider for luminescence linearity
5.2.(i) Luminescence spectra G52 NT
5.2.(ii) Luminescence spectra G53 NT
5.2.(iii) Luminescence spectra G57 RT
5.3.(i) Luminescence spectra H8 RT and NT
6.1.(i) Small cryostat and ball valve
6.2.(i) Absorption spectra G80
6.2.(ii) Absorption spectra G83
6.2.(iii) Qualitative behaviour of bands on re-irradiation after StageII F band bleaching

INDEX(Cont.)

Title

Figures(Cont.)

6.3.(i) Typical absorption spectrum 200keV Stage I G48
6.4.(i) Thermode construction
6.4.(ii) Thermal annealing of F centres in NaBr
6.4.(iii) Slow thermal annealing of 200 and 400 keV F centres
6.5.(i) Transient effects of re-irradiation G67
7.2.(i) Normalised P and W curves
7.2.(ii) Equivalent spatial variation of modified Pooley equation
7.2.(iii) Typical comparison between experiment G8 and computed Herrmann-Pinard curve
7.2.(iv) Typical comparison between experiment G69 and computed Herrmann-Pinard curve
7.3.(i) The Hayes-Nichols centre. Divalent-vacancy complex. Br_2^- -divalent-vacancy complex
7.3.(ii) Possible stabilised intermediate
7.4.(i) F centre concentration vs dose. G63 and calculation

Appendix..... Published work

ABSTRACT

Experimental procedures are described for the reproducible preparation and electron-beam irradiation of single crystal specimens of deliquescent alkali halides, and for the measurement of absorbed dose in the samples to ± 1% repeatability. Subsequent measurements of optical density, to ± 1%, at wavelengths known to within ± 5 nm (at 500 nm), were used to plot F band growth / dose curves for several alkali halides, with beam energies between 115 and 460 keV, at room temperature and at 77 K. Cathodoluminescence was measured during irradiation and the luminescent peak wavelengths were located to within ± 2 nm at 200 nm. Studies with a microscope and microdensitometer produced coloration/depth profiles which were used in conjunction with the optical density/dose measurements to determine the concentration of F centres produced in NaBr samples by irradiation. Studies of the effects of optically or thermally bleaching the F band on the absorption spectrum of NaBr led to the discovery of a series of V bands that had not previously been reported.

A study of the detailed kinetics of the radiolytic coloration of NaBr showed that at 77 K the growth curve was divided into two distinct saturating phases separated by a plateau whose "height" and "length" depended on the sample purity and beam energy respectively. At room temperature the growth curve had no inflection and a higher saturation value.

The final saturation concentration of F centres at a given temperature was found to be independent of the beam energy between 230 and 460 keV and the rate of production of F centres per unit dose was independent of the beam flux.

Theoretical and experimental studies of the variation of electron penetration depth with energy showed that the coloration penetration law differed significantly from that found by other workers at lower beam energies. The effective coloration depth p(micrometres) in NaBr was given by $p = 0.77V^{1.08}$ where V is the beam energy in keV. A beam orientation dependence of p was found for NaCl. For beam

energies $\geqslant$230keV it was found that irradiation enhanced the deliquescence of NaBr, presumably by ejecting Br^- from the surface, but this effect was not detected for beam energies $<$115 keV.

The cathodoluminescent behaviour of NaBr was seen to correlate with the F band growth behaviour. "Intrinsic" and "impurity" luminescent bands were identified by analogy with NaI.

Analysis of the coloration behaviour, taken in conjunction with the other experimental observation, showed a need for a new mechanism to explain the production of F centres in radiation-resistant alkali halides.

A synthesis of previously postulated mechanisms is shown to account for part of the observed behaviour, where the formation of anion defects is assisted by the presence of impurities. The experiments have shown that it is necessary to invoke an additional intrinsic coloration process.

The intrinsic coloration behaviour of NaBr is shown to be fully consistent with a process whereby radiation-induced cation defects enhance the subsequent formation of anion defects without involving large threshold energies in either step. One example of such a mechanism is examined in detail and is shown to be consistent with all the other experimental observations.

Detailed kinetic examination of a generalised intrinsic-enhancement mechanism limited by F centre re-ionisation is shown to describe the F band growth/dose behaviour of NaBr at high doses. Taking this in conjunction with the synthesised "impurity" mode, calculations yield an F band growth curve for NaBr which correlates with the experimental data more closely than any previously published result at 77K and can be extended to explain the room temperature behaviour and the apparent variation of the colorability of NaBr with temperature.

UNITS

Throughout the experiments, unless specifically stated, the cross-sectional area of the radiation beam was constant at nearly 1 cm^2. As the observed penetration/energy relationship was effectively linear, the absorbed dose in the specimen is reported in the measured units, i.e. millicoulombs (mC). The approximate conversion factors for conventional radiological units are as follows:

$$1 \text{ mC} \equiv 5 \times 10^{19} \text{ keV/cm}^3$$

$$\text{or } 1 \text{ mC} \equiv 2.5 \times 10^{8} \text{ rad.}$$

CHAPTER 1

INTRODUCTION

1.1.1 The interaction of radiation with condensed matter

The observation, measurement and control of the interactions between energetic particle or photon beams and matter in the condensed states has formed the basis of a great deal of recent experimental work in applied physics and chemistry. Without drawing fine distinctions between research disciplines, general classes of investigation are evident. In order to characterise radiation sources and qualities in terms of beam energy spectrum and beam flux, the interaction of various forms of radiation with solid or liquid substrates is studied with a view to eliciting information about the radiation itself. Given a well-characterised source and type of radiation, it is then possible to explore the properties of the materials with which it interacts.

In the great majority of common applications of energetic radiation to the study of materials, the experimental objective is to observe the effect of a material sample on a radiation beam; absorption, diffraction and refraction are common terms in non-destructive analysis. In most of such applications the material is not permanently and significantly modified by the radiation.

However as the specific energy available for the interacting process is increased, it becomes possible for the incident beam to significantly alter the properties of the substrate material and if the effects can be characterised and measured a new tool is created for materials analysis. In many cases the technological stimulus for such work is directed towards the mitigation of the damage caused by the interaction: a classic example is that of nuclear reactor fuel can distortion due to the swelling of fuel rods subject to intense neutron fluxes. In the field of chemical research the use of pulse radiolysis in the study of liquid phase reactions has opened a number of new avenues of enquiry and presents an example of radiation interaction with condensed matter being employed to inject energy adiabatically into

an otherwise isolated system.

Within the field of solid state physics we are concerned with the analysis of tightly coupled systems. Whilst the equilibrium states of such systems are, in principle, amenable to detailed mathematical modelling and precise experimental investigation, the response of the systems to very large adiabatic transients is not well understood. Interaction with energetic radiation can provide a useful experimental technique in this respect.

1.1.2 Phenomenology : The effect of ionising radiation on alkali halides

A detailed account of previous studies of radiation damage to crystalline alkali halides will be given in Chapter 7. For the present a brief phenomenological survey will suffice.

Most alkali halides acquire a pronounced visible coloration when subjected to fluxes of ionising radiation. The effect is generally persistent and initially is largely caused by the optical absorption of defects known as F centres. These centres have been shown to be identical in most respects to those created by heating the materials in an atmosphere of an alkali metal. Quenching prevents aggregation and leaves a substitutional excess of alkali metal. Evidence from paramagnetic and (recently) ENDOR spectroscopy, in addition to chemical analysis of the "additively-coloured" materials, supports the model proposed by de Boer (Rec. Trav. Chim. Pays-Bas 56 p 301 (1937)) for the F centre : an electron trapped at an anion vacancy.

At the same time as the F centre absorption band is introduced into the radiation-coloured crystals, so other optical absorptions appear. The alkali halides have been studied in detail because virtually every point defect or small aggregate has a characteristic optical absorption located in the near-UV to near-IR region.

It is therefore apparent that optical spectrophotometry can be used to investigate the response of at least some solid-state systems to large adiabatic energy inputs.

1.2.1 Displacement threshold estimation

During irradiation with a beam sufficiently energetic to produce F centres, it is generally found that a further (α) absorption band,

associated with the interaction of halide vacancies with the fundamental absorption of the material, is produced. Thus it has been confirmed that energetic radiation can eject anions from their equilibrium sites to generate vacancies.

On studying the quantitative aspects of radiation damage in alkali halides (and in crystalline solids generally) it is found that the energy required to create an ion vacancy is considerably lower than might be expected from the mechanical properties of the material, or from the interionic binding energies involved.

Experimentally the work involved in removing a negative ion from the surface of an alkali halide crystal is found to be 5-6 eV. In order to generate a vacancy within the bulk material it is necessary to add corrections for the energy required to move the surrounding ions (since the anions can generally be regarded as hard spheres in contact) and to take note of the fact that the bond co-ordination of a bulk ion is about twice that of a surface species. Seitz and Koehler (Sol. Stat. Phys. 2 p 305 (1956)) elaborated this simple argument and Sosin (ASTM Special Technical Publication 341 (1962)) has performed detailed calculations concerning the "relaxation" part of the total energy involved in displacing an atom from its lattice site in a number of materials.

It is generally held that in a perfect, strongly bonded material (which class includes the alkali halides) there is a "displacement threshold" of about 25 eV to be overcome before a vacancy can be created. There is, therefore, a need to explain how this amount of energy can be effectively invested in an ion as a result of interaction with ionising radiations. As work proceeds in the field of low-energy ($<$100eV) electron diffraction, so evidence is becoming available that radiation damage and vacancy creation occur even at these low beam energies: by any account there is a serious discrepancy between naive theory and experience.

Displacement thresholds are, of course, related to the adiabatic investment of energy in a single atom or ion. In order to explain the relative ease with which damage occurs it is therefore expedient to discuss the range of co-operative phenomena available for the

transfer of energy between the incident beam and the displaced particle, and for the transmission of the momentum of this particle.

1.2.2 Brief review of co-operative energy - transfer processes

In the case of particle (eg proton, alpha, electron) radiation there is a possibility that direct collision between the particle and the struck nucleus may transmit enough energy to the recoil atom to overcome the displacement barrier E_d. The 25 eV required can, in general, only arise from collisions between electrons of >1 MeV kinetic energy and light nuclei. This point will be discussed more fully in Chapter 7.

The co-operative energy-transfer mechanisms proposed to date fall into the following three broad categories:

(a) Inhomogeneity-assisted vacancy creation

Motion of edge dislocations (Seitz: Rev. Mod. Phys 26 p7 (1954)), mosaic and twin boundaries or voids in a matrix can introduce approximately equal concentrations of positive and negative ion vacancies into the bulk of the material If the boundary creep rate is slow the vacancies may diffuse apart as isolated entities evenly distributed through the material. The anion vacancies can then trap electrons from a low-energy ionisation process to form F centres. Although not strictly a co-operative energy-transfer process in the sense of polyatomic interaction with the incident radiation, this is a co-operative process which lowers the apparent creation energy of F centres. A similar effect can be postulated whereby impurities enhance the radiolytic susceptibility of alkali halides.

(b) Interaction between an ionised anion and its neighbours

An energetic photon interaction with a single anion is unlikely to invest the ion with more than about 6 eV of kinetic energy (Varley : J. Phys. Chem. Sol. 23 p 985 (1962)) in a state with a lifetime long enough to produce a vacancy. However an ionised anion could interact with a neighbour to form a V_k centre (two adjacent anion cores with a shared valence electron and the nuclei slightly displaced from their lattice points) or in the case

of a doubly-ionised ion, an $X^+ - X^-$ complex similarly located. The kinetic energy produced by a V_k-electron interaction (Pooley, Proc. Phys. Soc. 87 p245(1966)) and X^+-X^- de-excitation collapse (Howard, Vosko and Smoluchowski: Phys.Rev. 122 p1406 (1961)), have been investigated. The details will be discussed in Chapter 7 but we can note for the present that neither system gives more than 5 eV kinetic energy to a Br^- ion in alkali bromides.

(c) Ionisation of close sets of anions

If a close set of lattice anions are simultaneously ionised by radiation into either X^o or X^+ states, there will be a real or effective mutual repulsion between the resultant species which will give rise to momentum directed along the internuclear vectors of the set.

This type of mechanism has received the most support in the published literature but imposes certain conditions that will be discussed in Chapter 7.

1.2.3 Co-operative momentum-transfer mechanisms

Apart from the direct displacement of an energetic ion moving by "brute force" from its equilibrium site to create a vacancy, we must, in the light of the energy limits imposed by the available energy-transfer mechanisms, find an alternative means of transporting an ion away from its normal site, with either a lower E_d or reduced recombination rate.

There has been a recent growth of interest in co-operative momentum transfer by replacement collision sequences and channelon propagation. These phenomena have been dealt with in detail in reviews (eg Chadderton: Radiation Damage in Crystals : Methuen (1966)) but will be briefly described here, and considered more deeply in Chapter 7.

If the primary particle (the energetic "struck" daughter of an ion-radiation interaction) collides with an ion at an equilibrium lattice site, it may be possible for the second ion to be substitutionally replaced by the primary. The second ion (now the secondary daughter product of the radiation reaction) acquires momentum, relative to the lattice, along the internuclear vector at the moment of collision. If this vector

lies in or near a close-packing direction then it can be shown that the process may be repeated and the momentum acquired by the primary interaction can be propagated along a close-packing direction. Some energy loss will be incurred at each collision and ultimately the struck ion will not have enough energy to displace its neighbour, and will take up an interstitial position. Thus a widely separated Frenkel defect pair can be produced with very little extra energy than would be required to produce a close pair. Consequently there is a reduced probability of interstitial-vacancy recombination compared with a random-displacement pair created by the same primary interaction and the effective value of E_d may be reduced at temperatures where recombination is significant. The replacement sequence length is critically dependent on the "focusing" effect of the surrounding ions and any disturbance of the lattice periodicity(eg by phonons) will reduce it.

The allied phenomenon of channelling involves the propagation of energetic particles (which may be subatomic particles or small ions) along the lines of potential saddles in the matrix. In highly symmetrical crystals it is often possible to predict lines along which the mean electron density is very low: for example the line joining the midpoints of Cl^- - Cl^- vectors in NaCl. A particle initially incident in such a special direction will suffer less energy loss to matrix electrons than if its incidence were in any general direction, and consequently for a given initial kinetic energy it will penetrate the crystal more deeply in these preferred directions. Thus radiation damage may occur in deeper layers of the material than would be expected if the material was homogeneous or amorphous. The reduced recombination rate due to the greater dispersion of a given number of defects may lower the apparent displacement threshold energy.

1.3.1 Comparative studies of alkali halide radiolysis

As a class, the alkali halides range from molecular weight 26 (LiF) to 260 (CsI) and most have the interpenetrant f. c. c. lattice structure in the solid state. Consequent upon their chemical similarity and similar crystal structures it is often possible to predict the physical properties of one member of the class by studying the homology of its neighbours. Thus the peak wavelengths of the absorption bands corresponding to the various point defects have been found, in general, to be related to the lattice unit cell length;

eg by the Mollwo-Ivey relation for the F band (Phys. Rev. 72 p 341 (1947))

$$\lambda(F) = 703\, d^{1.84} \text{ (units of } 10^{-10}\text{m)}.$$

However the energy required to create an F centre does not vary in such a convenient manner. Rabin and Klick (Phys. Rev. 117 p1005 (1960)), deduced, from the slope of the [F] vs dose curve, the energy E_F absorbed from an X-ray beam per F centre generated at 4K. E_F was plotted as a function of S/D where S is the space between the Goldschmidt anion radii in ⟨110⟩ and D is the halogen atom diameter. For S/D greater than 0.45 it was found that E_F is substantially independent of S/D and is about 1100 eV. As S/D decreases below 0.45 so E_F becomes approximately proportional to -log(S/D), with NaBr the "hardest" material investigated, having $E_F \simeq 8 \times 10^5$ eV and S/D ≃ 0.28. The terms "hard" (to colour) and "soft" (easy to colour) will be used in the present thesis to distinguish between those alkali halides with E_F substantially greater than 1 keV and the remainder.

Of the soft alkali halides, KCl has been studied extensively, and most of the work cited in the detailed review in Chapter 7 refers to X-ray coloration of KCl. Of the hard materials KI presents some curious phenomena (eg Hersh, Phys. Rev. 105 p 1158 (1957)) and NaCl has been the chief material of interest : its S/D ratio and ionic radius ratio make it the structural archetype of the light alkali halides.

Previous work has revealed the following general features:

1. E_F is substantially independent of impurity concentrations at 4K, but is generally reduced by the presence of impurities at higher temperatures, in all alkali halides.

2. Irradiation at 4K produces F, α , and H centres (Cl_2^- molecule-ions at anion sites) only. H centres are unstable at 77K but a variety of spatially larger V centres are formed by hole trapping. The V_k centre has already been described (1 2.2) and is the best-understood of these. V-band absorptions have been found in most alkali halides.

3. E_F generally increases with increasing temperature for the soft members, but decreases for the hard members of the alkali halides.

From time to time other specific information will be drawn into the present argument from the published literature, but it should be noted here that there is very little published work on NaBr. Apart from brief mentions in general surveys the number of papers published annually and dealing specifically with radiation damage in NaBr is about ten, compared with several hundred concerning each of the "popular" halides. In consequence at the outset of the present project only two radiation-induced absorption bands (F and α) had been characterised in NaBr.

1.3.2 Reasons for studying NaBr

The reported values for λ(F) and λ(α), the wavelengths at the absorption band peaks for NaBr, were seen to fit the homologous series very well but in view of the experimental results of Rabin and Klick (op. cit.) it seemed that further investigation of the mechanism by which these centres are produced was in order. With the Van de Graaff electron source available it was possible (see Chapter 7) to deliver up to 15 eV kinetic energy to a Br^-ion, and in view of the reported high E_F it was therefore possible that a significant fraction of the F centres formed might have been generated by a more or less direct displacement of anions from lattice sites. It was therefore hoped that there would be a discontinuity in the response to increasing beam energy, and this would indicate the nature of the displacement processes responsible for colour centre production.

Again, as a result of the high value of E_F, NaBr was thought to be a useful material for the study of cathodoluminescence since a considerable radiation dose could be absorbed before the material exhibited significant optical absorption. The importance of a full study of cathodoluminescence arises from the potential application of colour centres as information storage elements with very small effective volumes. This is discussed in 5.1.1.

Motivation for investigation also sprang from the reported temperature dependence of E_F in NaBr. The material had been shown by many authors (see 3.4.1) to be easier to colour at room temperature or at 4K than at 77K, and this phenomenon demanded a thorough investigation and explanation since it contains elements of both "hard" and "soft" alkali halide behaviour and might have illuminated further the mechanisms by which F centres are created.

Finally it was hoped that the use of a powerful means of introducing radiolytic defects at 77K in NaBr would lead to the discovery of the V bands which had not been previously noted since they are not formed at 4K and are not stable at room temperature.

CHAPTER 2

EXPERIMENTAL METHODS AND EQUIPMENT

2.1.1 Aims and conditions of experiments

In general the intention of the experiments described in this thesis can be summarised as the measurement of the optical absorption characteristics of samples prepared under reproducible conditions and subjected to known doses of electron irradiation at known temperatures.

The temperature range covered was from room temperature (RT) to the boiling point of nitrogen (NT). Sample size was generally of the order of 1 cm square x 0.05 cm thick with the electron beam incident on the square face, absorbed doses from 100 to 25,000 microcoulombs being obtained from a beam flux of 0.05 to 25 $\mu A/cm^2$ and nominal energy 100 to 400 keV.

Sample preparation was standardised as NaBr, the chief material of interest here, is highly deliquescent in normal atmospheres. Sample irradiation was carried out with a 400 keV Van de Graaff accelerator with the flight tube maintained at a vacuum of better than 10^{-5} torr throughout the experiments.

With the foregoing conditions in mind the instrumentation and constructional program divided into well-defined categories which will be reported in the present chapter. The underlying concept linking the separate sections is the experimental necessity for conducting the optical absorption measurements as soon as possible after irradiation without changing the temperature and ambient atmosphere of the specimen. In fact the time lapse from switching off the irradiating beam to precise optical density measurement at a fixed wavelength was kept below 60s and reliable data was obtained concerning the short-term changes of optical properties after irradiation ceased.

2.1.2 The experimental sequence & broad layout of equipment

Specimens were prepared by cleavage from monocrystalline boules in a drybox (the boules being stored in a desiccator between experiments) and were transferred in the drybox to the tail of a cryostat which was then

assembled in the dry atmosphere and sealed. This assembly was taken into the accelerator enclosure.

The cryostat was arranged to have an optical path perpendicular to the electron flight path. The inner tube was coupled to a motor which allowed the specimen to be rotated to intercept either the electron beam or the analytical beam of an optical spectrophotometer kept in the radiation enclosure. During irradiation the specimen temperature and absorbed dose were measured continuously.

The electron beam was either pulsed or continuous, the pulse length and p. r. f. being selected to keep the mean specimen temperature in limits specified by the experiment. Periodically the electron beam was deflected away from the sample which was then moved into the "measuring" position and optical measurements were made without switching off the Van de Graaff .

After irradiation some specimens were recovered from the cryostat, sectioned, and photographed under a microscope. Other specimens were subjected to optical bleaching and/or thermal annealing and re-measurement.

2.2.1 The electron beam source : description of basic instrument

The energetic electrons used in these experiments were obtained from a Van de Graaff electrostatic accelerator model AS400 built by High Voltage Engineering (Europa)NV, Amersfoort, Netherlands and purchased by Dr M. R. Tubbs with a research grant from the Science Research Council. The accelerator was housed in a concrete enclosure within the laboratory and in June 1969 was transferred to an essentially identical enclosure in the new Physics Building.

The AS400 high voltage terminal shell is contained in a tank holding an insulating mixture of N_2, CO_2 and SF_6 at 7 kgf/cm^2. Within the terminal shell is contained a triode gun and the short accelerating tube. The gun elements are driven from a set of stabilisers deriving their power from a generator within the high voltage terminal and itself driven by the charging belt. Manual control of gun settings is achieved by switching a set of motors housed in the main tank and

connected to potentiometers by long perspex rods passing into the terminal.

Terminal voltage is measured by a rotating sectored vane chopper and a capacitive pickup plate feeding an amplifier. The terminal charge is leaked down a column of resistors linking equipotential planes in the accelerating tube and in conjunction with the terminal voltage measurement this provides a control signal to the belt charge spray-on stabiliser. Stability of ± 2 kV was achieved at voltages >50 kV.

Console controls are provided for belt charge, shell voltage, beam current, cathode emission and Wehnelt cylinder potential. The last three controls are in fact servo-motor switches and there is no provision for pre-setting the beam condition, nor can the standard stabilisers be used to pulse the beam. Both these limitations were overcome by a simple switching system described later (2.2.2).

The flight tube contains pre-limiting apertures, X-Y symmetrical deflection plates driven from $2 \times \pm 2$kV variable stabilised supplies at the control console, and a focus coil similarly controlled. A nominal 400 keV/100 μA beam could be focused to a 1 mm spot and steered across the 2" exit gate of the flight tube by using these controls. Setting-up was accomplished with the aid of an aluminium end-window coated on the outside with a mixture of grease and ZnO : the luminescence could be clearly observed on a CCTV link.

2.2.2 Beam switching system

Warm-up time to reach a stable beam condition was about 120 s, which limited the minimum useful irradiation period since the beam current and voltage fluctuated considerably during that period. Additionally it was intended to investigate the behaviour of samples irradiated with large beam currents at low temperature : in consequence it was necessary to provide some means of switching the beam of electrons without altering the gun settings.

This was achieved by focusing the beam on to a 1 mm dia hole drilled in a watercooled aluminium plate (Fig 2.2.(i)), and adding a 700V pulse to the beam steering deflector plates in one plane. An essentially square pulse of electrons could then be produced by driving the beam

across the plate on to the aperture. It was then possible to set the accelerator up with the beam aimed at the plate, and monitor the total beam current before directing the beam on to the specimen. During optical measurements of the specimens, the electron beam was deflected away from the aperture to avoid the production of cathodoluminescent noise on the optical record.

Spurious radiation scattered from the edges of the aperture was absorbed by a precollimator described later (2.4.5) and caused no problems in the experiments.

2.2.3 Calibration of accelerator beam energy

The capacitive pickup voltmeter supplied with the accelerator is an inherently linear device and is specified to ±2% maximum deviation from linearity. Nevertheless its absolute accuracy depends upon a number of variable factors which cannot be independently checked : for example, if the mark/space ratio of the chopper is not exactly unity, the output may depend upon the chopping rate, and the dielectric properties of the separating gas may change with time and temperature. It is therefore necessary to calibrate spot points on the accelerator panel voltmeter in absolute terms.

Two systems were proposed by the author:

(1) analysis of the electron diffraction pattern from gold foil

(2) calorimetry of absorbed dose in a copper Faraday cup.

The first approach was taken up by Miss I. Henrich, and an extensive set of results indicated that an instrument voltmeter reading of 400 keV corresponded to an electron energy of 460 keV (±2%), the scale error being linear with scale deflection. A feasibility study of the second method was carried out by the author, using a ~100g copper block. The block was bored out with a $\frac{3}{4}$" dia blind hole and capped by a copper plug with a $\frac{1}{4}$" dia entry hole. The block was supported on thin Perspex insulators and placed in the flight tube near and behind the beam switching aperture, and a thermocouple was greased into a small hole in the bulk of the block which was earthed through a dose integrator (2.3.1). Although irradiations were not carried out with the same attention to detail as those of Miss Henrich the results

were reproducible to within $\pm 5\%$ and were within -0 +10% of the diffraction results at 400 keV nominal.

Secondary emission losses were restricted by the system geometry and by polishing the copper block, and with the block-beam tube wall separation about as large as the block diameter, cooling corrections were of the order of 0.1°C in 10°C temperature rise following a 50 second irradiation. Thermal leakage paths were reduced by using thin thermocouple wires, taken to a fully-floating amplifier so that the thermocouple leads could also be used as beam current leads without introducing offset errors in the dose integrator.

In view of the magnitude and linearity of the discrepancy between meter indications and calibrated beam energies the actual meter deflections are recorded in the "experimental" chapters of this thesis and only in a few areas of Chapter 7, where the "maximum possible beam energy" is used to test an argument , are the calibrated values used : these will be unambiguously apparent. No inconsistency of argument arises from this convention.

2.3.1 Beam dose measurement system

Dosimeter inaccuracy has been a major shortcoming of experimental work in radiation damage, and a disproportionate effort is often required to measure the dose producing a given effect. There often remains, when a repeatable dosimetric system has been established, an unknown "quality dependence" which precludes intercomparison of results from different radiation sources. Distinguishing between "standard" and "absolute" dosimetry we note that Ritz has employed glass block dosemeters (Phys. Rev. 133 p 1492 (1964)) which were compared with Fricke oxidation standards in a separate experiment. However although such methods are widely used as standard techniques it is by no means established that they are absolutely consistent, and in any case they cannot be employed to measure the beam actually irradiating the test sample. Furthermore it is impracticable to plot detailed damage / dose curves with such dosemeters as they require a separate and complicated analytical process to establish each dose point. Counter-scaler devices based on cascade ionisation or scintillation counting are inappropriate to the very large doses required

in radiation damage experiments (and have been shown to suffer from damage effects themselves).

What is required for charged-particle radiolysis experiments is an absolute local absorbed dose integrator with an indication of specimen current during irradiation. Then from an absolute energy calibration (2.3.3) and a knowledge of the projectile penetration characteristics (Chapter 4) it is possible to correlate experiments with a high degree of confidence.

The basic categories of electronic integrator are (Fig 2. 3.(i))

(1) small capacitor ("tipping bucket") integrator

(2) large capacitor ("filling bucket") integrator

(3) areal integrator - graphical analysis of i/t plot

(4) electromechanical register ("clock").

Type (1) instruments depend on the close tolerance of a small-value capacitor working between known voltage limits as a charge integrator which is discharged at a preset level to produce a frequency-analogue of the input current. Although used in high-accuracy digital instrumentation the system requires stringent attention to zero-drift since random fluctuations do not cancel (there being no frequency-analogue of a negative input). This is achieved either by automatic recalibration (not appropriate to continuous measurement systems) or specialist design of input or counting circuitry. Thus although the ultimate precision is theoretically superb there were disproportionate practical obstacles to its achievement in this case.

(2) uses the familiar capacitor feedback loop in a summing circuit. However despite the familiarity of the circuit there are very grave restrictions on its applicability to systems with a large dynamic range. Electrolytic capacitors do not approximate very closely to the ideal V=Q/C characteristic so although the zero-drift problem is less acute than for type (1) systems of comparable complexity, the linearity is suspect.

(3) suffers only from the drawback of the unavoidable tedium in measuring areas by hand. With a good potentiometric recorder and a sensibly drift-free amplifier (which is anyway working in a purely linear-amplification mode) a very high degree of repeatability is

obtained from commonplace laboratory instruments. High-precision work demands little more than that the chart speed be constant and the use of a Kelvin disc planimeter offers good measurement accuracy.

(4) requires that a low-inertia motor should have a linear voltage / velocity characteristic. Driven from a gain-stabilised current-to-voltage transducer circuit its speed is proportional to the input current to the amplifier.

The best intrinsic precision of these systems is obtained by methods (1) and (3). The integrating range of systems (1), (3) and (4) is unlimited (resetting (2) automatically or manually merely reproduces (1) with a buffer preamplifier). Types (1) and (3) have the best transient response and (3) produces a permanent record of the beam current. Both (3) and (4) have visual rate indication, and are consequently the easiest to calibrate.

Eventually (1) was discarded on the basis of projected development time, (2) was rejected after a short trial confirmed the inapplicability of simple operational techniques to long-term integration of the signals involved in the irradiations and (3) was discarded on the grounds of the tedium involved in calculating a series of short individual doses. However (3) will give very accurate values of $\int_0^t i\,dt$ and its use was therefore recommended to Miss I. Henrich who has extended the range of the system to the nanoamps x hours region by using a low-drift FET input system.

Method (4) was adopted, with an Electro-Methods mechanical integrator type 921/4L. Operating at a nominal 6V input this produces 60,000 counts/hr on a clock face scaled in 100 divisions with a 100 : 1 revolution scaler in addition to the directly driven pointer. Z_{in} was arbitrarily set at 100Ω to prevent damage from accidental short-circuits and then with Z_f = 360 kΩ each clock division corresponded to 10^{-6} coulomb passing through the amplifier input circuit. As the normal condition of a dose integrator is with the input effectively open-circuit there was no need to provide any offset current compensation and the only back-off requirement was the E_{os} potentiometer recommended for the Comtec A6/1 amplifier used

(hence the need for Z_{in}). Ranges of 10, 100, 1000 μC/rev were provided by switching Z_f = 3.6 MΩ, 360 kΩ, 36 KΩ and the backoff could be set to less than $^1/_{100}$ rev/hr in either direction on all ranges although thermal instability of E_{os} was evident on the 10μC/rev range. A 2μF polystyrene capacitor was used to shunt the feedback resistor to smooth the response to pulsed irradiation.

Calibration was straightforward : a good microammeter (Avo model 8 usually) was connected across the input terminals after the amplifier had been set for zero open circuit offset drift. The offset current flowing in the microammeter was compared with the rate of rotation of the clock on a suitable range and by using a constant-current source the interrange rationality was confirmed. After selection of Z_f from stock high stability components the systematic error of the dose integrator was found to be within $\pm$ 2.5% between 10% and 200% of nominal speed (1000 counts/min) on any range and better than $\pm$ 2% at nominal speed (limited by midrange calibration of Avometer). No systematic ageing drift was detected in two years' use.

2.3.2 Sample temperature measurement system

Sample thermometry was an important aspect of the irradiation monitoring scheme. Previous workers have employed germanium and carbon resistance thermometers at very low temperatures (4 - 15K) but it was felt that their reproducibility under conditions of large absorbed dose might be suspect and in any case pure metal resistance thermometry is quite adequate for most purposes at NT or above. However the sensitivity of a pure metal resistance thermometer is ultimately dependent on the mass of metal involved and again the resistivity of a metal is somewhat affected by energetic radiation damage.

The optimum combination of radiation damage insensitivity, low thermal inertia, ease of assembly and good temperature sensitivity was felt to be found in a thin-wire single copper-constantan-thermocouple. Since the cryostat tail was made of copper, accidental short circuits could be ignored by choosing the correct layout of the junctions and in this mode the thermal sinking efficiency of the

cryostat was checked (2.4.4). For the accelerator calibration experiments (2.2.3) a single junction was greased into the calorimeter and coupled via a junction in water at RT to a Fenlow A2 instrumentation amplifier (gain 100) with a 50 mV fsd meter. This amplifier has its own power unit and could thus be "floated" on an isolating transformer, allowing the thermocouple leads to act as dose integrator connections without introducing common-mode errors.

For general thermometry an Analog Devices AD111 amplifier was added to the instrument panel. Two operating modes were used (Fig 2. 3 (ii)). In the differential mode with $Z_{in} = 100\Omega$ and $Z_f = 75k\Omega$ the output displayed on a 125 mV meter corresponded to 10K fsd if both junctions were at ~NT. In the inverting mode the output from one junction (compared with one at RT) was summed with a backoff emf so that the scale read directly 0-300K with $Z_{in} = 100\Omega$ and $Z_f = 2.2k\Omega$. The linearity of the thermo-emf was good enough to provide $\pm$5K estimates of temperature from NT to RT.

Since the thermocouple leads, in either mode, represented virtual ground lines the single junction used for specimen temperature measurement was electrically insulated from the cryostat inner tube which acted as the beam current lead. By using 32 swg wires wrapped round the inner tube, stray heat conduction was kept to a practical minimum.

E_{os} adjustment of the amplifier provided the necessary zero set since input conditions did not vary in use.

2.3.3 Electron beam switching pulse generator

The principle of the pulse generator was derived from a circuit supplied by AERE Harwell. The original design used an Eccles-Jordan monostable fired by an oscilloscope timebase and working between rails at ground and -500V, to switch a valve operating between ground and +700V from cutoff to saturation. The Eccles-Jordan circuit was felt to be rather restricted in mark/space range for the present application and so the circuit of Fig 2. 3.(iii) was developed.

V1 is a highly asymmetric multivibrator which can free-run if R_a is shorted. The cycle time is set by R_t and the 0.22μF capacitor. Shorting R_t locks the system "on" and with R_a in circuit triggered operation is accomplished by applying positive spikes from the 1000 pF capacitor. At V1 cathodes the waveform is a positive-going asymptote. V2 is in a Schmitt trigger configuration with a fixed backlash of ~5V and an "on" point at ~60V. The setting of the 25kΩ potentiometer determines the mark/space ratio of the 100V square wave output from V_2a_2. The rise and fall times of the pulses are ~10μs.

The maximum positive excursion of the Schmitt output is that of terminal 8 (ground) and feeding this signal to V3 grid produces 700V square pulses at V3 anode. The rise time is ~100μs and fall time ~20μS. Terminals 6 and 7 are the power output pair and terminal 5 is a monitor point. Ripple is less than 3V at each state of the pulse.

Free running, the prf is almost exactly $1/2.2\ R_t\ s^{-1}$ (R_t in megohms) and in single-shot, $^1/_{25}\ R_t$. By switching R_t the generator was made to run with prf between 2.5mS and 10s with complete coverage of mark/space ratio from zero pulse width to zero space width.

2.3.4 A simple stopclock for calibration purposes

It was occasionally necessary to measure short intervals of time during the experiments, primarily as a means of determining irradiation currents from the integrator rate. A timer was therefore devised to count tenths of seconds using 50 Hz mains as a timebase.

In Fig 2. 3.(iv) V1 is an astable multivibrator with a free period of about 110 ms, stabilised by the use of good-quality components and a Zener diode clamp on the ht line. A 40V rms sinusoidal signal at 50Hz is inserted at V_1g_1 which locks the period at an exact multiple of 20 ms, ie 100 ms. Large coupling capacitors prevent noise spike triggering. V2 is a cathode-follower power amplifier with the counter as a load. Since the dc resistance of the counter is 2.3kΩ, V_2g can be driven negative with respect to the cathode and a 100V p-p wave appears across the counter which was adjusted to operate reliably at 10 Hz.

R_s was used to set the firing point by "pulling" the mark/space ratio to eliminate the possibility of the multivibrator locking to a 120 ms period. On 1000 s trial runs the counter did not deviate more than $\pm$ 0.1 s from a stopwatch and despite the wide statutory limits for mains frequency the error incurred during a normal working day was within acceptable limits for the experiments.

2.3.5 Optical density measurements : spectrophotometric apparatus

Having measured the dose and temperature for a specimen, it was necessary to extract optical density information. A Zeiss PMQ II single beam spectrophotometer was used for this purpose. This instrument produces transmission data in the range 185-2500 nm using tungsten and deuterium-arc lamps. The lamp output passes through a variable slit into a calibrated quartz prism and exits through a coupled variable slit and a chopper as an effectively parallel horizontal beam in the same vertical plane as the optical bench on which the monochromator and lamphouse are mounted. No sample cell was fitted and the photomultipler/PbS cell unit was mounted on an optical bench saddle to allow the optical path to pass through the various cryostats used in the irradiations. A synchronous demodulator/amplifier and galvanometer display, a monochromator wavelength scan drive, and a power supply unit, formed the remainder of the system.

The PMQ II was mounted on the apparatus trolley (2.5.1) with the optical path parallel to the long edge of the trolley shelf and at a height to intersect the electron beam tube axis. A support was built over the optical bench to hold the cryostat firmly in position. The wavelength scan control switches (go red, go blue, stop) were re-wired to accept remote control.

Careful layout of wiring eliminated electrical interference and the chopper/demodulator effectively reduced noise from room lighting. Set to read 100% transmission at 190 nm, the system recorded $<$0.05% when a soda-glass microscope slide was inserted in the beam, thus confirming the negligible level of stray-light error in transmission work.

Since the entrance and exit slits were coupled, transposition of the light source and detector head made no detectable difference to the performance : this was useful in the case of luminescence measurements as it allowed a more convenient layout of the apparatus. Beam divergence was so small that insertion of black paper tubes in the cryostat extension tubes (2.4.2) made no detectable difference to the output of the photodetector in either configuration. The use of bandpass filters in luminescence measurements confirmed the absence of stray light interference in either mode of operation.

The photodetector output was available as a 0-10mV DC signal on a 600Ω line brought out to sockets on the amplifier unit. To keep high-impedance leads short, the amplifier was mounted on the apparatus trolley and a co-axial line ran outside the accelerator enclosure from the 600Ω sockets. This line was terminated at a chart recorder. The wavelength scale on the monochromator was viewed via a CCTV link and the slit opening was monitored by mounting a 15kΩ potentiometer on the slit control knob and fixing the spindle in an arotary gimbal. By applying 15V across the track it was possible to monitor the rotation of the control knob by following the potential on the wiper. The slit control was driven from outside the enclosure by switching a reversible motor.

Drift on zero-scale readings for both transmittance indicator and chart recorder were of the order of 0.01% of fsd per day after a warmup period of 30 minutes and despite the fact that a single-beam spectrophotometer will record drift of the 100%-transmission point with lamp ageing or supply fluctuations, the power stabilisers maintained the "100%" recorded light output constant to better than 0.05% over a typical 8-hour day with random fluctuation no worse than 0.01% (the 1 second time constant of the galvanometer helped reduce apparent short-term fluctuations).

The manufacturers' dispersion curves were presented in terms of exit spectral bandwidth with entrance slit width as a parameter For most of the absorption work in the visible region the bandwidth was kept at about 1.5 n m (slitwidth ≈ 0.03 mm) but bandwidths were varied during luminescence runs.

The photomultipler response fell drastically beyond 700 nm and for wavelengths $>$650 nm the PbS cell was used as the detector. The higher background noise was not significant in this application and no cooling was provided for either cell.

2.3.6 Power supplies and other instrumentation

The dose integrator, thermocouple amplifier, band width telemetry receiver and a further amplifier and analogue divider module, were mounted on the same rack, with a Coutant ATB 100/15 power supply. Power supply drift was less than 0.1% maximum excursion over 24 hours (indeed the limit was probably due to the use of a four-digit DVM) and since all the analogue equipment was operated in heavy feedback modes there were no problems associated with long-term instability. The analogue divider module was intended for use in cathodoluminescence studies (see Chapter 5 for details).

The instrument rack also carried the time clock, motor driven switches and chart recorder. A simple shunt-stabilised power supply was constructed using a pnp-npn transistor pair and a zener diode to provide a +1V reference for the analogue divider : this too was built into the instrument rack.

2.4.1 Design criteria for the main cryostat

The crystal specimens to be used in these experiments were to be irradiated by the electron beam at a known temperature and then examined in the spectrophotometer. The short range of electrons in air precluded the use of a cryostat isolated from the main accelerator flight tube and the possible existence of transient effects (6.6.1) in coloration precluded a full study if the cryostat had to be isolated from the accelerator and transferred to a separate spectrophotometer. Vacuum-vacuum isolation by means of an aluminium window was undesirable since this would involve a degradation of the electron spectrum. It was thus necessary to design a cryostat to allow the crystal to be moved from the electron beam path into the sampling beam of the spectrophotometer without isolating the cryostat or (2.2.2) switching off the electron beam.

The spectrophotometer beam was arranged for convenience to run

perpendicular to the flight tube axis and the instrument was not found to suffer from radiation-induced ageing. Thus it was decided to rotate the specimen, from the "irradiate" to the "scan" position, about a vertical axis. Additional desiderata were:

(1) the spectrophotometer should be protected from X-rays generated at the sample holder during irradiation

(2) good thermal contact between sample and cryostat should not involve undue stress in the sample.

(3) sample temperature monitoring should be continuous

(4) the cryostat reservoir capacity should suffice for several hours' continuous running

(5) the specimen should be electrically insulated from the flight tube to allow dose integration

(6) the cryostat should be demountable for cleaning and replacement of the optical windows, and should be separable (and separately evacuable) from the accelerator

(7) It should be possible to mount the specimen into the cryostat in a dry inert atmosphere.

2.4.2 Cryostat design and construction techniques

Departmental workshop experience showed that 0.010" wall stainless steel could be fabricated into a robust cryostat and the instrument shown in 2.4.(i) and 2.4.(ii) was constructed in the Physics Workshop. The major design criteria were met as follows:

(1) the optical windows ($\frac{1}{4}$" thick Suprasil) were situated on extended tubes so that in the "irradiate" position the spectrophotometer "sees" the heatsink edge-on and filling the optical path, so that very little X-radiation escapes from the sample.

(2) the specimen is seated in a milled and polished recess in the sample clamp and is held to the heatsink by about 200 g force from two compression springs. The heatsink has a large thermal inertia and good conductivity (being milled from solid copper) to ensure rapid cooling during pulsed

beam irradiation, and a low thermal impedance for continuous irradiation. Half the area of a 2 x 1 cm specimen was in contact with the sink.

(3) thermocouple wires were led through glass-metal insulating seals in the top-plate and were coiled round the inner tube to reduce heat transmission. The point junction was sprung against the unirradiated (rear) face of the specimen.

(4) the 1 litre reservoir capacity sufficed for a 6 hr run at full accelerator output without total loss of coolant. Quiescent loss was reduced by polishing the inner tube and casing faces : at 10^{-5} torr operating vacuum the coolant required more than 15 hours to evaporate.

(5) the inner tube and top casing were isolated by a Perspex flange from the irradiation chamber which incorporated the pipework and collimator for connection to the accelerator.

(6) removal of six bolts allowed the casing to be completely dismantled and the optical windows were retained by knurled nuts clamping them down to O-rings. The inner tube assembly was retained by atmospheric pressure alone. The accelerator connector ran via a 1" dia Genevac ball valve and the pumping nozzle was led off to a mobile pumping unit. Open, the ball valve had an unrestricted optical path of 1" dia and closed it held off 10^{-6} torr with negligible leakage.

(7) a glovebox (2.5.2) was generally used for specimen preparation. The cryostat body could be manipulated into the box via the airlock provided. Inside the glovebox, handling was assisted by the recessed crystal mounting clamp and the use of hex-socket headed bolts for compressing the springs. Very little grease was needed to achieve a good thermal and mechanical contact with the specimen.

2.4.3 Cryostat manipulation and lubrication

The cryostat top plate was held down by atmospheric pressure to a 4" nom dia O-ring and was laterally located by a circumferential

ridge on the top flange of the casing. Thus a simple mechanism could be built to rotate the inner tube between the "irradiate" and "measure" positions. The atmospheric force was considerable (~180 lb wt) and consequently the drive mechanism was a fairly crucial part of the equipment since it had to operate rapidly between precise positions, with no sidethrust, yet had to be demountable in order to extract the inner tube and light enough not to vibrate the experimental trolley.

An MR 100 rpm / 20 lb in reversible motor was obtained and this was firmly bolted to a base plate on two 2" x 1" steel girders straddling the cryostat, with the motor shaft ending about 12" from the cryostat axis and some 6" above the top plate. A length of nylon torque tubing joined the motor to the input shaft of the worm-and-worm-wheel mechanism shown in Fig 2.4.(iii) which used a 2" dia brass wheel pinned to a $^3/_8$" silver steel shaft and driven by a $^5/_{16}$" BSF steel bolt. The output shaft ran through a long honed mild steel bearing and the worm-and-wheel were sprung together by a mild steel bar so that wear was progressively taken up. The final output shaft was coupled to the cryostat by a dog-clutch consisting of a steel bar lightly pinned to the shaft and engaging two nylon-insulated dogs on the cryostat top plate. The driving gear was mounted on a separate baseplate bolted to the transverse girders and could be swung out of the way on its flexible coupling to extract the cryostat. The shearable drive pins were placed in accessible locations and on the few occasions where the mechanism jammed these pins snapped harmlessly and were easily replaced.

Three Perspex cams fitted to the cryostat top plate were arranged to strike a microswitch on the cryostat body and thus acted as motor stops. By careful profiling of the cams <u>in situ</u> the setting accuracy on full-speed motor drive was better than $\pm$ 0.5° and the repeatability was such that a poorly-cleaved specimen had an apparent optical density change of less than 0.25% in five successive traverses from "scan" to "irradiate" and back again.

Heavy-duty motor vehicle greases were sufficient for the driving gear and no problems were encountered in this area, but the O-ring

required more careful selection of lubricants. The contact force on the line-seal at the O-ring was very large and the metal faces of the flanges were generally rubbing together. Excellent machining of these faces, and careful polishing during assembly, removed any "proud spots" and the surfaces were coated with Apiezon N grease. However this material (chosen for its high mechanical strength) often froze during use and it was therefore overlaid with Midland Silicones high-vacuum grease. Though thicker than the conventional optimum grease layer the combination did not fatigue or freeze and there was never any metal-metal binding problem in operation.

2.4.4 Cryostat performance : vacuum, thermal retention : fatigue

Under vacuum conditions the driving gear performed most reliably, moving the sample between the "irradiate" and "scan" positions in 45 s with no perceptible increase in leakage and consistent and negligible mechanical distortion. The shearable pins broke twice due to lubricant freezing (see above) but only once during operational runs.

The cryostat could be pumped down to a measured vacuum of 10^{-6} torr at the pumping head (probably 5×10^{-6} torr in the cryostat) after a thorough bake-out and without coolant. Pouring in liquid nitrogen improved the vacuum and rapidly cooled the heatsink to equilibrium. With two constantan leads bolted to the nitrogen-facing and specimen-facing areas of the copper heatsink the equilibrium sample temperature under the operating vacuum of the accelerator was found to be 82K referred to NT = 77K.

The first inner tube (2"OD) failed due to axial cracking after 9 months' use. After a considerable delay a replacement was made up but this warped during 3 months' use and was damaged during an attempt to re-align the specimen holder necessitated by the inconsistent optical data arising from the misalignment. A third tube, of $1\frac{3}{4}$" OD, was made up and functioned well for over a year despite the higher quiescent loss rate. In view of this experience it is recommended that large thin-wall stainless steel tubes for "production" use under thermal

cycling and shock should be selected by ageing before commissioning.

2.4.5 Beam alignment, collimation and measurement

In order to collect the majority of the electrons incident on the sample and feed them into the dose integrator it was necessary (a) to define the beam so that all the counted electrons struck the sample and not the sample holder, and (b) collect as much of the backscatter and secondary emission as possible. Forward scatter was in any case absorbed by the use of thick specimens.

Condition (a) was met by placing a collimator in the beam tube coupling : this was a 7 cm dural bar, 1" diameter, drilled axially to 0.7 cm dia and protruding 1 cm into the radiation chamber at the base of the cryostat, giving minimal clearance to the specimen holder rotation. The inlet side of this collimator was covered by a 5 μm aluminium diffuser and the output beam at the specimen was 0.9 cm in diameter and had a reasonably flat intensity distribution. A number of small NaCl crystals greased on to the specimen holder showed only X-ray coloration (rapidly bleached at RT) outside this diameter.

Backscattered electrons were collected by virtue of the thick copper sample clamp which was further extended into a Faraday cup by a 1.2 cm long dural cap drilled with a conical cavity and a 0.9 cm entrance hole (Fig 2.4.(iv)). In theory this cup should collect about 90% of the backscattered radiation if this were isotropic. Low energy experience indicates that there is in fact a polarity in secondary emission but it can at least be assumed that (i) a constant fraction of the total emission was collected and (ii) the 180° backscatter would consist of the higher energy components and these will arise from those incident electrons that have given up least energy to the specimen.

In those experiments involving the use of the beam switching aperture the penumbral and multiply scattered radiations were absorbed in the precollimator. This was a 10 cm dural bar with a 1 cm axial aperture and mounted in a flange that supported it centrally in the flight tube counterbore. For some luminescence work, and for irradiations in small cryostats without collimators, the beam was smoothed and broadened by putting the 5 μm foil on the accelerator side of the

precollimator.

Alignment of the cryostat with the main flight tube was simplified by the insertion of a length of 1" nom bore phosphor-bronze bellows between the ball valve and the flight tube coupling flange. The precollimator prevented electrons from striking the brass flange or bellows : less than 1% of the total beam current struck the walls of the apparatus beyond the precollimator, so the X-ray background was small. Visual alignment could be carried out to centre the specimen to within $\pm$ 1 mm. The beam tube accessories are shown in Fig 2.4.(v).

2.5.1 Apparatus trolley : description

The apparatus for use in the irradiation chamber was mounted on a heavy trolley with castor wheels. By constructing the trolley from 2" square box girders with 2" x 1" sub-frames and Formica-faced blockboard platforms the structure was made rigid and vibration-free. The trolley and optical apparatus are shown in Fig 2.5.(i). The wheels were packed away from the main frame to level the monochromator exit slit with the accelerator beam tube axis so that the centre of the measuring beam passed through the same portion of the sample as the irradiating beam.

2.5.2 High-purity glovebox preparations

The glovebox used for sample preparation was a standard model from Marine and Industrial Plastics Ltd, fitted with an airlock tunnel. The box was flushed with dry nitrogen boiled off from the liquid by a 65W soldering iron element in the reservoir Dewar. A safety valve, blowing off at 2 psi, a silicone oil outlet trap, and an outlet psychrometer were fitted to the drybox. Psychrometer temperature was measured with a copper-constantan thermocouple. The maximum flushing rate was $\sim$1000 l/hr with an overpressure of 2" WG measured on the Bourdon gauge supplied with the box. Dewpoints of -190°C (corresponding to $<$0.001 ppm water) were recorded after 36 hours' flushing when the system was plumbed with semisoft polished nylon tubing (use of rubber raised the best dewpoint to -80°C (1 ppm water)). To preserve the very dry working conditions despite the restricted size of the airlock

tunnel a skirt was made up from Stayflat polythene tubing to link the tunnel to the cryostat casing. The cryostat inner tube could then be slid from the box into the cryostat entirely in a nitrogen atmosphere.

2.5.3 Specimen sources and cleavage

Samples were cleaved from large boules of material. The Harshaw Chemical Co, Cleveland, USA, produced 5 x 2 x 1 cm blocks of all of the materials studied : these blocks were monocrystalline. When the effect of moisture on the colorability of NaBr had been noted (Chapter 3) a new boule, grown in an argon atmosphere from optical quality material, was ordered from BDH Ltd, Poole, Dorset. This boule was delivered in a desiccated jar and kept in the glovebox. On trial cleavage it broke into three main grains, two having the boule axis as $\langle 110 \rangle$ directions but with 45° misalignment, and the third having no obvious orientation with respect to the others. As the boule was about 2" long x $1\frac{1}{4}$" dia rather fewer useful specimens were obtained than from a comparable volume of Harshaw material.

Impact cleavage was found necessary for work in the glovebox although continuous pressure produced better specimens in ambient air. Dry NaBr chips and blunts ordinary stainless razor blades and scalpel blades were used for cleavage. Under all conditions it was possible to produce a specimen of the required 2 x 1 cm dimensions at 0.05 - 0.10 cm thickness with no more than three macroscopic steps in the surface : most samples had none. Specimens with visible lamellar faults were discarded to avoid having them break up under thermal shock. Very few samples suffered macroscopic disintegration during irradiation.

2.5.4 Microscope examination of irradiated material

In addition to specimen transmittance measurements, irradiated materials were subjected to scrutiny under the microscope to elicit information concerning the surface damage due to irradiation and the coloration / depth profile of the damage products. The experimental methods used will be described in this section as they have certain common facets.

Standard microscopic techniques were slightly modified to compensate for the transience of some of the phenomena, due to thermal and optical annealing, and the deliquescence of the specimens. There was no time available for the preparation of covered and protected microscope slides and these are at best unsuited to high-magnification surface studies. Instead the samples were recovered from the cryostat, brought rapidly to room temperature in the glovebox, and smeared with silicone grease. This material was sufficiently impermeable to moisture to allow a short working period in ambient air and the refractive index disparity ensured that there was no loss of apparent surface detail. Streaks in the grease were revealed as periodic regions of low contrast and could be identified and ignored in microscope studies. The microscope employed was a Zeiss Ultraphot photomicroscope with an automatic exposure meter : significant detail was photographed for later examination. Tungsten or mercury-arc lamps were employed for illumination. Surface studies were carried out with the microscope in standard reflecting mode.

By sectioning the specimen in the plane of the electron beam and observing the transverse coloration profile it was possible to prepare sets of plates for measurement with a Joyce-Loebl scanning microdensitometer. Attempts to scan samples directly with this instrument were unsuccessful since the specimen tended to deliquesce during the scan, giving rise to an uneven baseline. Further, it was easily possible to adjust the microscope to provide a parallel output from the condenser and to focus sharply on the top surface of the specimen. Specimens of various thicknesses cleaved from the same irradiated sample produced virtually identical scan profiles under these conditions, showing that face-reflections and refraction were not significant factors in the apparent density-penetration characteristics. By scanning each plate in several positions a mean microdensitometer trace could be built up to eliminate spurious detail due to grease striations and surface irregularities.

CHAPTER 3.

F. BAND GROWTH CURVES IN NaBr.

3.1.1. General Description of Experiments on F Band Growth.

Samples cleaved from boules of crystalline NaBr were mounted in the cryostat described in Chapter 2 and the assembly was transferred to the accelerator chamber and clamped in the spectrophotometer beam path as described earlier. With the specimen temperature determined by the cryostat coolant, the specimens were irradiated by the electron beam, rotated into the spectrophotometer path, and returned to the electron flight path. Beam current and sample dose were measured during irradiation with the dose integrator previously described.

The production of the F absorption band is the most obvious effect of irradiation of alkali halides. In NaBr it has been generally reported as a simple bell-shaped band whose peak wavelength and halfwidth are temperature dependent. For the temperatures of chief interest here (77&293K), these are, respectively 525 nm (NT) and 538 nm (RT) (by experiment); 0.29 eV (NT) and 0.50 eV (RT). Halfwidth, the bandwidth at half the peak absorbance, is taken from Hughes, Pooley, Runciman, Rahman; A.E.R.E. R5604 (1967). By virtue of the strong absorption of green light by the F band, irradiated NaBr has an intense magenta coloration when viewed in white light. The F band absorbance is linearly related to the number of F centres present in the material; the precise relation will be discussed later.

With the spectrophotometer set to measure the absorbance at the F band peak for the temperature chosen, plots of F band absorbance against absorbed electron dose were obtained for a variety of specimen preparation and irradiation conditions. Extensive sets of sampled points were obtained by these means, the observed optical density being that found some 45 s after cessation of irradiation. A modified system, using simultaneous irradiation and transmittance measurement with the crystal at 30° to the incident beam, was later

used to provide continuous semiquantitive confirmation of some of the effects noted in the sampled results: this experiment will be referred to from time to time in the following text, and the optical system is shown in Figure 3.1.(i). The cryostat described in Chapter 2 was modified for this experiment by adding two extra windows.

3.1.2. Anticipated Results and Strategy of Experiments.

It was expected that there would be an impurity dependence of colorability in NaBr since it had been widely reported that the presence of divalent impurities such as Ca^{2+} (Rabin and Klick, Phys. Rev 117 p 1005 (1960)) or hydride/hydroxyl inclusion (e.g. Etzel and Allard, Phys Rev Let 2 p 452 (1959)) increased the rate of formation of F centres by irradiation at temperatures $>$4K.

Since NaBr is highly deliquescent it was not possible to cleave a sample in air and mount it in the cryostat without the surface becoming sensibly wet and in consequence most of the experiments conducted prior to the delivery of the glovebox were characteristic of NaBr containing atmospheric moisture, presumably present as $H^-/H^+/OH^-/O_2^-$/etc. The parent boule for all these experiments was Harshaw material. On receipt of the glovebox the B.D.H. material was obtained (2.5.3) and this, with the remaining Harshaw blocks, was kept and handled in the dry nitrogen atmosphere. As can be seen from the Certificate of Analysis there are considerable differences between the materials, not only in the Ca concentration but also in other impurities such as K and Si. The water concentrations reported are almost certainly pessimistic; this point will be discussed in 7.3.3.

A flux dependence of damage/dose curves has been reported from time to time but has never been adequately explained. Unlike the previous experiments with X rays it was possible here to vary the beam flux over a very wide range without modifying its spectral quality and, by pulsing the beam, to maintain a constant specimen temperature regardless of the peak flux during the "mark" periods. Continuous bombarding current densities as low as

0.05 $\mu A/cm^2$ were employed from time to time and the conditions could be rapidly changed to give 50 $\mu A/cm^2$ pulsed at <0.5% duty cycle. Since in practice fluxes of 2 $\mu A/cm^2$ made no appreciable difference to the specimen temperature at a nominal 77K it was possible to examine the flux dependence of the F band generation kinetics for all types of sample.

The dependence of the coloration kinetics on beam energy could be studied in a rudimentary fashion with the equipment employed here, by varying the beam energy during irradiation. Owing to the spectral degradation of the beam in the thick specimens employed here the interpretation of the results was less simple than for the other kinetic experiments but had the advantage over previous work of using the same specimen at all energies, thus making the results substantially independent of the specimen history.

The results are presented here under the headings of the various dependencies tested rather than in strict chronological order of acquisition. A schematic illustration of the terms "plateau" and "saturation" used in the following discussion is given in Fig. 3.1.(ii).

3.2.1. The Effect of Moisture on the Coloration of Harshaw NaBr.

Figure 3.2(i) shows the F band density/dose curve for specimen G4 irradiated at NT with 300 kV electrons. This specimen had been cleaved in air and was visibly damp when the cryostat was assembled. Apart from one point at ~12 mC dose the general tendency of the coloration was a rapid increase with a steadily decreasing rate as irradiation proceeded. Changing to 200 keV irradiation reduced the rate of coloration further and a tendency to a saturation value of optical density is noticeable. The apparent plateaux in the coloration curve will be discussed later (3.5.1.). Each point recorded had a standard error ~ ± 0.02 optical density units and ± 2% on the dose axis, although, as described in Chapter 2, the dose repeatability was probably a good deal better than the absolute accuracy of ± 2%. Specimen G 5 (Figure 3.2(ii)) was used to test the current-dependence of irradiation but also demonstrated the salient features of the irradiation of damp NaBr, namely a rapid initial coloration followed by a

decreasing slope, and final optical density >0.45 for 300 keV irradiation. The exact shape of the coloration curve will be discussed later (Chapter (7), but the general shape and magnitude of the parameters are of interest here.

For the purpose of comparison we may consider the optical absorbance of the dry-cleaved Harshaw specimen G 30 at 5mC dose. (Figure 3.3.(i)) The rapid initial rise of coloration passed through a plateau region more marked and more rapidly attained than for damp specimens of the same source material, and at 5 mC the optical density of the specimen F band was only 0.16 compared with >0.2 (G4) and 0.4 (G5). 300 keV coloration of a number of damp specimens produced saturation optical densities (by extrapolation) in excess of unity whereas the mean for some ten dry specimens was 0.33 ± 0.02. The extrapolation technique will be described in 7.2.2.

3.2.2. The Effect of Non-Aqueous Impurities: Comparison of Harshaw and BDH Material (NT).

Figure 3.2 (iii) shows the behaviour of samples of B.D.H. NaBr. irradiated at NT. There is a faintly discernible inflection in the 400 keV curve at ~2mC but the inflections observed with B.D.H. material were in general less well defined than for the Harshaw material. The F centre concentration/dose curves of Figure 3.2. (iv) show that for Harshaw material prepared under the same conditions the curves are similar but saturate at a lower value of optical density. Without entering into detail at this juncture we can note that in all cases of dry materials irradiated with electrons at NT it was possible to discern an inflection in the F band growth curve and a tendency to saturation at high doses. The mean plateau optical densities for the whole set (some sixty samples of NaBr approximately evenly distributed through the table) are given in Table 3.2.1.

The decrease in standard error for Harshaw materials with decreasing beam energy reflects the larger number of samples irradiated at 200 keV whereas for B.D.H. material the results were generally more tightly grouped, since the crystal boule was fresher than the Harshaw material and had been more carefully handled.

The extrapolated saturation optical densities were similarly analysed and the mean values are tabulated in Table 3.2.2.

The wide discrepancies between the source materials will be discussed later (3.7.1) but it is sufficient to note here that the B.D.H. material was always easier to colour than the Harshaw NaBr. Since the water content of the B.D.H. boule was certainly lower than for the Harshaw crystals we must assume that either an impurity was responsible for inhibition of F centre formation in the Harshaw materials, or an impurity enhanced F centre production in B.D.H. NaBr. A strong absorption band was found in B.D.H. NaBr at 300 nm, and the absorption of this band was unchanged by irradiation. Although not specifically identified it seems likely that this band was due to a V-type centre stabilised by the high Ca^{2+} concentration trapping electrons that would otherwise annihilate the V centres.

3.2.3. Qualitative Confirmation of "Plateau".

The estimates of plateau optical density given above are necessarily subjective since, as mentioned previously, the optical data points were always a discrete set. However by using the apparatus shown in Figure 3.1.(i) it was possible to obtain definite confirmation of the existence of an inflection in the coloration curve. A continuous transmittance/dose curve was obtained from 200 keV irradiation of a sample of B.D.H. NaBr and by changing the gain of the amplifier it was possible to expand the scale of the chart recorder to precisely locate the inflection. The slope of the curve was measured at several points. Results are shown in Figure 3.2.(v) as the rate of change of absorbance with dose. The scale divisions on both axes cannot be referred to the discrete data since the sample was not irradiated normal to (100) and the beam was not defined by the usual collimator and cup assembly. However the axes are scaled linearly and it was observed that after 16 mC dose the coloration rate had fallen to less than $\frac{1}{1000}$ of its initial value, then rose again to about $\frac{1}{10}$ of the initial value, passed through a long inflection, and turned towards a saturation optical density. During the interruptions for changing scale factors the

coloration decreased in an exponential manner, the decrease involving a time constant of ~20s and being about 10% of the total coloration at all times, thus confirming that the time lapse in obtaining the sampled data produced a small but consistent decrement in apparent optical density. In view of the large available scale expansion for this experiment it is felt that the existence of a plateau region, during which the rate of F centre generation falls virtually to zero, is fully proved.

3.3.1. The Effect of Beam Flux on the F Band Growth Curve at NT.

Figure 3.2.(ii) showed the effect of varying the beam current at constant energy during irradiation of a damp specimen. The currents quoted were peak measurements, and the beam was pulsed at 1s prt, <10% duty cycle, to maintain the specimen surface temperature within 5K of its equilibrium value. As can be seen from the part of the growth curve shown here, increasing the peak current produced no discontinuity in the normal growth curve at A, and again the curve is continuous at C. At B, however, decreasing the peak current led to an apparent drop in optical density followed by a recovery and even at D, where the growth rate was very small the decrease in peak flux reduced the growth rate, which again later recovered and went on to exhibit the usual saturating behaviour.

Figure 3.3.(i) has already been cited as an example of the behaviour of a dry Harshaw specimen under the same type of irradiation conditions. Here the beam current was changed after the plateau region had been passed and again it can be seen that reducing the peak current (in this case maintaining the mean current constant by adjusting the duty cycle of the high-flux pulses) has reduced the F band optical density, whereas increasing the peak current had no analogous effect. The phenomenon was found to have quite general applicability for all specimen sources, beam energies, and doses prior to change of flux. It can be viewed as directly analogous to the short-term bleaching described in 3.2.3.

In contrast to the "dynamic" effect of beam flux variation it was found that the "static" effect of flux on the shape of the F band growth curve was nil. No systematic variation was noted between samples irradiated at different constant fluxes of the same beam energy: the random fluctuation of growth curve parameters due to spurious contamination and experimental errors was sufficient to mask any departure from a strict linearity of growth rate with current (at a given dose) smaller than about an "$I^{1.2}$" dependence and there was certainly no evidence for a square-law relationship of growth rate to current, provided there was no significant rise in sample temperature. The linearity of growth rate with current was seen to hold in the range 100 - 400 keV and 0.05 - 50 $\mu A/cm^2$.

Whatever the "static" flux employed, the short-term bleaching on cessation of irradiation had the same characteristic behaviour and it was therefore concluded that if irradiation produced a dynamic equilibrium concentration of F centres this was about 10% greater than the equilibrium value in the absence of radiation. Another phenomenon, that of "transient" bleaching, was observed when irradiation was interrupted (for a period long compared with the time constant for the establishment of equilibrium) and re-initiated. This will be discussed further in 6.5.1. For the present it suffices to note that there was in all cases a small decrease in F band absorbance before the expected recovery on re-irradiation, but the necessary "waiting time" was several orders greater than the space width of pulsed irradiation used in the current-dependence experiments.

3.3.2. The Beam Energy Dependence of the F Band Growth Curve.

Figure 3.3.(iii) shows the effect of changing the energy of the bombarding electrons whilst maintaining a constant flux. The portion of the curve shown here indicates that an increase in beam energy during what would otherwise have been the "plateau" region of the growth curve in fact added a further "Stage I" portion to the curve, which then turned over into a plateau and rose again on continued irradiation. Beyond the limit shown in Figure 3.3.(iii) the curve assumed the normal "Stage II" saturating form.

As had already been demonstrated incidentally in 3.2.2. the most

obvious beam energy dependence was found in the saturation and plateau optical densities of the F band. In fact within the energy range studied it was generally true that for a fixed dose the optical density increased with the energy of the electrons responsible for that dose. However the beginning and end of the plateau region were also found to be energy-dependent. In general, for Harshaw material, the plateau region could be regarded as beginning at, say, 2.5 mC dose and continuing to 4.2 mC for 400 keV irradiation, whereas with a beam energy of 200 keV produced a marginally later inception and the plateau ended at ~3.5 mC. Figure 3.3.(iv) shows a typical result for 100 keV bombardment:at this energy there are definitely two "stages" to the growth curve but no distinct plateau separating them. Just as the plateau height was seen to correlate with the impurities in the specimens (being significantly different in Harshaw and B.D.H. material - see Table 3.2.1) so the plateau inception point and length were found to vary widely depending upon the precise preparation conditions of the specimens. Additionally the location of the inception and termination points was a somewhat subjective choice when the discrete nature of the data points was taken into account. Accordingly no attempt was made to assign a numerical relationship to the energy-inception dose-length observations.

In those cases where the beam energy was changed during irradiation it was found that the behaviour of the growth curve was such that if the electron energy were <u>increased</u> the material exhibited the behaviour expected of an <u>earlier</u> stage of coloration, and <u>vice versa</u>. For example, at any dose, increasing the beam energy produced a sharp rise in absorbance followed by a plateau and another rise going into a saturating curve, whereas it was possible by continuing the first irradiation long enough, to produce "stage II" behaviour on reducing the beam energy although the plateau had not in fact terminated before the energy was changed. Anticipating a discussion of electron penetration depth (range) as a function of energy, it seemed that each lamina of the material had to pass through

a plateau in its coloration behaviour and increasing beam energy merely involved the coloration of regions of the crystal that had not previously been irradiated. Similarly since we can expect the beam to be degraded both in flux and energy with increasing depth into the specimen, the observed effect of reducing beam energy was held to show that the front surface layers of material reached the second stage coloration before the deeper layers.

3.4.1. The Temperature Dependence of the Coloration Growth Curve.

It has been generally reported in the published literature that the effect of impurities on radiolytic F band growth in alkali halides is more pronounced as the temperature rises, and this had led to the employment of liquid helium cooling for such precise studies as that of Rabin and Klick (Phys. Rev. 117 p.1005 (1960)) of the energy required to produce an F centre. However the work of Hughes, Pooley, Runciman and Rahman (AERE R. 5604 (1967)) lent support to some early observations in the present series of experiments that the "colorability" of NaBr increased with temperature above NT, but also demonstrated that the colorability increased with decreasing temperature below NT. Both types of behaviour have been noted in other alkali halides (e.g. as quoted by Pooley: Proc. Phys. Soc. 87 p. 245 (1966)) and have been variously explained in terms of thermally activated diffusion of hole traps and phonon interference with the F centre production mechanism. However the existence of both effects in NaBr, plus a conveniently attainable temperature at which the F centre creation energy is apparently at a maximum (70 - 80K) provides an excellent opportunity for closer study of the temperature dependence. As has been shown it was possible to produce useful concentrations of F centres by electron irradiation of NaBr at NT and some experiments were therefore carried out at RT. Without coolant it was not a simple matter to maintain a working vacuum in the cryostat since any contaminants evaporated from the irradiated zones were not rapidly trapped. However with careful cleaning it was possible to obtain sets of data which led to growth curves such as those shown in Figures 3.4.(i) and 3.4(ii).

Careful analysis of low-dose behaviour such as 3.4.(i) revealed no significant plateau region that could not be accounted for merely in terms of beam current fluctuation. Extrapolation of high-dose curves proved difficult as the rate of change of optical density with dose ($dD/d\Delta$) remained large until the spurious effects of specimen contamination and surface damage contributed significantly to the optical absorption. However the results shown in Figure 3.4(ii) were part of extended irradiations which were extrapolated to give the saturation densities of Table 3.4.1.

Regarded either in terms of the initial slope of the coloration curve at $\Delta = 0$, or in terms of the saturation optical density, the creation energy of an F centre was found to be an order of magnitude smaller at RT than at NT, for both sources of material. RT coloration of "damp" NaBr was too rapid to be measured accurately.

There was no significant departure from the linear relationship of dD/dt with beam current, apart from the short-term type of dependence discussed in 3.3.1, when the irradiation was performed at RT.

It was not possible to investigate the behaviour of samples irradiated at liquid helium temperatures with the apparatus used here, and it was felt to be more useful to extract the maximum available data from experiments conducted in the region 70 - 300 K rather than to construct specialised apparatus for very low temperature work. Fortunately a good deal of published data already exists on the production of F centres in alkali halides at 4K and this will be referred to in later discussions.

3.5.1. Summary of Experimental Observations.

1. Electrons with beam energies between 100 keV and 400 keV can generate F centres in NaBr between NT and RT.
2. The F band absorbance has a generally asymptotic growth with increasing absorbed dose.
3. At NT or RT the growth of the F band is greatly enhanced by the presence of moisture.

4. Other impurities appear to affect the rate of growth and final absorbance of the F band at NT.
5. At NT, though not at RT, there is an inflection in the growth curve (plateau).
6. The "height" of this plateau depends upon the impurity concentration present.
7. The "length" of the plateau depends upon the beam energy.
8. Growth curves are substantially independent of beam current (flux) provided this is steadily maintained.
9. Differences between growth curve shapes resulting from different beam energies can be ascribed to the variation of electron penetration with beam energy (but see 3.6.4. et seq)
10. The rate of growth and final saturation absorbance of the F band at RT are about ten times those at NT.

3.6.1. The Saturation Concentration of F Centres : Smakula's Formula.

In order to correlate the experimental optical density measurements with a quantitative theory of F-centre creation it is necessary to convert them to values of F-centre concentration. The most widely accepted relationship between optical density and colour centre concentration is Dexter's modification of the formula given by Smakula (Zeits f. Physik 59 p 603 (1930)):

$$Nf = 0.87 \times 10^{17} \times \frac{n}{(n^2 + 2)^2} \alpha W$$

(Dexter; Phys. Rev. 101 p. 48 (1956)) where

N = concentration of colour centres (cm^{-3})

f = oscillator strength of absorption band.

n = refractive index of host material at peak wavelength of absorption band

α = peak absorption coefficient (cm^{-1})

W = absorption band width (eV) at half-height.

The oscillator strength of the F band in NaBr is not reported in the literature as an experimental value. After an unfruitful attempt to measure it in the present series of experiments it was decided to adopt the value 0.5 used by Hughes et al (A.E.R.E. R.5604 (1967)). W is determined by spectrophotometric analysis and is generally agreed to correspond to a wavelength halfwidth of ~50 nm centred on 525 nm at NT. This was confirmed here and at RT the value was found to be ~75 nm centred on 540 nm. These values are equivalent to energy halfwidths of 0.25 and 0.40 eV respectively, but for the sake of consistency with the most extensive available review (Hughes et al A.E.R.E. R.5604) the values 0.29 and 0.50 eV were adopted for the purpose of further calculation; the scaling factor being virtually identical in both cases and certainly smaller than the uncertainty in f (~ ±60%). It should be noted that much earlier work on the "soft" alkali halides employed the Smakula constant 1.26×10^{17} as against the present (Dexter) value of 0.87×10^{17}, which has been used in all the most recent published work on "hard" materials.

Taking n = 1.64, in the absence of any published value for NT, we have :-

$$N = 2.99 \times 10^{16} \times \begin{Bmatrix} 0.29 \\ 0.50 \end{Bmatrix} \times \frac{\text{Optical density(D)}}{\text{Thickness of coloured region(t)}}$$

3.6.2. The Assumed Distribution of F Centres in the Irradiated Material.

The determination of α from specimen optical density requires a knowledge of the thickness of the absorbing layer and the distribution of absorbing centres in it. Previous work has been concerned either with additively coloured crystals, giving a virtually homogeneous concentration of colour centres, or with short range projectiles or X-rays. Low energy electrons (Hermann and Pinard, Phys. Let. 29A p 584 (1969); Shulman and Gel, Fiz. Tverdogo Tela 2 p 524 (1960)) or protons (Pooley, Brit. J. Appl. Phys. 17 p 855 (1966)) deposit all their energy in a short range and can be considered to give rise to a rectangular distribution of colour centre

concentration with depth. X-rays (e.g. Rabin and Klick, Phys. Rev. 117 p 1005 (1960)) produce a virtually even distribution of centres throughout the specimen. However with energetic electrons, even at 2 MeV (Ritz, Phys. Rev 133A p 1452 (1964)) it is necessary to use thin specimens to ensure a constant rate of energy deposition and a homogeneous distribution of centres. Even at 2 MeV Ritz found it necessary to polish the specimen surfaces and this technique, in the light of Section 3.2.1, would obviously be inappropriate for NaBr.

Assumptions were therefore made, and will be justified later (7.2.3) concerning the colour centre distribution. Figure 3.6.(i) shows a fixed range of coloration within which the distribution of centres is triangular at the plateau and rectangular at final saturation. Initially the practical range of coloration was taken to be 0.053 cm at 400 keV incident energy (from measurements reported in the following chapter) and calculated as 0.019 cm from the "$V^{3/2}$" power law proposed by Shulman and Gel (op cit) for 200keV electrons.

3.6.3. The Saturation Concentration of F Centres in NaBr.

Using the figures given in the last section the saturation concentrations of F centres were as shown in Table 3.6.1. (dry materials only). It is first noticeable that these values are at least an order of magnitude lower than those assigned to other alkali halides by other workers. Herrmann and Pinard (op cit) regularly measured RT concentrations in excess of 10^{19} F centres/cm^3 in NaCl and predicted saturation at $>10^{20}$ cm^{-3}. This point will be dealt with in later discussion (Chapter 7) but it is also apparent here that the saturation concentration increases with decreasing beam energy. Before discussing this point in detail it is useful to invoke the concept of "numerical concentration".

The NaBr lattice has a lattice parameter of 5.973 A, so there are about 1.88×10^{22} anions/cm^3 in the perfect material. Thus it is possible to reduce the bulk concentration of F centres to the number of F centres associated with each anion site, giving table 3.6.2.

Since the "numerical concentration" can be regarded as the fraction of lattice anions converted into F centres it is a useful concept and quite unambiguous if used as a dimensionless quantity.

Now anticipating the experimental determination of the penetration of coloration (Chapter 4) we ignore the prediction of Shulman and Gel (op cit) which was in any case based on low-energy electron studies, and rewrite table 3.6.2. on the assumption that the penetration of coloration is linear with incident energy. This gives rise to table 3.6.3.

The maximum discrepancy between vertical pairs of results is now 4% and at high energy the saturation concentration of F centres is substantially independent of the energy of the bombarding electrons.

3.6.4. The Plateau Concentration of F Centres in NaBr.

The plateau optical densities given in Table 3.2.1. reduce to the numerical concentrations of Table 3.6.4.

3.7.1. Contingency Relations of Plateau and Saturation Concentrations of F centres.

The differences in behaviour between the B.D.H. and Harshaw materials can be seen by constructing tables of the ratios of the concentrations of F centres at the plateau and saturation levels. The titles of the tables are self-explanatory (3.7.1., 3.7.2.)

The standard error of the figures in Table 3.7.1. is $\sim \pm$ 10%, indicating that the lower right figure is significantly different from the others. Similarly in Table 3.7.2. the lower right figure is significantly higher than the mean of the other three. We therefore conclude that the plateau concentration of F centres for B.D.H. material is significantly lower for 200 keV bombardment than could be expected from straightforward extrapolation of the other data. It is therefore essential that the first stage of coloration be considered in detail in arriving at an explanatory mechanism for F centre production. This matter will be taken up again in Chapter 7.

CHAPTER 4

OPTICAL MICROSCOPY OF IRRADIATED MATERIALS

4. 1. 1. The necessity for determining colour penetration depth

In order to calculate the concentration of colour centres produced by irradiation it is necessary to know the optical absorption coefficient α, of the material being studied and to know how the centres are distributed in the coloured region (see Section 3. 6. 1). If an uncoloured sample transmits an optical beam intensity I_o and a coloured sample transmits an intensity I under the same conditions then we define optical density D and transmission coefficient T as

$$D = \log_{10}\left(\frac{I_o}{I}\right) = \log_{10}\left(\frac{1}{T}\right) \qquad \ldots\ldots \quad 4.1.1.(a)$$

For a material with refractive index n, the reflectance R is

$$\frac{(n-1)^2}{(n+1)^2}$$

at normal incidence, and in a homogeneous medium of thickness t and absorbance α, we can write

$$T = (1-R)^2 e^{-\alpha t} \qquad \ldots\ldots \quad 4.1.1.(b)$$

$$\therefore \alpha = \frac{1}{t}\ln\left(\frac{1}{T}\right) - \frac{1}{t}\ln\frac{1}{(1-R)^2}$$

$$= \frac{2.303D}{t} + \frac{2}{t}\ln(1-R) \qquad \ldots\ldots \quad 4.1.1.(c)$$

provided there are no significant multiple reflections.
Where t does not describe a homogeneous absorber, an "equivalent thickness" may be substituted to correspond with a chosen α, or a mean α may be deduced for a chosen value of t representative of the absorbing entities. In the present case of electron-beam-coloured thick NaBr specimens, the optical absorption change of interest occurred in less than 0.5mm thickness and no mechanical division existed between the coloured and uncoloured regions. Therefore to a good approximation, the R.H.S. of 4.1.1.(c) is separable into two components such that a plot of 2.303D/t' vs Δ describes the growth of the absorption band and 2/t(ln(1 - R)) is nominally independent of dose.

In the usual case where $t \simeq 2t'$, putting $n = 1.64$ shows that the second term is not greater than 5% of a typical saturation value of the first.

By setting up a single-beam spectrophotometer to read $T = 1$ for the uncolored specimen, it is therefore possible to derive changes in D, and hence in α, from transmittance measurements provided only that the distribution of colour centres (for which a value of t' may be derived) is known and R does not vary during irradiation.

In practice, R will appear to vary significantly only if the crystal surface is damaged.

4.1.2 Surface damage investigations

All the extrapolated saturation data reported in the previous chapter were calculated from the optical density / dose behaviour of samples given finite doses of radiation of short range projectiles. In consequence it is conceivable that in fact R may not have been constant throughout the experiments since a great deal of energy from the beam must have been dissipated near the specimen surfaces. Qualitative investigations were undertaken in this area and will be reported later in this chapter but it is sufficient for the present to note that the samples generally retained their superficial appearance in vacuo to all dose levels employed and severe superficial damage only occurred in samples exposed to ambient air after irradiation. There was no reason to suppose that variations in R caused more than about $\pm$ 2% systematic variation in the extrapolated saturation figures, and the doses required to produce plateau behaviour were generally too small to give rise to visible surface damage at all.

4.2.1 A feasibility study : colour penetration in NaCl

Fig 4.2 (i) shows the photograph obtained by irradiating a sample of NaCl at NT and photographing it under the conditions described in

2.5.4 with tungsten light. The salient features of the penetration of colour centres in an electron-irradiated alkali halide are

(1) a penetration of ~650 μm (300 keV electron beam)

(2) an apparently even distribution up to a sharp cutoff at the penetration depth (15 mC dose, well into stage II coloration)

(3) penetration of colour centres into a penumbral region behind the cryostat clamp.

(3) is indicative of a great deal of electron scattering within the sample, or a preferential direction of energy transfer for F centre production. These points will be considered in detail later but the shape of the tail of the microdensitometer trace (4.2.(ii)) should be noted.

4.2.2 Colour penetration in KI : effect of stress

Photograph 4.2.(iii) shows the colour penetration on either side of a step in a KI crystal surface. In preparing the crystal for irradiation area A was subjected to considerable bending stress and was deliberately roughly cleaved whereas area B was part of a clean flat surface. With 400 keV irradiation at NT the penetration of coloration at high doses (>7mC here) can be seen to be not more than ± 5% dependent on the mechanical stress history of the material. The region in the immediate vicinity of the step, although too brittle to produce a photographable surface, did not exhibit any apparent deviation from this rule.

4.2.3 Bleaching effect of storage and microscope illumination

Photograph 4.2.(iv) shows the colour penetration in 300 keV-irradiated KI after a 20 minute period on the microscope stage with maximum illumination from the mercury-arc lamp, followed by 12 hr in the dark at RT. The cracks perpendicular to the irradiated face were initiated after irradiation, during specimen preparation, and immediately after preparation the coloured region extended to the edges of the crack.

Optical bleaching and storage had little effect on the penetration of the coloration but the colour centres near the cracks can be seen to have annealed out or migrated away from their initial positions.

4.2.4. Summary of preliminary results

1. Coloration penetration from high-energy electrons exceeds that

predicted by extrapolation of low-energy results, eg Shulman and Gel, Fiz. Tverdogo Tela 2 p 524 (1960). The figure for NaCl (4.2.1) is >50% higher than predicted from their formula.

2. The assumed rectangular distribution of F centres at saturation (3. 6. 2) appears to be a good approximation to the observed distribution.

3. Penetration is unaffected, at least in stage II, by previous mechanical stress.

4. Optical bleaching does not significantly alter the apparent penetration depth if the exposure is short and the sample unstressed.

4.3.1 Coloration penetration in NaBr irradiated at NT

In view of the success of the preliminary investigations reported above, the experiments were repeated using NaBr crystals irradiated at NT with 200 keV and 400 keV electrons. Difficulties were immediately encountered due to the deliquescence of the material but these were overcome by application of the grease-coating technique described in 2.5.4. It was soon noticed that the samples irradiated at 200 keV did not retain their coloration at RT and consequently the working period was very short. Only two samples gave rise to visible photographic evidence of the coloration / depth profile and the better of these is depicted in Fig 4.3.(i). Tungsten light and an ortho plate were used to minimise the possibility of F band bleaching whilst maintaining contrast since the mercury spectrum contains strong lines at higher energies than the F band absorbance whereas a normal tungsten filament lamp has a continuous emission peaking in the region 520-550 nm.

In contrast the samples irradiated by 400 keV electrons produced consistent coloration / depth profiles of which Fig 4.3.(ii) is an example. The use of tungsten illumination was found to produce better negative gradation and by bracketing exposures it was possible to obtain photographs with detail visible throughout the coloured region : these were scanned in the microdensitometer to give coloration / depth profiles such as that shown in Fig. 4.3.(iii). Mercury-arc light, with a green filter, gave rise to higher contrast negatives which, although demonstrating the cutoff more dramatically, did not prove the existence

of the colour saturation implicit in 4.3.(iii) since no detail was visible in the densely coloured region. Fig 4.3.(iii) was obtained by averaging eight scans across different portions of the negative : the general shape of the curve could then be easily distinguished from the spurious noise due to surface reticulation and cracks in the specimen.

The "practical coloration range" for the electron energy and irradiation temperature was found by projecting a tangent through the inflection of the sigmoid portion of the profile to intercept the horizontal line representing the mean background "noise" level from the remainder of the material. The "mean" drawn here was the mean for ten samples and this was 530 μm ± 12 μm. Both microscope magnification and microdensitometer scan ratio were marked on scales on the instruments and were checked with a microscope graticule photograph : the systematic error was insignificant compared with the standard error of the mean penetration depth.

4.3.2 Colour penetration in NaBr irradiated at RT : evaluation of precision

After the discovery of the thermal instability of F centres generated in NaBr by 200 keV electrons at NT it was decided to approach the problem of determining the NT penetration characteristics by an indirect comparison with the behaviour of material irradiated at RT. Since the optical density obtained at RT was an order of magnitude greater it was also easily possible to verify the technique employed by measuring the apparent penetration in sections of different thickness (measured in the direction of the microscope axis) and comparing the microdensitometer plots. Any discrepancy due to surface reflections, or non-parallel or non-uniform field illumination would then be revealed as a systematic variation of apparent penetration depth with sample thickness.

The photographs of Figs 4.3.(iv)a, b, and 4.3(v)a, b, depict sections of NaBr irradiated at RT by 400 keV and 200 keV electrons respectively. Section thicknesses were 0.2 mm, 3 mm and 0.3 mm, 4 mm, respectively. It is immediately noticeable that the 400 keV-irradiated material is very similar in coloration profile to the sample shown in 4.3.(ii) and that the

appearance of the photographs is independent of section thickness. Figs 4.3.(vi) and 4.3.(vii) show the microdensitometer plots of these photographs which were taken with mercury-green illumination to maximise the available contrast (since the high saturation density produced at RT reduces the sensitivity of the technique to optical bleaching compared with that produced at NT) and it can be seen that the apparent practical penetration depth does not vary significantly with section thickness even in the extreme cases investigated. A typical "1 mm - thick" plot is also shown in 4.3.(vi) : this was the thickness generally employed in these experiments.

It was found that the mean colour penetration depth at RT, for a number of 400 keV - irradiated samples, was indistinguishable from the NT value. In the absence of conflicting data it was therefore assumed that the NT value for 200 keV irradiation could be similarly inferred.

For all the specimens examined, with both NT and RT coloration, the penetration depths, p, were found to be 250 and 530 μm for incident energies (V) of 200 and 400 keV respectively, with standard errors $\sim \pm 10$ μm in each case.

Now suppose	p	=	AV^n (V in keV)
then	250	=	$A.200^n$ and 530 = $A.400^n$
whence	n	=	1.08 and A = 0.77.

(Alternatively, we may consider the <u>calibrated</u> values of V. Since the calibration scale factor was constant the value of n is unchanged but A becomes 0.70).

The relationship is significantly different from that found by Shulman and Gel (Fiz.Tverdogo Tela 2 p 524 (1960)) for a number of other alkali halides. They obtained A values between 0.03 and 0.07 and n from 1.5 to 1.7 for electron energies up to 15 keV. Even allowing the maximum error in penetration lengths the departures from the Shulman and Gel relationship is significant and the departure from linearity in V is significant at the 90% confidence level, although too small to affect the calculations of the previous chapter. Useful values of p are given in table 4.3.1.

The remarks of 4.2.1 have already indicated that extensions of low-energy empirical penetration formulae are inadequate at energies $\geqslant$200 keV for NaCl and in consequence a more detailed theoretical approach was made to explain the discrepancies at higher energies.

4.3.3 Projectile penetration and colour penetration : a résumé and discussion of published work

The penetration of the coloured region in electron-irradiated alkali halides has received little attention in the published literature, with the paper by Shulman and Gel (op cit) prominent among the few available. Ehrenberg and Franks (Proc Phys Soc 66 p 1057 (1953)) and Ehrenberg and King (Proc Phys Soc 81 p 757 (1963)) have studied the luminescence-depth behaviour of numerous substances (including a few alkali halides) at incident-electron energies up to 80 keV.

The trend in the results of Ehrenberg and King was such that the proportionality between integrated electron path length (of the kE^n type) and experimental practical(luminescence) range worsened with increasing beam energy E. Practical range measurements from transmission data (eg Katz and Penfold, Rev Mod Phys 24 p 28 (1952)) and Lane and Zaffarano (Phys Rev 94 p 959 (1954)) generally bear a more constant ratio to their theoretical values (for transmission through Al foils of electrons with E above and below 100 keV respectively in the cases cited). It is thus possible that the processes responsible for initiating luminescence have a higher mean inception energy than those responsible for energy loss in metal-foil transmission experiments. We cannot, therefore, expect to predict coloration range directly from electron penetration range in a material such as NaBr for which the coloration inception energy may be large.

The relationships plotted by Ehrenberg and King and by Kobetich and Katz (Phys Rev 170 p 391 (1968)) indicate that for a given incident electron energy E_o the proportion of the penetration depth for which the electron yields less energy per unit distance travelled than an arbitrary critical value (dE_c/dx) decreases as E_o increases, provided of course dE_c/dx is less than the maximum value dE_m/dx that can be transferred to the matrix.

The value of dE_m/dx along the electron track can be found from the well-known formula (Bethe : Handbuch der Physik 24 p 519).

$$\frac{-dE}{dx} = \frac{2\pi q^4}{mc^2} N\left\{2 \ln\left(\frac{2mc^2}{\bar{I}}\right) + 3 \ln\frac{1}{1-\beta^2} - \ln 8 + \frac{1}{8}\right\}$$

where q = charge of one electron

N = $N_o . Z$ = electron density of target

$\bar{I}$ = mean ionisation potential of target

m = mass of electron, and the other symbols have their usual significance.

This expression has a minimum for electrons with energies $\lesssim$ 0.5 MeV for most dense solids and in consequence as an electron slows down from this region of energy its specific energy loss will increase. However if an energy loss pathway involves a critical value $E_c > 0$ the probability of this being followed will pass through a maximum since at some point the primary particle will have less energy than E_c. Relieved of this energy-loss regime the real range of the primary particle will therefore "straggle" beyond the practical range of its damage effect.

Direct electron-nucleus collisions will have only a marginal effect on dE/dx but are important in considering coloration penetration since they are the means by which direct atomic displacement may be initiated.

As a result of the considerable large-angle scattering and numerous ionisation processes available for electron energy loss it can generally be stated that the electron flux ϕ in a thick target decays as

$$\phi = \phi_o e^{-\mu x}.$$

μ/ρ, the mass absorption co-efficient for a target of density ρ, has been given by Schumacher (Electron and Ion Beam Science and Technology; Ed. R. Bakish; John Wiley & Sons Inc (USA), 1965) as an approximate constant value of $2.4 \times 10^6 \; E_o^{-2}$ virtually independent of the nature of the target. This value has not been thoroughly tested for $E_o > 200$keV but is probably constant within $\pm$ 15%. For NaBr, $\rho = 3.2$ g cm^{-3} and we can calculate table 4.3.2..

4.3.4. Comparison of coloration and projectile ranges in NaBr Limitation of theoretical validity

Considering the data of Section 4.3.2, we have a practical coloration range of 550 μm for 400 keV electrons. From table 4.3.2 we can deduce the relative residual electron flux at this depth as

$$\phi_r^{400} = \frac{\phi_{550}}{\phi_o} = e^{-48 \times 0.055} \simeq \frac{1}{15}$$

and for 200 keV electrons $\phi_r^{200} \simeq \frac{1}{100}$.

Even allowing a $\pm$ 30% variation in μ it is only just possible that $\phi_r^{400} = \phi_r^{200} = \frac{1}{30}$ but it is highly unlikely that the values tabulated in table 4.3.2 for μ^{400} and μ^{200} are respectively 30% high and 30% low. It must therefore be concluded that the residual electron flux at the practical limit of coloration is considerably higher for 400 keV incident electrons than for those of 200 keV initial energy. Now considering the results of Ehrenberg and King regarding straggling, we can say that this phenomenon is consistent with there being a critical energy below which a primary electron cannot create any F centres, and taken together with the energy-loss / depth relationships this can be used to predict the coloration range. Further, the electron penetration law and the coloration rate penetration law are not identical in a thick specimen.

Although the Bethe energy-loss formula is exact in the energy range concerned in these experiments (except for small bremsstrahlung and Cerenkov losses) it only applies to the case of non-scattering energy loss in a homogeneous medium. No account is taken of the periodicities of electron density in the target and in consequence the effects of random incidence and multiple scattering are ignored. On the other hand the exponential flux-decay formula is an empirically confirmed result, despite the lack of precision above 200 keV, and the two approaches cannot be readily reconciled to approach the "coloration threshold" energy determination.

4.3.5 Empirical depth / energy relationships

Let r = practical range of electrons (g cm^{-2})

w = energy of electrons (keV)

A = mass number of absorber } or weighted mean, for

Z = atomic number of absorber } compound absorbers

t = thickness of absorber (g cm^{-2})

η = fraction of incident electrons transmitted.

Then Weber (Nucl Instr Methods 25 p 261 (1964)) proposed an empirical formula of the type

$$r = Pw\,(1 - Q/1 + Rw) \qquad \ldots\ldots 4.3.5(a)$$

where P, Q, R are empirical constants:

$$P = 5.37 \times 10^{-4} \text{ g cm}^{-2} \text{ keV}$$
$$Q = 0.9815$$
$$R = 3.1230 \times 10^{-3} \text{ keV}^{-1}$$

and Rao (Nucl Instr Methods 44 p 155 (1966)) proposed

$$\eta = (1 + \exp(-gh)) \,/\, \left[1 + \exp\left(g\left({}^{t}/_{r} - h\right)\right)\right] \qquad \ldots\ldots 4.3.5(b)$$

where g, h are empirical relationships:

$$g = 9.2\, Z^{-0.2} + 16\, Z^{-2.2}$$
$$h = 0.63\, ({}^{Z}/_{A}) + 0.27.$$

Kobetich and Katz (Phys Rev 170 p 391 (1968)) used these equations to calculate the energy deposition / depth relation by writing the residual energy $W(r, t)$ of an electron of practical range r after travelling through a thickness t of absorber as

$$W(r, t) = w(r - t) \qquad \ldots\ldots 4.3.5(c)$$

then the energy transmitted through t is ηW and the energy deposited at depth t by a beam containing one electron/cm^2 is:

$$E = d(\eta W) \,/\, dt \qquad \ldots\ldots 4.3.5(d)$$

Backscatter is ignored in this treatment by assuming the energy scattered from t into t-δt to be compensated by that from t + δt.

Kobetich and Katz demonstrated that for elemental absorbers over the range 300 eV to 20 MeV their empirical calculations compared favourably with experiment and with Spencer's (Phys Rev 98 p 1596 (1955)) classic ab initio calculations. Consequently their approach was used here, with $\bar{Z} = 23$ and $\bar{A} = 52$, to calculate the energy/depth distribution for electrons in NaBr.

Equation 4.3.5(a) was used to calculate the Weber ranges shown in Fig 4.3.(viii)and by combining this with equation 4.3.5(b), and

approximating to the differential form of $d(\eta W)/dt$ via a 10-step interpolation of each Weber range, the curves of Fig 4.3.(ix) were generated.

The implicit lack of correction for surface backscatter, and the "sampling" errors, can be ignored in comparison with the salient features displayed even by the crude calculation employed here. It is noticeable that the energy/unit depth is virtually constant for a considerable portion of the range, that there is a pronounced "ionisation peak" just before the practical range limit, and that for most of its range the specific energy loss from the 200 keV beam is greater than that for the 400 keV beam and the 200 keV ionisation peak is higher. The effect of this difference will be seen to account for variations in the equilibrium between F and a centres at high doses (6.2.5), and (4.4.4) coloration range maxima.

We note that the shape of curve 4.3.(viii) is indicative of the inapplicability of low-energy (eg Shulman and Gel) penetration characteristics to high energy electrons : at energies below 100 keV the curve tends to a higher-order dependence on V.

4.4.1 Background considerations regarding direction dependence of coloration depth in NaCl

The effect of variation of angle of incidence on colour penetration and F band density has been investigated piecemeal by a number of workers including Shulman and Gel (op cit) and Ritz (Phys Rev 142 p 505 (1966)). The latter author found the F centre production rate "less than 20%" dependent on the orientation of the incident beam with respect to a number of soft alkali halides whereas the former authors, using 15 keV electrons, found a significant departure from a "$\cos\theta$" colour penetration dependence on angle of beam incidence for both NaF and NaCl.

Attention was aroused by the discovery of the lenticular edge of the coloration in KI (Fig 4.4.(i)) which showed a more pronounced anisotropy of distribution than NaCl (Fig 4.2.(i)). However further investigation showed this to be a spurious effect of bleaching as mentioned in 4.2.2.

Choudury, Chaudri and Goswami (Phys Rev 186 p 885 (1969)) irradiated a cylindrically ground rotating NaCl crystal and measured the optical

density/angle of incidence profile before and after grinding away the surface layers of the crystal. They found optical density maxima in the $\langle 100 \rangle$ and $\langle 110 \rangle$ directions, with $D_{\langle 110 \rangle} > D_{\langle 100 \rangle}$ after a very large (Stage II) dose of 25 keV electrons at RT. The colour penetration depths were also maximal in the low-index directions, with $p_{\langle 110 \rangle} < p_{\langle 100 \rangle}$. In view of the known susceptibility of coloration to impurities it was decided that the experimental data here should refer to dry-cleaved samples only.

NaBr was held to be an unsuitable material for investigation owing to the thermal instability of the NT coloration and the difficulty of measuring penetration in a single specimen with any degree of precision. Further, the long irradiation time and preparation delays would have spread the experiment out over a considerable period whereas the necessity for preparing all the photographs under identical conditions militated in favour of using the microscope for a continuous session without altering its parameters. Consequently it was decided to investigate NaCl.

4.4.2 Experimental results : polar penetration plot

Samples F8, F9, F10 of Harshaw NaCl were cleaved and greased onto the tail of the large cryostat in contact with a thermocouple. Despite the absence of a specimen clamp the surface temperatures achieved were lower than 85K with liquid nitrogen coolant. Without the sample clamp it was possible to alter the angle of incidence of the electron beam by rotating the cryostat inner tube.

Since F band growth per unit time had been shown proportional to beam intensity for $\langle 100 \rangle$ incidence (Chapter 3) it was decided to give each specimen a dose $\Delta \sec \theta$ where θ is the angle $\langle 100 \rangle \wedge \langle$incident beam$\rangle$. Beam energy was held at 400 keV and current at $0.8 \pm 0.03\ \mu A$. Then in the absence of any orientation dependence the penetration characteristics should have been identical for all samples. After irradiation each specimen was sectioned as close as possible to the point of intersection with the beam axis and photographed in the Ultraphot microscope, using plates from a single batch, developed together, with identical exposure conditions and section thickness 1 mm $\pm$ 0.1 mm

(The effect of specimen thickness was dealt with in 4.3.2). Two sets of plates were prepared, one with half the exposure of the other. The plates were scanned by the microdensitometer and the ranges ρ_{10}, ρ_{25}, ρ_{50} at which the plate transmission had fallen to 10, 25 and 50% of its maximum respectively, were determined. Three specimen orientations with $\theta = 0$, $22\frac{1}{2}^{o}$, 45°, were examined. The polar plots of $\frac{\theta}{\rho}$ sec θ vs θ are shown in Fig 4.4.(i).

The standard error of each value of $\frac{\theta}{\rho}$ from the microdensitometer trace is less than $\pm$ 2 μm so the shape of the mean curve is significant. The significance is heightened by the similarities between the curves and also with an earlier, though less precise, determination. The polar plot of the "half exposed" plates at the 25% level was indistinguishable from that shown here.

4.4.3 Discussion of penetration / angle of incidence experiments

Ehrenberg and Franks (Proc Phys Soc 66 p 1057 (1953)) showed that the distribution of luminescence excited by electrons inan irradiated solid conformed to a hemispherical region surrounding the point of incidence of the narrow beam. As the beam energy increased so the luminescent region tended to become columnar. Extension of this work (Ehrenberg and King; Proc Phys Soc 87 p 751 (1963)) to 80 keV showed similar effects with the "ionisation peak" (4.3.5) visible as a luminescent intensity peak. Although the authors treated the effects as isotropically distributed about a point whose depth into the crystal increased with energy the energy distributions of Fig 4.3.(vii) for NaBr at higher energies are more in keeping with a columnar-distribution approach to radiation effects at these energies.

Shulman and Gel (op cit) dismissed their observed orientation dependence of penetration by noting that at grazing incidence there was still some coloration penetration. The diameter of the "column of damage" surrounding the projected incident flight path of a narrow electron beam is therefore finite and observable even at $<$15 keV beam energy, and the non-linear penetration / cosθ relationship arises from this width.

However if the effective coloration range of the electrons were isotropic with respect to angle of incidence (regardless of its relation to the

"practical range") and in consequence the dimensions of the damage column associated with each electron were constant regardless of the angle of incidence, then turning points in θ_ρ must be such that the normal penetration of coloration measured along $\langle 100 \rangle$ due to normally-incident electrons must be a minimum if the column diameter is finite. In the present case, however, the penetration for $\theta = 0$ was not a minimum and must, by symmetry, have been a maximum (unless local maxima occurred in the region $0 < \theta < \pi/8$).

The aspect ratio of the effective damage column was next investigated. Photograph 4.4.(iii) shows a NaCl crystal irradiated through a $^1/_{16}$" dia hole in a lead sheet, with collimated 400 keV electrons. The central coloured section is depicted in the photomicrograph 4.4.(iv) and it can be seen that the coloration has spread as far in the plane of the lead sheet as it has perpendicular to the sheet, indicating that the "column" of damage referred to above has a width commensurate with the effective coloration range. We would not, therefore, expect there to be a minimum ρ between $\theta = 0$ and $\theta = \pi/4$ unless the angular distribution of ρ has other than a simple "cos θ" type dependence. However 4.4.(i) is interpreted there is a pronounced minimum in the coloration range in the region $0 < \theta < \pi/4$ and it therefore seems that the effective path length of the electrons depends to some extent on the angle of incidence of the primary beam, with the $\langle 100 \rangle$ and $\langle 110 \rangle$ directions giving increased coloration range compared with intermediate ones. It may be argued that $\pi/4_\rho > 0_\rho$ is not a significant result since the distribution of damage around the incident flight path has not been adequately described, but the existence of a minimum ρ for θ in the region of $\pi/8$ is a significant experimental result.

4.4.4 Theoretical considerations : extension to NaBr

Most of the energy of an incident electron will be scattered out of the initial line of flight by processes such as secondary emission and ionisation, which tend to dissipate the incident kinetic energy more or less isotropically. Consequently any anisotropy shown in an effect dependent upon the incident beam transferring energy to the matrix must either indicate a very strong preference on the part of the matrix for damage to be caused by electrons travelling in a specific

direction, or must be indicative of reduced energy dispersion for electrons travelling in initially preferred directions, leading to greater effective ranges.

In the case of NaCl it appears that at least ⟨110⟩ and possibly ⟨100⟩ incidence leads to enhanced effective penetration of electrons. Now in ⟨100⟩ there are potential saddles in the NaCl lattice at $(\frac{1}{4}, \frac{1}{4}, 0)$ and preferential electron channelling in this direction has been reported by Nip, Hollis and Kelly (Phys Let 28A p 324 (1968)). An electron travelling in the direction $(\frac{1}{4}, \frac{1}{4})$ is intuitively relatively free from the probability of interaction with a matrix electron and in consequence its energy loss / unit range will be small and its effective coloration range large. In ⟨110⟩ however there are no such saddles but it is in this direction that momentum is most easily propagated and focused along the closepacked Cl^- ion rows. Since F centre creation demands the removal of an anion from a lattice site it is intuitively conceivable that the injection of momentum in ⟨110⟩ will give the optimum yield of F centres at any finite radius from the primary event.

In essence this is the argument propounded by Choudury et al. (op cit) but extended to a higher incident beam energy where, since p ⟨110⟩ > p ⟨100⟩, we must assume the momentum-transfer function to be more important than the electron-channelling range enhancement. We have seen (4.3.(ix)) that the energy loss to matrix electrons is in any case smaller for high-energy incident electrons and the channelling effect will thus be relatively less important to the range of 400 keV electrons than to that of a 25 keV beam, compared with the momentum-transport enhancement.

Although no experiments were conducted here on NaBr, as explained in 4.4.1 we could expect, on the basis of the above argument, to see a greater orientation dependence since the near-critical radius ratio of NaBr implies that the anions are effectively in hard-sphere contact in ⟨110⟩. As explained earlier, a sampled-data experiment would be very difficult to conduct but a modification of the direct observation methods used by Ehrenberg and co-workers, and Shulman and Gel, could be set up. A CCTV system could be employed to measure

penetration of both luminescence and coloration with a microscope set up on an axis orthogonal to the electron beam and a redesigned cryostat allowing the specimen to be rotated with the microscope axis parallel to the irradiated face.

4.5.1 Surface damage : techniques and results for NaCl

Within the programme of microscope studies outlined in the previous sections it was a simple matter to investigate the surface damage caused by irradiation, both transmission and reflection modes being available without major resetting of the microscope. As before, NaCl was investigated as a preliminary experiment.

Fig 4.5.(i) shows the appearance of a sample of NaCl viewed in transmission after irradiation with 300 keV electrons at NT. In reflection-mode (4.5.(ii)) it can be seen that there is an increased granularity in the irradiated zone although the apparent increase in large-scale surface features is possibly due to the enhanced contrast in the region backed by the absorbing layer. On increasing the magnification further the reflection photograph 4.5.(iii) was obtained in the coloured region. Two flat circular plateaus on the right, and the "circularity" of a number of other features, were characteristic of the appearance of the irradiated zone. Similarly the planar regions between the major features display a granularity which was absent from the unirradiated area. The apparent broadening of longitudinal cracks in the coloured region was seen to be due to the appearance of severe pitting in the region near the crack.

A remarkable aspect of the circular plateaus is that the narrow rills in the surface are continuous across the edges of the plateaus. The edges rise smoothly from the plan of the surface and turn smoothly into the tabular plane without overshoot. Apart from these features the edges of other surface irregularities appeared to be "rounded" by irradiation.

4.5.2 Revised method of study : NaBr

The irradiated and unirradiated faces of the sections cleaved for penetration depth measurements gave a more representative picture of the effect of irradiation on surface damage in the case of the hygroscopic NaBr, since

both surfaces were then subject to the same atmospheric contamination (the unirradiated portion of the NaCl crystal described in 4.5.1 had been partially covered by the heatsink during irradiation) and backed by similar absorbing material. Use of the thin grease film (see 2.5.4) kept atmospheric moisture from the surface during examination but did not obscure fine detail.

Figs 4.5.(iv) and (v) show respectively the irradiated and unirradiated faces of an NaBr specimen (200 keV, NT), and the appearance of material irradiated with 400 keV electrons was generally similar. The irradiated faces appear granularly reticulated compared with the others, similar in appearance to material exposed to ambient air. On exposure to ambient air the irradiated areas appeared to deliquesce most rapidly.

Irradiation with 100 keV electrons, although producing measurable F centre concentrations in the same way as at other beam energies, produced no visible surface damage, as evidenced by Figs 4.5.(vi) and (vii) (irradiated and unirradiated faces respectively). The "softening" effect on surface contours is not as noted for NaCl but is due to depth-of-field restriction leading to mis-focusing of most of the area in an attempt to focus the few distinct features on the surface. Over the whole of the irradiated zone the concentration of distinct features was the same as for the unirradiated face.

It must therefore be concluded that the nature of the surface damage produced in NaBr at NT depends on the energy of the bombarding electrons to the extent that a large dose (12 mC in this case) of 100 keV electrons produces less macroscopic breakup of the surface than a small dose (generally around 4 mC) of 200 or 400 keV particles, and has less effect on surface deliquescence.

4.5.3 Discussion of results in the light of published work

Townsend and Kelly (Phys Let 26A p 138 (1966)) showed that surface sputtering (as distinct from evaporation) was caused by the incidence of low energy electrons on KI, and Townsend and Elliott (Phys Let 28A p 587 (1969)) demonstrated the same effect with UV radiation, producing a surface very similar to 4.5.(iv).

Obviously, from Fig 4.3.(vii), 100 keV electrons would have contributed more to surface evaporation than those of higher energy, so the observations of 4.5.2 must be taken as indicating a threshold incident energy for superficial pitting. The following UHV work is illustrative.

The existence of a surface potential to be overcome before sputtering commences, was shown by Townsend and Kelly (Phys Let 25A p 673 (1967)) who found this potential to be dependent on beam energy and current, and sample temperature.

The present results may therefore be explained in terms of an energy-dependent surface potential tending to suppress surface sputtering and competing with increasing momentum transfer as the beam energy is raised. Townsend and Kelly found the mean effective surface potential of Na Cl to be approximately dependent on $E^{\frac{2}{3}}$ where E was the incident electron energy : for a relativistic electron the maximum collision transfer of energy to an ion increases approximately as E^2, giving the correct condition for a threshold sputtering energy.

The apparent enhancement of deliquescence by irradiation may be explained by the observation of Palmberg and Rhodin (J Phys Chem Sol. 29 p 1917 (1968)) that the first species sputtered from electron-irradiated alkali halides in UHV is the halide ion, with the alkali metal being removed later by a highly temperature-sensitive evaporation process. In the case of extended irradiation of NaBr at NT we may expect to build up a stoichiometric excess of Na^+ near the surface. In the presence of the high incident and secondary electron flux this may give rise to a region effectively doped with Na^o neutral atoms which will react vigorously with atmospheric moisture. The heat of reaction and subsequent solvation of NaOH will further enhance the surface degradation.

Thus the observed surface effects in NaBr are consistent with the transfer of momentum from the incident beam to Br^- ions in the matrix, which have a threshold energy requirement for motion.

No adequate explanation can be given for the circular plateaus of Fig 4.5.(iii). They do not appear to have been caused by evaporation of surface moisture, nor do they have the crystallographic orientation

of surface features noted by Hibi and Ishikawa (J Phys Soc Japan 13 p 709 (1958)). In fact their properties more closely resemble epitaxial growth or nucleation of or at impurities, although their concentration militates against this.

CHAPTER 5.

CATHODOLUMINESCENCE OF NaBr and NaI

5.1.1. The Importance of Cathodoluminescence as an Analytical Tool.

Whilst an alkali halide is being bombarded with electrons it emits photons with energies in the visible or UV region. This phenomenon is known as cathodoluminescence and is directly attributable to the bombarding electrons since the decay of luminous intensity after irradiation is very rapid. Spectral analysis shows the radiation to consist of distinct bands (compared with the continuous Cerenkov spectrum) which may extend into the UV region.

Several authors have noted cathodoluminescence in alkali halides and a good summary is given in Hughes et al (A. E. R. E. R. 5604) of the bands seen during irradiation of all the alkali halides at 4K. There is general agreement on the existence and wavelength of bands generated at this temperature.

The importance of luminescence studies in a survey of radiation damage springs from the fact that luminescent radiation is the only information available during the damage process. Even though it is possible (3.1.1) to measure colour centre concentrations during irradiation, each centre is essentially the end-product of the damage-producing event whereas luminescence is concerned with a dynamic process active only during irradiation.

It is, therefore, only from a study of luminescence that we can hope to elicit direct evidence of the mechanism by which electrons interact with alkali halides. Further, by correlating changes in the luminescent spectrum with dose it may be possible to identify the causes of the multi-stage appearance of the F band growth curve and other damage effects (e.g. 7.4.4.)

A potential application should serve to emphasize the importance of cathodoluminescence studies. As mentioned earlier (1.3.2.) one of the broad aims of the present programme of work was to

investigate the application of radiolytic defects as information storage elements. The theoretical maximum packing density of information then depends on the minimum defect separation obtainable.

Optical readout, however, is limited to a resolution of ~5000 Å. If it were found possible to excite cathodoluminescence only in the absence of a damage centre then a scanning electron probe could be used to excite luminescence which can be detected by more conventional optical means despite the fine resolution of the scanning beam (~10 Å diameter being routinely achievable). Postulating a photodetector with a 5 - photon response over, say, 95% of a spherical distribution it should be possible to read information to 20 Å diameter from a specimen saturated with a defect concentration of 10^{-3}, provided only primary electrons excite luminescence.

5.1.2. Experimental Details.

As explained in 2.3.5. it was a simple matter to modify the spectrophotometer to produce luminescence spectra and specimens were merely greased to the cryostat tail without a clamp and irradiated with the (100) face at 45° to both the incident beam and the spectrophotometer path.

Ideally the lowest possible irradiating beam current should be employed in luminescence experiments to avoid undue interference from absorption by the colour centres resulting from irradiation. Since the accelerator beam stability was suspect at current settingsbelow 1μA the circuit of Figure 5.1(ii) was set up to divide the luminescent intensity by the beam current and reduce the apparent fluctuation due to current instability. However in the case of NaBr the resistance to coloration was for once turned to advantage, as was the deliberate inefficiency of the scattering foils and collimators employed, and a current of 0.05 μA at the specimen, derived from a 10μA beam, was slow to colour the sample and stable enough for the luminescence to be smoothed by the 1s time constant of the detector amplifier.

Peak wavelengths are quoted without correction for the response of the photomultiplier, but those reported elsewhere agree reasonably well with the scale readings found here. Wavelength measurements were made by simply scanning the monochromator drive and observing the scale on the CCTV link.

5.2.1. Initial Results: Harshaw NaBr, NT.

An "as found" sample of Harshaw NaBr was irradiated, at NT, with 100, 200, 300 and 400 keV electrons. A broad visible luminescence band was observed, with peak wavelength moving from 440 nm to 460 nm as the electron energy was raised. At 400 keV incident energy the wavelength scan was extended to 190 nm and further band peaks were found at 360 and 273 nm. The intensity ratio (uncorrected) was 20 (273): 0.5(360) : 1 (460).

A freshly-cleaved sample of NaBr, and a narrower monochromator bandwidth, showed the long-wavelength band to be resolved into two parts peaking at 390 nm and 485 nm. Using a PbS detector the scan was extended to 2.5 μm but no further bands were found. All the bands were found to be generated by 50keV irradiation, but current instability precluded analysis of the peak heights in this case.

5.2.2. Detailed Experiments at NT: Harshaw NaBr.

Measurements with specimen G53, prepared in the usual clean, dry conditions, confirmed that all the bands were characteristic of the Harshaw material and not due to airborne impurities or contamination from other material in the desiccator. The sample was cooled to NT and with an excitation flux of 0.05 μA at 400 keV emitted the luminescent bands shown as Curve A in Figure 5.2.(ii). The current was increased to 0.8 μA, with the specimen re-oriented normal to the beam and a dose of 3575 μC was absorbed. The luminescence spectrum was re-examined and the longer wavelength bands were considerablysuppressed (Curve B) whereas the 273 nm band was virtually unaffected. The 85% reduction of intensity was considerably greater than could be accounted for by an optical density commensurate with those found in the coloration experiments (Chapter 3) at this dose which predict a maximum of

<20% absorption at 525 nm and even less at 450 nm.
After 50 min. in the dark at NT the sample yielded the luminescence curve C in the visible-near UV region, showing partial regeneration of the longer wavelength bands compared with that at 390 nm. A short re-irradiation transformed this behaviour to curve D, suppressing the longwave bands. The 273 nm band was substantially the same as for A and B. After a further 45 min wait a very small 360 nm band was found but no detail appeared at longer wavelengths. Using 0.8 μA exciting flux, which also heated the sample, curves E1 and E2 were obtained: as the irradiation proceeded so the long-wave emission increased at the expense of the shorter wavelengths.

Finally the beam was changed to 1.2 μA at 200 keV and produced spectrum F in which the longer wavelengths were depressed compared with the 360 nm band.

On those occasions for which no 273 nm band is shown it was deliberately suppressed with a filter to reduce the possibility of stray-light interference with the fainter visible bands.
This filter did not affect the 390 nm band measurably.

5.2.3. Conclusions from Cathodoluminescence Experiments at NT.

(1) The only cathodoluminescent bands generated in Harshaw NaBr at NT between 195 and 2500 nm are
   (a) a strong band peaking at 273 nm.
   (b) a band peaking at 360 nm.
   (c) a band peaking at 390 nm.
   (d) a band peaking at 485 nm, not well resolved from (c)

(2) (b) decreases slightly on irradiation in Stage 1 (stages of irradiation defined from coloration curve: see Chapter 3)
   (c) and (d) are completely removed by irradiation in stage 1.

(3) (c) and (d) are regenerated on standing in the dark at NT provided stage II has not been reached.

(4) (b) is not significantly regenerated in the dark at NT at any stage of coloration.

(5) (c) and (d) are regenerated on heating, and increasing the beam energy enhances (d).

(6) None of the bands can be associated with "atmospheric" impurities (except perhaps nitrogen).

(7) Although not reported above, the ratio of intensities of (a) to (b), (c), and (d) is greater the higher the energy of the incident electrons. This may be due to the converse of (5), namely that the low energy electrons heat the specimen more discontinuously and to a greater extent in the region where they can also excite cathodoluminescence.

It is thus clear that the long-wavelength bands are to be associated with exhaustible processes which occur more readily at higher temperatures or in the easy stage of F centre formation, and may be reactivated on standing.

5.2.4. Cathodoluminescence of NaBr Irradiated at RT.

The next step in the experiments was to examine the luminescence of an RT-irradiated specimen. Sample G 57 was cleaved in ambient air and irradiated at 1.6 μA beam current, 200 keV. The spectrum (5.2.(iii) A) of the cathodoluminescence showed a considerable reduction in the UV band at 273 nm, and an apparent shift of this band to a broad peak centred at 290 mm. Faint shoulders were found at 360 and 380 nm on a band which peaked at 450 nm. After receiving a dose of 2420 μC the "450" peak was observed to have decreased to ~60% of its original intensity, and the "290" peak had decreased to less than 50% of its original intensity. The beam energy was decreased to 100 keV and spectrum B was obtained. This shows a decrease in the relative strength of the 380 nm shoulder, which was regenerated by stepping up the beam energy to 400 keV (C) despite the continuing drop in overall luminescent intensity. Increasing the beam current by 100% at this stage produced spectrum D, with virtually the same shape as C at the long wavelength end but an apparently exaggerated 290 nm peak: whereas the ratio of intensities ^{450}D: ^{450}C is 2:1, at 290 nm the ratio is nearer 4:1. Reducing the beam energy to 200 kV produced spectrum E which shows a lower intensity at the shorter wavelengths.

5.2.5. Summary: The Effect of Temperature on NaBr Cathodoluminescence.

In view of the foregoing sections it is apparent that the luminescent bands must be associated with the conditions of the experiment thus:

(1) The longer wavelength bands are certainly characteristic of the high-temperature processes.

(2) Although not apparently at NT, the "360" and "390" bands have a projectile-energy-dependent intensity at RT.

(3) The "273" band exhibits a reduction in intensity with increasing dose, at RT: this behaviour has not been noted at NT.

(4) The three longer wavelength bands exhibit a reduction in intensity during irradiation: at NT they effectively decrease to zero after Stage 1 irradiation has been achieved; at RT the decrease is continuous and more gradual than that of the "273" band. This decrease is not commensurate with increasing colour centre absorption.

(5) Since the wavelength periodicity of the luminescent bands is similar at RT and NT, it has been assumed that the bands observed at RT correspond to those found at NT, with a temperature-induced wavelength shift increasing the wavelength of the "273" band and decreasing those of the others.

5.3.1. Cathodoluminescence of NaI: Comparison with NaBr.

One sample of NaI was examined in order to obtain its cathodoluminescence spectrum. Excitation with 0.3 μA 400 keV electrons at RT produced spectrum 5.3.(i) A, with peaks at 313 nm, 387 nm, 483 nm and intensity ratios 2:1:1 respectively. No other bands were detectable within the spectrophotometer range.

The specimen was then cooled to NT and re-irradiated. Luminescence was detected as 5.3.(i) B, with peaks at 443 nm and 299 nm (ratio 1:20) and a shoulder at 384 nm. A peak detected at 340 nm when the NT spectrum was scanned with a 380 - 500 nm passband filter in the optical path (to cut out stray light from the 299 nm band) was assigned to an interaction of the filter passband tail with the tail of the 299 nm luminescence, and it is not recorded here.

The heights ratio of the "443" and "438" RT bands was 4:1, giving an 80:1 ratio for the NT "299" : RT "438", without correction for photomultiplier response and sample absorption. Consequently the scales for the two curves in Figure 5.3.(i) are not identical.

There is an obvious comparison between the behaviour of NaI and that of the NaBr reported earlier. The overall luminescent intensity is temperature dependent and concentrated in a narrow region of the blue-near u.v. portion of the spectrum. The short-wave band appears to be a single band with a highly temperature-dependent intensity though the temperature coefficient of wavelength is of different sign for the two compounds. Likewise the temperature coefficients of the wavelength of the longer-wave luminescences are of opposite sign for the two compounds, and are of opposite sign, in each case, to that of the short-wave luminescence, as shown in Table 5.3.1.

The exception to the general rule here is the "387" (NT) band in NaI. Since the observed band in this region appears only as a shoulder at RT in the present measurement its temperature dependence will not be featured in the subsequent discussion.

5.4.1. Comparison with Other Authors' Results. Theory of Intrinsic Cathodoluminescence.

Measurements of X-ray excited luminescence at 4°K have been published by Hughes et al (AERE-R5604 (1967)) who obtained peaks at 269 nm (NaBr) and 293 nm (NaI) with relative intensities of 1:3. Although the equipment used here cannot be said to provide direct correlation between samples, owing to the current dependence of the luminescence and the unknown sensitivity characteristic of the photomultiplier, the relative intensity ratio at NT for the short-wave bands was broadly similar, and the band peak wavelengths show a reasonable correlation with the present observations. The work of Hughes et al makes no mention of any longer-wavelength bands and in view of the temperature dependence of their intensities observed here it is doubtful whether they would have been detectable at 4K using standard equipment.

Kabler and Patterson (Phys Rev Let 19 p 652 (1967)) have analysed the data (Table 5.4.1.) for luminescence of most of the alkali halides and have explained the shortest-wavelength lines observed here in terms of a forbidden transition of a V_K centre + electron (self-trapped exciton) system. They consider the ground state of this system to have the electronic configuration $(\sigma g.np)^2 (\pi u.np)^4 (\pi g.np)^4 (\sigma u.np)^2$, which is an unstable $^1\Sigma g^+$ state, relaxing spontaneously into two separate anions. The lowest excited states are then .....$(\sigma u.np)^1(\sigma g\ (n+1)s)^1$ which is either $^1\Sigma u^+$ or $^3\Sigma u^+$ and is in both cases bonding. There is an obvious transition $^1\Sigma u^+ \rightarrow {}^1\Sigma g^+$ but the transition $^3\Sigma u^+ \rightarrow {}^1\Sigma g^+$ is forbidden by the multiplicity change involved. Consequently the authors invoke a mixing from the $^1\Pi u$ state $(\sigma g.np)^2 (\pi u.np)^3 (\pi g.np)^4 (\sigma g.np)^2 (\sigma g(n+1)s)^1$ and similar states. The resultant transition then can be shown to have the observed polarisation reported by Murray and Keller (Phys. Rev 153 p 993 (1967)) for Na I and by Kabler and Patterson for NaBr. The longer wavelength bands are associated by Van Sciver (Phys Rev 120 p 1193 (1960)) with Tl impurity luminescence in NaI, (425 nm at NT) and with excess I^- (375 nm at NT) although there does not appear to be a reliable account of the origin of the longer-wavelengths bands in NaBr.

5.4.2. Implications of Theory and Notes for Discussion.

We note for later discussion that there is no report in the published literature of the luminescence of the "allowed" transition in NaBr, and no higher energy luminescence than 270 nm was observed in the present experiments. We also note that the observed lifetime of the excited state for the forbidden transition, as reported by Kabler and Patterson, corresponds more closely to the lifetimes for the allowed transition in all the other alkali halides, being several orders of magnitude less than for the forbidden transition in, say, NaCl. The authors suggest the discrepancy can be assigned to the variation in halogen spin-orbit coupling, but the discrepancy between the "forbidden lifetimes" of KCl and KBr is not commensurate with that found here. An alternative explanation is advanced in 7.4.4.

In connection with the observations of Section 4.4. we note that the intrinsic luminescence intensity reported by Van Sciver had an orientation dependence on the polarisation of the incident exciting light, such that alignment of the E vector along (110) directions enhanced the luminescent output.

It should be possible, in principle, to investigate this latter effect, and to obtain information concerning the polarisation of the luminescent bands to confirm the assignment of origins. However it was felt that these experiments would be beyond the scope of the present investigation. In view of Van Sciver's results (and others) confirming the sensitivity of cathodoluminescence to trace impurities it is worth considering the analytical table given in Chapter 3. It seems highly probable that Fe or Ca could be held responsible for some or all of the long-wave luminescence observed in the irradiation of NaBr, but there is no published precedent for this assignment and, again, an investigation was felt to be beyond the limits of the present project.

CHAPTER 6.

OPTICAL SPECTROPHOTOMETRY OF NON F-BANDS IN NaBr AND THE EFFECT OF THERMAL AND OPTICAL BLEACHING OF THE F BAND.

6.1.1. Introduction : Previously Published Studies of Non-F Bands in NaBr.

Prior to the present work there had been little published data concerning the absorption bands (other than the F band) produced by irradiation of NaBr. A generally comprehensive list compiled by Klick (Schulman and Compton: Color Centres in Solids, Pergamon (1963)) of all the well established absorptions due to trapped-carrier defects in alkali halides mentions only the F and α bands for NaBr, and gives the peak wavelength of the α band as 199 nm (at 90K). This value fits well in the homologous series with λ^{α}_{NaF} = 131 nm, λ^{α}_{NaCl} = 174 nm. The α band has been unambiguously associated with the perturbation of the fundamental absorption edge by vacancies in the halide submatrix, and is consequently usually found in materials irradiated at low temperatures, along with the F band.

Jacobs and Krishna Menon (Phys. Stat Sol 35 K 143 (1969)) published the results of a study of the UV absorption at NT of NaBr samples X-irradiated at RT and additively coloured by the Van Doorn method. They positively identified a band at 6.31 eV (196 nm) as the β band, a perturbation of the fundamental absorption by F centres, and assigned an absorption peaking at 5.76 eV (215 nm) to the α band. They also found a shoulder on the β band "correlated" with the β, designated β′ and so far unexplained. The same authors have reported (J Chem Phys 41 p 2920 (1968)) work on the K and M bands (arising respectively from higher excited states and aggregate pairs of F centres) in NaBr X-irradiated at RT and cooled to NT. They were unable to resolve the K band but found a small M band at 1.5 eV (825 nm).

Since it had been shown possible to create appreciable concentrations of F centres at NT by electron irradiation it was decided to use the present apparatus to investigate the non-F bands generated by the same irradiation and if possible to correlate their stability with the susceptibility of the F band to optical and thermal bleaching. The V-series of bands (holes trapped at anion defects) had not been characterised in NaBr prior to this investigation since X-irradiation is hardly effective in creating damage centres in NaBr at NT and V-centres are unstable at RT.

6.1.2. Experimental Procedures.

Preliminary feasibility studies were performed with the large cryostat (Section 2.4) and Zeiss single beam spectrophotometer in the accelerator enclosure. However the limitations implicit in using a single-beam instrument for scanning over a range of wavelengths necessitated a departure from the ideal criteria of 2.4.1. and a small cryostat and ball valve (Figure 6.1.(i)) were employed to allow the irradiated crystal to be transferred under vacuum and at NT to the sample chamber of a Perkin Elmer Model 450 spectrophotometer. This instrument covers the range of wavelengths of interest here (185 - 750 nm) in two stages and by virtue of being a double-beam device could be used to plot absorbance or transmittance curves directly, against a compensated baseline.

The small cryostat was not fitted with a Faraday cup charge collector and in consequence the dose measurements obtained could not be directly compared with those from the main cryostat system. However the inner tube and top flange assembly was electrically insulated from the outer case by a Perspex collar and the dose integrator was employed : it was found that doses $<$10 mC were clearly insufficient to take the F centre coloration beyond Stage 1, whereas doses $>$25 mC corresponded to Stage II coloration. Owing to the restricted clearance in the sample chamber there was not room for the final collimator and in consequence the measured beam was spread over a greater area than in the larger cryostat.

The Zeiss spectrophotometer was used to provide the F band bleaching light for some experiments, and for others a 50W projector bulb was run under controlled voltage conditions and the light filtered through a Wratten tricolour green gelatine filter.

6.2.1. Absorbance of Irradiated B.D.H. NaBr (400 keV, NT) and Effect of Optical Bleaching of F Band.

Figure 6.2.(i) shows the absorbance spectra of a sample of NaBr (G80) from the B.D.H. boule, after 400 keV electron irradiation and optical bleaching of the F band. The baselines for both visible and UV spectra were set horizontal before irradiation, so that the bands seen must all have arisen from the treatment applied to the material. The numbered curves correspond to:

(1) 8 mC dose.

(2) 8 mC dose followed by 3 hr bleaching in tricolour green light.

(3) 9 mC dose.

(4) 34 mC dose

(5) 34 mC dose followed by 3 hr bleaching in tricolour green light.

(6) 35 mC dose.

The behaviour of the absorption spectrum shows that, in Stage 1, bleaching the F band (525 nm) enhances all the absorption bands with $\lambda < 250$ nm. There is no strong evidence of the formation of a band with $\lambda_{peak} = 215$ nm on irradiation but bleaching treatment does produce such a band. Any F' shoulder (caused by F' centres - two electrons trapped at a vacant anion site) is below the limit of detection and any decrease in the β band due to bleaching of F centres is masked by the growth of the band peaking at ~200 nm. There is some evidence of a band system in the region between 215 and 235 nm after bleaching the F band. A short re-irradiation restores the F band, reduces the heights of those bands between 195 and 205 nm, and enhances all the intermediate bands: new structure becomes apparent in the 250 nm and 475 nm regions.

Irradiation into Stage II still fails to reveal the 215 nm band reported by Jacobs and Krishna Menon (op cit) but the β band

is increased along with the F band. Bleaching the F band again enhances all those bands with $\lambda < 250$ nm but now a broad band centred on 275 nm appears, whereas in Stage I this region was bleached with the F band. The fractional depletion of the F band was about 75% of that which was brought about by the same bleaching treatment in Stage I. F band bleaching again fails to produce an F' band, enhances the 200 nm band (but sharpens it owing to the decreasing overlapping β band) and gives marginal evidence of an absorption structure in the 205 - 220 nm region. Finally re-irradiation restores the F band (though not as completely as before) and the β band, produces some structure between 230 nm and 474 nm, and reduces the 200 nm region whilst maintaining the β band.

The behaviour of the 200 nm band seems to bear a directly proportional anticorrelation to that of the F band and the absence of a 215 nm band throws some doubt on the findings of Jacobs and Krishna Menon. In the light of the experiments just described it seems more reasonable to suppose that the α band is as listed by Klick (op cit) peaking ~199 nm. In view of the large oscillator strengths calculated for the α band (e.g. Delbecq Pringsheim, Yuster : J. Chem. Phys. 19 p 574 (1951) calculate values greater than unity), it is eminently reasonable that the behaviour of the region between 195 and 210 nm can be ascribed to an α band peaking at about 200 nm.

6.2.2. Behaviour of B.D.H. NaBr Irradiated at 200 keV, NT.

Figure 6.2.(ii) shows a set of absorbance curves obtained from NaBr after

(1) 8 mC dose.

(2) 16 mC dose.

(3) 16 mC dose followed by 3 hr bleaching in tricolour green light.

Some of the apparent UV absorption must be ascribed to a baseline malfunction in the spectrophotometer but the salient features of the curves are similar to those reported for 400 keV irradiation.

There is again no evidence for a 215 nm band generated by irradiation alone although the 215 nm region is "filled" on bleaching the F band. The fractional enhancement of absorbance at ~200 nm correlates with the fractional depletion of the F band on bleaching and the behaviour of the 240 - 310 nm region is similar at high dose levels to that described for 400 keV irradiation.

Evidence from this and other samples led to the conclusions that:

(a) the behaviour in Stage 1 was comparable with that found in 400 keV-irradiated material but the fractional depletion of the F band (and 200 nm enhancement) for a given bleaching treatment was not significantly dependent on dose.

(b) brief re-irradiation after bleaching the F band (stage II) reduced the F band but scarcely affected the 200 nm band.

(c) protracted re-irradiation increased the F band but decreased the 200 nm band initially, after which both bands increased towards a saturation level of absorbance.

(b) and (c) are illustrated semiquantitatively in Figure 6.2.(iii).
(b) was not tested in Stage 1 as the F band absorbance was too small to produce a detectable effect. Both effects will be discussed later (6.5.2 and 6.2.5).

6.2.3. Discussion of F band optical bleaching results and UV absorbance measurements.

Some of the evidence for this discussion is drawn, in fact, from the experiments whose description follows: in later sections of this chapter it was found to be advantageous to measure transmittance curves and a more extensive set of data is available than for absorbance measurements. However this is an appropriate juncture for presenting some observations on the optical bleaching of F centres in NaBr and its effect on other bands.
No evidence was found to suggest that the 215 nm band is a primary product of irradiation at NT. We cannot, therefore, expect that this is the α band. It appears that the 200 nm band has a saturation absorbance which can be approached by irradiation at NT. If, therefore, this is the α band then it is quite possible that it was not

formed to any significant extent during the experiments reported by Jacobs and Krishna Menon, since at the temperature of their irradiation (RT) any "unfilled" vacancies in excess of the thermal equilibrium concentration could have annealed out or migrated to clusters. The absence of the 215 nm band from additively coloured material or Ca^{2+}- doped irradiated material (Jacobs and Krishna Menon, op cit) then indicates that it may arise from a centre complementary to a bleached F centre.

The enhancement of the 240-310 nm region on bleaching stage II F centres seems to indicate some qualitative difference between the products of irradiation in Stage I and Stage II. The decrease in this region seen in 6.2.(i), curve 1, can almost certainly be ascribed to the bands riding on the tails of the longer-wavelength complex whereas the enhancement in Stage II is unequivocal.

There appears to be a difference in stability with respect to optical bleaching between F centres generated by 400 keV and 200 keV electrons, to the extent that some of those formed by 400 keV irradiation in Stage II are more difficult to bleach than the stage I centres, whereas no such difference was found between 200 keV Stage I, 200keV Stage II, and 400 keV Stage I.

6.2.4. "Homology" Argument for Re-Allocation of α Band.

Jacobs and Krishna Menon (op cit) quoted the results of Eby, Teegarden and Dutton (Phys. Rev. 116 p 1099 (1959)) who showed that NaBr has exciton bands peaking at 6.68 and 7.20 eV. The shifts responsible for the β and α bands were then tabulated, as in Table 6.2.1.

It is immediately obvious that the figure for NaBr α is the only homology misfit in the table. In the absence of a value for λ^{α}_{NaBr} one would assume, therefore, that it corresponded to about 0.66 eV difference from the first exciton level. This leads to a value of 205 nm (6.02 eV).

6.2.5. F/α Ratio: The Relative Concentrations of Filled and Unfilled Vacancies created by Irradiation.

It would be useful to apply the Smakula formula (Section 3.6.1) to the α band and thus follow the absolute value of the F/α ratio for NaBr,

in the same way as typified by the work of Ritz (Phys. Rev. 133A p 1452 (1964)) on KBr. However the necessary constants for the α band are still less well known than for the F band, especially in view of the present doubt as to the precise location of the α band. We can place an upper limit to W^{α}_{NaBr} by inspection of the absorbance curves, and show that the halfwidth is probably not greater than 0.5 eV, and, further, we can assume the spatial distributions of α and F centres to be identical. However n is unknown at this wavelength and temperature, and apparatus was not immediately available for its determination. Nevertheless it is reasonable to assume that all the unknown constants remain constant during irradiation, and that the effect of adjacent bands overlapping remains fairly constant : thus the qualitative changes in F/α ratio can be followed.

Although, as mentioned in 6.2.2., the curves of Figure 6.2.(ii) cannot be considered fully representative of the quantitative UV behaviour of the sample, adequate information was obtained from transmittance measurements to demonstrate that:

(a) the F/α ratio is constant for 400 keV irradiation regardless of dose.

(b) The F/α ratio for 200 keV stage I is similar to that for 400 keV irradiation, but rises by about 15% in Stage II.

It therefore seems that 200 keV radiation is more effective in "filling" vacancies than creating them, compared with 400 keV electrons. Referring to 4.3.5. and Figure 4.3(ix) we see that at a given depth of penetration a 400 keV electron will have lost less energy to ionisation events than a 200 keV projectile and is thus better able to initiate a high-threshold event such as anion displacement. On the other hand if an equilibrium vacancy concentration has been attained, the higher specific ionisation associated with a 200 keV electron will increase the number of free electrons and enhance the probability of α→F conversion by electron trapping. Provided this event is more probable than F centre ionisation (see 7.4.1) the F/α equilibrium will depend on the ionising capability of the incident radiation whilst

the beam is present, and will be "frozen in" as a metastable equilibrium when the beam is switched off.

6.3.1. A Survey of all the Absorption Bands in Irradiated NaBr Between 195 nm and 750 nm.

As explained in the foregoing sections, the measurements made in the "absorbance" mode of the double-beam spectrophotometer yielded good quantitative measurements of the principal band strengths where these bands were identifiable, but the scale was generally too compressed to allow resolution of any other bands, or study of band overlaps. However in the "transmittance" mode it was possible to increase the system gain to 0.01 transmittance/ordinate division and then to suppress the scale zero so that small deviations from 100% transmittance could be observed. At this scale expansion baseline stability was very suspect and the general opalescence of the samples (due to trapping of impurities in the vacuum system and consequent surface damage enhancement (4.5.2.)) increased as the experiments proceeded, so no quantitative measurements of absorption could be made to any greater precision than in the "absorbance" experiments. However it was possible to locate the apparent peak wavelengths of a large number of previously unresolved bands.

The location of a pair of weak and unidentified absorption bands at 260 and 280 nm by Didyk, Pashkovskii, and Tsal (Sov. Phys. Opt. and Spect. 20 p 462 (1966)) is one of the few previous reports of any radiation-induced absorption in NaBr between 220 nm and the F band. A search for K bands by Jacobs and Krishna Menon (see 6.1.1.) was inconclusive. Consequently any bands found here could only be associated with centres on the basis of the present work.

Figure 6.3.(i) shows the results of a typical broad-range scan after subtraction of the baseline (it was not feasible to completely flatten the baseline with the compensator at the scale magnification employed). The sample was cleaved from a Harshaw boule and shows a broad shoulder at 215 nm: it is worth noting in this context that Jacobs and Krishna Menon were unable to generate their 215 nm band in material doped with Ca, and the Harshaw material has been shown

(Chapter 2) to contain less Ca than the B.D.H. boule which was used for the experiments on absorbance and α-band location.

6.3.2. Tabulation of location, behaviour and possible identities of all bands found.

Table 6.3.1. contains the digest of some fifty spectra similar to 6.3.(i) obtained from ten Harshaw and two B.D.H. samples of NaBr irradiated and bleached at NT.

Any band which appeared consistently in three traces at different doses or in different materials, was listed for the tabulation in Table 6.3.1. along with its "distinguishability" from surrounding bands, and behaviour during optical bleaching of the F band (using the Zeiss spectrophotometer set at 525 nm, 60nm bandwidth, as the bleaching radiation source).

Probable identities are assigned from the following argument.

Bands 1 and 3 (or 4) are assigned by the arguments of the foregoing sections, with some doubt remaining as to whether 3 or 4 is the true α band : it seems more likely, from the "homology" argument, that 4 should fit the hypothesis but the higher absorption of 3 may indicate the large oscillator strength associated with the α band. The V bands are conventionally assigned such that $\lambda^{V_1} > \lambda^{V_4} > \lambda^{V_2} > \lambda^{V_3}$. Both materials have $[K^+] > 80$ ppm, dictating a strong V_1 band and V_1, V_3 are generally found, in other materials, to be sharper and more distinct at NT than the surrounding bands. The V_k band is assigned by virtue of a homology argument but the 340 nm band may be an equally good choice : however in view of the nature of the V_k centre (Kanzig and Woodruff : J. Phys. Chem Sol. 9 p 70 (1958)) and the arguments of Chapter 7 it seems possible that V_k centres are only formed as stable entities in NaBr by high-energy bombardment.

The K band appears in the expected position, with approximately the correct absorption strength and precisely correlated bleaching with the F band, and may be considered as a reasonably certain assignment. The band to the long wave side of the F band is unlikely to be the F' band since this is not generally formed in radiation-coloured materials and should anticorrelate with F band

bleaching. The only reasonable contenders for the associated centre are therefore the R_1 and Vk (second excited state); in view of the small F centre concentration the probability of finding three associated vacancies is small and the second Vk level seems the more probable assignment : this then throws a slight doubt on the assignment of band 13 to the Vk centre.

Those bands whose appearance was specific to material from one or other source have been assigned to the general "impurity" category and may arise from trapped-hole centres associated with an impurity cation.

The 215 nm band is somewhat problematic in view of the results of Jacobs and Krishna Menon. It could very well be associated with an aggregate defect and in fact its properties are consistent with di-vacancy (double α-centre) shifting of the fundamental absorption. Such an explanation would be consistent with its behaviour during F-band bleaching, its maintained absorption on re-irradiation, and its predominance over true α band absorption in samples cooled from irradiation at elevated temperatures. The apparently large [α]/[F] ratio leads us to expect any F-aggregate (e.g. M) band to be small even if it is stable.

6.4.1. Thermal Bleaching of F centres. Experimental Method.

It has already been noted (Chapter 4) that the F centres formed by 200 keV irradiation of NaBr at NT are unstable with respect to rising temperature. This effect was investigated quantitatively using the large cryostat by inserting the thermode shown in Figure 6.4.(i): this consisted of a 65W heating element embedded in a Dural block that made good contact with the cryostat heatsink. The thermode was used to drive off the coolant after irradiation at NT, and to raise the temperature of the specimen in a controlled manner. Sample transmittance at 525 nm was recorded with the Zeiss spectrophotometer and a chart recorder. Sample temperature was monitored continuously during rapid heating and estimated from a separate calibration during slow annealing to RT.

Specimen G 60 was irradiated at RT to an optical density of 1.05 (540 nm) with 200 keV electrons. After 11 hours in darkness there was no perceptible change in optical density. Similar confirmation was obtained of the stability of 400 keV - generated centres, and attention was then turned to the centres generated at NT.

Specimen G63 was irradiated to an O.D. of 0.125 (525 nm) at NT by 200 keV electrons. Annealing to RT over a period of 12 hrs. in darkness destroyed all the F coloration, even at 540 nm. For samples irradiated at NT by 400 keV electrons to F centre concentrations of the same magnitude, at least half the coloration remained after similar treatment. The effects were not found to be dependent on the source of material.

6.4.2. Detailed Results: Fast Thermal Bleaching.

Sample G 66 was irradiated at NT with 200 keV electrons to an O.D. of 0.28 (525 nm) and warmed to RT with the thermode, then cooled again to NT. The optical density had fallen to 0.12 but recovered rapidly on re-irradiation.

Figure 6.4. (ii) shows the effect of warming samples G70 (400 keV) and G 71 (200 keV) rapidly to RT after irradiation into Stage II. As the F band halfwidth increases with temperature it was felt that the optical density measured at 525 nm would suffice to demonstrate the behaviour of the F band. Thermocouple readings are annotated to the curves at salient features.

Considerable thermal inertia in the system accounts for the long period of virtually constant F band density but once the thermode was hot the band displayed a number of interesting features.

Violent oscillations were noted in the apparent absorbance of G71 at about 100 K. These were assigned to thermoluminescence which may have also occurred in G70 - obviously the rate of heating is critical to the observation of weak luminescence against the background of the measuring beam and its observation in the case of G71 was probably fortuitous despite the significance of the fluctuation.

Beyond this point there was a small, sharp, increase in F band absorbance, followed by a longer and less violent change. Then at about 200 K both samples showed a strong, shortlived, increase in absorbance equivalent to a 150% increase in F centre concentration for G71 and about 20% for G70. By the time the temperature had risen to about 210 K this feature had annealed out as suddenly as it grew, and the F band absorbance returned eventually to virtually the same value as it had immediately after irradiation.

6.4.3. Detailed Results : Slow Thermal Bleaching.

Experiments in this area were carried out by simply emptying the cryostat coolant and allowing the sample to warm to RT by ambient radiation heating. Optical density data was plotted continuously with a chart recorder and the minimum practicable measuring beam flux was employed to reduce optical bleaching.

Figure 6.4.(iii) shows the radiation heating curve with zones of thermal bleaching and recovery behaviour annotated. Although at the end of the "transient" period (similar to that found in fast annealing) both types of specimen had similar F band densities to those obtaining immediately after irradiation, those irradiated with 200 keV electrons exhibited slow thermal bleaching between 250 K and RT, with a measurable slope of F vs t even after 12 hours warming. The "fast bleach (200)" refers to about 45% decrease in F band absorbance in 1hr. whereas the "slow bleach (400)" refers to 15% decrease in 3 hr. Both samples were irradiated into Stage II.

6.4.4. Discussion of Thermal Bleaching Effects.

Reirradiation of thermally-bleached 200 keV samples cooled to NT rapidly regenerated the F band. It is therefore probable that the slow bleaching process involves transfer of F centre electrons to another trap rather than destruction of the vacancies. Unfortunately the opalescence of surfaces warmed to RT (due to recondensation of impurities frozen to the cryostat reservoir) prohibited detailed spectral analysis.

Some of the 400 keV - generated F centres appear to undergo a similar annealing, but the majority are "hard" (7.4.7).

The transient growth of the F band during fast heating is almost certainly due to electron traps emptying into a centres to give a nonequilibrium concentration of F centres which anneals out again. In the case of slow heating the equilibrium is more readily regained and consequently the transient is less marked.

Only two complete spectral records of any significance were obtained from annealing experiments, owing to the difficulty of keeping the specimen surfaces clean. There is some evidence of band 16 enhancement on warming, and a general annealing of bands 6 - 12 at about 240 K. Cooling to NT enhances bands 1 to 5 slightly and raises band 9 above the RT level : however comparison cannot be made with the original NT absorption since the RT opalescence remains on cooling and masks any evidence for F - V recombination.

6.5.1. Transient Bleaching Investigations: interrupted irradiation at NT.

It was mentioned in 3.2.2. that transient bleaching of the F band occurred on reducing beam flux at constant energy. The extreme case of interrupted irradiation was investigated here and a set of results is plotted in Figure 6.5(i) for 200 keV irradiation. Curve (a) shows the effect of re-irradiation after halting irradiation for 60 min. (in darkness) in the early-plateau region of the coloration curve. During the "waiting period" the optical density of the F band fell from 0.213 ($\pm$ 0.001) to 0.201 ($\pm$ 0.001) and on re-irradiation the behaviour was as shown. Curve (b) shows the result of repeating the experiment at a Stage II dose (initial F band density 0.312, falling to 0.305 in 60 min. waiting period). A repetition of the experiment leading to curve (b), using the same specimen, produced the same behaviour.

In order to obtain optical density and dose data to the degree of precision indicated it was necessary to use the large cryostat and Zeiss spectrophotometer : consequently no record was available of the behaviour of other bands.

6.5.2. Analysis of Transient Bleaching Results.

Sanchez and Agullo-Lopez(Phys Stat Sol 29 p 217 (1968)) developed an analytical approach to the transient-bleaching phenomenon just described, and applied it to RT γ- radiolysis of NaCl in the plateau region. Briefly, their argument ran as follows:

Let the sample be irradiated to an F centre concentration f_R, which falls to f_o during the waiting period. Let v be the concentration of vacancies, s the concentration of vacancy sources, and χ the probability of vacancy trapping at thermally activated sinks. Then on re-irradiation:

$$\frac{df}{dt} = \alpha v - \beta f \; ; \; \frac{dv}{dt} = \beta f - \alpha v + \delta s - \chi v$$

where α, β, δ are constants dependent on flux.

Then for $t \geqslant 0$

$$s = s_o + v_o + f_o - v - f$$

which can be used to eliminate v in the previous equations to yield

$$f(t) = C + Be^{\lambda_1 t} + Ae^{\lambda_2 t}$$

where

$$\lambda_1, \lambda_2 = -\tfrac{1}{2}\left\{(\alpha + \beta + \delta + \chi) \pm \left[(\alpha + \beta + \delta + \chi)^2 - 4(\alpha\delta + \beta\delta + \beta\chi)\right]^{\frac{1}{2}}\right\}$$

Then if $b = f_R - f_o$ and is small,

$$f(t) = f_R + (A - b)\, e^{\lambda_1 t} - Ae^{\lambda_2 t}$$

from a consideration of the conditions at t = 0. A is obtained from the first equation at t = 0 :

$$\because f'(0) = \alpha v_o - \beta f_o, \quad A = (\alpha v_o - \beta f_o + \lambda_1 b)/(\lambda_1 - \lambda_2)$$

and the re-irradiation behaviour of f is then composed of a decaying exponential $(A - b)\, e^{\lambda_1 t}$ overtaken by a growing exponential $Ae^{\lambda_2 t}$.

In the present case the transient curves were drawn from near-horizontal portions of the growth curve and there was thus no need to correct for the underlying F band growth. By geometrical approximation the curves were decomposed into pairs of exponentials using Δ instead

of t and optical density for f. Then the figures of Table 6.5.1. were obtained.

The values of b are probably not better than $\pm$ 0.003 in view of the reading resolution of the apparatus, it therefore appears that whilst the bleaching during waiting time is virtually independent of dose the radiation-induced bleaching parameter A is dose dependent, as are the rate constants λ_1, λ_2, which are probably within $\pm$ 15% of their true values.

Sanchez and Agullo-Lopez considered that electronic processes would proceed faster than ionic movements, giving $\chi, \delta \ll (\alpha + \beta)$. This is borne out by the 10 :1 ratio of λ_1 λ_2 here. The rapid re-colouring (compared with normal growth) indicates electron trapping in α centres, and the constant value of b suggests that interruption bleaching may be impurity activated. The increasing value of λ_1 with dose implies increasing β/α, hence increasing mean vacancy formation energy as irradiation proceeds.

The connection with the observations of 3.2.2. has been explained by the experiments of Agullo-Lopez (Phys. Stat Sol 22 p 483 (1967)) and Harrison (J. Chem. Phys. 37 p 388 (1967)) with reference to many other alkali halides : the constancy of b is also noted by these workers.

CHAPTER 7

KINETICS OF RADIOLYSIS OF NaBr AND A NEW MECHANISM FOR F CENTRE GENERATION

7.1.1 A general review of previous approaches to reaction kinetics of F band formation

Since the earliest quantitative work on the subject of radiolytic F band formation with electrons (eg Varley J. Nuclear Energy 1 p 130 (1955)) attention has been given to the possibility of examining the underlying mechanism of F centre production via the mathematical expression which approximates most closely to the observed dependence of F centre concentration on absorbed radiation dose. There are two general lines of approach : either a mechanism is postulated from considerations of the available energy transfer mechanisms and parameters are assigned by experiment to the detailed formula extracted from this mechanism, or a general form of curve is fitted to the experimental results and the relative magnitudes of the resulting parameters are matched against their likely physical interpretations. Typical of the first approach is the work of Wallis and Faraday (Phys Rev 133 p 1360 (1964)) on the results of Sonder and Sibley (Phys Rev 129 p 1578 (1963)) concerning RT irradiation of KCl. The second approach is characterised by the work of Hermann and Pinard (Phys Let 29A p 584 (1969)) on low energy electron irradiation of a number of alkali halides.
These two broad approaches can be distinguished as either involving a model that can be modified to describe the experimental results or a model which has a strong foundation in known physical phenomena and a correspondingly high initial "confidence level".

In this chapter the relevant published material is reviewed to identify the most appropriate mechanism for study. The experimental evidence presented so far will be compared with these mechanisms and some general curve fitting formulae will also be examined. In the light of the other experiments reported in Chapters 4 - 6 it is hoped to identify the mechanisms for the radiolysis of NaBr. Particular attention will be devoted to the fate of the species displaced during radiolysis, since this may be the rate-limiting part of the mechanism. The exact natures of most of the complementary damage products are

still not fully determined in the alkali halides.

7.1.2 The materials investigated in previously published literature

Hughes et al (AERE R5604) have classified NaBr among the "unpopular" alkali halides. The inherent difficulties of handling the material were mentioned in previous chapters, and its hygroscopy and resistance to radiation coloration, have discouraged studies of its coloration by X-rays. Only with the comparatively recent interest in high-energy electron radiolysis have NaBr and the "hard" alkali halides been investigated in any detail. Consequently most of the published work quoted in the present chapter is based on X-ray coloration of the softer halides and any extrapolation of these results to electron coloration effects in NaBr must be viewed with some caution.

7.1.3. Single curve parametrisation methods.

The first approach to kinetic analysis by the majority of workers in the field of F centre production has been to consider the F band growth curve as a single saturating phenomenon.

Sonder and Sibley (op cit) reported the F centre concentration in X-rayed KCl as a function of irradiation time, and also examined the M centre concentration. They explained their results in terms of a dynamic equilibrium between the undisturbed lattice, F centre concentration, and M centre concentration with the interconversion driving energy arising entirely and directly from the incident radiation. Interruption of the X-ray beam was thus held to "freeze" the system in its dynamic, possibly metastable, equilibrium state. Wallis and Faraday (op cit) parametrised these results, assuming no thermal excitation processes to be involved, and adequately approximated the experimental curve of F centre concentration with time in the form

$$n_F = (A/B)(1 - e^{-Bt}) \qquad \ldots\ldots (7.1.3(a))$$

where A and B are constants and n_F is the F centre concentration at time t during constant-beam-condition irradiation. In consequence the possibility of F→M conversion was shown to be an inadequate cause of the saturation of n_F since a Monte Carlo simulation of F and M band growth from random vacancy creation events yielded the wrong growth curves.

Whilst admitting to the possible contribution of the F→M interconversion to the saturation of n_F the authors made it implicit that the dominant cause of

saturation was annihilation of F centres by the incident X-rays.

In neither of the papers quoted was available-site saturation considered as feasible or even as a potential explanation for a single curve n_F behaviour, nor was the fate of the ejected species considered.

7.1.4 The F-complementary centre

Gebhardt (J. Phys Chem Sol. 23 p 1123 (1962)), Itoh, Royce and Smoluchowski (Phys Rev 137 p 1010 (1965)) and Crowe, Fuchs and Wiegand (Phys Rev Let 16 p 1154 (1966)) investigated the nature of the complementary centres produced when α and F centers are radiolytically induced in alkali halides.

Gebhardt and Itoh et al examined the thermal annealing of KBr X-rayed at 4K. Gebhardt's thermal resistivity measurements indicated several distinct stages of annealing and the magnitude of the resistivity was indicative of interstitial anion complements to the α and F centres. Itoh et al reached the same conclusion from a study of the 4-20K annealing of F centres by a process similar to that described here in Chapter 6, and showed that the Frenkel defects (shown by Gebhardt to be vacancy-anion pairs) annealed in four distinct stages indicative of three close and one wide separations between the pairs of annihilating defects. All these experiments involved X-rays of energies less than 100 keV.

Crowe, Fuchs and Wiegand (op cit) demonstrated that irradiation of NaCl with 300 keV X-rays produces pairs of Schottky defects at the concentration required to explain the observed F band. It therefore appears that as the bombarding energy or substrate "hardness" is increased so the fate of the anion ejected from a nascent F centre site increases in importance. Cadet and Gautier (Journal de Physique 28 p 445 (1967)) calculated ab initio the displacement energies required to initiate a replacement cascade in a number of alkali halides and showed that this energy is nearly the same for both ionic species in the "soft" halides, thus explaining the statistical equality of cation and anion Schottky defect concentrations.

7.1.5 Possible anion fates and vacancy creation sequences

The conceivable fates of an anion ejected from its equilibrium site during "intrinsic" production of a vacancy are:

(1) to become an interstitial

(2) to migrate to a macroscopic defect

(3) to become part of a crowdion or aggregate species.

(1) is a fairly obvious fate but the transit time to the interstitial position must be short compared with the anion-vacancy recombination time. Such direct displacement therefore requires a large initial kinetic energy transfer to the anion.

(2) requires a similar threshold energy but the greater potential energy loss to the system reduces the recombination probability.

(3) has been shown to occur, by Känzig and Woodruff (J. Phys Chem Solids 9 p 70 (1958)), at low temperatures where esr measurements showed the H centre to be a $\langle 110 \rangle$ oriented X_2^- ion located at an anion site. Above liquid helium temperatures this centre relaxes into an interstitial atom and a lattice-located anion.

We are now concerned solely with the production of F centres in pure, homogeneous material, and we therefore note that we may need to invoke an extrinsic concept such as an internal surface or a dislocation to explain type (2) loss of an ejected anion. Regarding type (1) loss we note that all the available directions of movement from an anion lattice site in a NaCl-type alkali halide involve interaction with another ion within a short range. Simple channelling can only take place if the channelled species moves first to a $(\frac{1}{4}, \frac{1}{4}, \frac{1}{4})$ position in the unit cell and then travels in $\langle 100 \rangle$ along the line of potential saddles : any deviation will result in defocusing and an increased recombination probability with the vacancy. Thus to remove an anion interstitial far enough from its equilibrium site to account for the thermal stability of F centres, by a direct displacement process, we require to give the anion a considerable kinetic energy. Varley (J. Phys Chem Solids 23 p 985 (1962)) has implicitly set an upper limit of 15 eV to the available energy from the X-rays generally employed since the lifetime of the ejected species decreases rapidly as its kinetic energy increases if the kinetic energy is obtained from ionisation of the lattice anion. Types (2) and (3) fates presuppose co-operative effects if the ejected anion is to reach its destination and if we add a phonon-destroyed co-operative momentum transfer to fate (1)

we can generate a plausible sequence of events leading to the required anion-vacancy separation. We consider a focused replacement sequence in which each anion collides with a neighbour and transfers a portion of its momentum. If the momentum loss to each involved ion is sufficient each ion moves into the position previously occupied by the struck ion and the momentum is propagated along a line by being invested in an anion whose identity changes periodically in space. Eventually momentum dissipated out of the "line of propagation" predominates and an anion does not have enough momentum to change places with the next, so the sequence terminates. Interaction with a phonon at this or an earlier stage will lead to sudden defocusing to a type (1) termination, or the sequence may terminate at an inhomogeneity as a type (2) fate. If the temperature is low enough the sequence may terminate in a charge redistribution between the dynamic crowdion and the vacancy, producing an F and an H centre (type (3) fate) : at a higher temperature we can expect there to be a region in which the focuson has a long effective range and the ejected particle may come close enough to a previously-created isolated vacancy to annihilate by thermal diffusion. If the temperature is raised further the focuson range will decrease until primary-site recapture becomes feasible. Thus the mean incident energy required to produce an F or α centre in pure alkali halides may vary with temperature due to variations in the recombination probability.

Quantitative analyses of momentum transfer in the solid state have been undertaken by a number of workers but whereas a high degree of confidence has been assigned to some analyses of one-component (eg metal) systems, models of the alkali halides have generally been strongly criticised by their creators. Robinson (Phil Mag 12 p 741 (1965) and 17 p 639 (1968)) has identified the foundation of much of this criticism by asserting that the nature of any computed displacement cascade is strongly affected by the exact form of interionic potential employed. Spherical symmetry may be satisfactory for metallic bonding but the isotropy of the alkali halides need not imply an underlying spherical symmetry of interionic field, and even granted this, the radial shape function remains to be chosen. Nevertheless the experimental advantage of the homology of behaviour of the alkali halides may be invoked in a theoretical prediction of the qualitative behaviour of a compound. Chadderton and Torrens

(Can J Phys 46 p 1303(1968)) described the channelling behaviour of knockon ions in KCl and NaCl arising from a number of computer models of these compounds with various interionic potentials. The general conclusion is that it is possible to channel an 80 eV Na^+ knockon in a ⟨112⟩ direction into an interstitial position some four lattice spacings (or more) from the site of the primary event. About half the knockon energy is dissipated in a ⟨110⟩ focuson along the Cl^- ions and the Na^+ moves down a ⟨100⟩ channel. K^+ ions require 0.5 MeV to initiate this event and the difference is entirely due to the radius ratio of the ions concerned in the two compounds, r^+/r^- being less for NaCl. Thus with r^+/r^- even smaller for NaBr we expect that

(a) Na^+ channelling will be enhanced further

(b) there is no a priori case for Br^- channelling, but

(c) there is a stronglikelihood of energetic focuson propagation in the Br^- sublattice.

In view of the work of Crowe et al (see 7.1.4) it may be necessary to invoke (a) in our consideration of F centre production of NaBr.

Before proceeding to a discussion of single-curve parametrisation of F centre concentration / dose curves we should note that if fate (2) is to be significant then cold-working the substrate before irradiation should enhance the F centre formation process. Ballaro, Chiarotti, Cubiotti and Grasso (J Phys Chem Sol. 26 p 729 (1965)) demonstrated that the final saturation concentration of F centres in X-rayed KBr did not vary despite an order-of-magnitude increase in dislocation concentration, although the initial rate of coloration was shown to be highly dependent on the history of the specimen.

7.1.6 Available-site saturation as a limiting process

Pooley (Brit J Appl Phys 17 p 855 (1966)) explained the results of F band growth measurements in proton-irradiated KCl by invoking a limiting concentration set by the "effective volume" associated with an F centre. Creation of a new centre in this volume would lead to annihilation of the existing centre by some process yet to be specified. Using the familiar Langmuir formalism for available-site saturation

Pooley derived a formula of the form

$$n_F = \frac{n_\infty \, t/\tau}{1 + t/\tau} \quad \text{where } \tau = \frac{n_\infty}{(dn_F/dt)_{t=0}} \quad \ldots\ldots \quad (7.1.6(a))$$

t indicates the duration of irradiation and τ is a characteristic time dependent on the temperature and irradiation conditions. n_∞ is the saturation F centre concentration as $t \to \infty$. By varying the restrictions placed on diffusion of the defect species introduced by irradiation, Pooley gave a reasonably satisfactory explanation of the behaviour of n_∞ with temperature (n_∞ falls with increasing temperature) but failed to provide a basis for discussing the behaviour of the "hard" halides for which E_F(1.3.1.) has a maximum near NT (Hughes et al (AERE R5604)).

7.2.1 Single-curve parameters based on dynamic equilibrium and site-saturation mechanisms. Comparison with experiment

If we accept the hypotheses leading to equations 7.1.3(a) and 7.1.6(a), we can compare the coefficients of their expansions, which are dissimilar beyond the second order.

$$\text{"P"} \equiv (t/\tau)(1 + t/\tau)^{-1} = t/\tau - t^2/\tau^2 + t^3/\tau^3 \ldots\ldots \quad (7.2.1(a))$$

$$\text{"W"} \equiv (1 - e^{-at}) = at - a^2t^2/2! + a^3t^3/3! \quad \ldots\ldots \quad (7.2.1(b))$$

with the W coefficients decreasing more rapidly. Consequently n_F saturates with different degrees of sharpness as can be seen from the graph of 7.2.(i). Thus whilst a pair of experimental points may be fitted to either curve any interpolation will in general be higher in P than in W.

An attempt to fit both types of curve to the results obtained for specimen G5 revealed the point just made. Values of optical density D at the F band peak absorption, and dose Δ, were substituted for n_F and Bt in 7.1.3(a) and for n_F and t/τ in 7.1.6(a). D_∞ was estimated by first choosing a value slightly higher than the largest obtained experimentally : all the experimentally generated points were then calculated for small shifts in D_∞. The P formula produced consistently high estimates for the intermediate experimental points, and values from the W formula were consistently low compared with experiment.

7.2.2. An approximate extension of the Pooley formalism to incorporate dose/depth effects.

Pooley's experiments (op cit) employed proton projectiles in order to confine n_F (with a uniform growth rate) in a short, sharply determined range in the substrate. Ritz (Phys. Rev. 133A p 1452 (1964)) used polished thin samples to absorb a known spectrum of the incident electron beam. This approach is inappropriate for NaBr and electron energies $<$1MeV and Ritz' published results are insufficient for kinetic analysis. Other workers have employed X-rays, where the interaction is weak enough to provide a nearly constant dose/depth distribution through the coloured region.

To provide a basis for argument, equation 7.1.6.(a) was taken as describing the behaviour of a lamina, thickness δx, absorbing a flux I at a depth x below the sample surface.

Considering only the first order effects (i.e. assuming P(I) behaves linearly with I) it is a simple matter to calculate $\int_0^p P\,dx$, where p = coloration depth as a function of absorbed dose $\Delta = \int_0^t I\,dx$, where t = specimen thickness.

Defining μ as in 4.3.3. and writing

$$I = I_o e^{-\mu x} \qquad \ldots\ldots 7.2.2.(a)$$

the equation

$$D = \frac{D_\infty}{\mu p} \ln \left\{ \frac{1 + \eta\Delta\mu}{1 + \eta\Delta\mu e^{-\mu p}} \right\} \qquad \ldots\ldots 7.2.2.(b)$$

was developed.

η is an arbitrary "efficiency" parameter.

Without doubt this formula contains many serious defects, mainly due to the implicitly non-linear behaviour of P(I) with I but it does represent a first-order correction for the "exhausted entity" (in anticipation of 7.3.2.) or "forbidden volume" saturation kinetics and will be referred to from time to time.

The effectiveness of the first-order correction was demonstrated by taking μ and p from the tables and fitting η and D_∞ to the data from the specimen G5. A curve through the "best fit" points was found always to lie between the curves predicted by 7.1.3(a) and 7.1.6(a) for the same D_∞, thus 7.2.2(b) was held to represent a better approximation to the experimental case of electron irradiation of a thick sample than either "P" or "W". In practice the fit was strongly dependent on D_∞ and thus the "best fit" values of D_∞ from 7.2.2(b) were retained for later comparison with Pooley's theory.

7.2.3 The spatial distribution of colour centres predicted by the foregoing argument

The family of curves

$$N = N_\infty A/(e^x + A) \qquad \ldots\ldots \quad 7.2.3(a)$$

has the same behaviour with respect to x and A as the x-dependent form of 7.2.2(b) has to x and Δ. In consequence we can expect that the family of curves of N/N_∞ vs. x will have some resemblance to microdensitometer traces such as 4.3.(iii). Fig 7.2.(ii) shows a family of curves of this form. As A increases so the exponentially decaying curve goes through a linear region into a convex form which becomes more rectangular as $A \rightarrow \infty$. When x is large N is small for any A. At the surface (x = 0), N tends asymptotically towards N_∞. This is the behaviour expected of a set of infinitesimal laminae which move towards saturation at a rate depending upon their separations from the origin in the manner of 7.2.2(a) and the approach was substantiated by several observations of "intermediate" microdensitometer plots conforming to each of the general forms of 7.2.(ii).

The change in the rate of growth of the area under the curve as the curve goes through the linear region was held to justify the assertion of Fig 3.6.(i).

7.2.4 The Herrmann-Pinard curve

Herrmann and Pinard (Phys Let 29A p 584 (1969)) observed saturation in the F band growth curves for KI, KCl, KBr and NaCl during irradiation

with 15 keV electrons. They fitted their results to the curve

$$N = N_\infty \left(1 - 1/\sqrt{(1 + bt)}\right)$$

with b as the fitting parameter. Substituting D, D_∞, and Δ for N, N_∞ and t, the results of the present work were fitted to this "H" curve.

The fitting program employed made use of the "H" equation at two data points (D_1, Δ_1) and (D_2, Δ_2) where $\Delta_2 > \Delta_1$. Then a trial value of D_∞ led to two estimates b_1, b_2 of b. If D_∞ was chosen too low then $b_1 < b_2$ and conversely for D_∞ too high $b_2 < b_1$. Thus by beginning with a trial D_∞ just larger than the largest D obtained experimentally it was a trivial exercise to extract an optimum D_∞ and b to fit a pair of data points, using a digital computer. The program also interpolated a point (D_3, Δ_3) with $\Delta_1 < \Delta_3 < \Delta_2$ for comparison with the interpolated value at Δ_3 on the experimental curves. A typical run, on the results of specimen G73, yielded values as follows:

Input Δ_1 = 1mC Δ_2 = 10mC. Exit values of b_1, b_2; 0.692, 0.688

Exit value D_∞ = 0.80 D_3(3mC) = 0.344 D_3(5mC) = 0.422

Experimentally D(3mC) = 0.342 D(5mC) = 0.422.

In no case, for sample G73, did the deviation of "H" from the experimental point exceed $\pm 5\%$; since the experimental values of D are known to have errors as large as $\pm 2\%$ it is worth considering the reason for the improved fit of the empirical "H" curve over "P" and "W". Expanding in terms of θ, a linear multiple of D, we have

$$D_H = D_\infty \theta_H \left(1 - \frac{3\theta_H}{2} + \frac{5\theta_H^2}{4} - \frac{7\theta_H^3}{8} + \ldots\right)$$

$$D_P = D_\infty \theta_P \left(1 - \theta_P + \theta_P^2 - \theta_P^3 \ldots\right)$$

$$\text{and } D_W = D_\infty \theta_W \left(1 - \frac{\theta_W}{2} + \frac{\theta_W^2}{6} - \frac{\theta_W^3}{24} \ldots\right)$$

so for small n the coefficient ${}^nC$ of θ^n obeys

$${}^nC_W < {}^nC_P < {}^nC_H$$

and for larger n

$${}^nC_W < {}^nC_P > {}^nC_H$$

ie. the Herrmann-Pinard formulation implies a steeper initial rise than

the other curves, but a saturating region intermediate between them.

Comparison with 7.2.2(b) is possible by writing

$$d = e^{-\mu p} \text{ and } \theta = \eta \Delta \mu$$

$$\text{then} \quad D = \frac{D_\infty}{\mu p} \theta \left((1-d) - \theta \left(1-\frac{d^2}{2}\right) + \theta^2 \left(1-\frac{d^3}{3}\right) - \ldots \right)$$

and again the arbitrary coefficient ^nC can be chosen to have the same properties as ^nC_H compared with ^nC_W and ^nC_P. Thus the improved fit of the Herrmann-Pinard curve to the experimental results can arise from its similarity to the depth/dose corrected Pooley equation, given correct choice of the relevant parameters, although the "H" parameters were not broken down into physically meaningful quantities in the original paper.

7.2.5 Comparison of the Herrmann-Pinard curve with 7.2.2(b)

D/Δ curves for thirty specimens of NaBr for which D(5 mC) was known from experiment were compared with the calculated optimal fit curves using both the Herrmann-Pinard equation and equation 7.2.2(b), with a view to the goodness-of-fit of D(5mC). By careful choice of b, the discrepancy between D_H(5mC) and experiment was in no case more than $\pm$ 5%, and choice of p in 7.2.2(b) gave a marginal improvement. Reducing the error in D(5mC) by choice of p increased the intersample variance of p above $\pm$ 5%.

The graphs 7.2.(iii) and 7.2.(iv) show the results of using the "H" formula to interpolate between doses of 1-5 mC and 1-14 mC respectively. As can be seen if the upper fitted dose is low the interpolation consistently overestimates D and if the upper fitted dose is high there is a consistent underestimate, despite the virtually identical irradiation conditions employed. With a fixed value of p similar objections hold for the fitting of formula 7.2.2(b).

7.3.1 The need for a two-curve model

In view of the remarks of the last paragraph we need to explain the consistent discrepancies between the theory so far considered and the experimental evidence. In Chapter 3 mention was made of the plateau in the D/Δ curve for F band growth. Differentiation of any of the curve-fitting equations so far given does not lead to $dD/d\Delta = 0$ except

for $\Delta \rightarrow \infty$ and indeed $d^2D/d\Delta^2$ is always negative, thus there cannot be a sigmoid inflection on any of these curves. We therefore need to investigate, ab initio, the possibility of saturation occurring in two distinct mechanisms with separately defined kinetics. This approach then includes, as special cases, the possibility of a single complex mechanism with a sigmoid development curve and the possibility of two nominally similar processes occurring but with differently-defined saturation levels.

7.3.2 The work of Mitchell, Wiegand and Smoluchowski : two curve parametrisation

Etzel and Allard (Phys Rev Let 2 p 452 (1959)) published one of the earliest investigations of the plateau region, in NaCl X-irradiated at RT. They found that the "first stage" duration and coloration intensity were directly proportional to the OH^- concentration and concluded that "the entity responsible for the enhanced initial coloration rate in synthetic (ie OH^- - bearing) crystals is no longer effective for F centre production after prolonged irradiation". For low doses they showed that $\Delta/[F]$ vs Δ was a straight line, indicating

$$D = \frac{\Delta}{a + b\Delta} \qquad \ldots\ldots (7.3.2(a))$$

which was not true for natural (OH^- free) material.

The authors noted the similarity of Etzel's report (Phys Rev 87 p 906 (1952)) demonstrating that $[F] \propto [Ca^{2+}]$ after short X-irradiation of Ca-doped NaCl at RT. The D/Δ behaviour of 7.3.2(a) was also found, and this was explained by Seitz (Rev Mod Phys 26 p 63 (1954)) and will be discussed later.

Mitchell, Wiegand and Smoluchowski (Phys Rev 117 p 442 (1960)) considered the description of the D/Δ curve obtained by Etzel and Allard after the plateau region as well as in Stage I. Considering KCl they explained the results in terms of "initial" and "generated" vacancies. The "initial" vacancies were supposed to be released from a source (given in a later paper, Phys Rev 121 p 484 (1961) as thermally activated clusters) according to a law of the form

$$\frac{df_i}{dt} = b(n - f_i) \qquad \ldots\ldots (7.3.2(b))$$

where n is the concentration of initial vacancies in virgin material and b is the electron capture rate constant for converting these vacancies to F centres. Similarly the "generated" centres are formed as

$$\frac{dfg}{dt} = c(at - f_g) \qquad \ldots\ldots (7.3.2(c))$$

with a capture rate constant c applied to vacancies generated at a rate a by the radiation.

Then by combining and integrating 7.3.2(b) and (c);

$$f = f_i + f_g = n(1-e^{-bt}) + at - {}^{a}/_{c}\,(1-e^{-ct}) \ldots\ldots (7.3.2(d))$$

this expression has the required inflection but does not saturate in Stage II.

The essential distinction between 7.3.2(c) and the approach of Etzel and Allard is between the earlier assumption of an exhaustible entity limiting the Stage I concentration and the assertion of Mitchell et al that the capture probability of an existing vacancy is the rate-limiting quantity. The original paper contains the implicit criticism of this approach, for widely different values are assigned to b and c. In the absence of data suggesting a shift of the F band peak absorption with dose we cannot regard the environment of a "generated" F centre as being widely different from that of an "initial" centre, as far as concerns the trapped electron, so there is no a priori justification for an order of magnitude difference between b and c. The UV work of Rolfe (Phys Rev Let 1 p 56 (1958)) and the soft X-ray work of Etzel and Patterson (Phys Rev 112 p 1112 (1958)) show F centre saturation concentrations of the same order as (OH^-) in KCl, KBr and NaCl : thus the original explanation of Etzel and Allard seems most attractive. We note the similarity of 7.3.2(a) and the Pooley equation 7.1.6(a) and the similarity of their theoretical foundations.

Although neither Etzel and Allard nor Mitchell et al observed or attempted to explain a Stage II saturation, all the more recent work at high absorbed doses of ionising radiation confirms the observations of Chapter 3 in this respect and therefore demands an explanation. In this respect the assertion of 7.3.2(c) is insufficient since the last two terms of 7.3.2(d) are such that for any $t=t_1$ we can choose a later time $t_2 > t_1$ and

$$at_2 - {}^{a}/_{c}\,(1-e^{-ct_2}) > at_1 - {}^{a}/_{c}\,(1-e^{-ct_1})$$

so there is no inherent saturation in 7.3.2(d) if a and c are positive, which is implicit in their definition.

7.3.3 The two-curve approach reappraised with particular respect to NaBr Stage I

From the work of Etzel and Allard, Rolfe and others quoted above, we see that the behaviour of X-ray coloration in Stage I is generally described by 7.3.2(a) or the equivalent 7.1.6(a). The discussion of 7.2.2 shows this basic approach to be satisfactory also for very strongly interacting projectiles, since protons (Pooley) and X-rays (Etzel and Allard) give rise to similar growth curves. It is therefore reasonable to examine the application of the medium-range projectile modification to equation 7.3.2. (a), (i.e. 7.2.2(b)) to Stage I and to seek an alternative explanation for the behaviour of Stage II.

Differentiating 7.2.2(b) we have

$$dD/d\Delta = \frac{D_\infty}{\mu p}\left\{\frac{\eta\mu}{1-\eta\Delta\mu} - \frac{\eta\mu e^{-\mu p}}{1+\eta\Delta\mu}\right\}$$

so as $\Delta \to 0$ the initial slope is

$$dD/d\Delta = \frac{D_\infty \eta}{p}\,(1-e^{-\mu p}) \qquad \ldots\ldots (7.3.3(a))$$

Now if D_∞ is taken as the plateau height, μ and p being known, η can be determined from the initial slope of the D vs Δ curve. We expect D_∞ to reflect the impurity concentration and η to be dependent to some extent on the nature of these impurities. Considering the Certificate of Analysis (3.1.2) we see that the total concentrations of impurities with valency $>$ +1 in Harshaw and BDH specimens were 40 and 130 ppm respectively, or 10 and 30 ppm discounting Si (which will almost certainly be present as atomic Si or fully combined SiO_2, and not as an ionised substitutional species). Total spectroscopic impurity was 320 and 210 ppm respectively : water contents are "loss on heating" and are probably entirely due to moisture accumulated in transit to the analytical depot.

Comparing the analyses with the plateau concentrations of F centres from 3.2.2, and ignoring the differences between different irradiation energies, we must explain respective plateau concentrations of about

1.6×10^{-4} and 2.2×10^{-4} F centres. Whilst Rabin and Klick (Phys Rev 117 p 1005 (1960)) and others, have shown Ca^{2+} to enhance F centre formation in NaCl at RT its effect is far less marked at NT, and we do not therefore expect a priori that there will be a great divergence of behaviour attributable to divalent impurity levels. On the other hand the K^+ concentration is about three times as high in Harshaw material as in BDH. Saidoh and Itoh (J. Phys. Soc. Japan 29 p156 (1970)) have demonstrated that the presence of monovalent alkali impurities can stabilise intermediate complexes in a radiation damage process and thus may effectively reduce the value of E_F. We can expect this effect to be particularly significant where a large impurity ion e.g. K^+, is present in a "hard" alkali halide, as here, and this will probably tend to offset the divalent-impurity effect between samples from the two sources.

Although we can thus approximate to an explanation of the F centre plateau concentrations, the anomaly of Table 3.7.4 must be investigated. From the previous paragraph we may deduce that the effect of divalent-impurity enhancement is increased with increasing irradiation energy : this presupposes:

(a) that the final saturation concentration of F centres is an intrinsic property of the pure host matrix, and

(b) the plateau concentration arises from the exhaustion of enhancing centres.

(b) has been justified earlier in this chapter and (a) will be dealt with later.

7.3.4 The Hayes-Nichols centre : stabilisation of focuson termination

Fig 7.3.(i) depicts a V-type centre stabilised by the presence of a divalent cation, in a monovalent fcc matrix. Such a centre was first described by Hayes and Nichols (Phys Rev 117 p 993 (1960)) to explain their observations of V-type bands formed during low temperature X-irradation of a number of alkali halides. The X-ray energy was not specified but was presumably $<$100 keV and the authors could not produce the centres in NaBr.

In Chapter 6 two absorption bands (7 & 9) were reported formed in Stage I coloration of Harshaw material by 400 keV irradiation, but not

by 200 keV electrons, and annealing ~ -30°C. We can examine the possibility that these are due tc similar centres and that the centres play a part in Stage I coloration by reducing E_F in a non-regenerative, i.e. "exhaustible" process.

If we suppose that the production of an F centre requires anion displacement via a focuson sequence a centre such as this can stabilise the intermediate of Fig. 7.3. (ii) (A,B or C $=M^{2+}$) which is an adequate endpoint for a type (3) fate (7.1.5). This mechanism requires both a significant impurity concentration and enough primary event energy to initiate a replacement sequence. The difference between the 200 keV and 400 keV-irradiated BDH NaBr F centre concentration ratios reported here can thus be ascribed to the energy-dependence of this stabilisation. As $[Ca^{2+}]$ is low in the Harshaw material the effect will only be marginal in any case; but when $[Ca^{2+}]$ is commensurate with [F plat], as in the BDH material, it becomes important to know whether or not this stabilisation has been effected.

7.3.5. Application of impurity-stabilised centres to Stage I coloration.

The applicability of equation 7.3.3(a) to Stage I coloration was tested by inserting the values obtained from analysis of all the available coloration/dose curves for NaBr (NT) with D_{plat} substituted for D_∞ to produce Table 7.3.1. Values of μ and p are obtained from Tables 4.3.1 and 4.3.2 to yield Table 7.3.2.

The subjective assessment employed in determining plateau heights (D_{plat}) and initial $dD/d\Delta$ throws doubt on the standard error for 400 keV Harshaw material, and since preparation conditions were substantially improved during the course of the experiments the subjective reliability of η values in Table 7.3.2 increases from left to right. With this in mind we can proceed with the gross assumption that η depends only on the energy of the incident radiation and not on the source of material.

In deriving equation 7.2.2(b), η was not assumed dependent upon D_∞ Thus variation of D_∞ between samples does not imply variation of η, and we can separate the variables so that η is an intrinsic property of the host matrix and bombarding radiation whilst $D_{plateau}$ is a function of the number of fates available to the primary-event daughter

species in Stage I : so D_{plat} may be energy- and material-source-dependent. A complete explanation of the saturating behaviour of the F band growth curve is therefore possible if D_{int} is a value associated with saturation in the pure host matrix in Stage II and we write

$$D_{sat} = D_{int} + D_{plat} .$$

This implies that only D_{int} is energy-dependent : the ratio D_{sat}/D_{plat} will then nave an energy dependence which anti-correlates with that of D_{plat} and the anomaly of Table 3.7.4 is fully explained in terms of an impurity - stabilised centre associated with Ca^{2+} (or less probably Si) in BDH NaBr. Doubtless several similar centres could be invoked in this explanation, but the Hayes-Nichols centre is the simplest available entity that entirely explains the anomaly and suits the argument of Sec. 7.3.4. Hayes and Nichols themselves developed the argument demonstrating the high creation energy of the centre in NaBr and in consequence we may place the threshold beam energy for creation at between 200 and 400 keV. The constancy of D_{sat}/D_{plat} for Harshaw NaBr indicates that any K^+-enhancement is energy-independent in the range studied.

Ignoring Ca^{2+} concentration for 200 keV irradiation gives a concentration ratio of all other polyvalent impurities ($I_{Harshaw}/I_{BDH}$) of ~0.8, the same as the "F plat" ratio given in Table 3.7.3. It would therefore appear that the plateau concentrations of Table 3.7.3 can be explained by each polyvalent ion enhancing the formation of about ten F centres : if, however, we allow for an "intrinsic" process background and take note of the large K^+ concentrations, an enhancement factor of about three F centres/polyvalent cation is possible.

We therefore conclude

(a) Coloration, up to D_{plat}, can be entirely ascribed to impurity enhancement.

(b) there is strong evidence for a threshold energy requirement in Stage I coloration via a Hayes-Nichols (or similar) centre termination to a focussed replacement sequence

(c) there is some degree of numerical correlation between the impurity cation concentration and the plateau F centre concentration. The absence of a detectable OH^- or U band in

the absorption spectra of well-prepared specimens prior to irradiation rules out the possibility of ascribing Stage I coloration to aqueous impurity.

7.4.1. Stage II coloration : the need for an intrinsic coloration mode and some possible mechanisms.

We have seen that Stage I coloration can be adequately explained in terms of impurity species assisting the creation of F centres and reducing the apparent creation energy E_F.
The saturation of Stage I coloration , at a density consistent with the impurity concentration, indicates that such impurity enhancement is exhausted by sufficient irradiation at NT. It is therefore necessary to consider what means are available for the continued and increasing rate of F centre production in the region beyond the plateau and for the final saturation as $\Delta \rightarrow \infty$.

Apart from colour centre generation, irradiation of an alkali halide has a mechanical effect, increasing both sample volume and lattice parameter. Balser, Piesl and Waidelich (Phys. Stat. Sol. 28 p207 (1968)) found that X-irradiation of NaCl at RT led to
(a) a single saturating curve for mean lattice parameter vs dose
(b) an inflected curve, with a plateau, for sample volume vs dose.

Now any ion displacement process can alter a specimen volume since processes occuring near the surface can lead to ion ejection and surface growth (4.5.1.) but only an event giving rise to an uncompensated local strain can affect the mean lattice parameter. Thus an impurity-activated or an intrinsic process can alter sample volume, but the former, involving regions of the matrix strained before the event, will have far less effect on the sample lattice parameter. We can therefore suppose that an intrinsic ion-displacement process leads to lattice parameter distortion and occurs continuously throughout irradiation.

Whatever process is selected as a mechanism for the intrinsic mode of coloration, it must imply a number of observed features of the coloration process, for example :-
(a) a plateau length correlating with bombardment energy

(b) a value of E_F corresponding with that found by Rabin and Klick at 4K (where impurities are ineffective).

(c) the differential thermal stability of F centres produced by different radiation qualities.

(d) the phenomenon of transient bleaching.

(e) the decreasing intrinsic luminescence during irradiation.

7.4.2. Stage II coloration. General kinetic theory.

We have seen that the theoretical approach adopted by Mitchell et al does not lead to a saturation of the second stage of F band growth, and that the overall saturation predicted by the methods of Pooley, and Herrmann and Pinard, does not arise from a theory consistent with an intermediate inflection. A crude calculation demonstrates the inability of the Pooley theory to explain the results obtained here. For a typical penetration depth $\sim$ 200μm and a saturation optical density of 0.25 estimated, say, from the Herrmann-Pinard relationship or equation 7.2.2.(b), we obtain a concentration of $\sim 10^{17}$ F centres/cm^3 i.e. an "effective radius" of $\sim$40 lattice parameters is associated with each F centre. For this concentration to impede further coloration, either by virtue of lattice distortion or by the cascade product of a new centre annihilating an existing centre, places unreasonable demands on the long-range interactions of the matrix on the one hand and focuson length on the other.

Pooley (Proc. Phys. Soc. 89 p723 (1966)) presented a detailed investigation of the kinetics of coloration in the case where saturation results from the inhibition of F centre formation by electron-trapping impurities. This work was followed by a series of experiments (Journal of Physics C 1 p323 (1968)) involving pulsed and interrupted irradiation of KCl, both "pure" and doped with Pb.

Whilst the present work did not involve the large range of beam intensities (10^{-4} to 40μA/cm^2) employed by Pooley, it is nevertheless apparent that the intensity dependence of $dn_F/d\Delta$ found by Pooley was not exhibited by the NaBr samples used here. Furthermore, the reported decrease of F centre production rate with increasing

Pb concentration is contrary to the present experience where (at least at 400keV beam energy) the high Ca^{2+} concentration in B. D. H. material was consistent with a high final saturation value of $[F]$ and a generally more rapid coloration rate.

Pooley's later paper must obviously be viewed in the light of the transient bleaching experiments reported here (Section 6. 5. 1.). There is no explicit evidence for, or prediction of, a change in the transient bleaching parameters with increasing dose whereas in the present case the Stage II phenomenon is markedly different from the Stage I.

Consequently it seems possible that although impurity-inhibition of F centre production may account for the saturation of either first- or second-stage coloration in the present instance, it cannot be held responsible for both. Since the impurity concentrations involved here have already been shown barely sufficient to account for Stage I formation, it is unlikely that impurity-inhibition is significant in Stage II saturation and we must therefore consider other means by which n_F may be restricted at high Δ.

It is therefore necessary to return to the possibility that the incident radiation is responsible for both the creation and the destruction of F centres. This concept was implicit in the discussions of Sonder and Sibley quoted earlier, and of a number of other workers. One course of inquiry is to examine the possibility of the incident radiation re-ionising the F centres. Krumhansl and Schwartz(Phys. Rev. 89 p1154 (1953)) and Simpson(Proc. Roy. Soc. A 197 p269 (1949)) have shown the ionisation energy of F centres to be between 3 and 5 eV from the ground state.

The growth curve will saturate when the probability of creating a new F centre is the same as that of ionising or otherwise destroying an existing one. We can now examine the equilibrium in terms of the reaction rates, for a homogeneous rate of deposition of energy dE/dt throughout material containing initially N occupied anion sites. We assume the probability of an anion vacancy trapping an electron to be very high in the absence of radiation. Then if E_f is the formation energy

of an F centre and E_i the ionisation energy, formation proceeds at a rate

$$\frac{dn_f}{dt} = \frac{A}{E_f} \cdot \frac{dE}{dt} \cdot \frac{N-n}{N} \qquad \ldots\ldots (a)$$

and ionisation produces the reverse reaction for which

$$\frac{dn_i}{dt} = \frac{B}{E_i} \cdot \frac{dE}{dt} \cdot \frac{n}{N} \qquad \ldots\ldots (b)$$

where A and B are constant. For equilibrium,

$$\frac{dn_i}{dt} = \frac{dn_f}{dt}$$

$$\therefore \quad A\frac{(N-n)}{NE_f} = \frac{Bn}{NE_i}$$

extrapolating $t \rightarrow \infty$ we know $n \ll N$ in practice, so

$$A/B \simeq n_\infty E_f / NE_i \qquad \ldots\ldots (c)$$

Since $(N-n)/N \simeq 1$ we can write (a) as

$$\frac{dn_f}{dt} = k_2 \text{ essentially independent of } n$$

and (b) as

$$\frac{dn_i}{dt} = k_1 n$$

so at any time $\frac{dn}{dt} + k_1 n = k_2$

so $n = n_\infty (1 - e^{-k_1 t})$ using approximation (c).

Transforming to the parameter of absorbed energy, Δ', we have

$$n = \frac{N.E_i A}{E_f B} \left\{1 - \exp\left(\frac{-B\Delta'}{NE_i}\right)\right\}$$

essentially independent of the incident flux. We know, or can estimate, E_i and E_f for any process, and A, B are projectile interaction probabilities for these processes. E_i need not be associated specifically with ionisation and we are free to choose another process during the later discussion.

7.4.3. A review of previously postulated intrinsic F centre creation processes, referred to NaBr, and the foundation of a new mechanism

Referring to Table 3.6.4 we see that as $\Delta \rightarrow \infty$ a typical value of n/N at NT for NaBr will be $\sim 4 \times 10^{-4}$. We narrow the field of likely mechanisms by considering that about 25 eV must be provided to create

an anion vacancy and about 5 eV to ionise an F centre. Thus if our kinetic argument holds we need $A/B \sim 10^{-3}$.

Varley (J Phys Chem Sol. 23 p 985 (1962)) showed how the creation energy could arise from multiple ionisation of an anion, and demonstrated that the ionisation cross-section of an anion decreases by a factor of about ten for each electron removed. Thus at first glance a 3- or 4- fold ionisation would account for the observed A/B ratio but would not provide the necessary kinetic energy. To approach the threshold of 25 eV, or even 15 eV, would give rise to a drastic reduction of cross-section to give $A/B < 10^{-5}$ which is unreasonable.

Howard, Vosko and Smoluchowski (Phys Rev 122 p 1406 (1961)) proposed the "de-excitation" collision process between a Br^+ (formed by Auger double ionisation) and a lattice Br^- neighbour ion to give the required kinetic energy. Whereas Sharma and Smoluchowski (Bull.Am. Phys.Soc.7 p 178 (1962)) showed the applicability of this theory to KCl, the same authors (Phys Rev 137 p 259 (1965)) and Ritz (Proc Int Symp Colour Centres, Stuttgart (1962)) show that it is inappropriate to KBr and "hard" bromides generally, since the resultant Br^o carries a maximum kinetic energy of ~4 eV.

Similarly Klick's adjacent-pair-ionisation theory (Phys Rev 120 p 760 (1960)) has been shown insufficient by Howard et al (op cit) on account of the short lifetime of two Cl^o atoms in an ionic environment : for bromides the situation is even less favourable.

Turning to the possibility of direct displacement of anions, we consider the most favourable case of 460 keV electrons interacting with Br^- ions. The maximum recoil energy is Tm = 18.3 eV. If we allow the displacement barrier energy E_d to be as little as 15 eV we have a displacement cross-section

$$\sigma_d = 1.526 \times 10^{-22} \left[\left(\frac{Tm}{Ed} - 1\right) - 0.686 \ln\frac{Tm}{Ed} + 1.504 \left\{ 2 \left[\left(\frac{Tm}{Ed}\right)^{\frac{1}{2}} - 1 \right] - \ln\frac{Tm}{Ed} \right\} \right] \text{cm}^2$$

(McKinley and Feshbach, Phys Rev 74 p 1759 (1948))

whence σ_d = 15 barn, so a dose of 10^{16} electrons (1.6 millicoulomb) per cm^2 will produce a maximum concentration of 1.5×10^{-7} displacements. This figure is still too small to be considered important in the present situation and Tm ≃ 7 eV for 230 keV electrons precludes any direct-

displacement contribution from the lower energy irradiations although Stage II coloration has been noted here for 100 keV bombardment.

Bearing in mind the discussion of 7.1.5 we consider the probability of Na^+ ions being displaced directly by the incoming radiation. Tm for Na^+ rises from 10 eV with 100 keV electron projectiles to 70 eV for 500 keV electrons. In the light of the work of Chadderton and Torrens (see 7.1.5) we find it quite probable that Na^+ ions can be ejected into interstitial sites by all the qualities of radiation used here, since $T_m = 3E_d$ gives $\sim 3 \times 10^{-5}$ displacements for 10^{16} incident electrons. The work of Mapother, Crookes and Maurer (J. Chem. Phys. 18 p231 (1950)) demonstrated that the thermal diffusion coefficient of Na^+ in NaBr is considerably lower than for the "soft" halides and we can therefore suppose that the ejected ion will not diffuse rapidly back to the original site. Now we consider the reaction

$$Br^- + \varepsilon^- + h^+ \rightarrow Br^- \text{ interstitial} + \text{F centre} + \text{hole trapped elsewhere.}$$

Electron-hole pairs are produced by ionising radiation and obviously the presence of a hole-trap will reduce the reverse (recombination) rate. A convenient hole-trap would be a cation vacancy, whilst the proximity of Na^+ interstititals could stabilise the nascent F centre. Thus dn_F/dt can be increased, whatever the F centre production mechanism, by allowing cation interstitials to be formed before the F centres and we have seen that the cation interstitial creation probability is higher than that of a direct-displacement F centre. For future discussion this phenomenon will be termed "intrinsic-enhancement" by analogy with the impurity-enhancement processes described earlier.

7.4.4. Analysis of a possible mechanism having detailed consistency with the experimental results.

In terms of the argument of 7.4.2. we need to explain $n/N \sim 5 \times 10^{-4}$ as $\Delta \rightarrow \infty$. We require ((b) 7.4.1) that $E_f/A \simeq 9 \times 10^5$ eV, whence B = 0.011 if E_i = 5eV. Approximating with a linear range/energy relationship, this leads to a bleaching exponent of ~ 0.18 mC^{-1} in the treatment of 7.4.2 which is, within bounds of reasonable error, the same as λ_1 (Stage II) deduced in 6.5.2 for the transient bleaching phenomenon. However, we still need to account for the difference between Stage I and Stage II transient bleaching rates.

We can construct a Stage II formation mechanism strongly analogous

to that proposed for impurity-enhancement, in terms of the possible stabilised intermediate centre of Fig. 7. 3. (ii). This could arise from a transient situation in which a focuson has been propagated along the line-of-contact of the anions. Normally the triple-nucleus species would relax very quickly and depending on the momentum involved in its formation would either propagate or dissipate the focuson but the cation vacancy (due either to one of A, B, C being divalent, or to previous cation ejection) allows the intermediate to relax in other modes and consequently prolongs its lifetime. Suppose that one of the terminal nuclei of the crowdion traps one of the electrons and relaxes to its normal lattice site. The remaining pair of ions constitute a metastable H centre in a highly anisotropic environment. There is a strong electric field between the cation vacancy and the effective charge of the perfect lattice (or the double charge of a divalent impurity), mitigated somewhat by polarisation of the re-formed negative ion. In this environment there will be a degree of Jahn - Teller splitting of the lower energy levels of the H centre and a distortion of the transaxial symmetry of the Σ states. Thus the $^1\Pi_u$ mixing required in 5. 4. 1 to explain the UV cathodoluminescence is promoted by the necessary condition for the formation of the species, while the distortion-sensitive $^1\Sigma_u^+ \rightarrow {}^1\Sigma_g^+$ transition is hindered by the anisotropic field. Unlike the V_k centre discussed by Kabler and Patterson (see 5. 4. 1) we are now dealing with a pseudo-H centre whose lifetime <u>must</u> be very short since it is not in thermal equilibrium. Decay of this centre may lead to a halogen interstitial (which may trap an electron) but in any case a halide vacancy remains in the line of the initial focuson and may trap an electron to become an F centre.

Above NT we can expect phonon interaction to assist the decomposition of the pseudo-H centre (see Pooley (Proc. Phys. Soc. <u>87</u> p245 (1966))) and the "extra" halide can diffuse away from the site which can relax into the state exemplified by the first part of 7. 3. (i): this can once again function as a low energy termination to a replacement sequence.

Thus at RT (1) the saturation density of F centres will be greater than, though commensurate with, D_{sat}(NT); (2) impurity effects will be more evident; (3) impurity effects will mask the inception of Stage II.

Now the field anisotropy associated with the Stage II formation process is weaker than for Stage I (impurity assisted) so on re-irradiation the probability of an ionised Stage I centre being re-formed is greater than for Stage II, giving rise to the apparent discrepancy in λ_1.

First we note from 5.2.4 that UV cathodoluminescence falls off rapidly during RT irradiation. We therefore conclude that the intrinsic process cannot stabilise the pseudo-H centre at RT and that the impurity-activated stabilisation only is effective. This observation is in agreement with that of Kăntzig and Woodruff (J. Phys. Chem. Sol. 9 p70 (1959)) concerning the thermal dissociation of H centres. Varley (J. Phys. Chem. Sol. 23 p985 (1962)) presented a theoretical argument involving trapping of halogen atoms at positive vacancies. This strengthens the case presented above concerning the pseudo-H centre decomposition and the temperature dependence of the coloration rate, In consequence the equilibrium state of a sample irradiated at low temperatures will contain a higher proportion of halogen atoms so trapped and will thus be more readily susceptible to F band bleaching (since the trap is shallow) than the equilibrium system of samples irradiated at NT.

Our final analysis concerns the thermal stability of centres produced by different radiation qualities. The probability of a very long replacement sequence giving rise to a widely separated α-interstitial pair will be small unless the beam energy is high, but if the temperature is subsequently raised the probability of recombination will be less than for a short range replacement. In the event of an F centre being thermally ionised or destroyed by thermally activated vacancy-interstitial ion recombination the "stable" α centre is available to trap the released electron and n_F remains constant. Realising that the mean separation range will rise rapidly with incident energy we can offer support to Varley's conjecture (op cit) that V_3 centres (halogen atoms located in cation vacancies) are formed at large separations from the associated F centres, giving rise to "hard" (Varley's terminology) F-V_3 pairs at high incident energies.

7.4.5. Kinetic implications of generalised first-order intrinsic enhancement processes.

Without necessarily involving the detailed mechanism just proposed, the general kinetics implicit in an intrinsic-enhancement mechanism 7.4.3 will be discussed. Let C_p, C_n denote positive- and negative-ion vacancy concentrations. Since these have maximum values of unity $\frac{dC_p}{d\Delta} = kp(1 - C_p)$ (where kp is the formation rate constant of positive ion vacancy-interstitial pairs appropriate to a given set of irradiation conditions) since cation defect pairs are assumed to be the first product of irradiation. Then $C_p = 1 - e^{-kp}$ We assume that the cation defect pairs have a first-order effect on the rate of production of anion defects, as indicated by the process mentioned in 7.4.3.

so $$\frac{dC_n}{d\Delta} = C_p k_n (1 - C_n) \qquad \ldots\ldots \quad 7.4.5\ (a)$$

whence $-\log(1 - C_n) = k_n\Delta + \frac{k_n}{k_p} \cdot e^{-k_p\Delta} + D.$

D is the constant of integration. Consideration of initial conditions at $\Delta = 0$ gives $D = -k_n/k_p$

$$\therefore \quad C_n = 1 - e^{-k_n\Delta} \exp\left\{\frac{k_n}{k_p}(1 - e^{-k_p\Delta})\right\}.$$

The dimensions of k_n and k_p are $[\Delta]^{-1}$ so an approximate value of k_n should be obtainable from the slope of the coloration growth curve at an appropriate point in the "intrinsic" region. As we have ascribed Stage I coloration to impurity enhancement the most useful area will be just after the plateau.

Obviously $C_n \ll 1$ at this point and without formal justification we can initially take C_p equal to the plateau F centre concentration. Since the α-centre concentration cannot be estimated, owing to overlapping bands, we assume from the work of Ritz (Phys Rev 142 p 505 (1966)) and the discussions of 6.2.5 and 7.3.5 that $[\alpha]/[F]$ is in equilibrium in the region of interest, so C_n need only refer to F centres.

The slope at the inflection of the post-plateau coloration curve 7.4.(i)A is 1.75×10^{16} mC^{-1} cm^{-3}. Converting to numerical concentrations gives $dC_n/d\Delta = 6.67 \times 10^{-5}$ mC^{-1} using the penetration depth for 200 keV electrons. For other qualities this slope of the coloration curve anticorrelated with penetration depth such that $dC_n/d\Delta$ was virtually independent of beam energy in this region (although possibly 5-10% lower at 100 keV). From the data of 7.4.(i)A it was a straightforward matter to fit parameters k_p, k_n, C_p starting from the assumed $C_p = [F_{plat}]$ and varying the parameters in an on-line computer program to obtain the observed slope $dC_n/D\Delta$.

For specimen G63 the following best-fit values were obtained, giving curve 7.4.(i)B:

"inception value"	C_p (3mC) $= 5.6 \times 10^{-5}$	$\pm 0.5 \times 10^{-5}$
	$k_p = 1.9 \times 10^{-5}$ mC^{-1}	$\pm 0.5 \times 10^{-5}$ mC^{-1}
	$k_n = 0.53$ mC^{-1}	± 0.05 mC^{-1}.

Quoted uncertainties arose from word-length limitations in the program but the original data did not justify further refinement by indirect

calculation or double-word arithmetic since intersample experimental variance was equivalent to ± 2 in the second significant figures quoted here. Within these precision limits there was no observed beam quality dependence.

It can be seen that C_n is very small until the end of the plateau region is reached, so we do not expect re-ionisation of F centres to be immediately significant with regard to the intrinsically-formed centres. However if the conjecture of 7.3.5 is correct we expect an eventual saturation. The long region during which C_n is undetectable allows Stage I to go to equilibrium before Stage II production is apparent. Thus the intrinsic-enhancement theory predicts a plateau (in impure material) and a final saturation of the inherently sigmoid growth curve of the coloration in pure material.

The "length" of the plateau has been shown in 3.3.2 to correlate with bombardment energy. Now the energy required to produce an F centre in Stage I is generally low so the behaviour of Stage I will be essentially beam-quality-independent in the region of interest. However the energy deposition/unit depth is greater for the less penetrating electrons (owing to the known non-linearity of the range-energy relationship) so by the time the Stage I enhancing impurities have been exhausted the value of C_p will be relatively greater for low beam energies. Consequently Stage II inception must be advanced by reducing the beam energy.

7.4.6. Kinetics of Stage II saturation.

Since we have calculated the rate of energy deposition throughout the substrate, it is possible to examine k_n in terms of the energy required to produce an F centre, and to compare this value with those obtained by other workers.

Expressing 7.4.5 (a) in physical terms we see that 1.6×10^{16} electrons (1mC) striking 1 cm^2 of material at 230 keV convert $0.53 \times 5.6 \times 10^{-5}$N anions into F centres, where N is the number of anions in a volume of 1 cm^2 x (230 keV penetration depth). From the calculations outlined in Chapter 4 this implies a "formation energy" of 900 keV/F centre in NaBr at NT, in the intrinsic mode of the process of production. This value corresponds well with that given by Rabin and Klick for

X-irradiation at 4K (850 keV) at which temperature impurities have little effect and there is no Stage I masking of the intrinsic process. We can account for the temperature dependence of the formation energy (E_F) reported by Hughes et al (AERE R5604) by noting that at 4K the only important process will be the intrinsic enhancement coloration and that the absence of thermal annealing will oppose the back-reaction in the cation vacancy production step : thus at low temperatures we expect the intrinsic process induction period to be drastically reduced and the initial slope of the coloration curve then indicates the same E_F as reported here. At NT the impurity processes predominate at small doses and since Hughes et al studied the "linear" portion of the growth curve we must assume that they were studying the plateau region where E_F is apparently very large (see Monpagens (Compt. Rend. Acad. Sci. Paris 266^B p1607 (1968) for an example where a similar assumption in the case of LiF is dismissed on further irradiation). At RT the apparent reduction in E_F may be due to the even greater role played by impurity enhancement, masking the early stages of the intrinsic process and giving a single continuous growth curve. Few authors have carried RT irradiation of NaBr to a high enough dose to observe the non-linearity of this curve.

7.5.1. A summary of the arguments presented so far and a complete kinetic description of F centre generation in NaBr.

The generation of F centres in NaBr by electron irradiation must be considered, in the light of the previous arguments, to take place in two distinct modes, one involving impurity species and the other being intrinsic to the pure host material.

F centres can be created by the agency of electrons whose energy is nominally far too low to displace Br^- ions from their equilibrium positions directly, or as a consequence of any cooperative process involving only Br^- ions, with the possible exception of multiple ionisation of a single anion : this process, however, leads to too small a cross-section to account for the occasionally rapid rate of coloration (at $\Delta = 0$ and just after the coloration plateau).

At NT the two coloration modes are separately distinguishable by virtue of a plateau in the coloration/dose curve. Below this plateau the coloration behaviour correlates with the concentration and identity

of the cation impurities andthe coloration kinetics in this region are indicative of a low value of E_F associated with exhaustible entities. The first coloration mode ceases to operate at a dose sufficient for the exhaustion of these entities. A first-order depth/dose correction to a Langmuir-type kinetic expression fits the experimental details well.

Above the plateau, the coloration behaviour is wholly consistent with an intrinsic process in which radiolytically-produced cation vacancies assist the subsequent formation of anion vacancies. One detailed mechanism (7.4.4) has been proposed which accounts for the experimental phenomena listed as (c) to (e) of 7.4.1. The arguments of 7.4.5 and 7.4.6 show that the kinetic implications of a general first-order intrinsic-enhancement process are fully consistent with criteria (a) and (b) of 7.4.1.

Saturation of the second stage of coloration can be wholly accounted for by a process of re-ionisation of F centres in the case of NaBr. The saturation concentration is too small to imply a significant contribution from F→M conversion or any similar process, and recombination-saturation places a very stringent demand on the long-range interactions of anions and F centres. However, it is possible to describe the F band saturation in terms of the incident beam ionising the F centres to α -centres, which exist in greater numbers and can therefore regain an equilibrium concentration at a faster rate.

At temperatures below NT it is generally agreed that impurities play a much reduced part in alkali halide coloration. The value of E_F deduced for the intrinsic mode here is consistent with that found at 4K by other workers.

At RT there is no detectable plateau in the coloration curve. This is consistent with the increased mobility of impurities at elevated temperatures, and phonon-interference suppressing the appearance of intrinsic-mode coloration : this is again consistent with a wide range of possible intrinsic-enhancement mechanisms utilising cation-vacancy assistance, and particularly suits the detailed mechanism advanced here.

Reference No.....

Johnson Matthey Chemicals Limited

Analytical Laboratories
Orchard Road Royston Herts
Telephone: 0763 2021

1st December, 1969.

Certificate of Analysis

To The University of Warwick.

Dear Sir(s),

We have examined the two samples of Sodium Bromides Reference Harshaw and B.D.H. received from you ~~on the~~ recently and submit the following report:

Element	Estimate of Quantity Present Results as parts per million	
	Harshaw	B.D.H.
Aluminium	<1	3
Calcium	2	20
Iron	5	5
Magnesium	<1	<1
Potassium	270	86
Silicon	30	100
Strontium	<1	1
H_2O Approx.	4%	2%

The following elements were specifically sought but not detected:- Ag, As, Au, B, Ba, Be, Bi, Cd, Co, Cr, Cs, Cu, Ga, Ge, Hf, Hg, In, Ir, Li, Mn, Mo, Nb, Ni, Os, P, Pb, Pd, Pt, Rb, Re, Rh, Ru, Sb, Se, Sn, Ta, Te, Ti, V, W, Zn, Zr, Tl.

for Johnson Matthey Chemicals Limited.

P.W. Gerrard

P.W. Gerrard,
Superintendent, Analytical Laboratories.

J.M. 550

BEAM ENERGY keV	HARSHAW	BDH
400	0.17 ± 0.03	0.30 ± 0.01
300	0.11 ± 0.02	-
200	0.096 ± 0.003	0.13 ± 0,01

Table 3.2.1.

MEAN PLATEAU OPTICAL DENSITIES: NT-IRRADIATED DRY NaBr.

BEAM ENERGY keV	HARSHAW	BDH
400	0.47 ± 0.02	0.79 ± 0.005
300	0.33 ± 0.02	-
200	0.24 ± 0.01	0.42 ± 0.005

Table 3.2.2.

MEAN SATURATION OPTICAL DENSITIES: NT-IRRADIATED DRY NaBr.

BEAM ENERGY keV	SATURATION O.D.
400	4.1
200	2.0

Table 3.4.1.

SATURATION OPTICAL DENSITIES: RT-IRRADIATED DRY HARSHAW NaBr.

Table 3.6.1

BEAM ENERGY keV	HARSHAW (NT)	HARSHAW (RT)	B D H (NT)
400	0.768×10^{17}	1.16×10^{18}	1.29×10^{17}
200	1.09×10^{17}	1.57×10^{18}	1.92×10^{17}

SATURATION CONCENTRATION OF F CENTRES IN NaBr (cm^{-3})

Table 3.6.2

BEAM ENERGY keV	HARSHAW (NT)	HARSHAW (RT)	B D H (NT)
400	4.10×10^{-4}	6.16×10^{-3}	6.86×10^{-4}
200	5.79×10^{-4}	8.35×10^{-3}	10.21×10^{-4}

NUMERICAL SATURATION CONCENTRATION OF F CENTRES IN NaBr.

Table 3.6.3

BEAM ENERGY keV	HARSHAW (NT)	HARSHAW (RT)	B D H (NT)
400	4.10×10^{-4}	6.16×10^{-3}	6.86×10^{-4}
200	4.09×10^{-4}	5.89×10^{-3}	7.20×10^{-4}

NUMERICAL SATURATION CONCENTRATION OF F CENTRES IN NaBr ASSUMING LINEAR PENETRATION/ENERGY RELATION.

Table 3.6.4

BEAM ENERGY keV	HARSHAW (NT)	B D H (NT)
400	1.49×10^{-4}	2.61×10^{-4}
200	1.64×10^{-4}	2.21×10^{-4}

PLATEAU CONCENTRATION OF F CENTRES IN NaBr LINEAR PENETRATION/ENERGY RELATION.

BEAM ENERGY keV	[F]BDH/[F] HARSHAW (SATURATION NT)	[F]BDH /[F]HARSHAW (PLATEAU NT)
400	1.67	1.75
200	1.71	1.35

Table 3.7.1

CONCENTRATION RATIOS FOR DIFFERENT SOURCES.

BEAM ENERGY keV	$[F]_{sat}/[F]_{plateau}$ (HARSHAW NT)	$[F]_{sat}/[F]_{plateau}$ (BDH NT)
400	2.75	2.62
200	2.50	3.26

Table 3.7.2

CONCENTRATION RATIOS FOR DIFFERENT STAGES OF COLORATION.

BEAM ENERGY keV		PENETRATION DEPTH
INDICATED	CALIBRATION	(MICROMETRES)
400	460	530 ± 10(Exptl.)
300		370(Calculated)
200	230	250 ± 12(Exptl.)
100		112(Calculated)

Table 4.3.1

COLOUR PENETRATION & INCIDENT ELECTRON ENERGY: NaBr.

E_0 (keV)	μ (cm^{-1})
400	48
300	111
200	192
100	770

Table 4.3.2

CALCULATED ABSORPTION COEFFICIENTS FOR ELECTRONS IN NaBr.

NaBr	NaI
273(+)	313(-)
360(-)	387(-)
390(-)	438(+)
485(-)	

Table 5.3.1

WAVELENGTHS (nm) OF OBSERVED CATHODOLUMINESCENT BANDS AT NT AND $d\lambda/dT$ BETWEEN NT & RT: FOR NaBr & NaI.

	«ALLOWED» TRANSITION		«FORBIDDEN» TRANSITION	
	E(eV)	τ(ns)	E(eV)	τ(μs)
NaCl	5.6	<5	3.38	295
KCl			2.32	5000
RbCl			2.27	5500
NaBr			4.60	0.49
KBr	4.42	~9	2.27	130
RbBr	4.20	~11	2.10	180
NaI			4.20	0.09
KI	4.15	~9	3.34	4.40
RbI	3.95	~9	2.30	11

Table 5.3.2

RESULTS QUOTED BY KABLER & PATTERSON. (See text).

MATERIAL	β	α
KCl	0.40	0.81
NaCl	0.58	0.80
KBr	0.35	0.67
NaBr	0.37	0.92
KI	0.32	0.60

Table 6.2.1

ENERGY DIFFERENCES FROM FIRST EXCITON BAND (eV).
(AFTER JACOBS & KRISHNA MENON).

PARAMETER	STAGE I	STAGE II
b	0.012 ± 0.003	0.007 ± 0.003
A	0.030 ± 0.005	0.018 ± 0.005
λ_1	$-0.045\ mC^{-1}$	$-0.20\ mC^{-1}$
λ_2	$-0.0023\ mC^{-1}$	$-0.025\ mC^{-1}$

Table 6.5.1

PARAMETERS OF FIGURE 6. 5. (i).

no.	λ_{peak} (nm)	400 keV				200 keV				Identity
		Stage I		Stage II		Stage I		Stage II		
		visibility	F-bleach	visibility	F-bleach	visibility	F-bleach	visibility	F-bleach	
1	197	sh. on 3 & 4	decreased	sh. on 2	riding on 4	shoulder on bands 3&4	ride on 4	sh. on 2	ride on 4	β
2	198			poor				poor		β′
3	200	broad	r. on 4	peak > 4	r. on 4	broad, > 4	enhanced	broad, > 4	enhanced	α ?
4	205	peak	enhanced	peak	enhanced	peak	enhanced	peak	enhanced	
5	215	not seen	? enhanced	broad, faint	enhanced	justvisible	enhanced	broad, faint	st. enh.	see text
6	230	broad peak ~ 233 nm	sl. enh.	less evident than StageI	sl. enh.	sharp	sl. enh.	sharp	sl. enh.	V_3
7	235		nil		sl. enh.	---------- not found ----------				impurity
8	240	not res. from 7	nil	stronger	nil	shoulder	sl. enh.	not resolved		V_2
9	260	shoulder	sl. enh.	peak	enhanced	peak'	enhanced	broad flat absorption	enhanced	impurity
10	290	shoulder	sl. enh.	peak	enhanced	shoulder	nil		nil	V_4
11	300	not res. from 10	nil	shoulder "	nil	peak"	nil	peak"	nil	impurity
12	340	peak	sl. dec.	peak	sl. dec.	clear shoulder	v. sl. dec.	clear shoulder	decreased	V_1?
13	390	sh. on 12	st. dec.	sh. on 12	sl. dec.	not found		poorly resolved	st. dec.	V_k
14	490	sh. on 15	decreased	shoulder	decreased	shoulder	decreased	shoulder	decreased	K
15	525	F band								F
16	550	sh. on 15	v. sl. dec.	sh. on 15	v. sl. dec.	sh. on 15	v. sl. dec.	sh. on 15	v. sl. dec.	R_1 or V_1

" Harshaw material only ' B.D.H. material only

Table 6.3.1 Bands in NaBr irradiated at NT, and effect of F band optical bleach

SOURCE	HARSHAW			B D H		
BEAM ENERGY keV	400	300	200	100	400	200
$\frac{dD}{d\bar{\Delta}}_{(\Delta \to 0)} / D_{plateau}$	1.04	1.14	0.69	0.78	0.81	0.72
STANDARD ERROR	0.12	0.14	0.03	*	0.10	0.04

Table 7.3.1

L. H. S. OF EQUATION 7. 3. 3(a).

* ONLY TWO ESTIMATES AVAILABLE: DEVIATION $\pm$ 0.05 FROM MEAN.

SOURCE	HARSHAW				B D H	
BEAM ENERGY keV	400	300	200	100	400	200
η (MILLICOULOMB^{-1})	600	430	174	89	468	182
STANDARD ERROR	69	53	36	-	58	10

Table 7.3.2

VALUES OF η FROM TABLES 4. 3. 1., 4. 3. 2., 7. 3. 1.

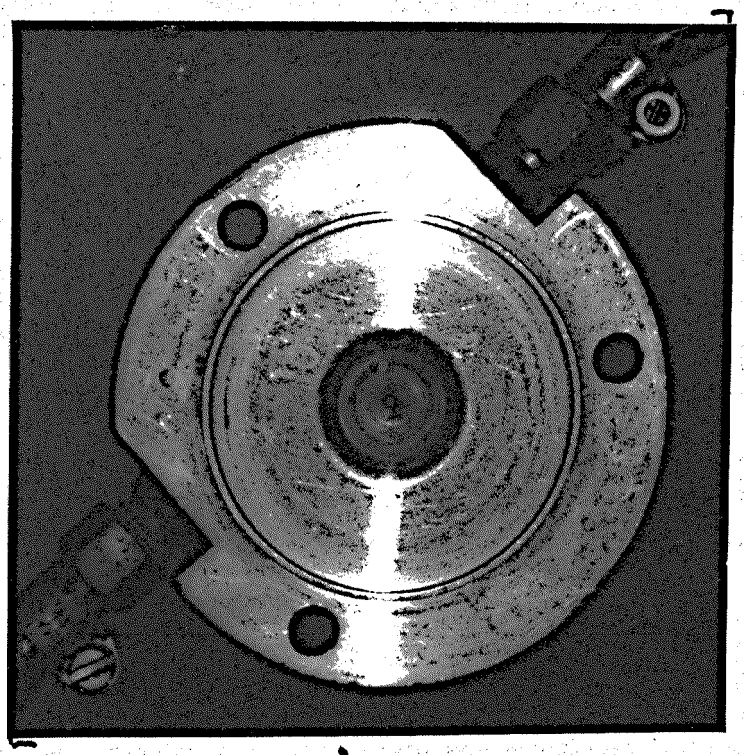

Fig 2.2(i) Beam switching aperture

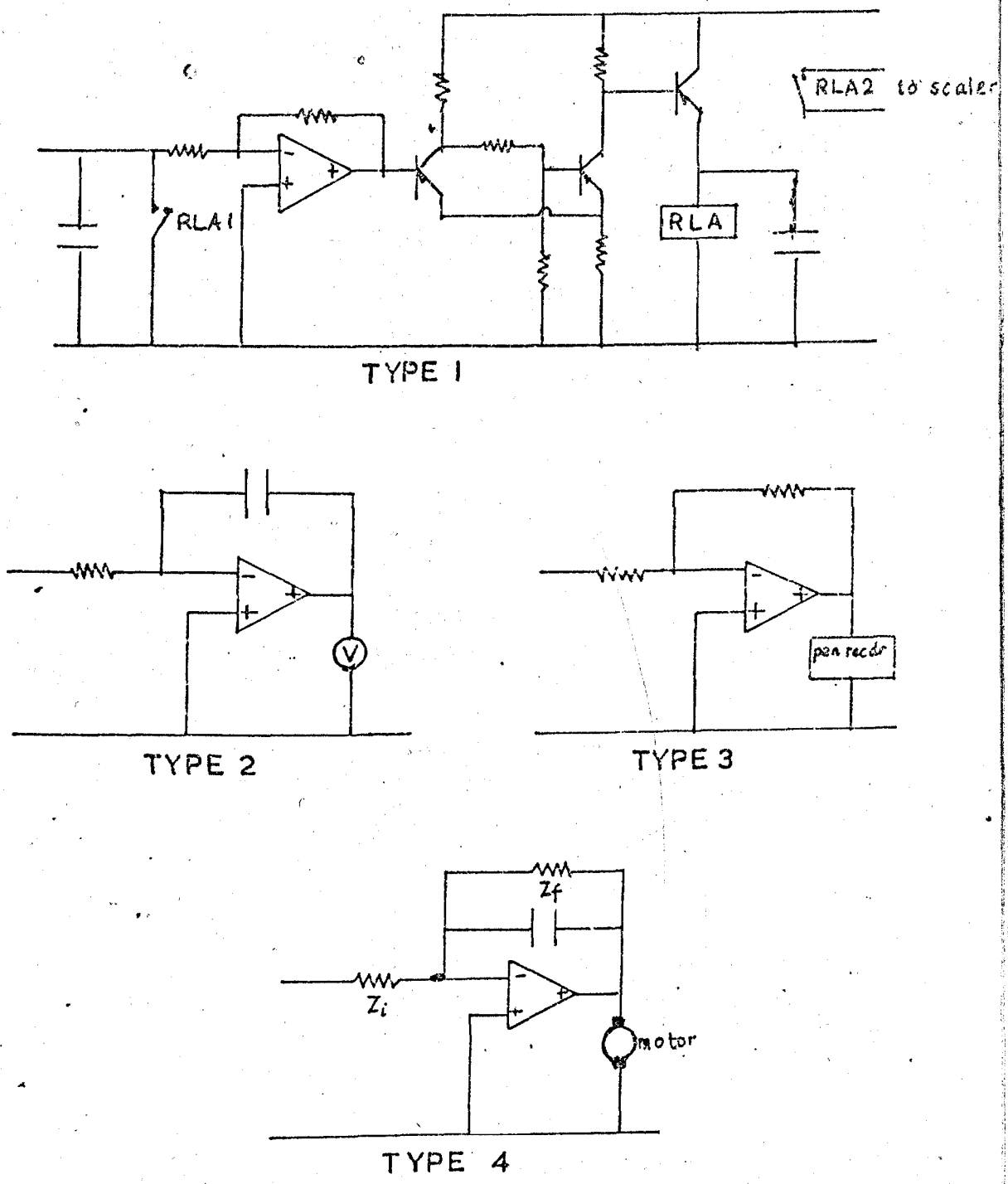

Fig. 2.3.(i) Schematic diagrams of the four types of dose integrator discussed

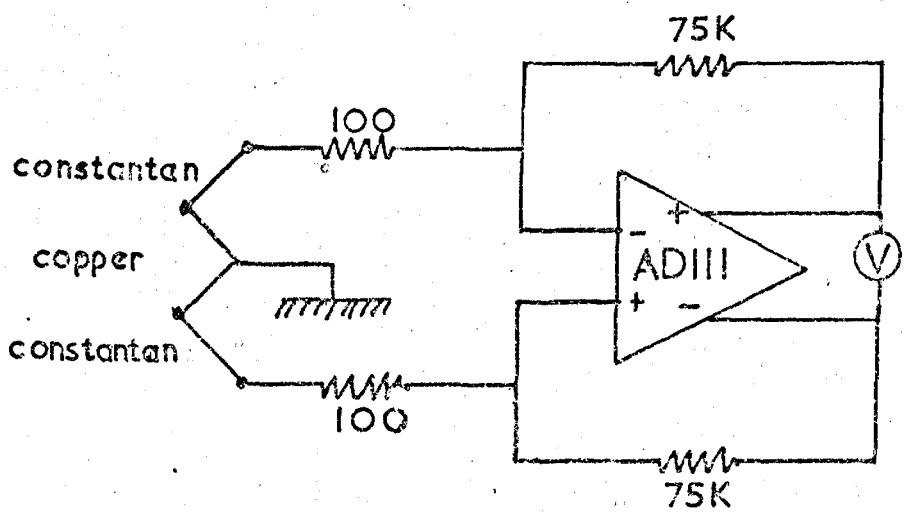

DIFFERENTIAL

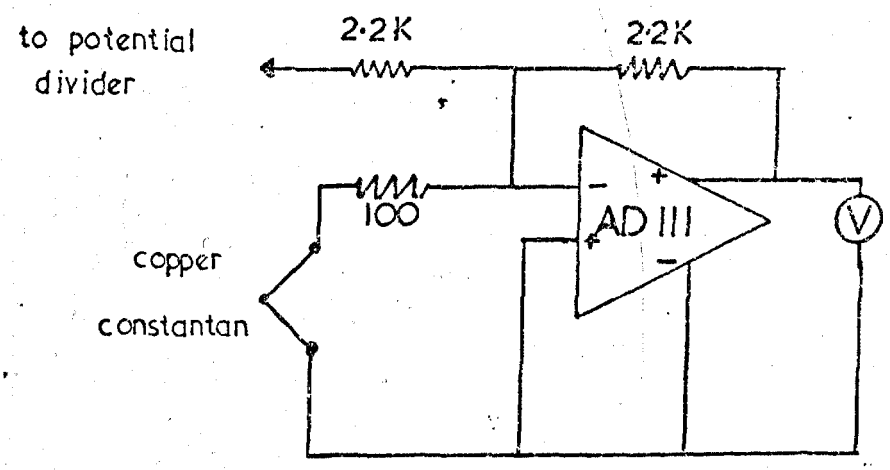

SUMMING

Fig. 23.(ii) Thermocouple amplifier configurations.

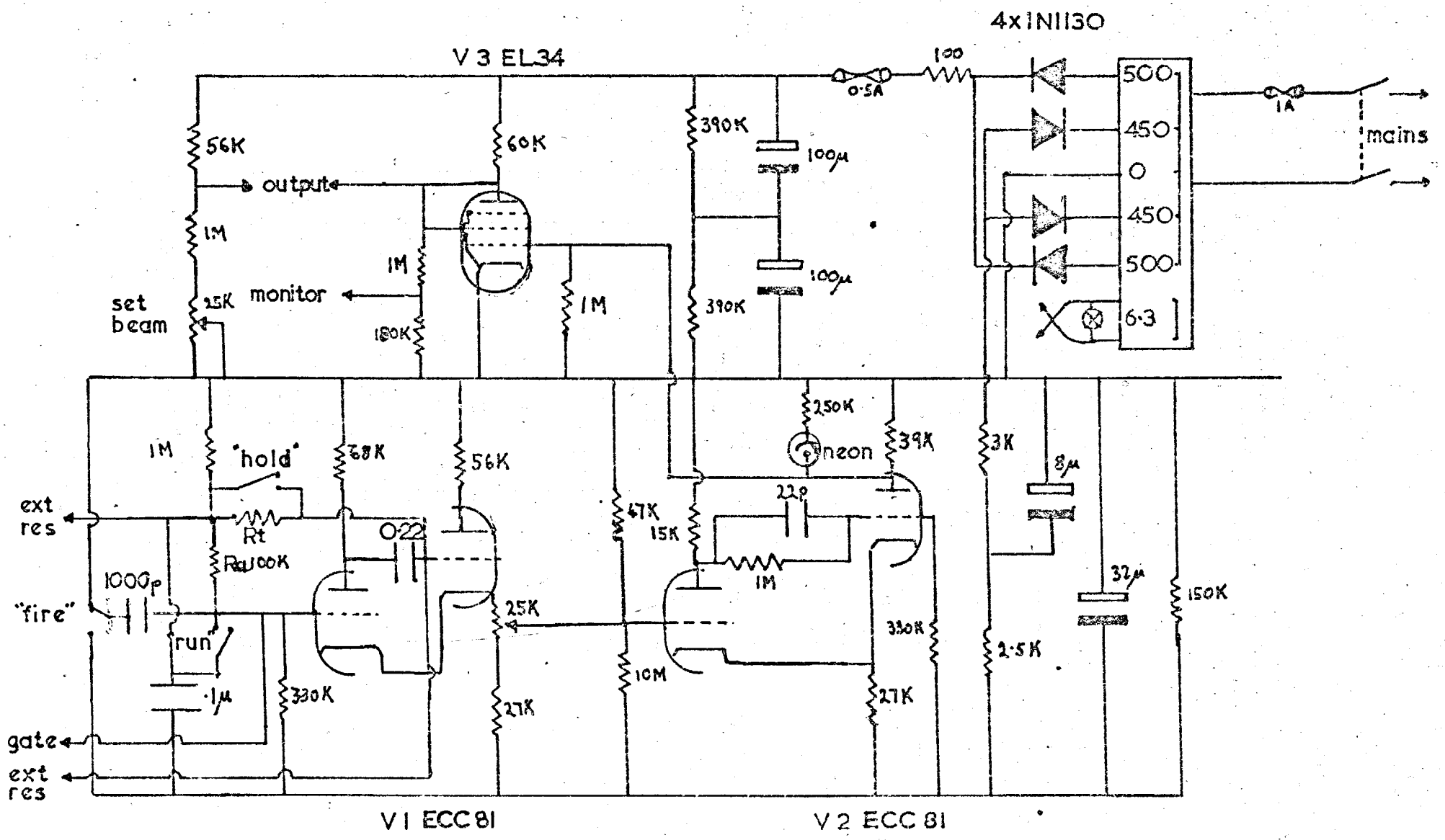

Fig.2.3.(iii) Pulse generator

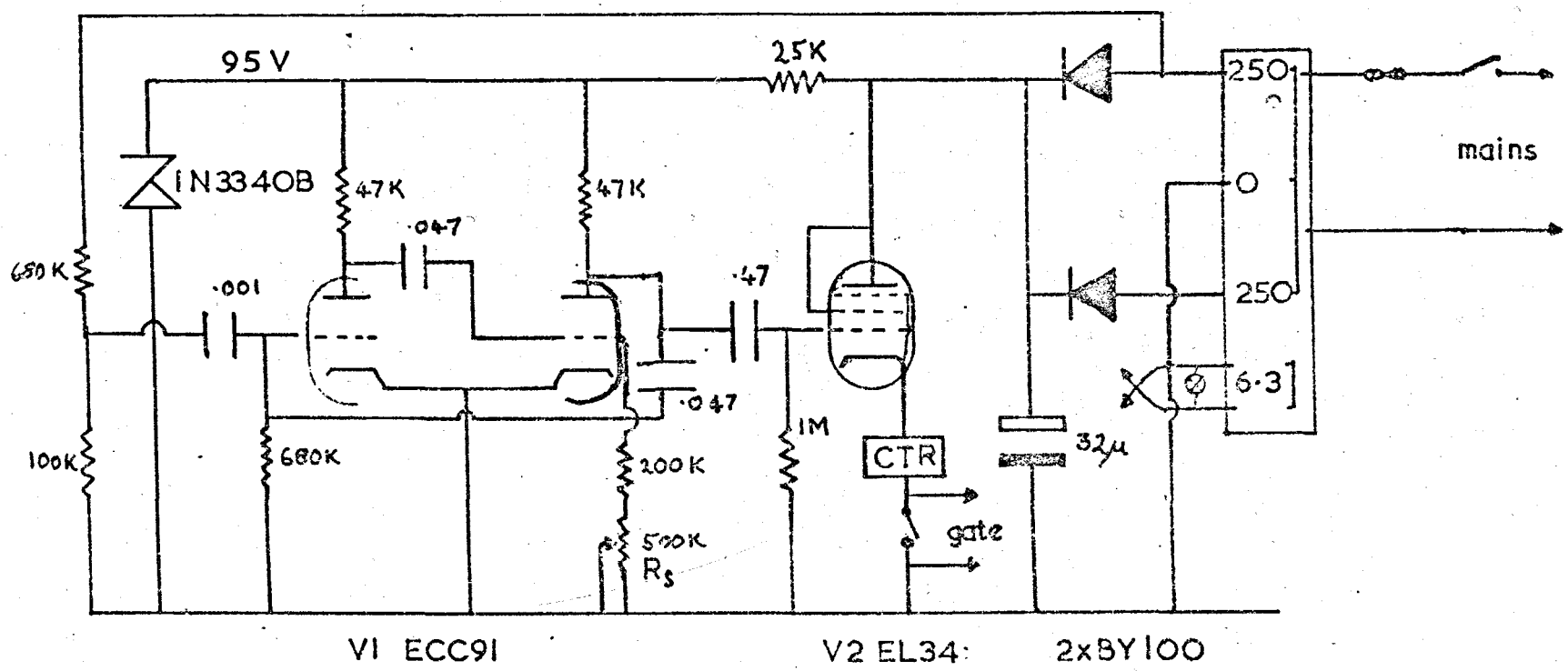

Fig.2.3.(iv) Time clock

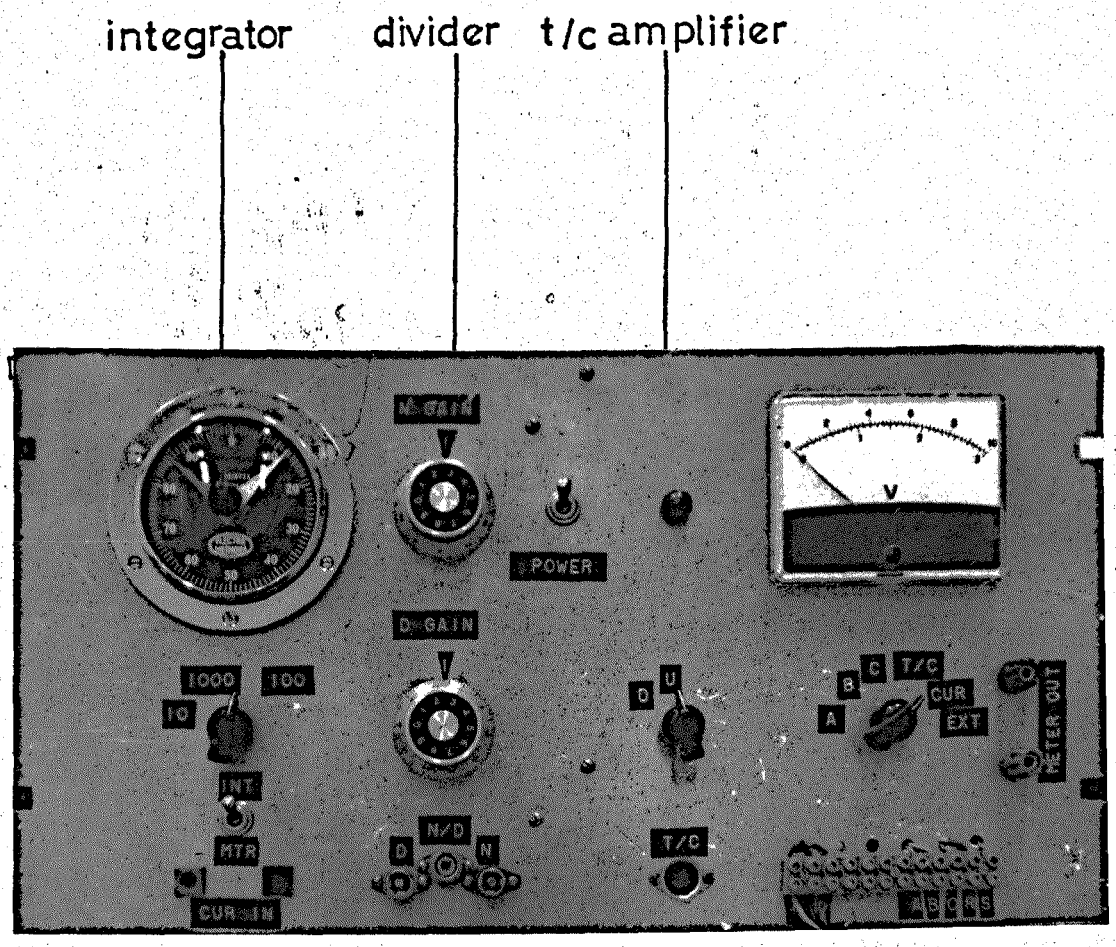

Fig.23.(v) Integrator, divider, and thermocouple indicator panel

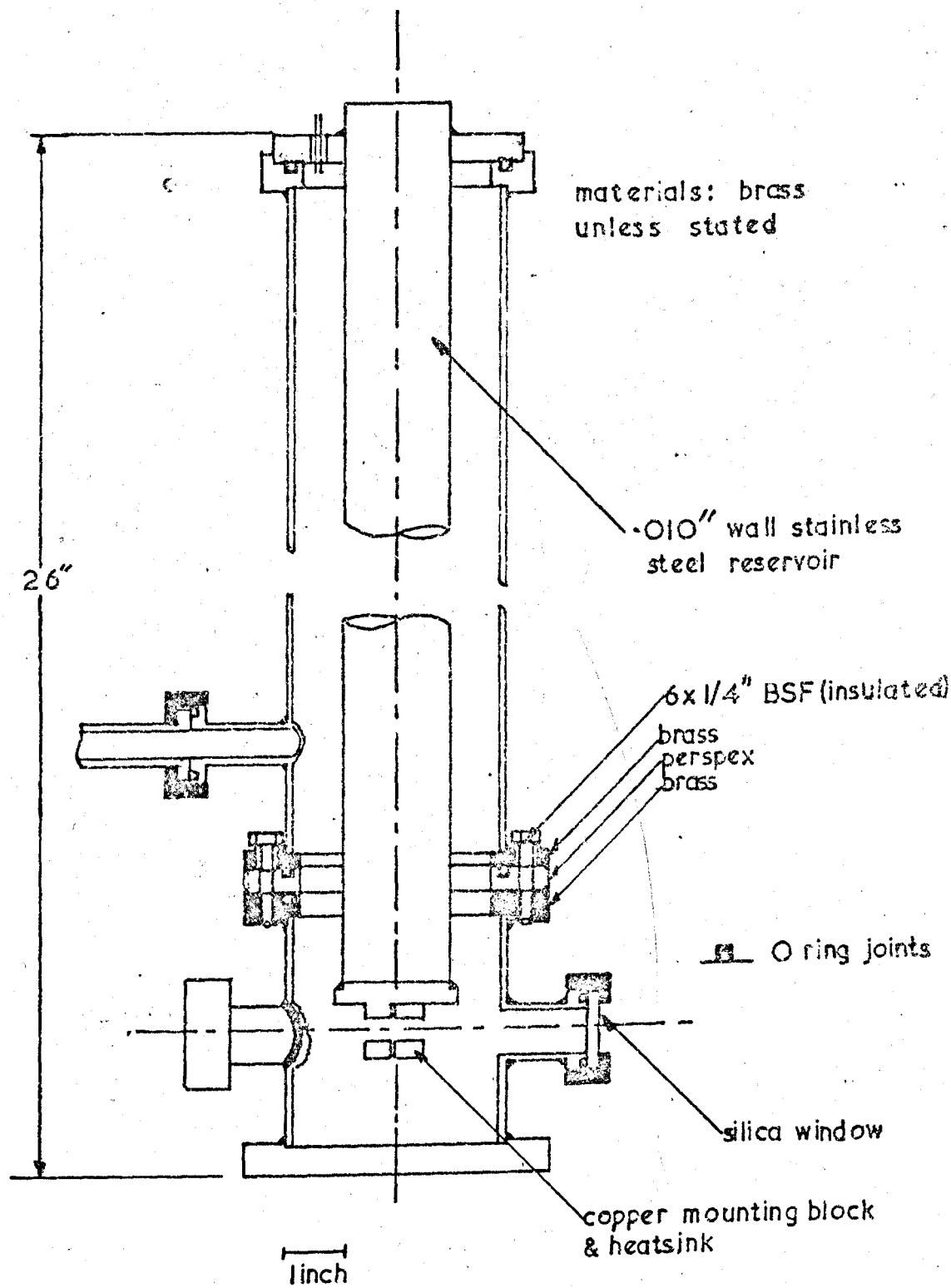

Fig. 2.4.(i) Cryostat section

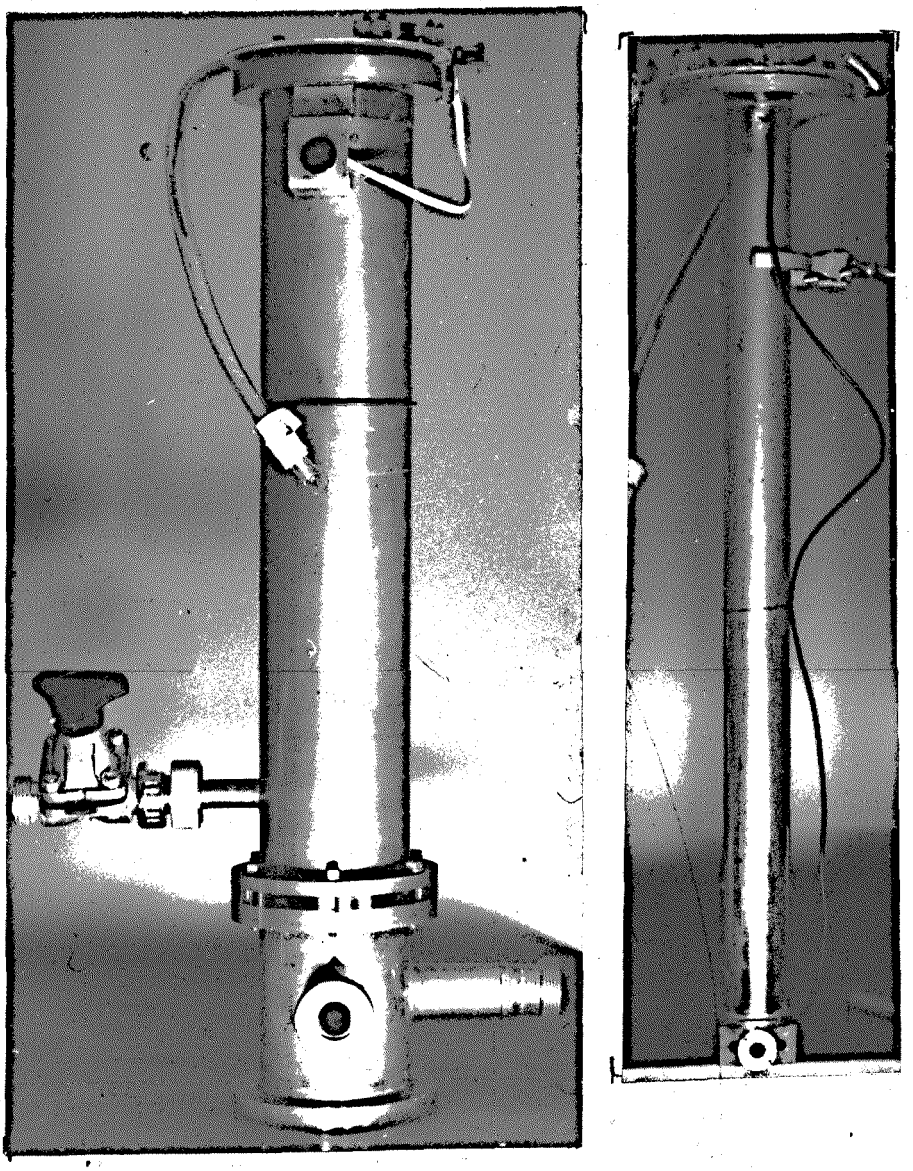

Fig.24(ii) Cryostat case and inner tube

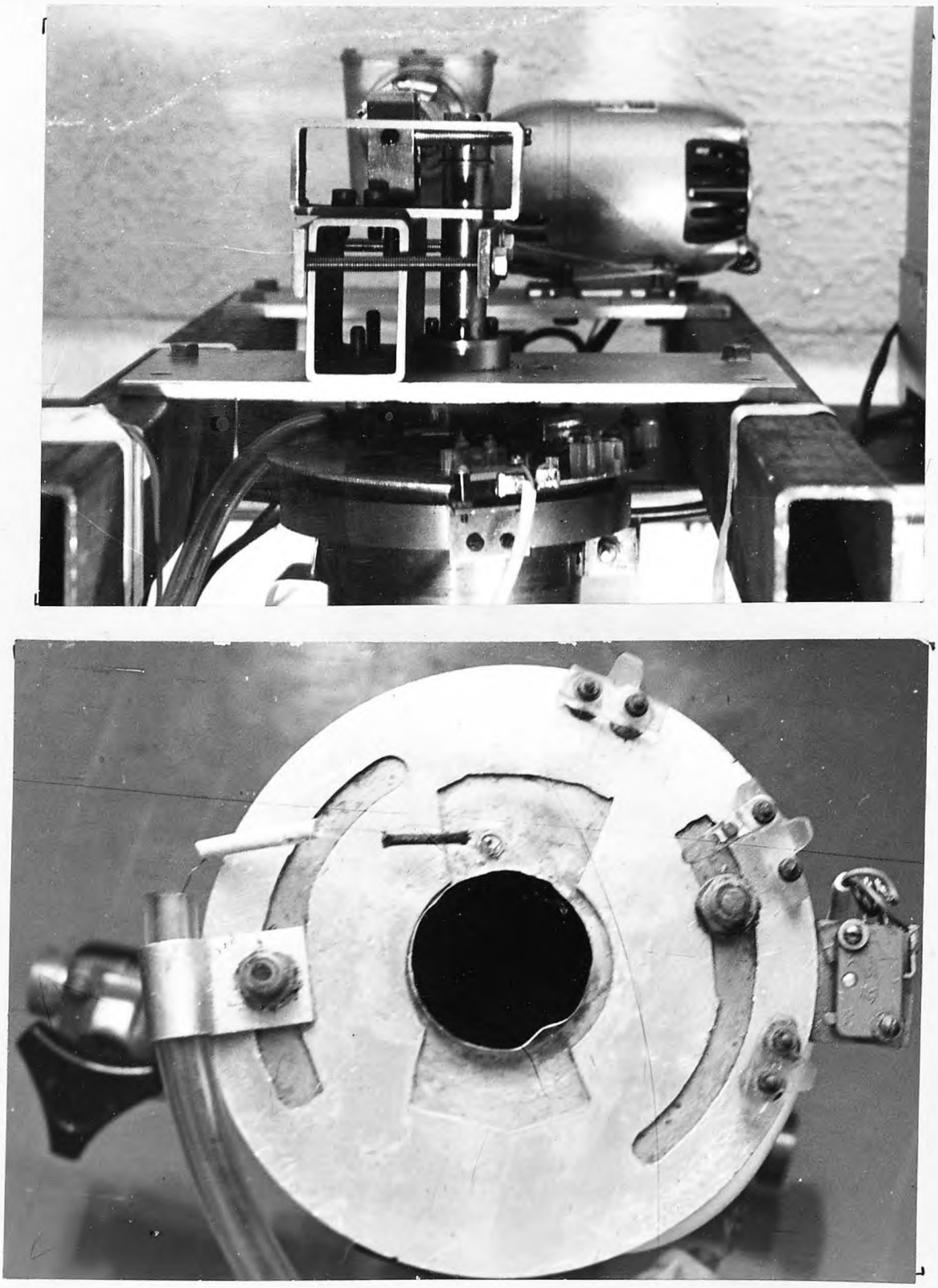

Fig.2.4.(iii) Alignment drive and cam switch with thermocouple lead-through

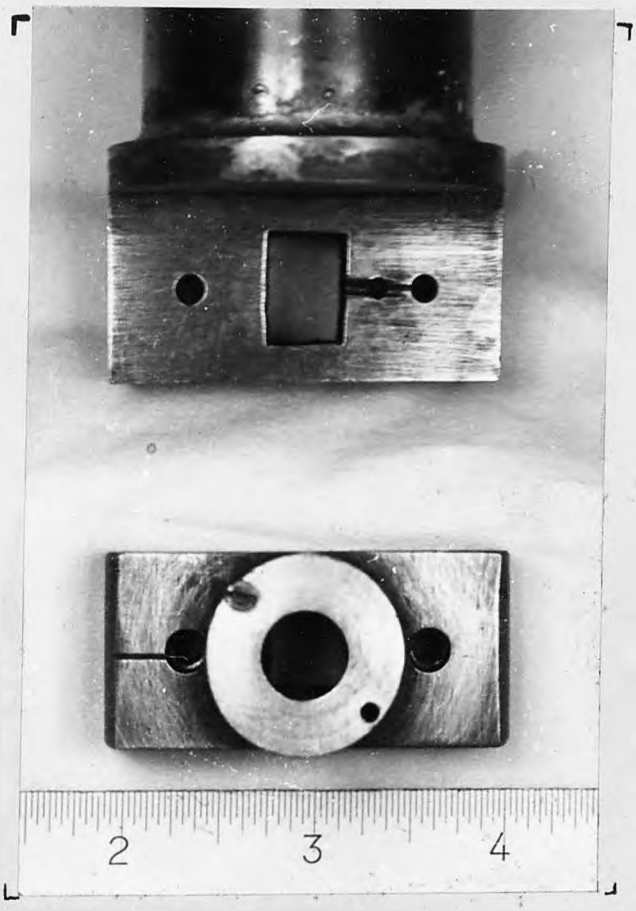

Fig.2.4.(iv) Sample holder, clamp, and Faraday cup

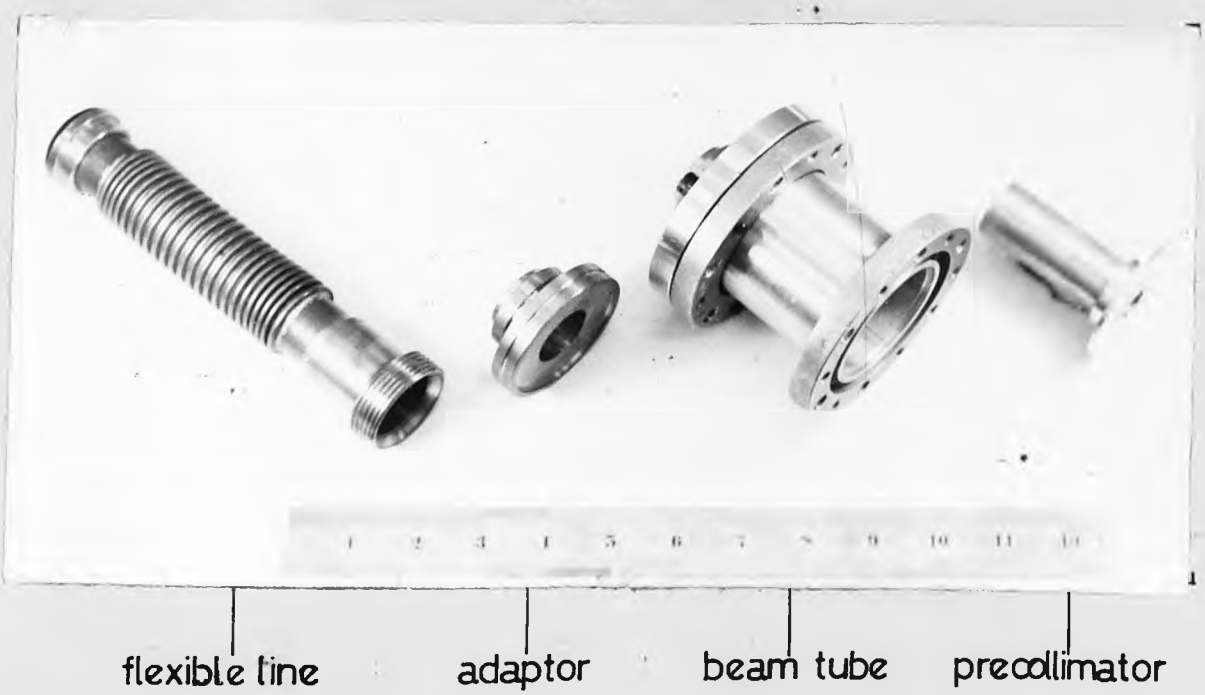

Fig. 2.4.(v) Beam tube alignment accessories

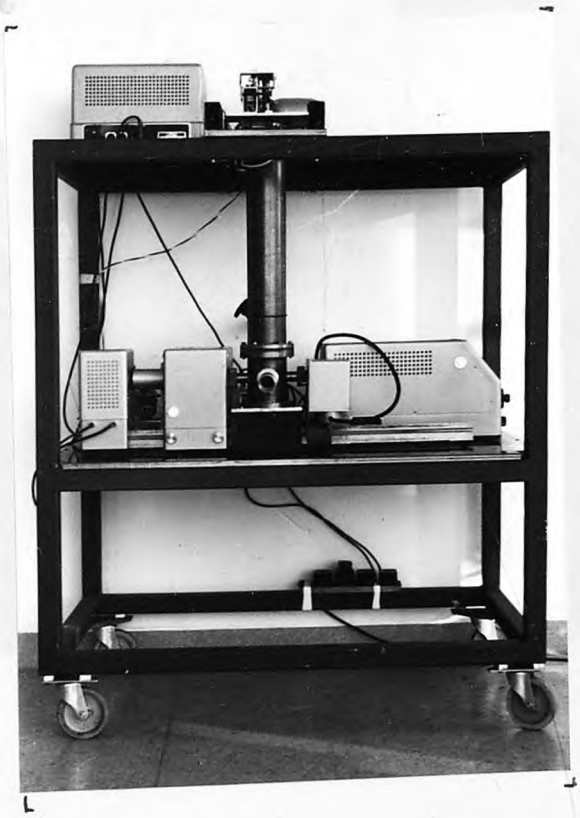

Fig.2.5(i) Apparatus trolley

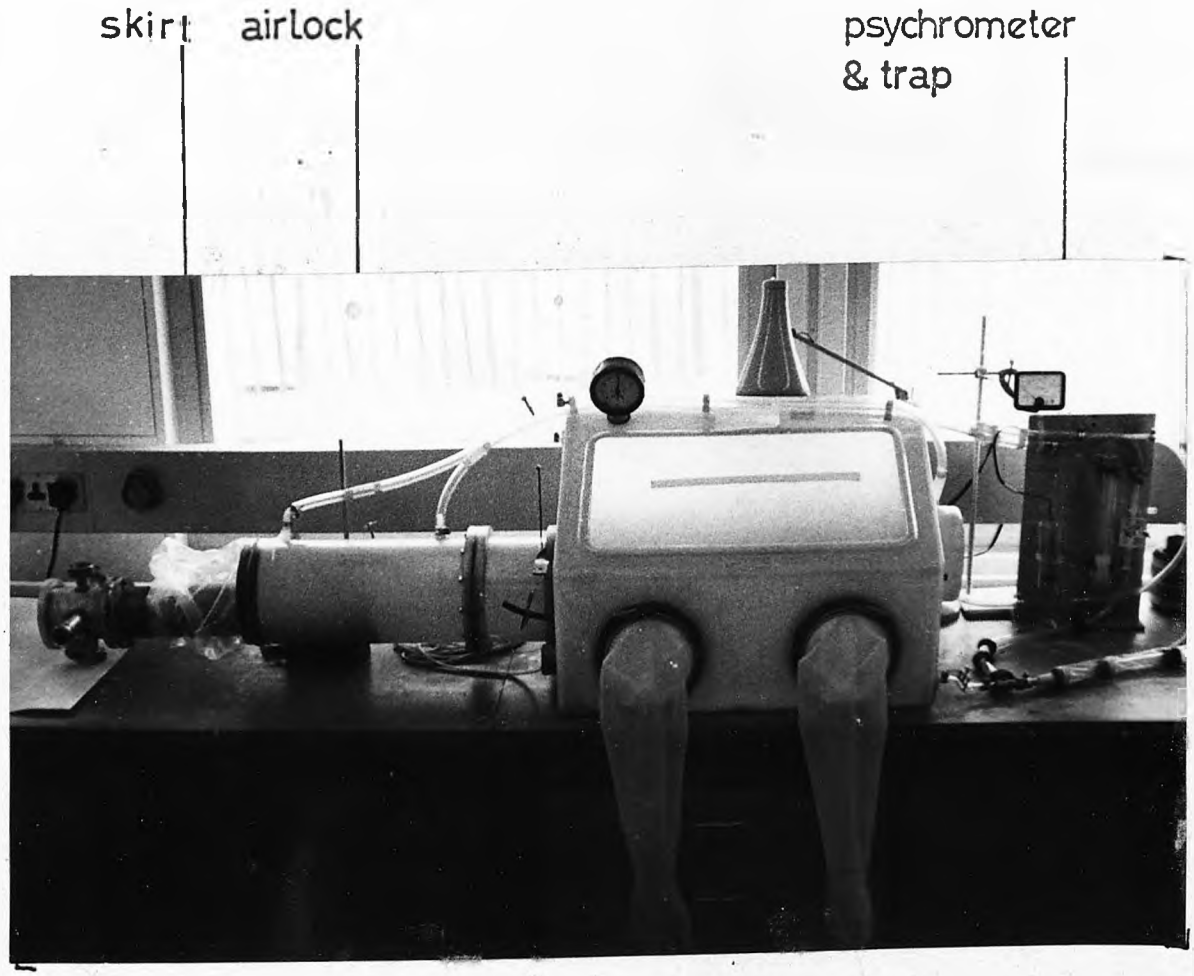

Fig.2.5(ii) High-purity glovebox

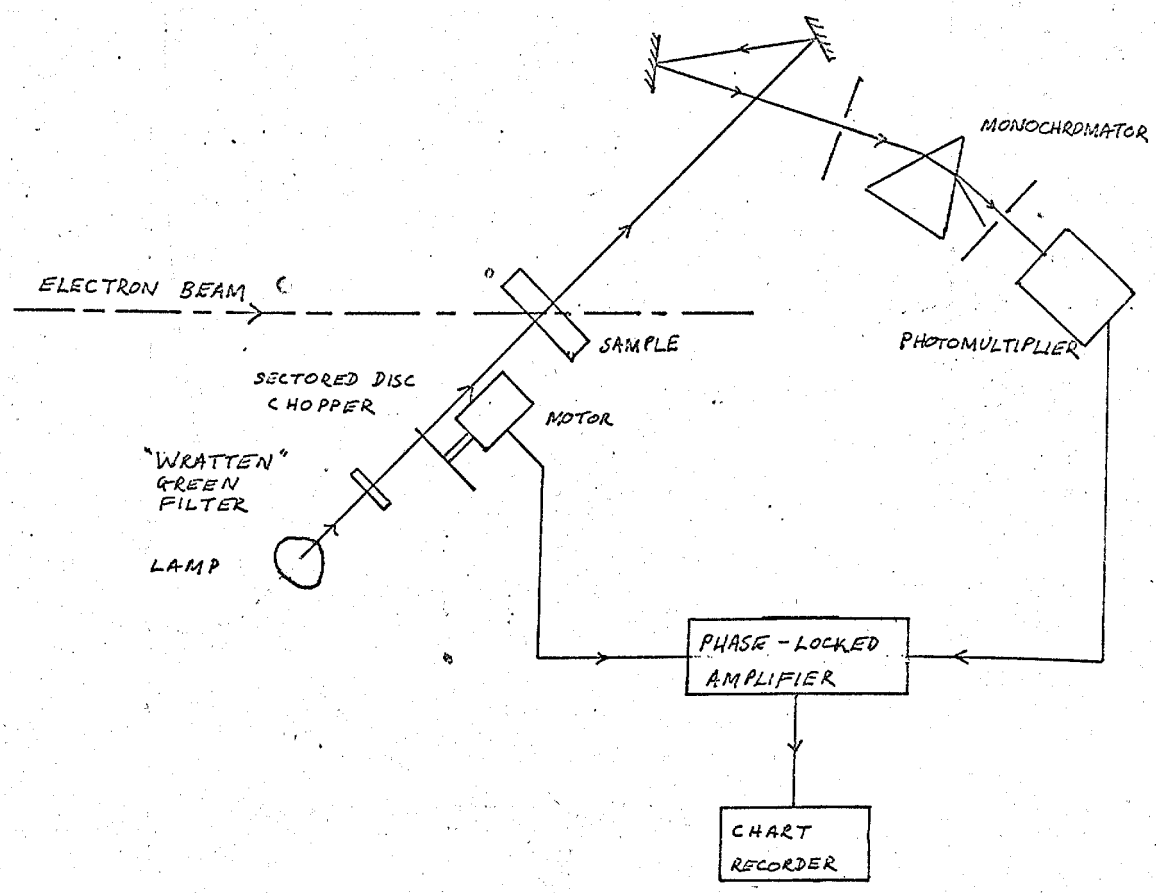

Fig. 3.1(i) Continuous measurement - schematic

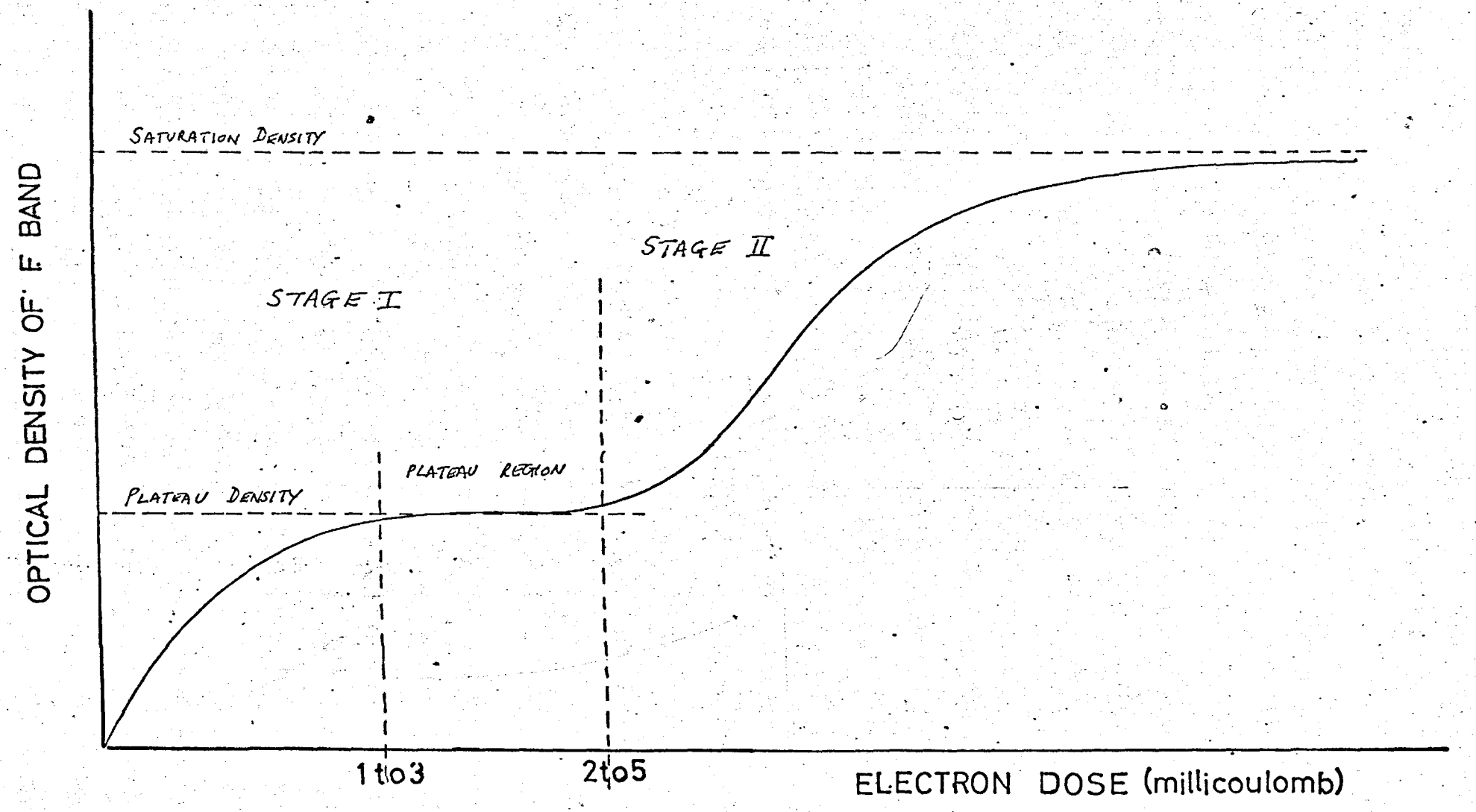

Fig 3.1.(ii) Schematic "growth curve" illustrating terms used in the text

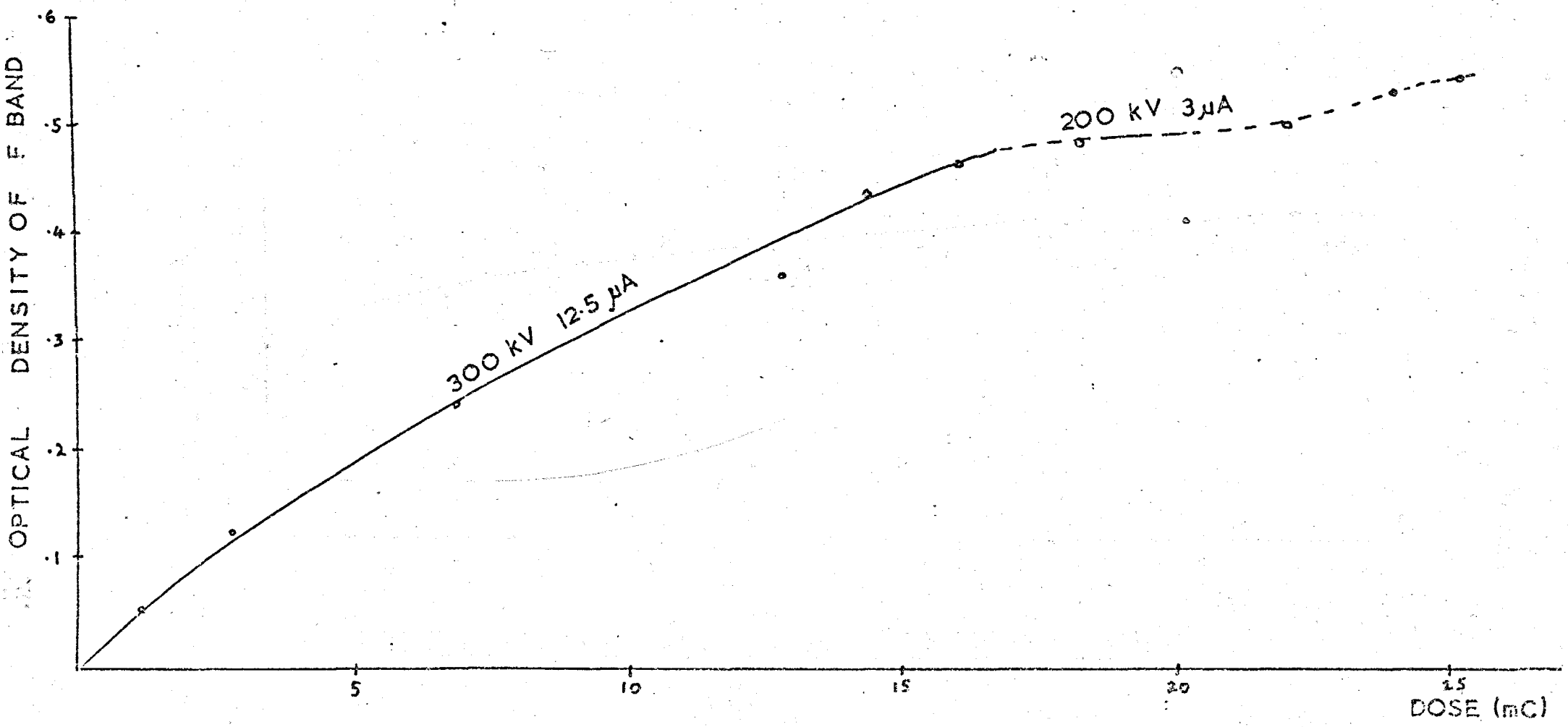

Fig. 3.2.(i) F band optical density as a function of dose: NaBr G4

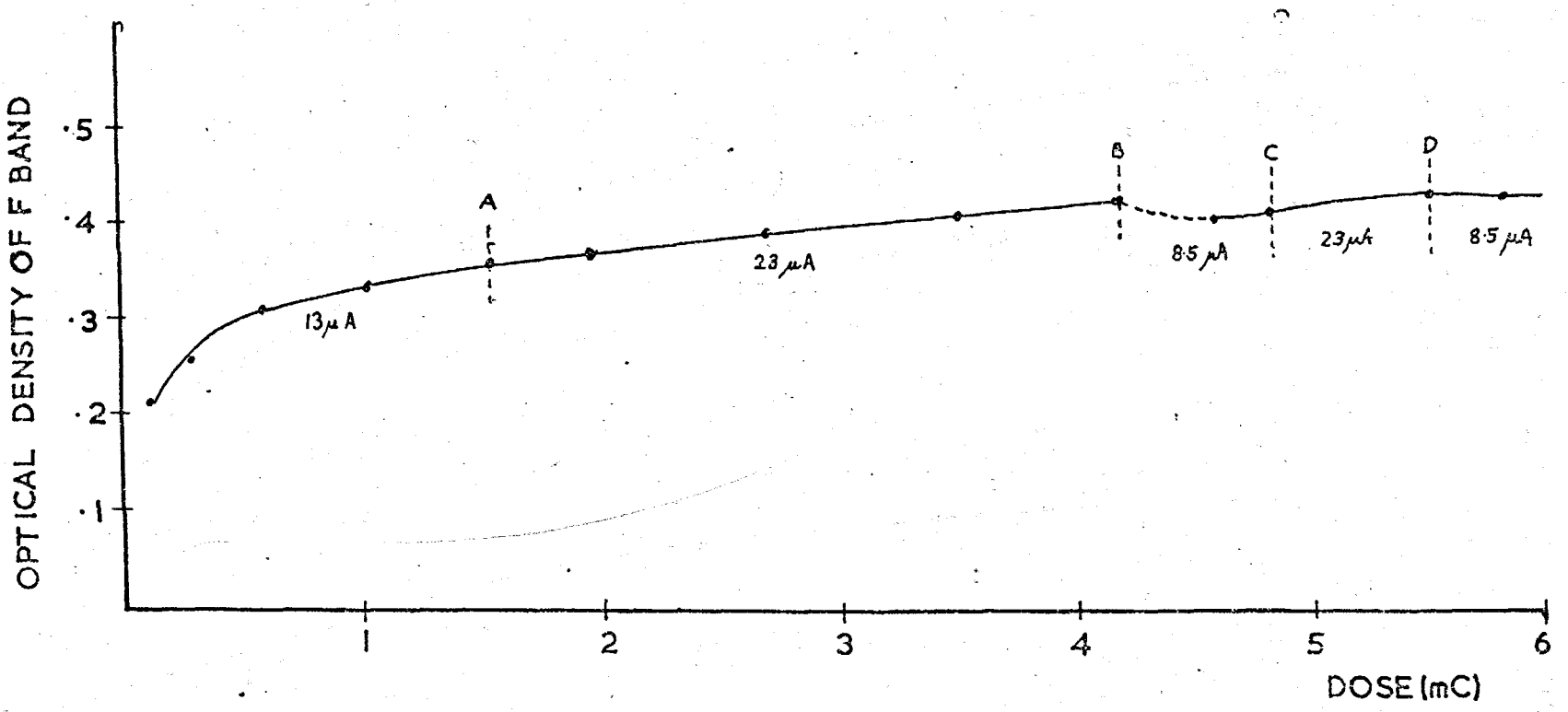

FIG. 3.2.(ii) Current dependence of F band growth

300 kV G5

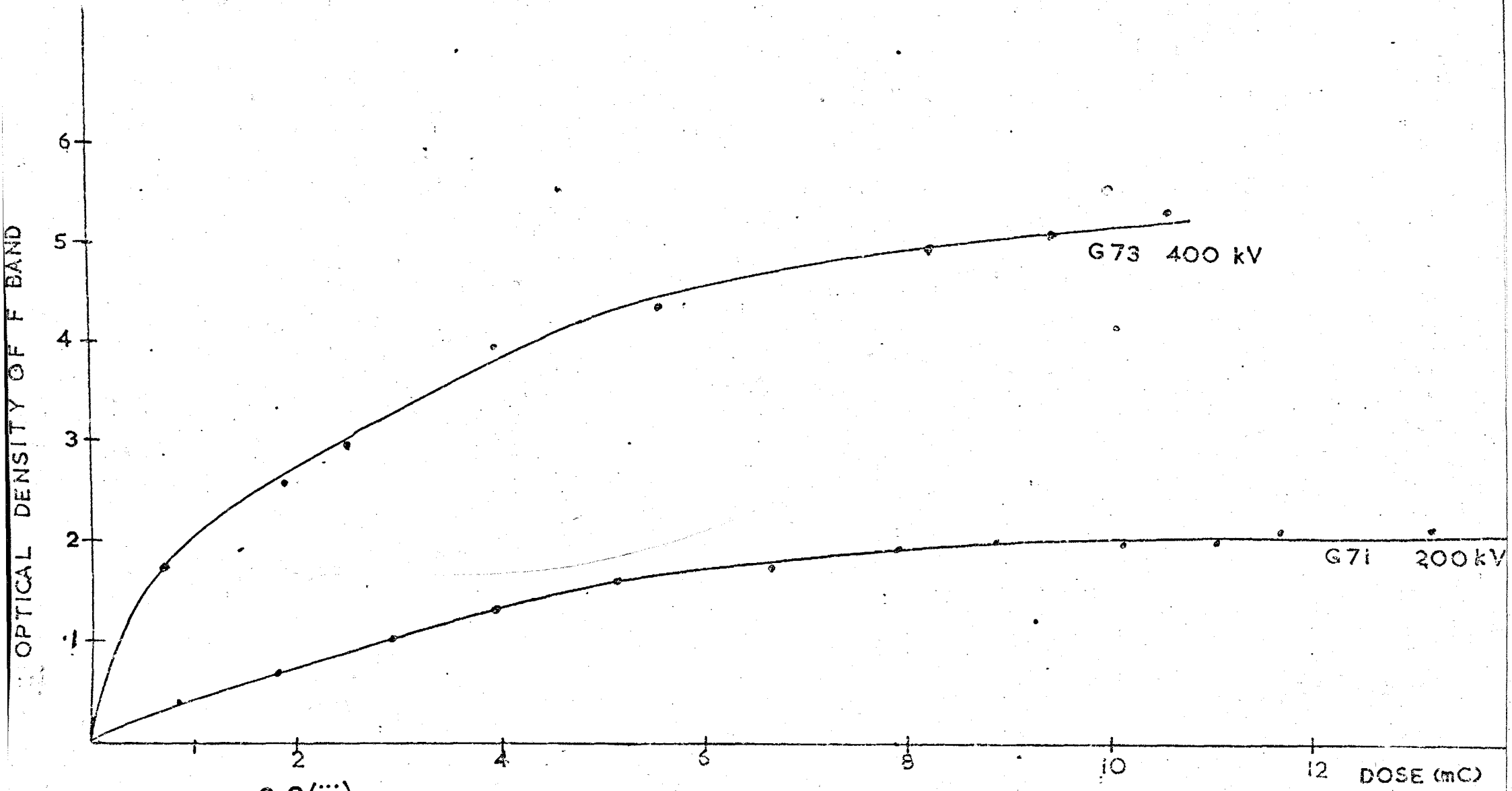

Fig. 3.2(iii) F band growth in B.D.H. NaBr

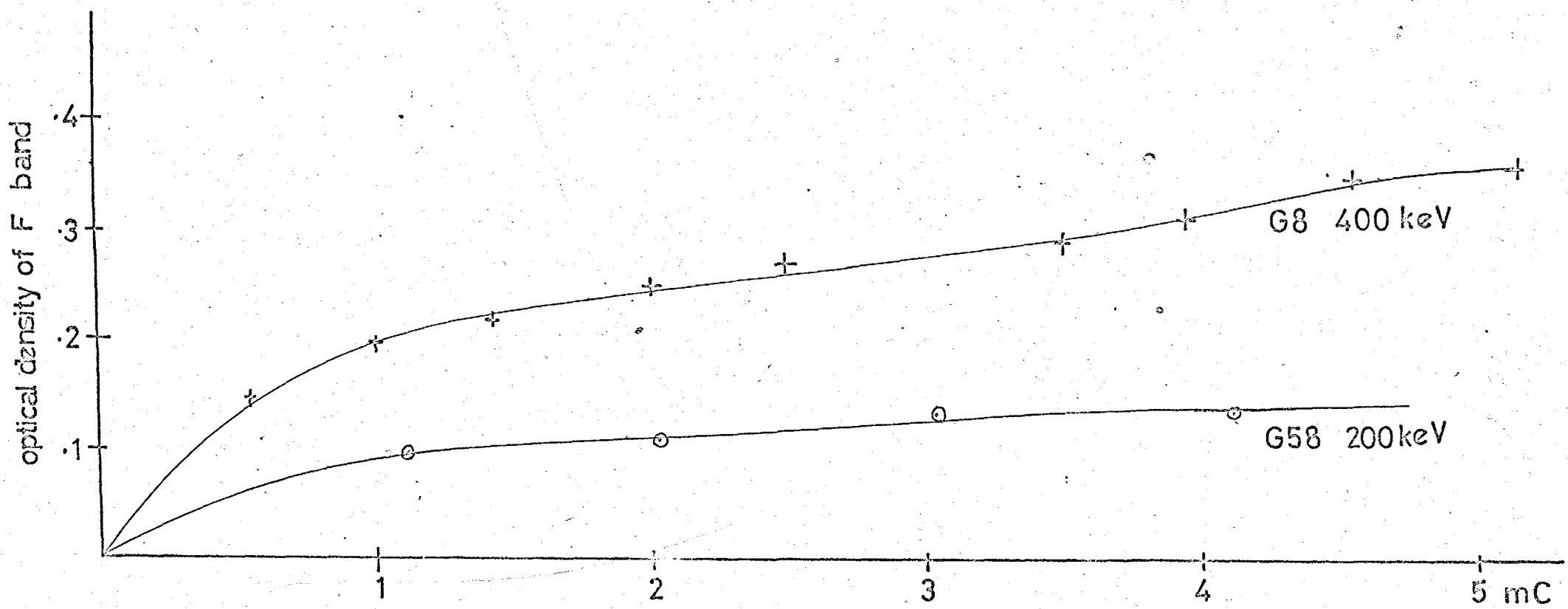

Fig.3.2(iv) F-band growth in Harshaw NaBr (NT)

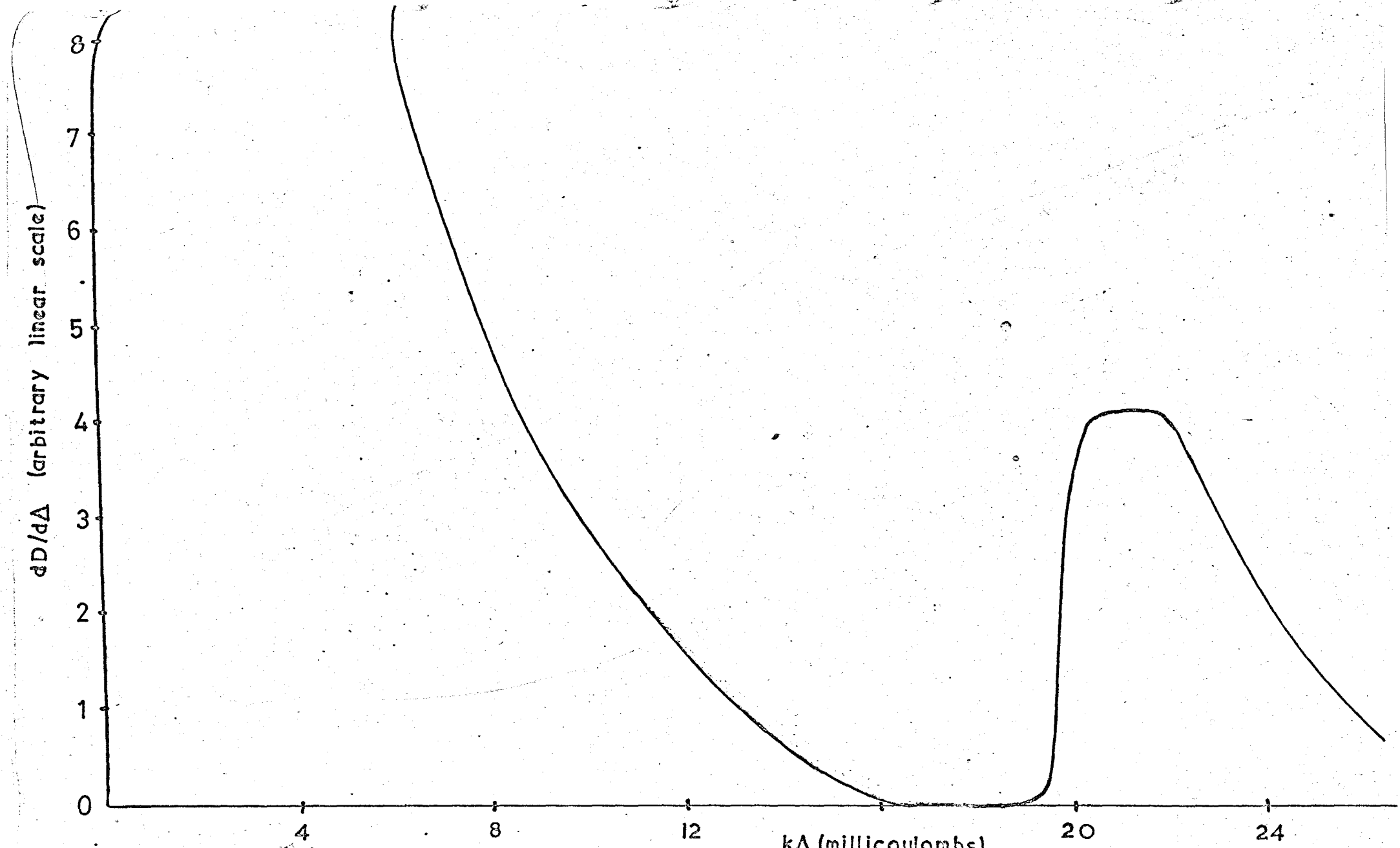

Fig 3.2(v) Differential of continuous F-band growth curve

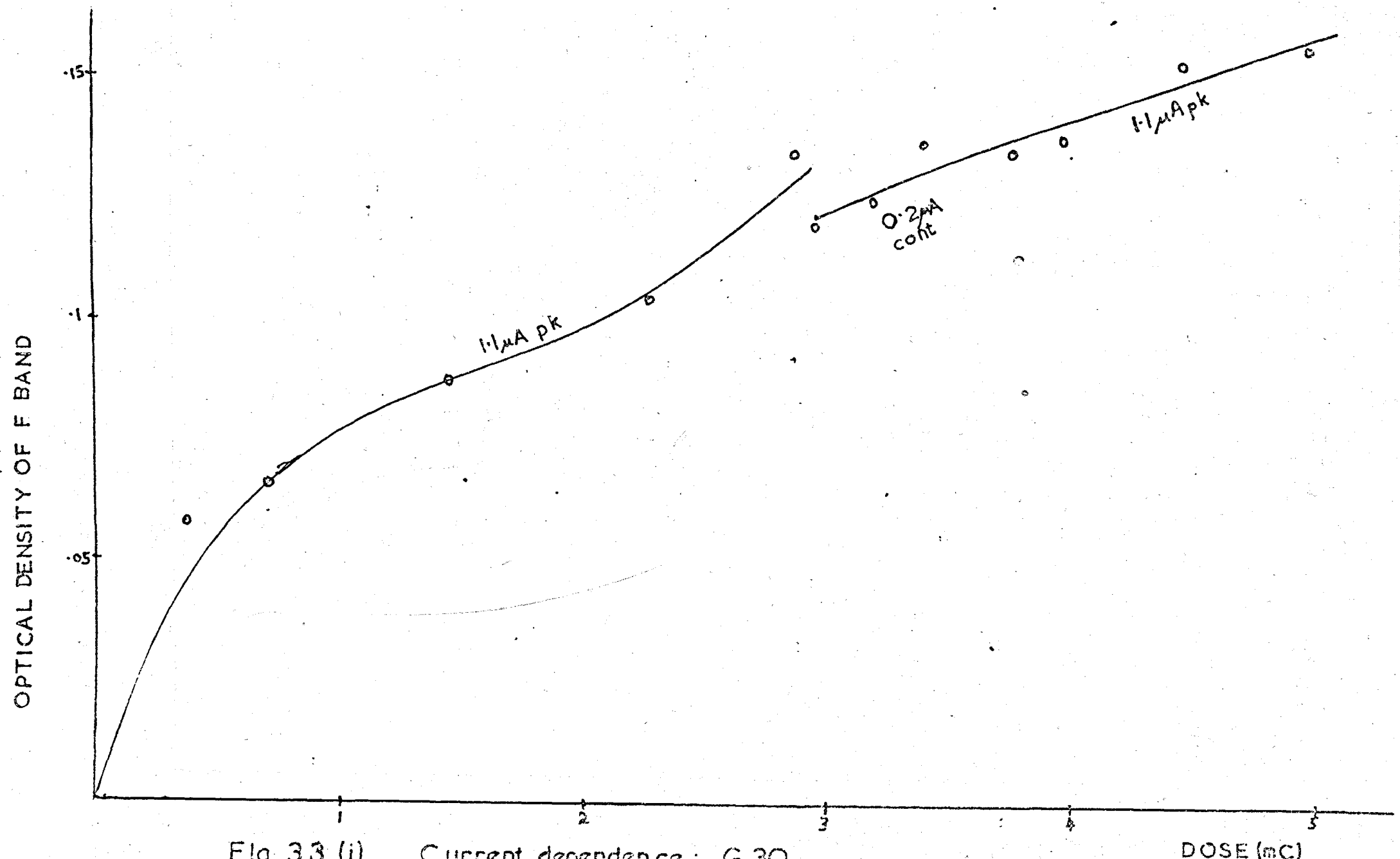

Fig 33 (i) Current dependence : G 30

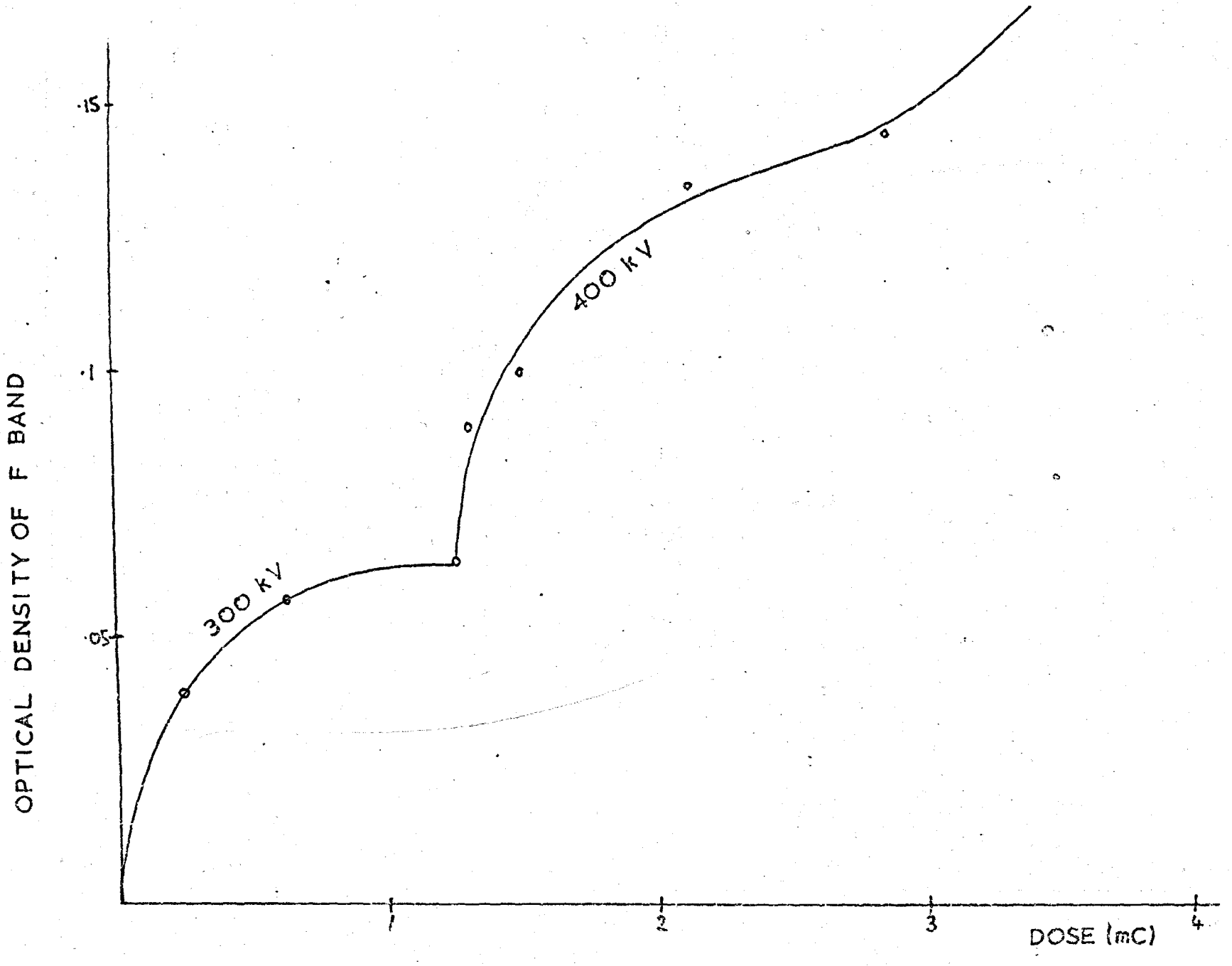

Fig. 3.3 (iii) Voltage dependence: G14

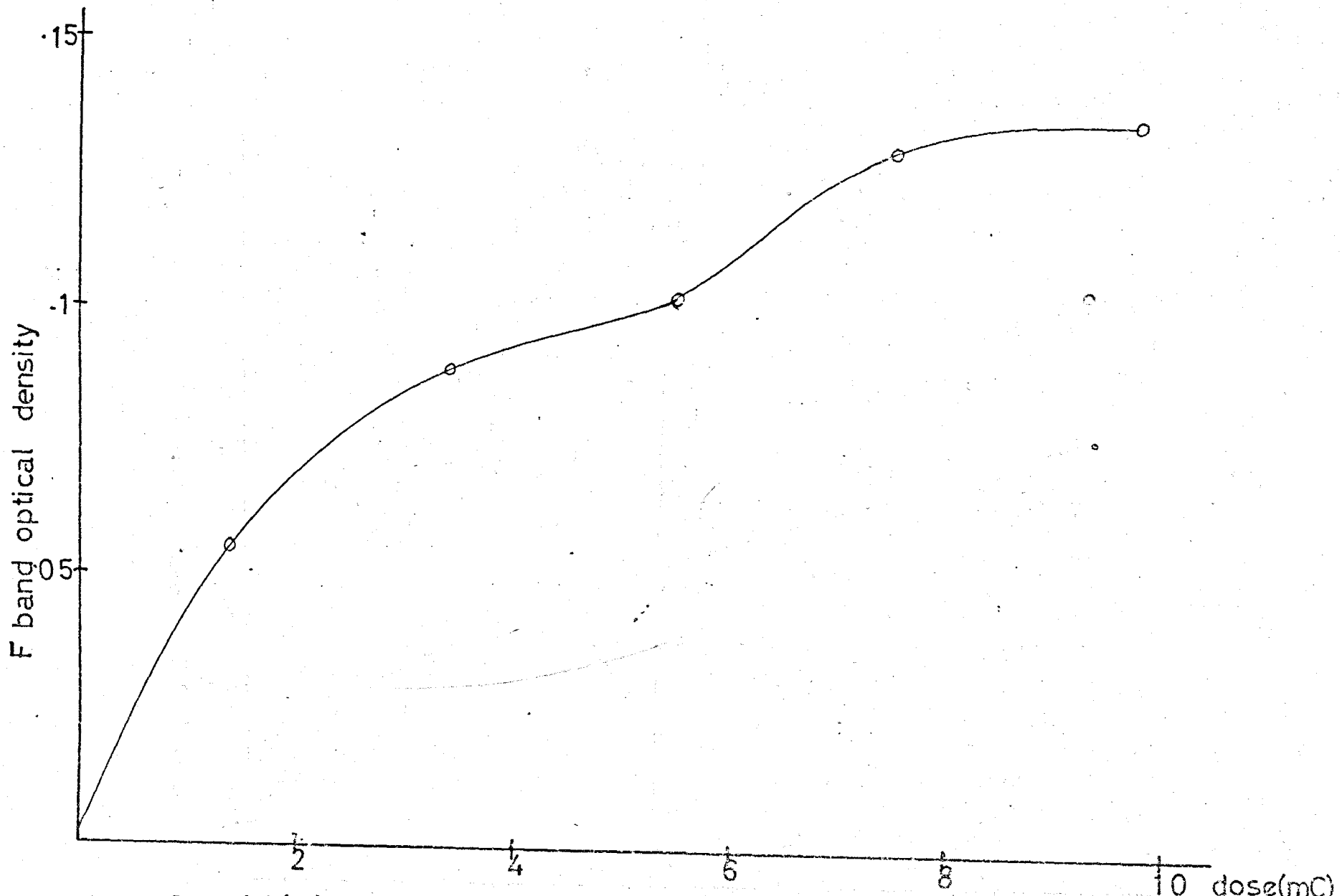

Fig. 33(iv) 100 kV growth curve: G64

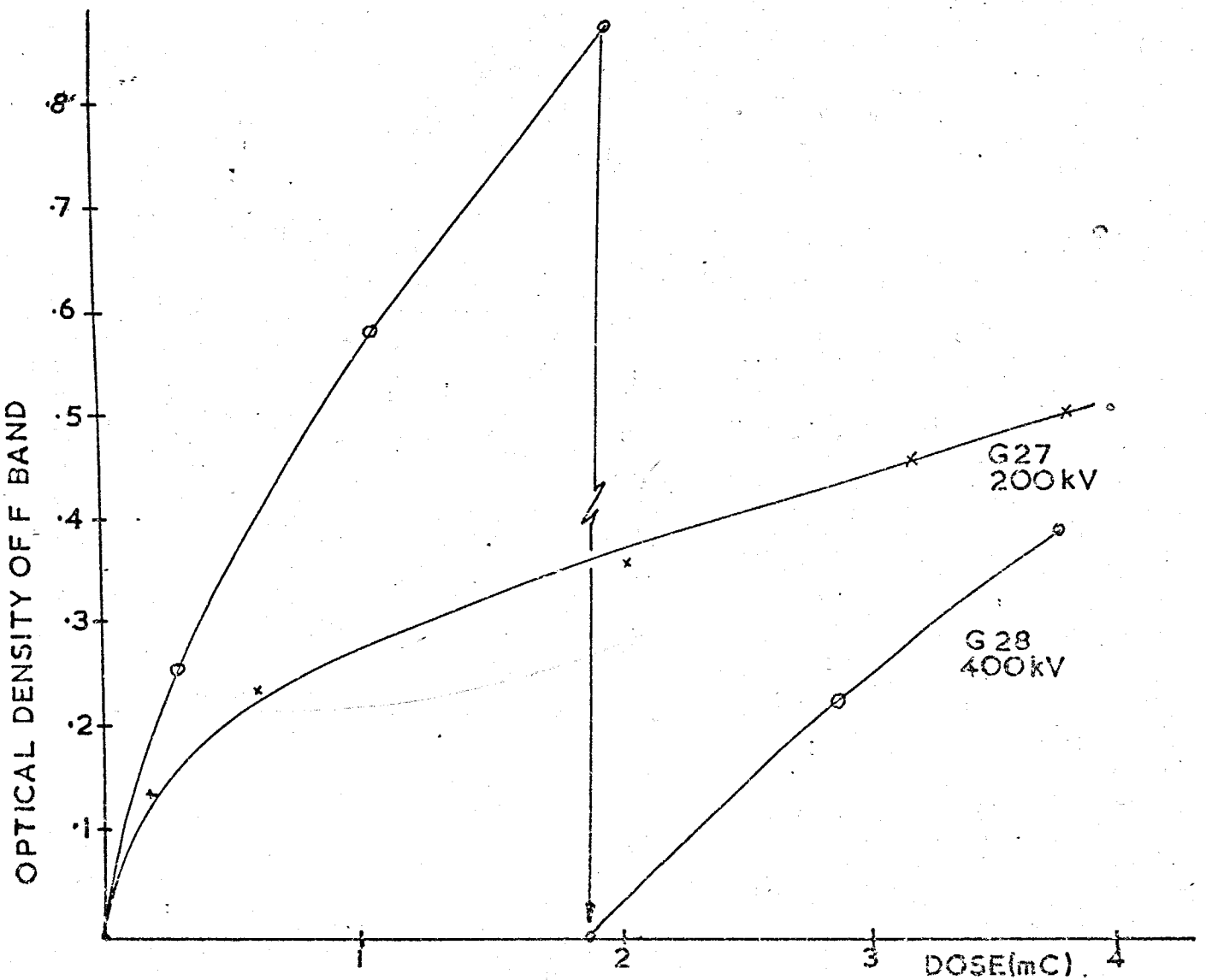

Fig.34(i) Growth of F band at RT: Harshaw NaBr

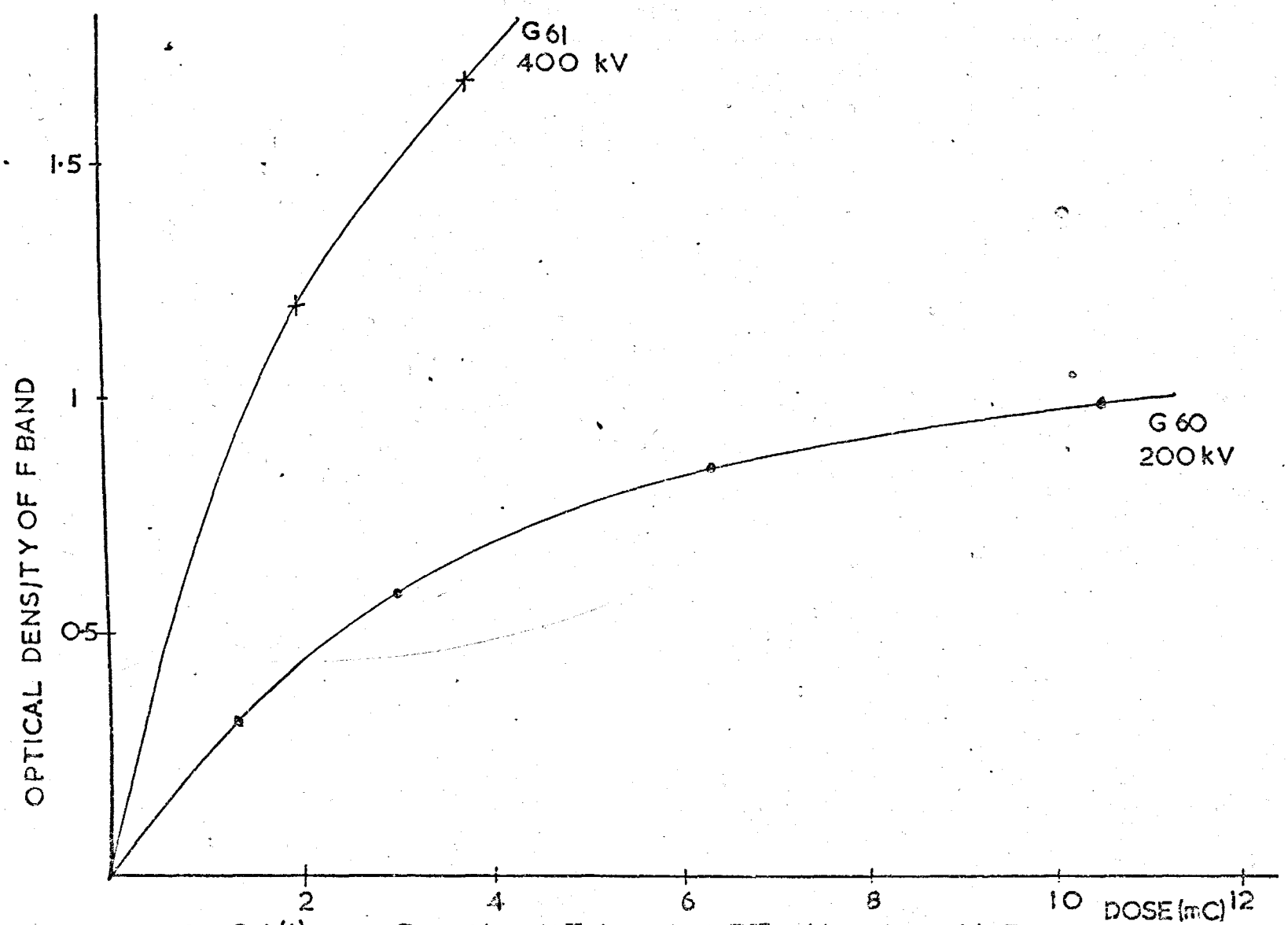

Fig 34(ii) Growth of F band at RT : Harshaw NaBr

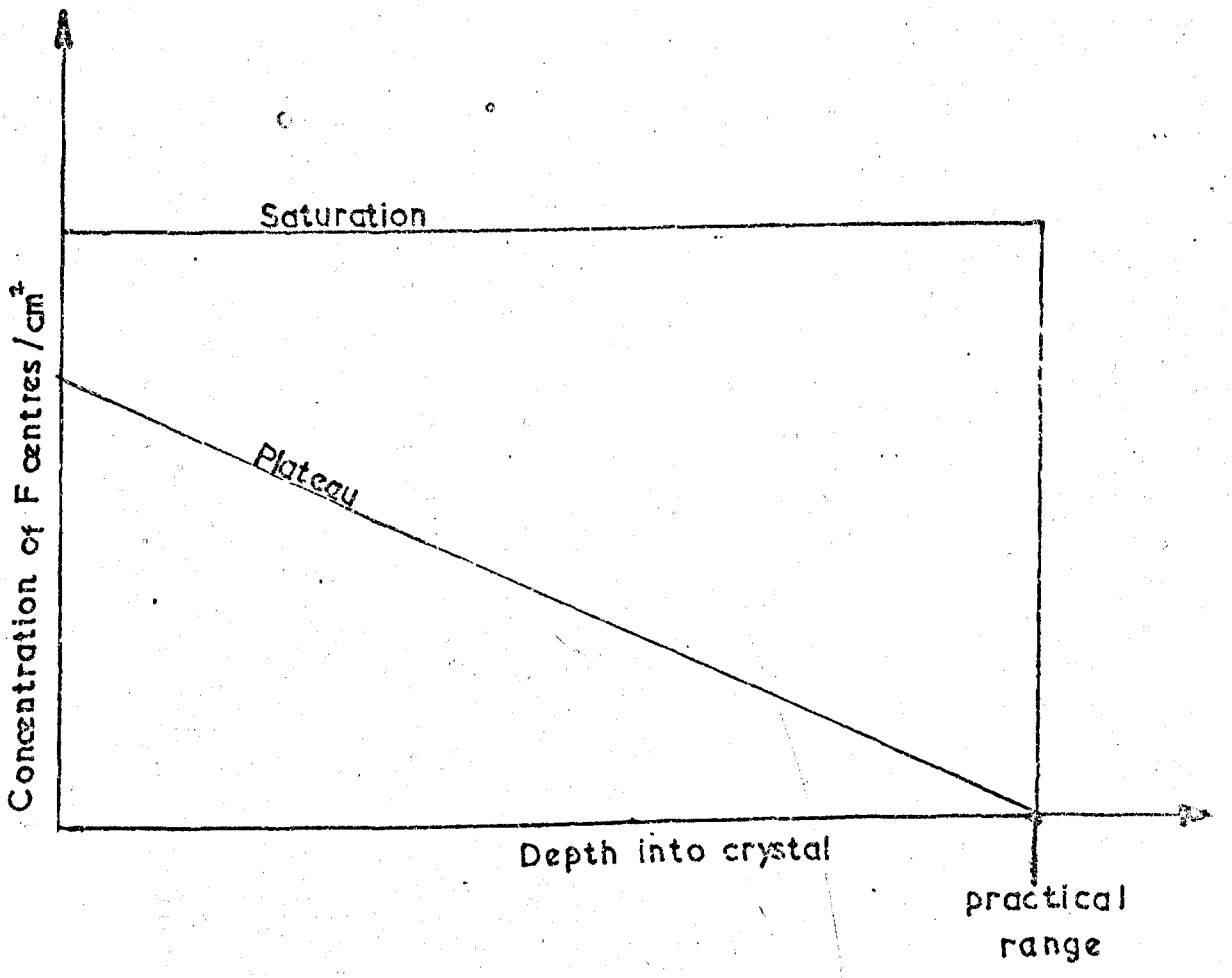

Fig. 3.6.(i) Assumed distributions

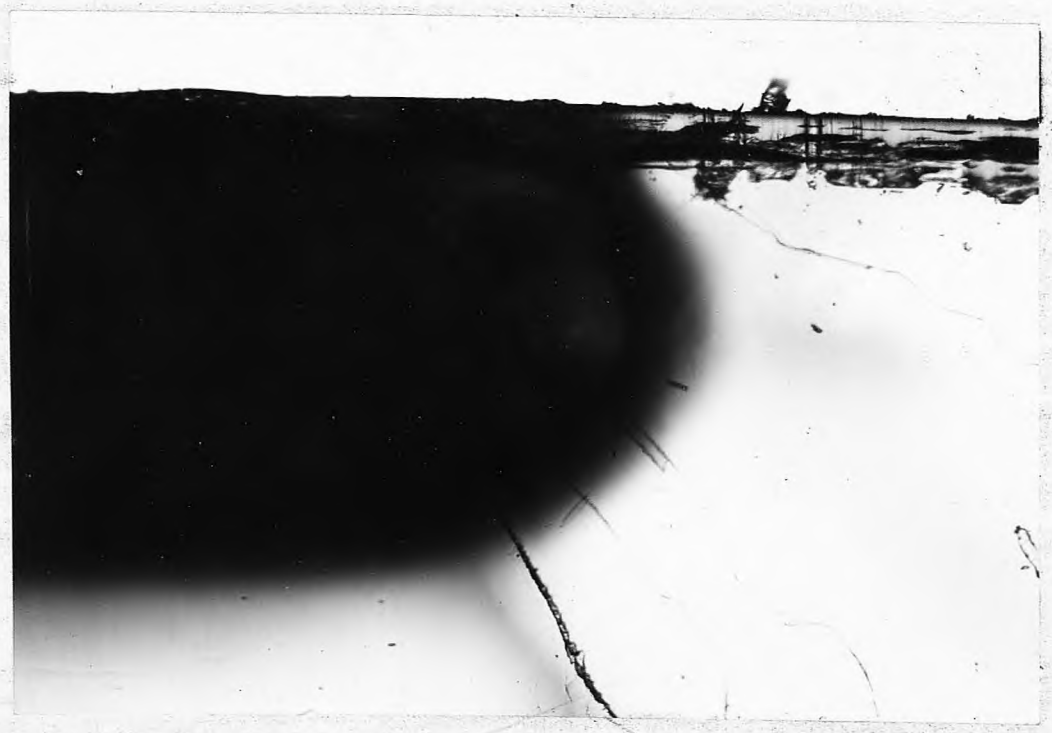

Fig. 4.2.(i) NaCl : colour penetration x100

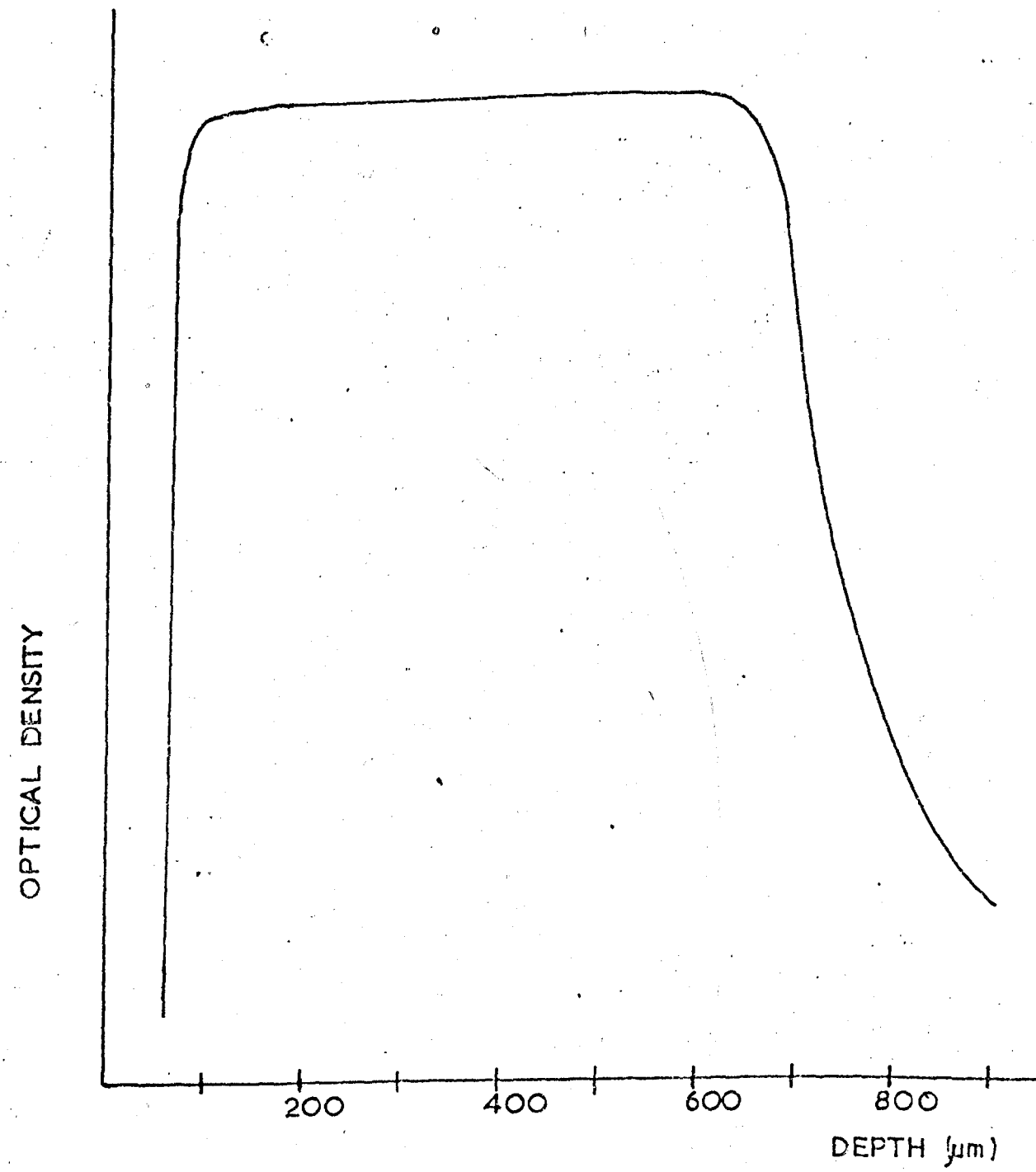

Fig. 4.2.(ii) Microdensitometer trace of 4.2.(i)

Fig. 4.2.(iii) KI: colour penetration in stressed material x80

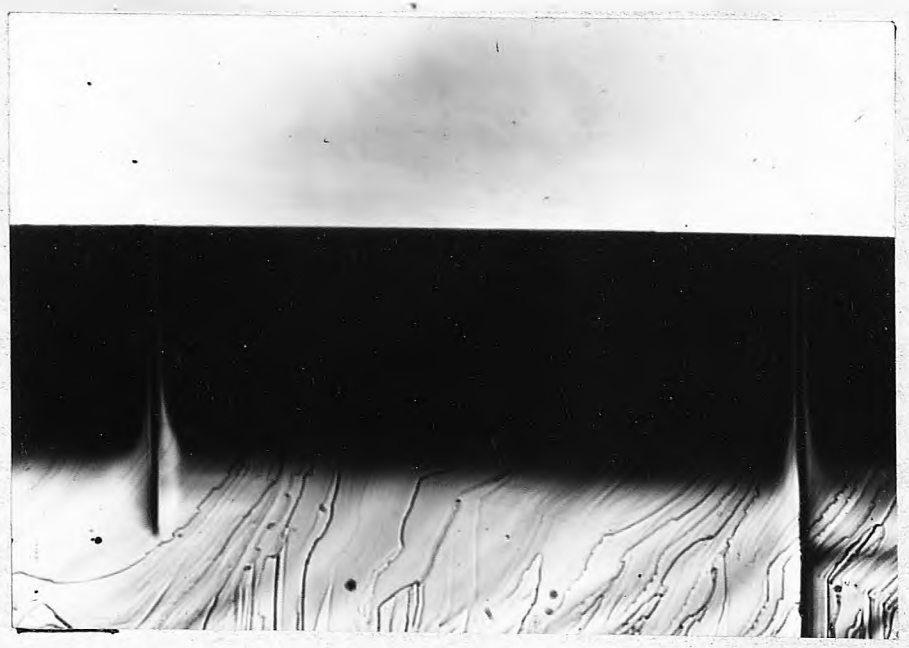

Fig.4.2(iv) KI: bleaching effect of storage x100

Fig.43.(i) x125

Fig.43.(ii) x100

NaBr colour penetration 200 kV & 400 kV : NT

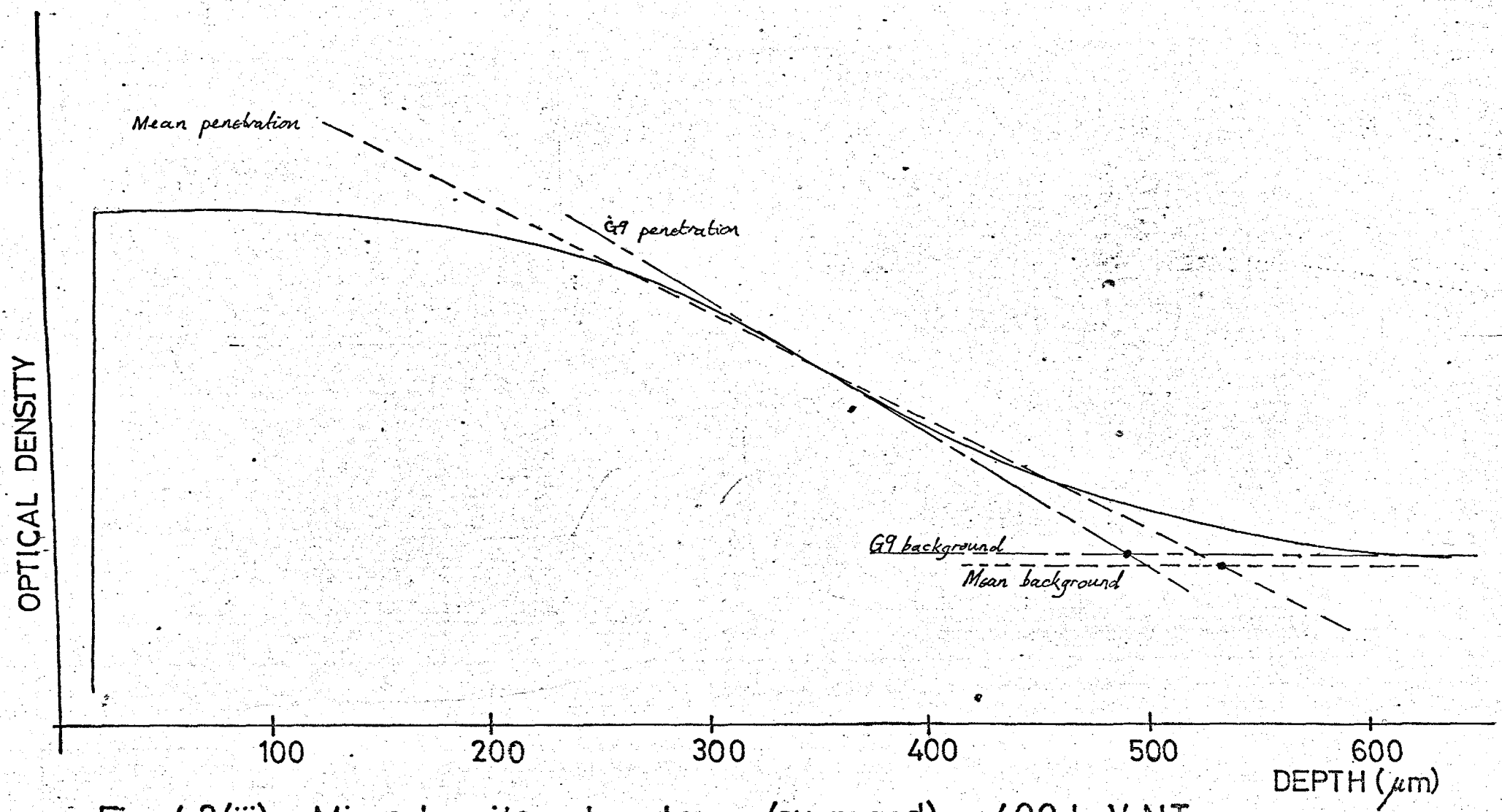

Fig 4.3(iii) Microdensitometer trace (averaged) 400 keV, NT Specimen G9, showing practical range.

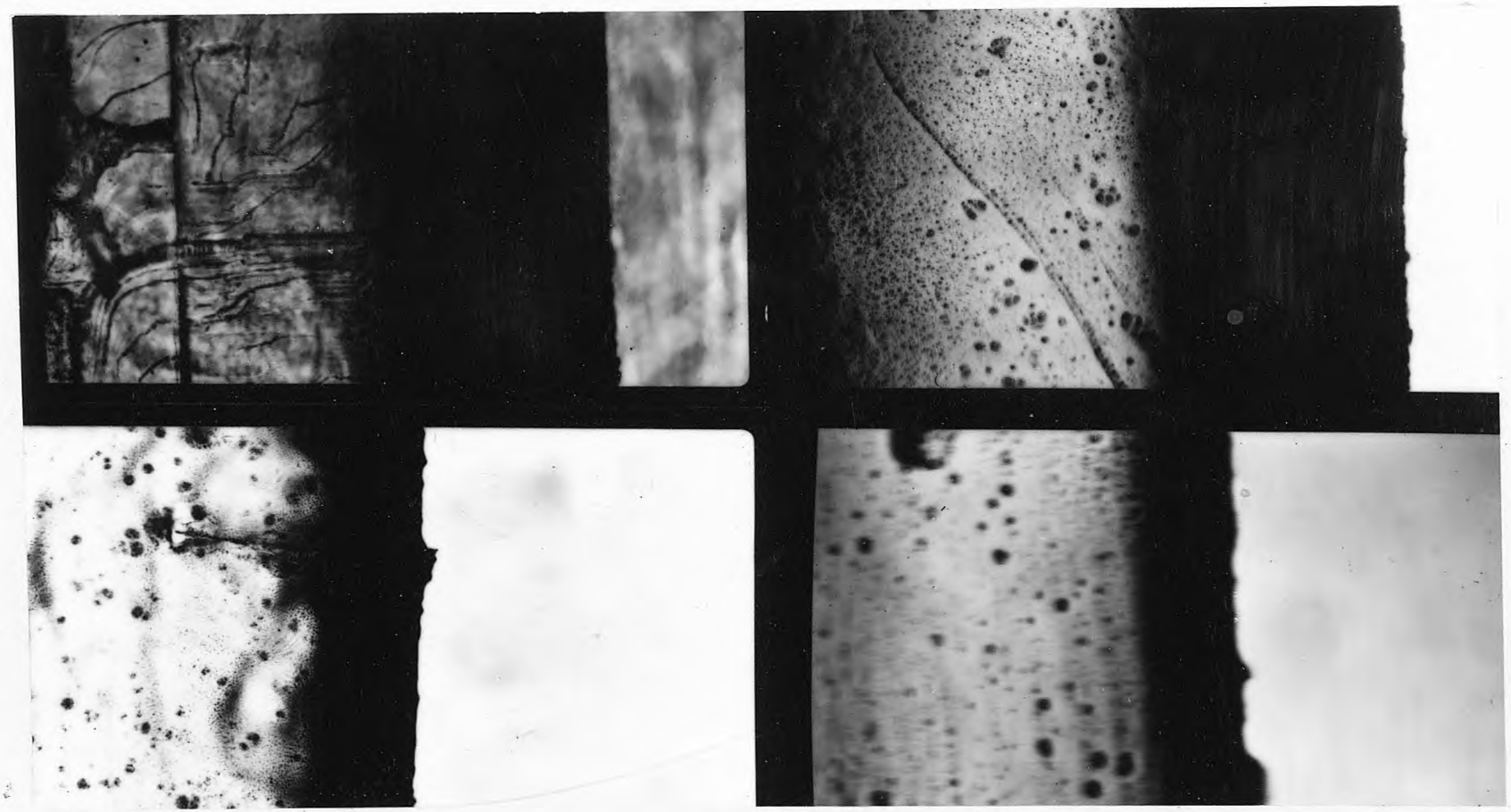

02mm	30mm
03mm	40mm

Fig 43(iv), (a)&(b)

Fig 43(v), (a)&(b)

Variation of apparent penetration with sample thickness

(NaBr, 400 & 200keV, RT, x80)

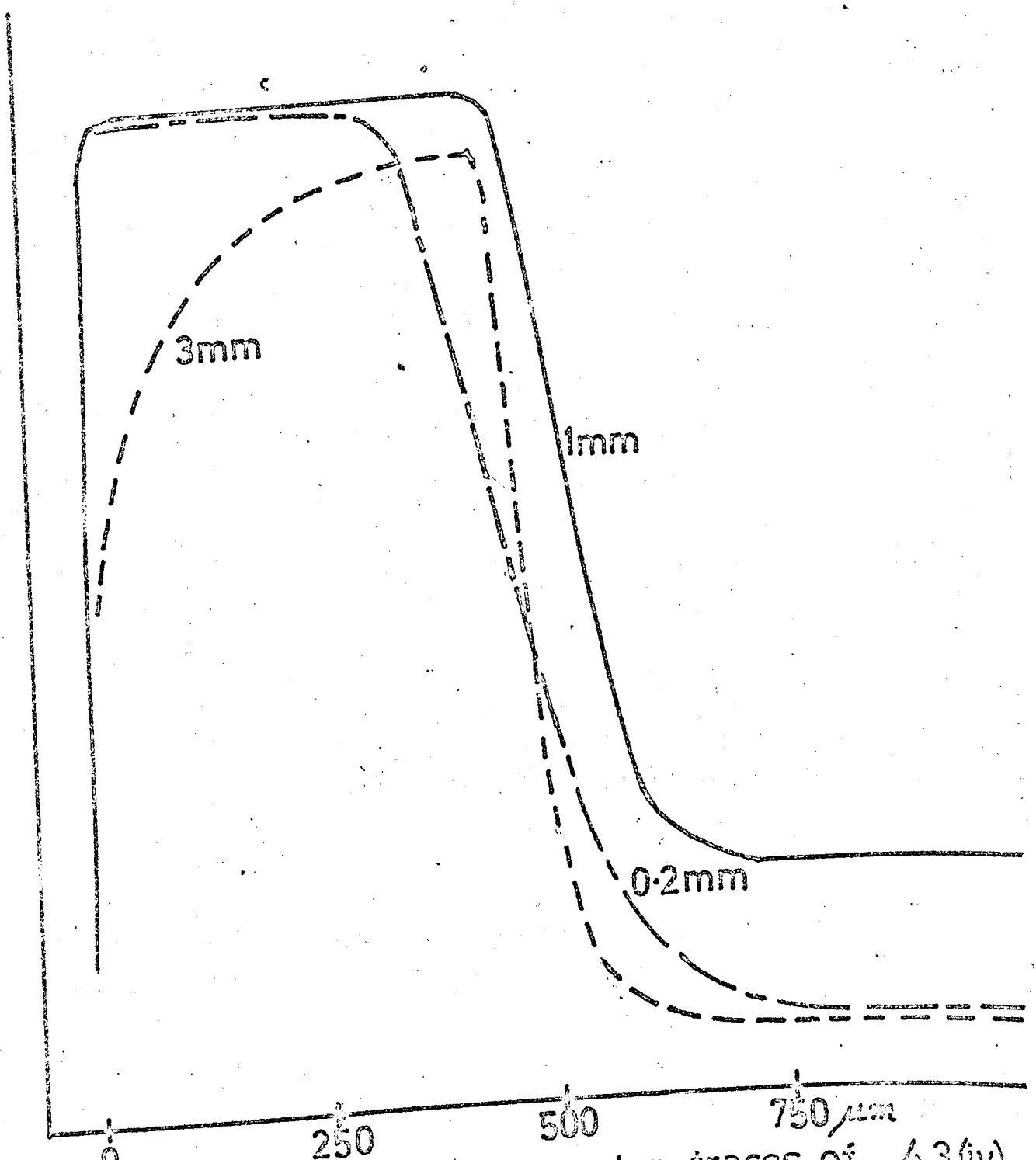

Fig. 4.3(vi) Microdensitometer traces of 4.3(iv)

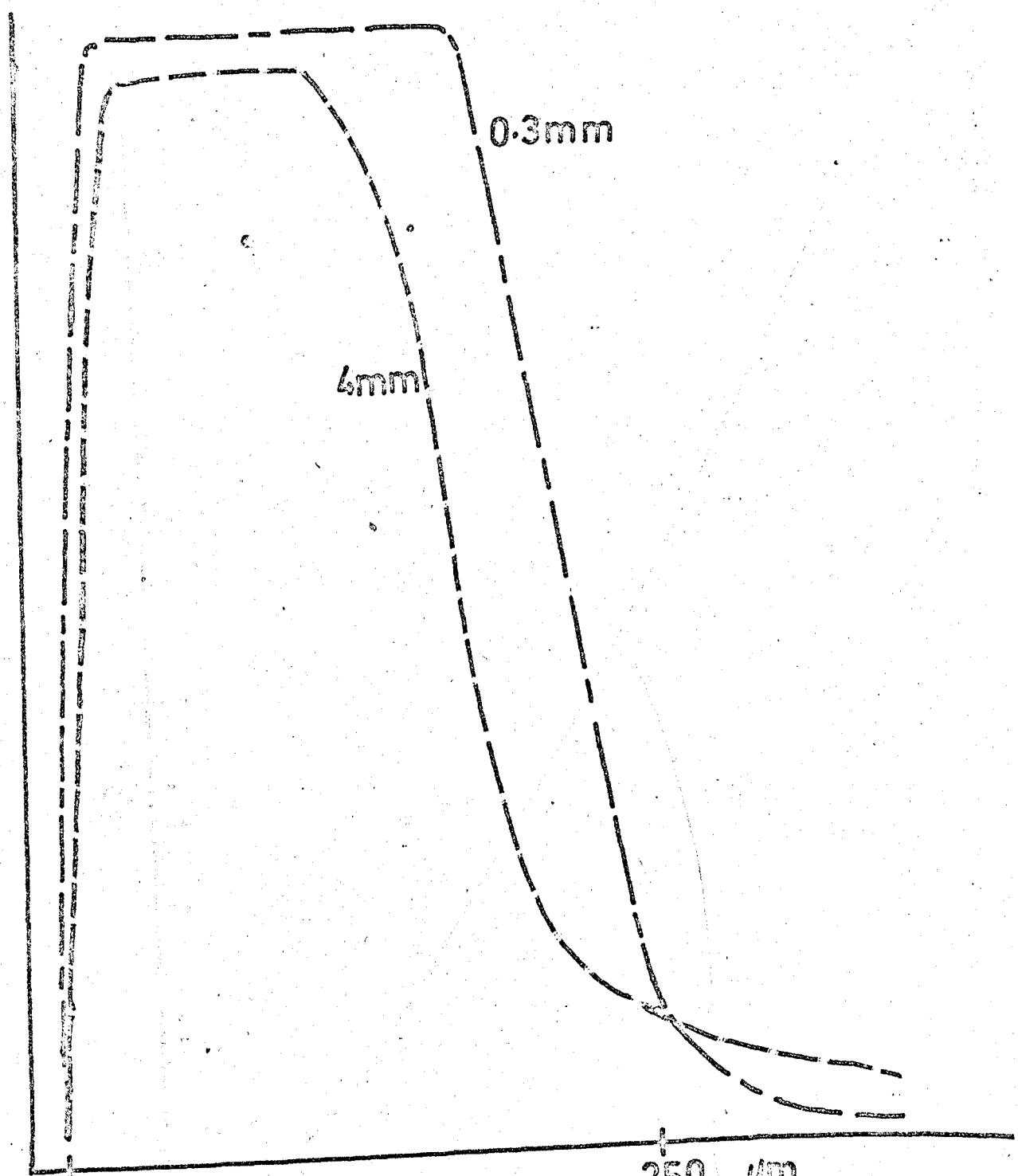

Fig. 43(vii) Microdensitometer trace of Fig. 4.3.(v)

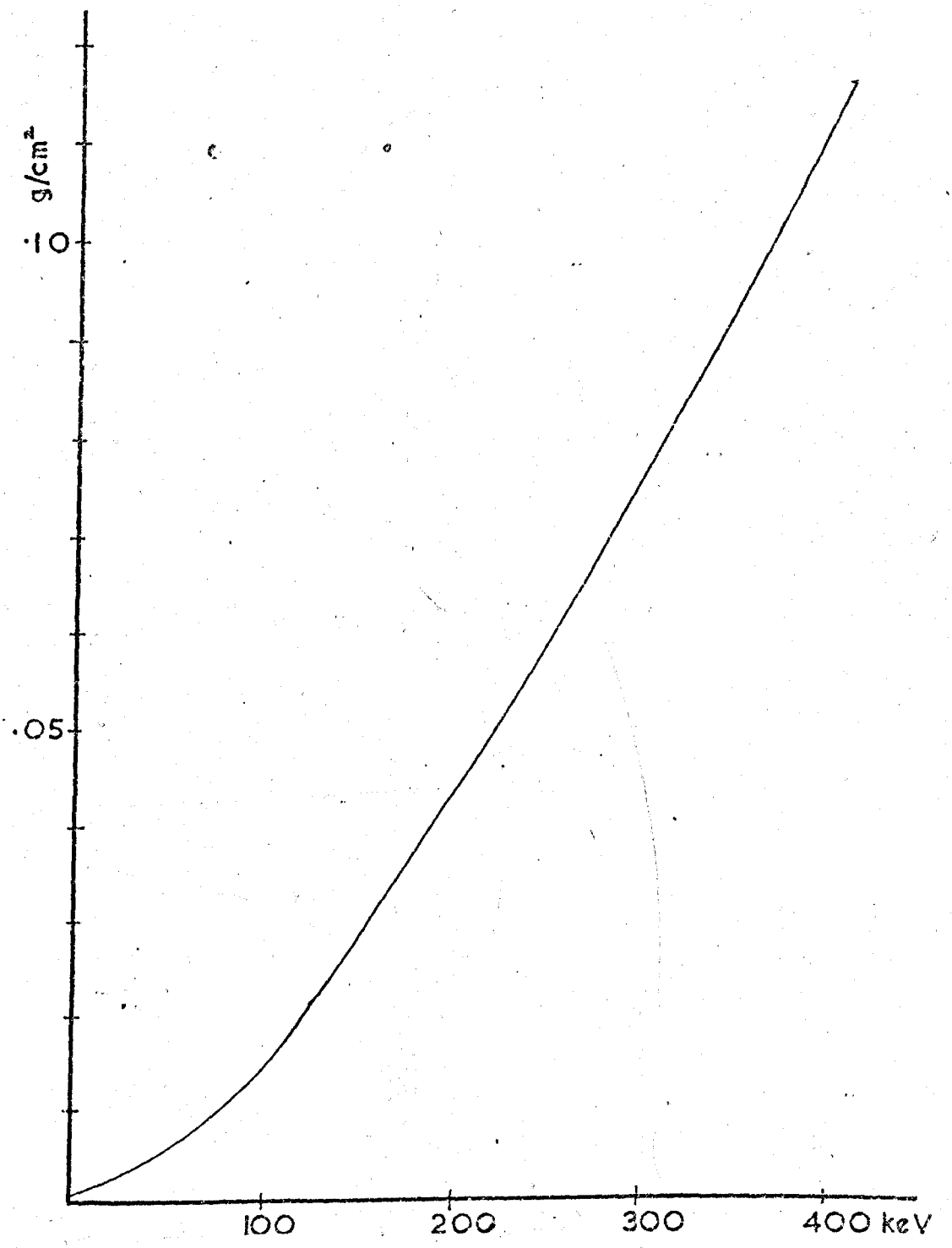

Fig 4.3(viii) Weber practical range vs. energy

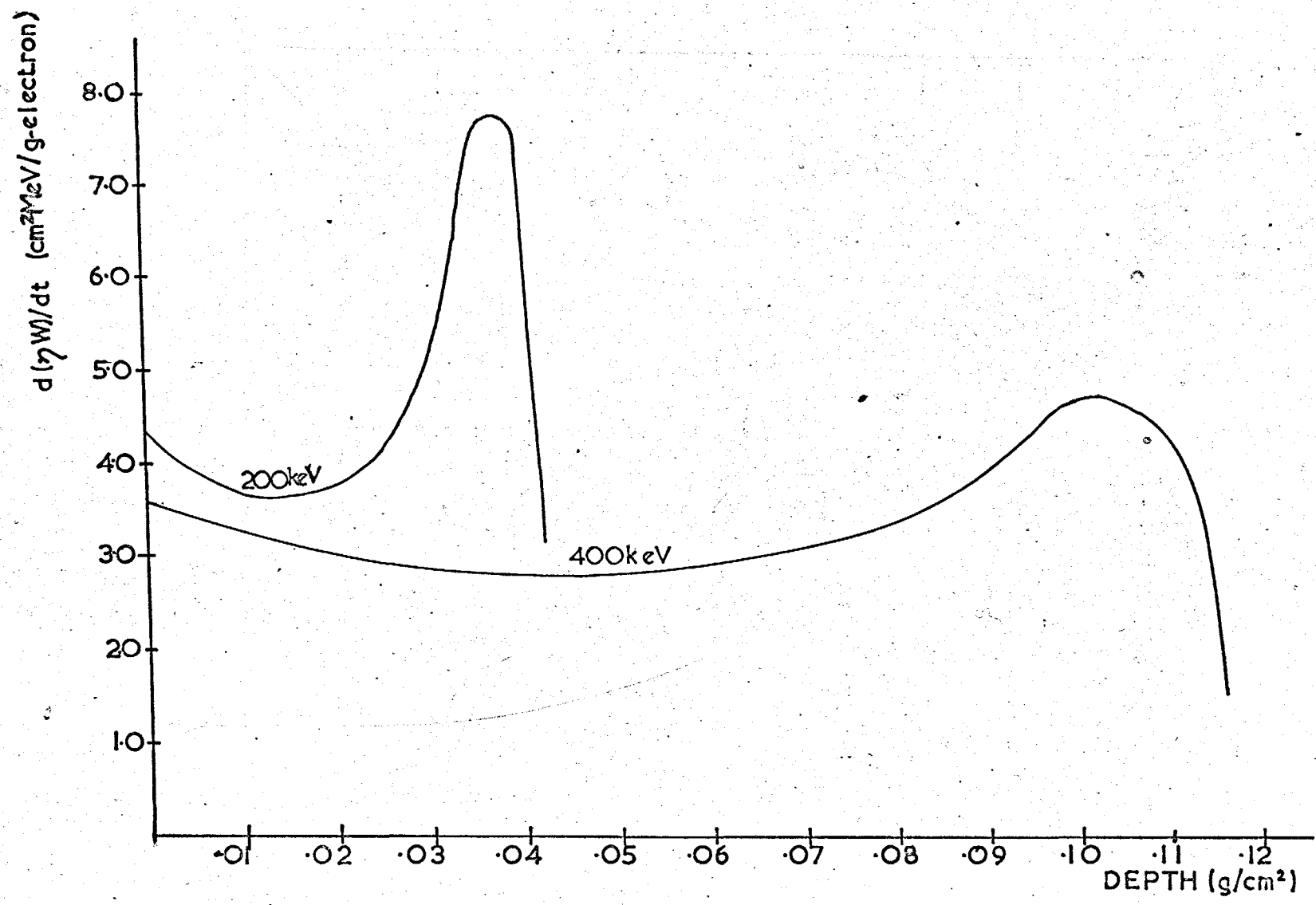

Fig.4.3(ix) Rate of deposition of energy as a function of depth and incident electron energy (NaBr)

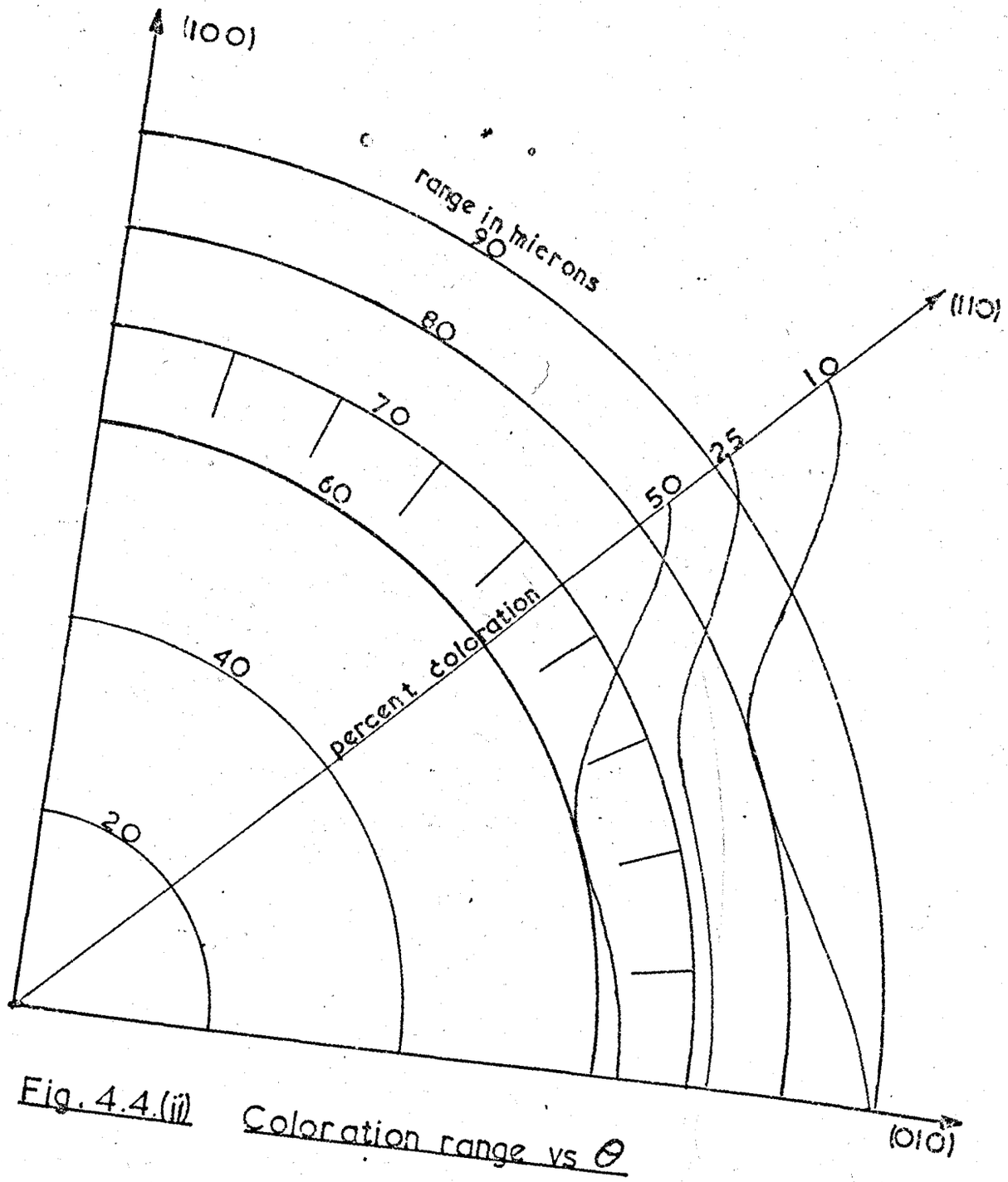

Fig. 4.4.(ii) Coloration range vs θ

Fig 4 4 (ii) KI: coloration anisotropy x 80

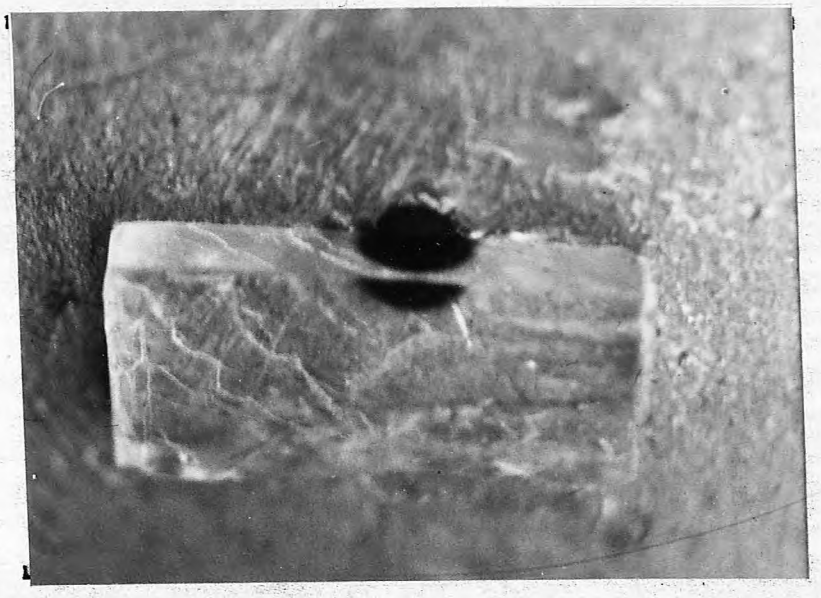

Fig. 4.4(iii) Experimental

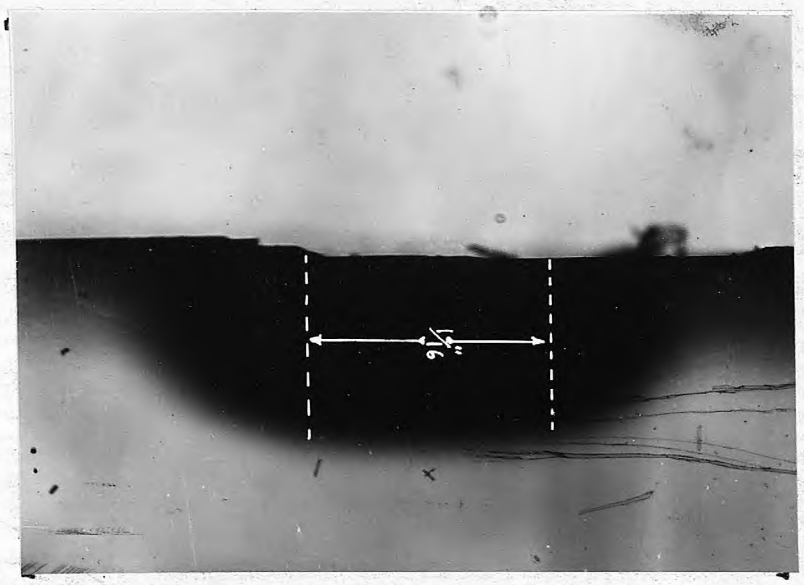

Fig. 4.4(iv) Section

NaCl: lateral spread of coloration

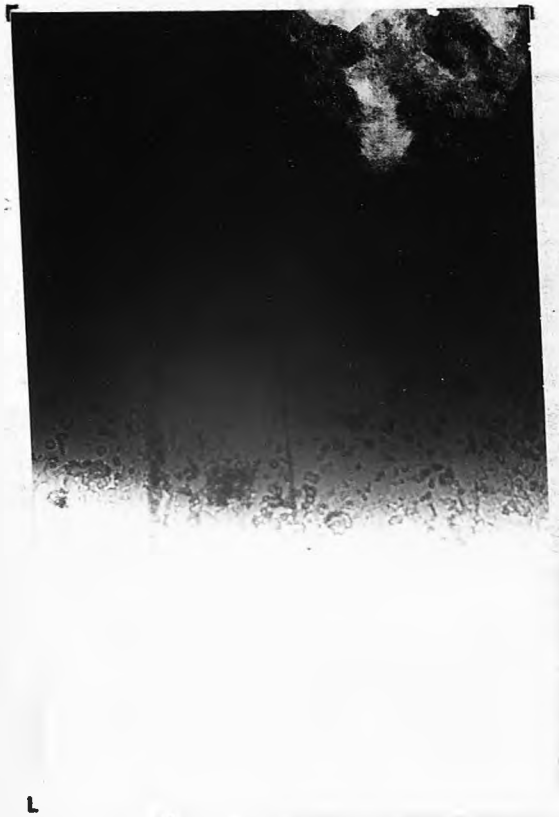

Fig.4.5.(i) x100

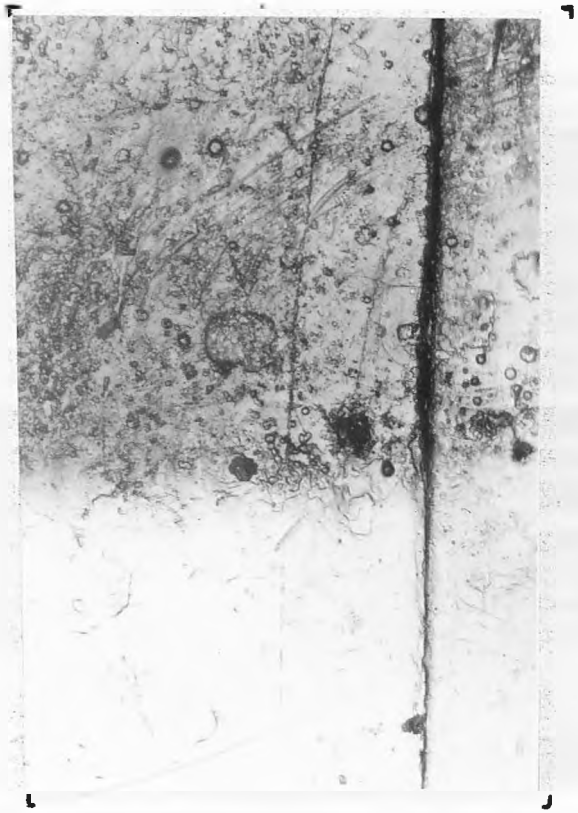

Fig.4.5.(ii) x100

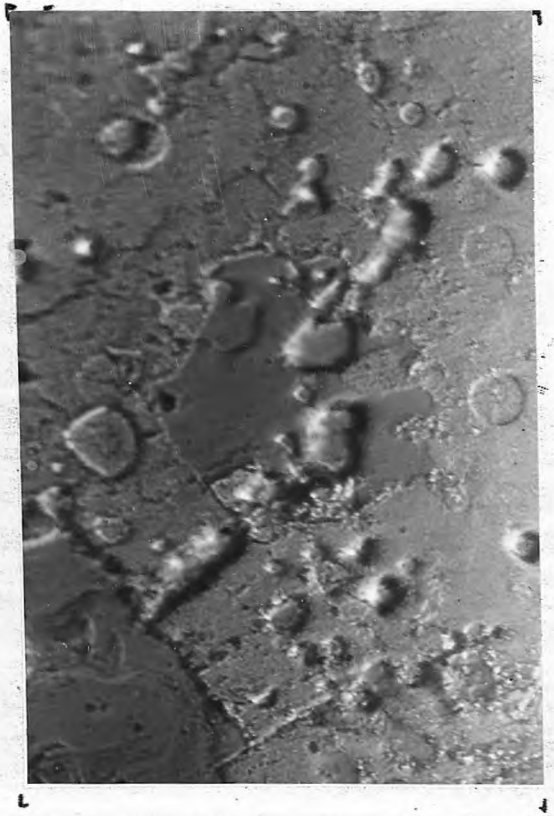

Fig.4.5.(iii) x500

NaCl: surface damage

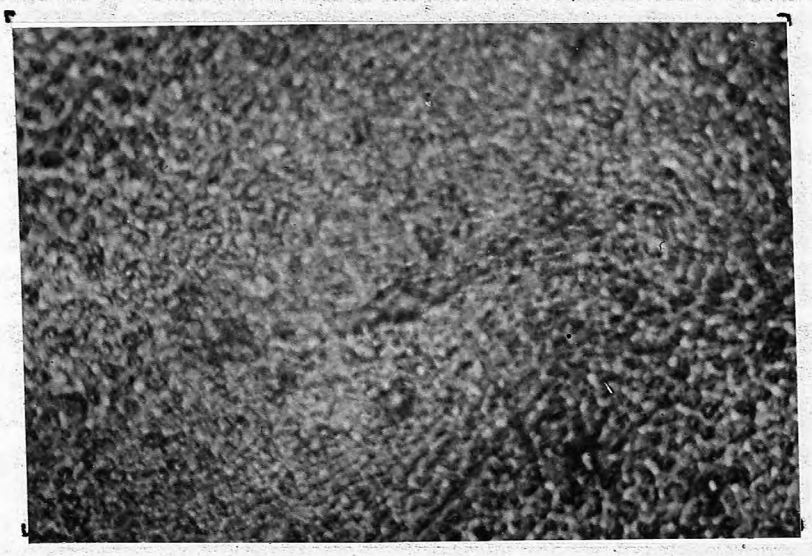

Fig. 4.5.(iv) x80

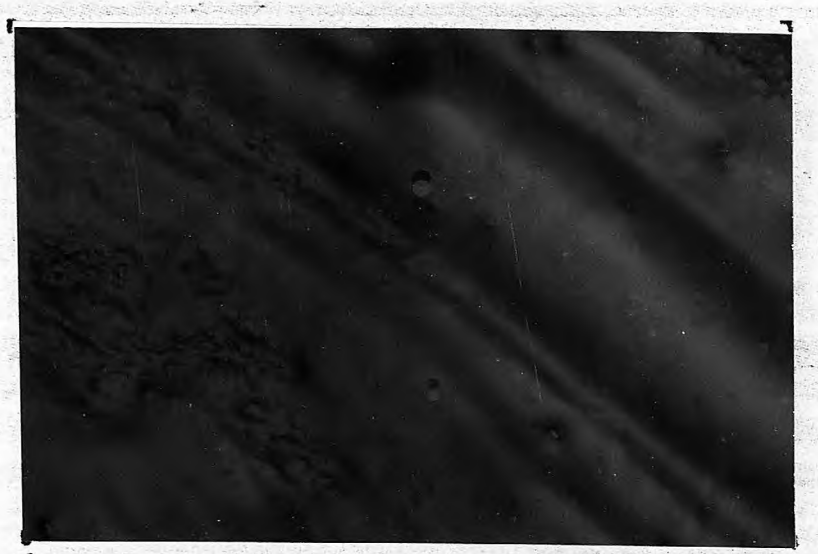

Fig.4.5.(v) x80

NaBr: surface damage 200 kV

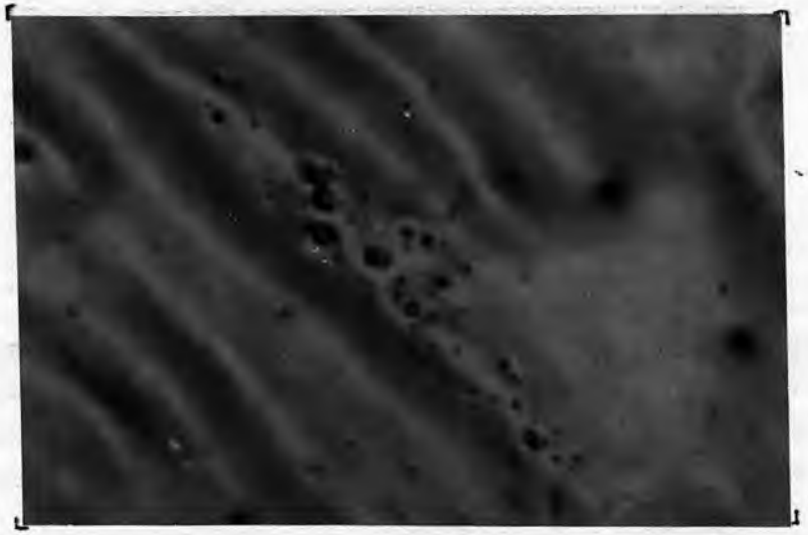

Fig.4.5.(vi) x 80

Fig 4.5.(vii) x 80

Na Br: surface damage 100 kV

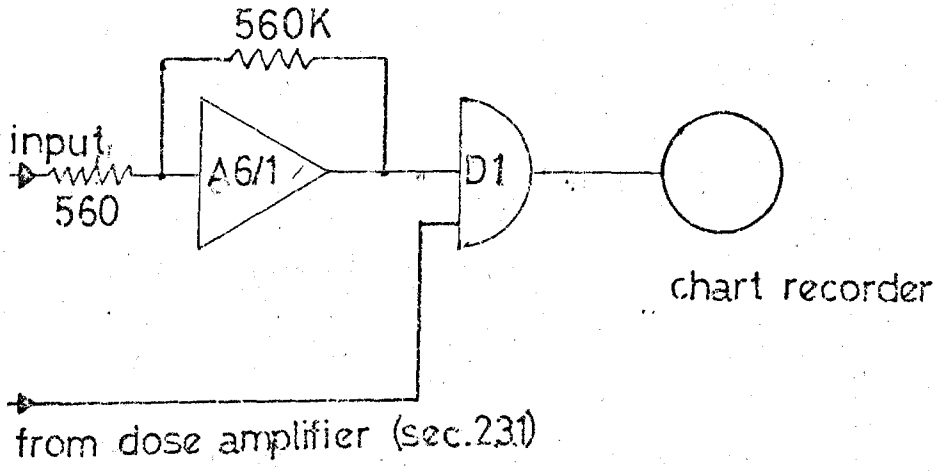

Fig 5.1(i) Principle of analogue divider for luminescence linearity

D1 is an Aricom 2-quadrant divider module

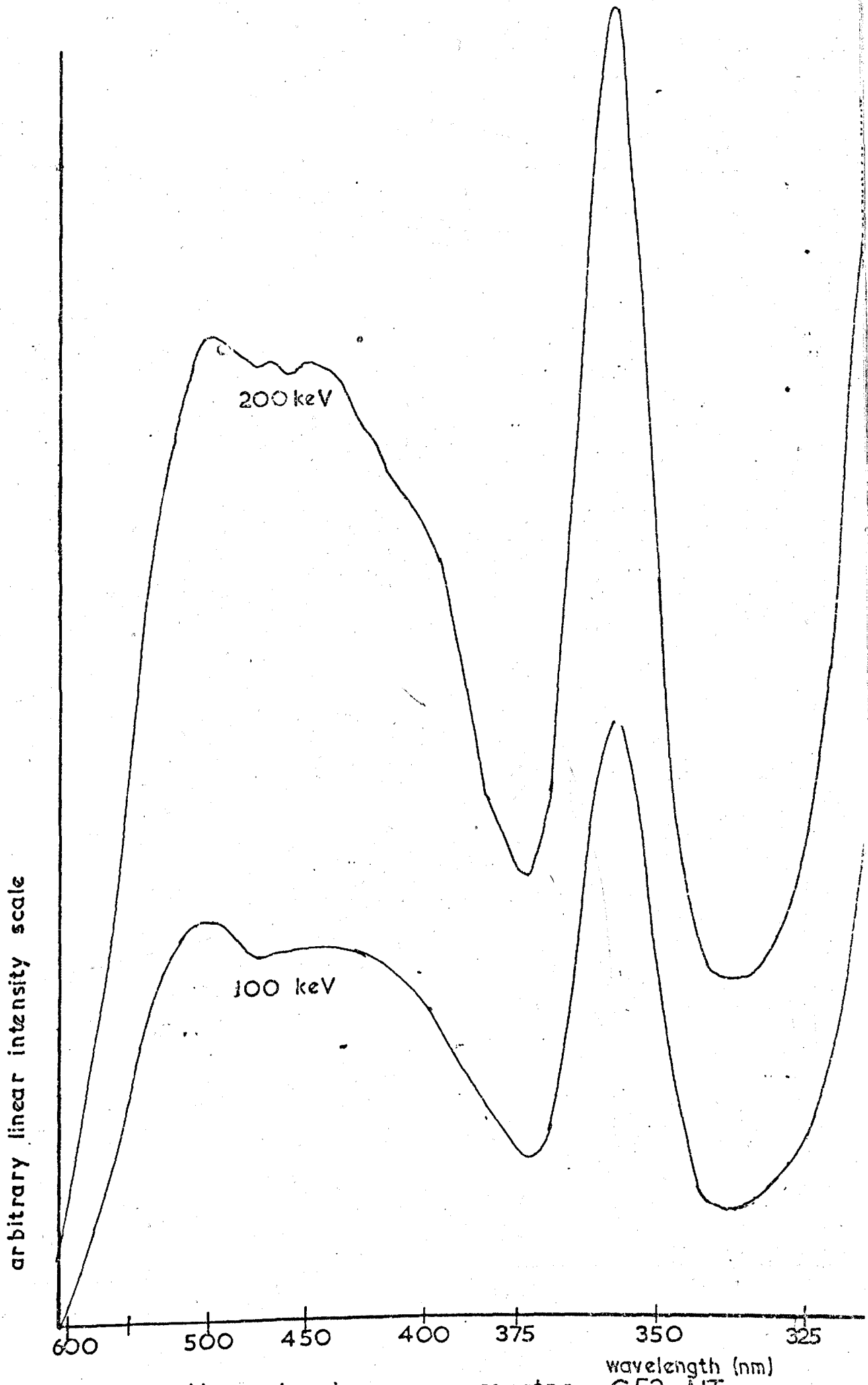

Fig. 5.2(i) Luminescence spectra G52 NT

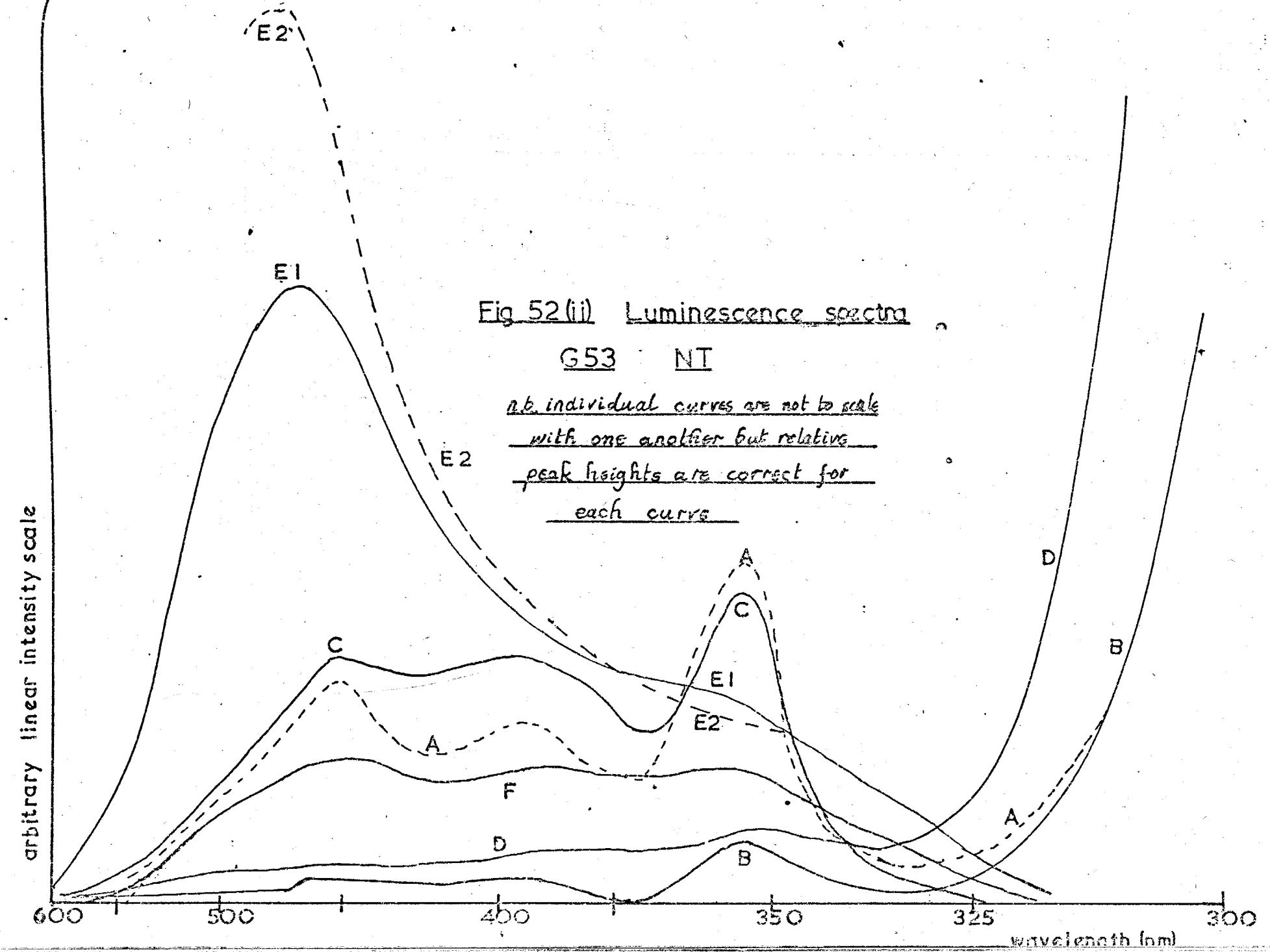

Fig 52(ii) Luminescence spectra

G53 NT

n.b. individual curves are not to scale with one another but relative peak heights are correct for each curve

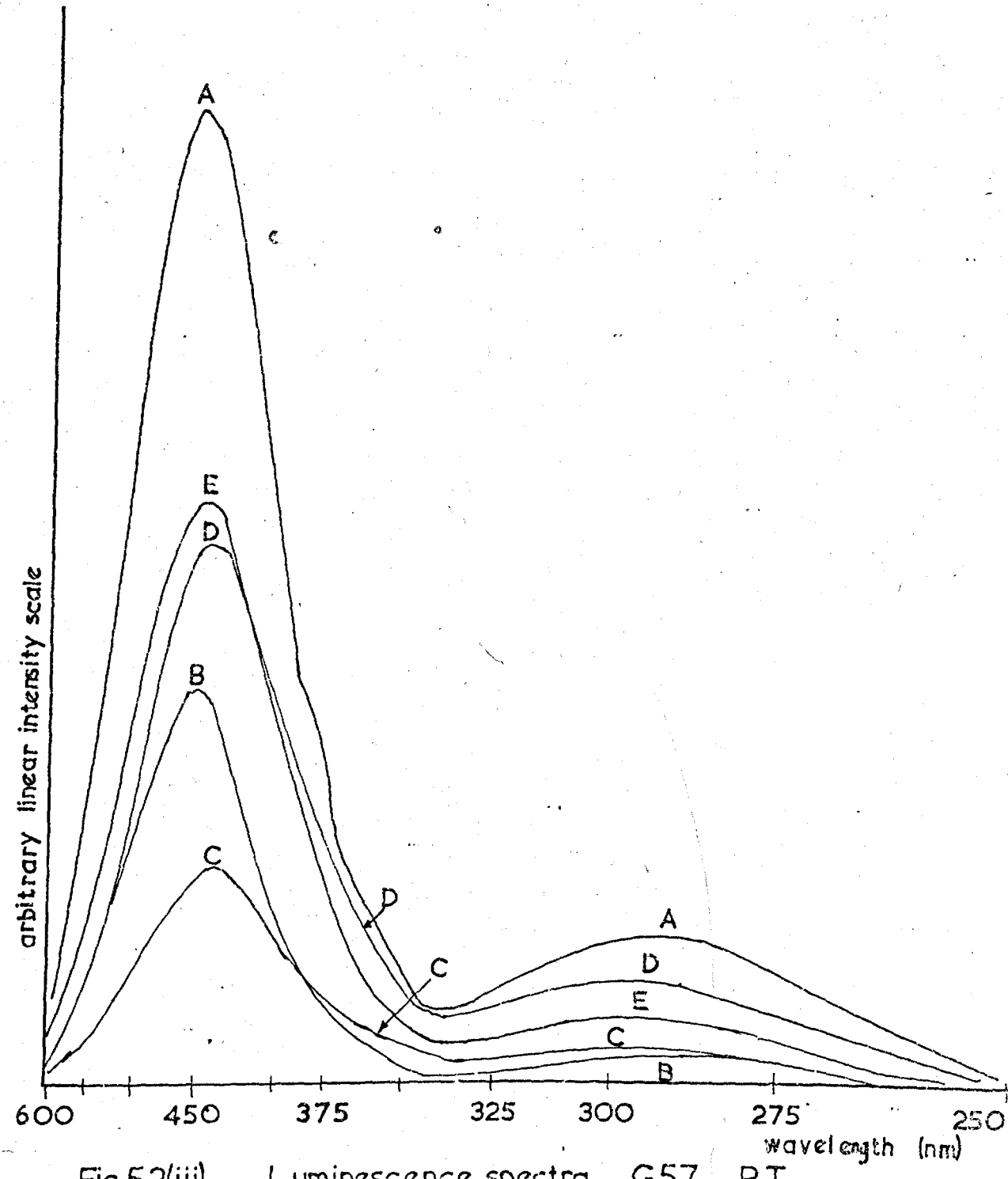

Fig 52(iii) Luminescence spectra G57 RT

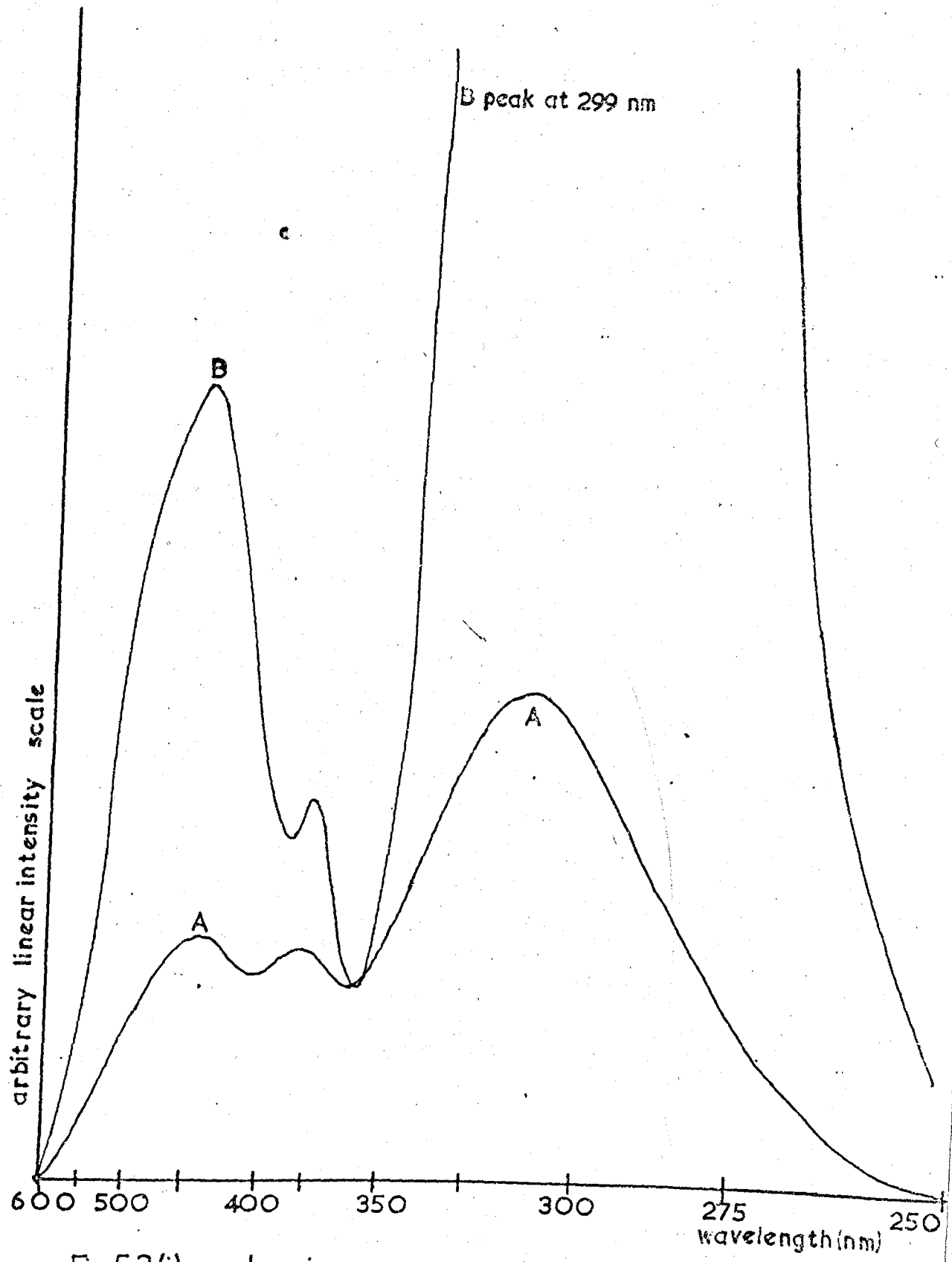

Fig.5.3(i) Luminescence spectra H8 RT & NT

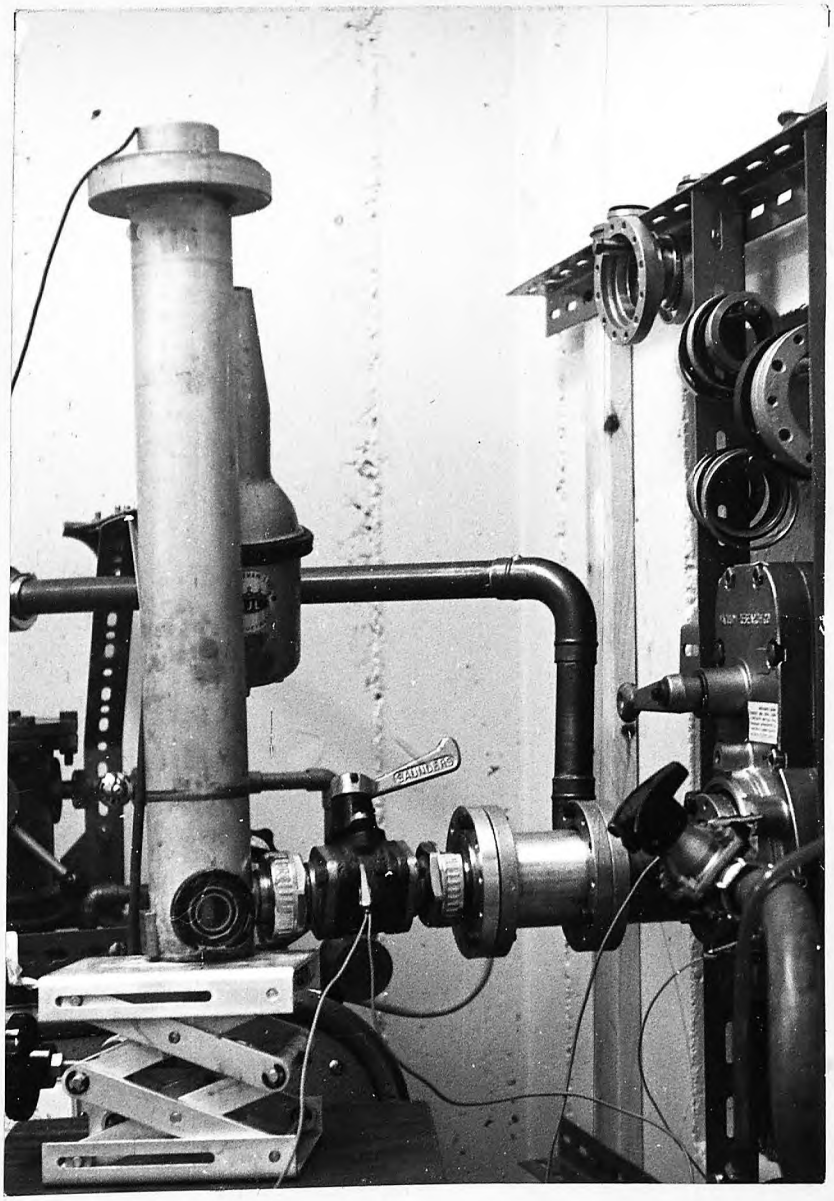

Fig. 6.1.(i) Small cryostat and ball valve

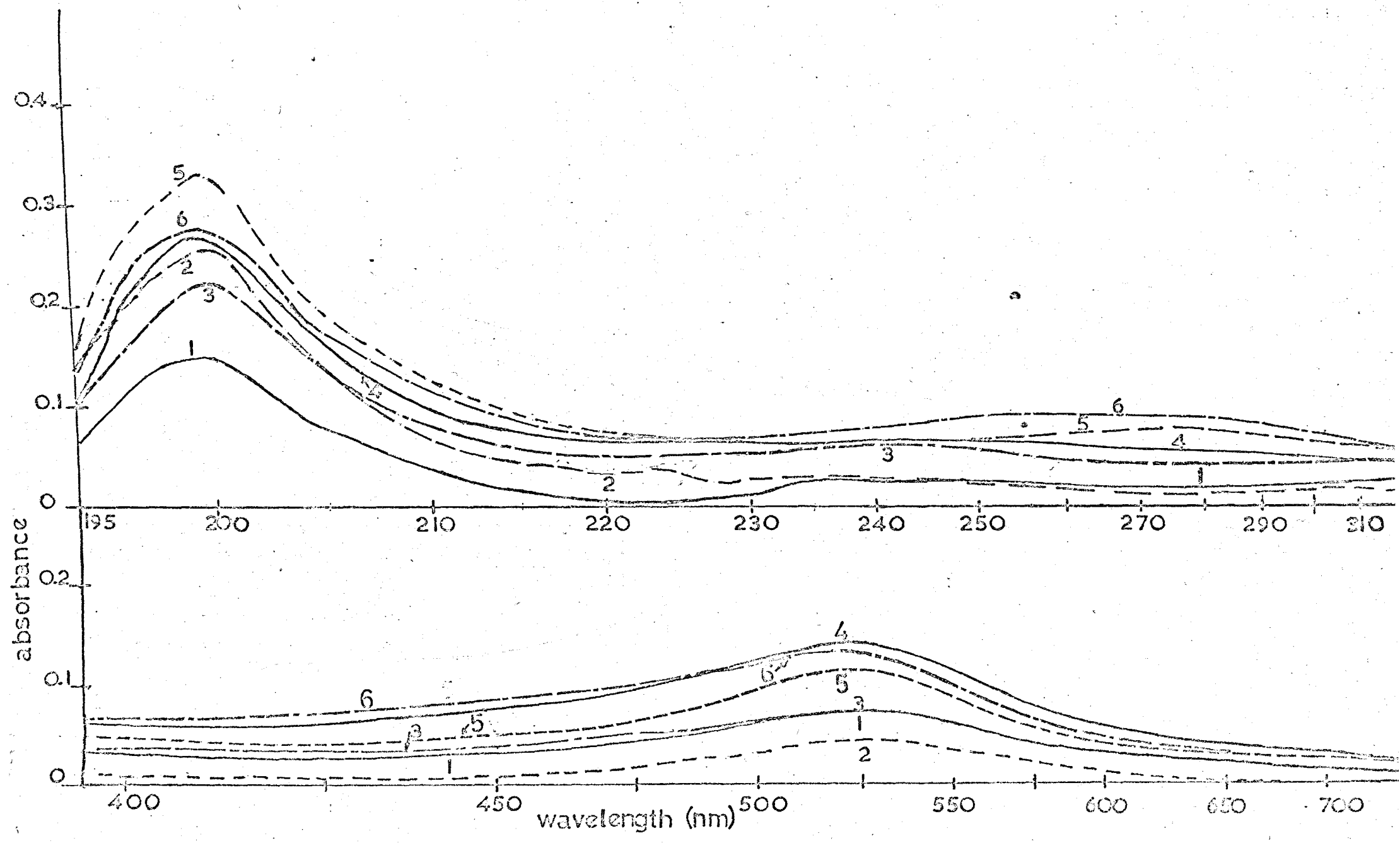

Fig. 6.2(i) Absorption spectra : G80

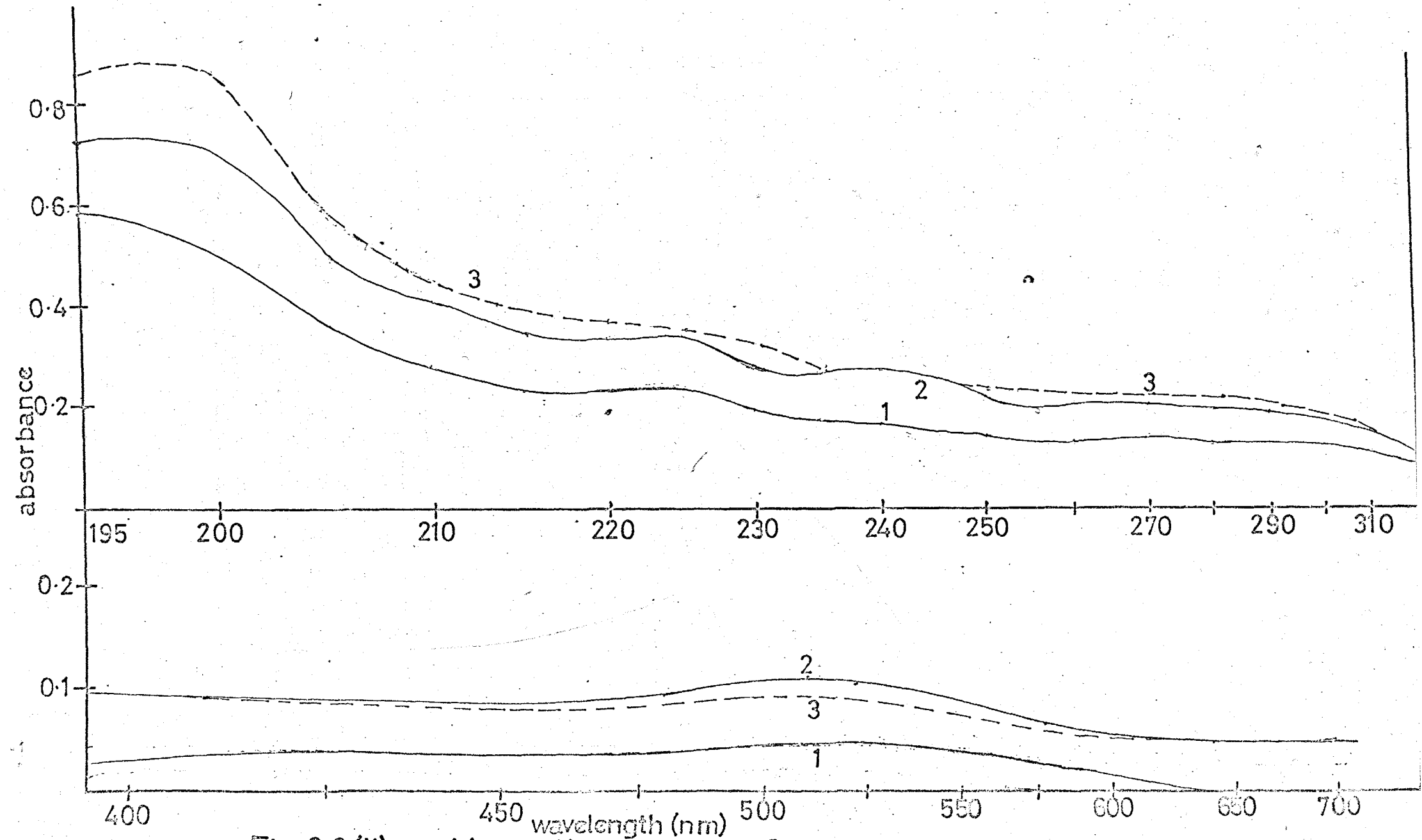

Fig 6.2.(ii) Absorption spectra: G83

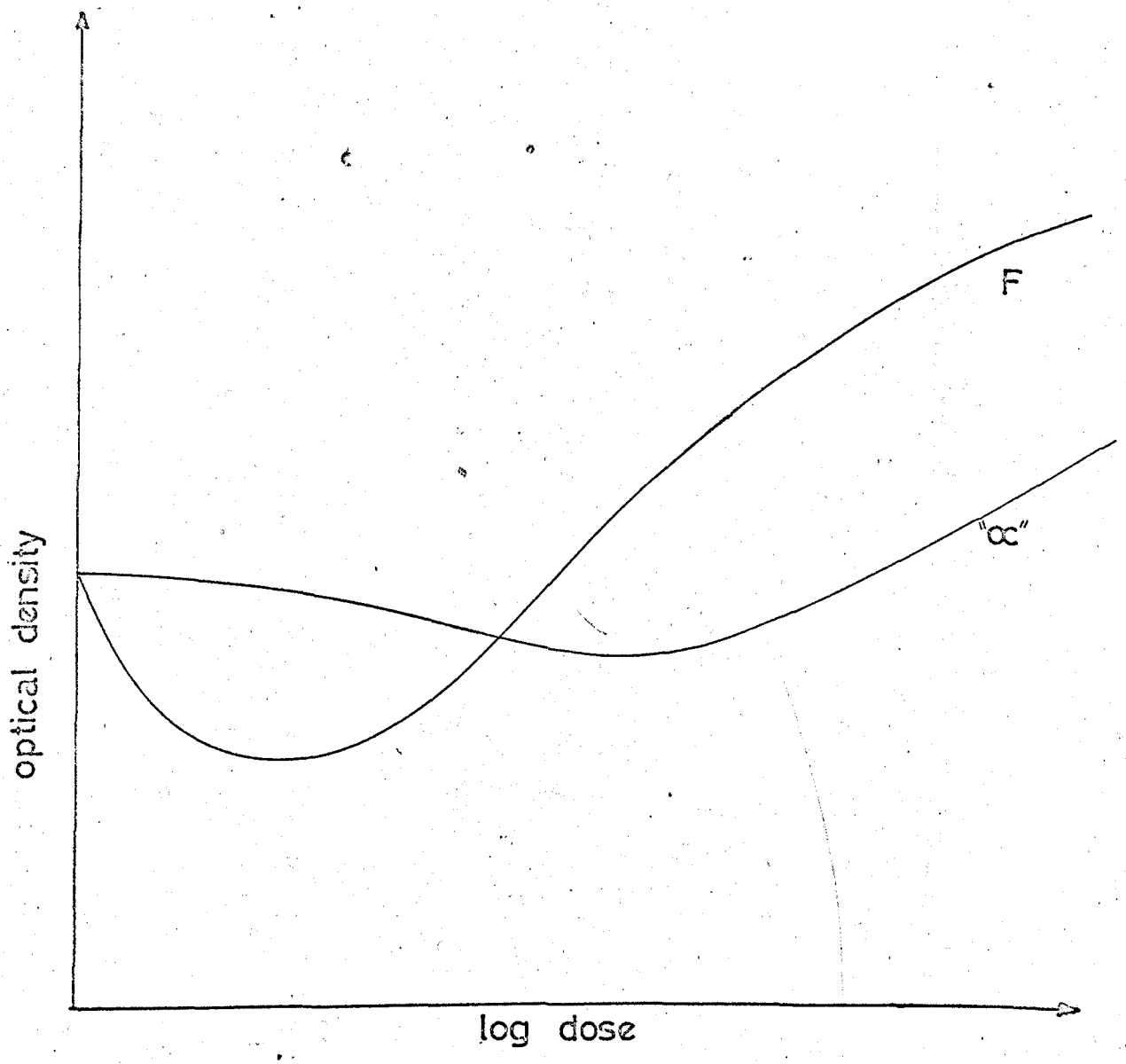

Fig. 6.2.(iii) Qualitative behaviour of bands on reirradiation after stage II F band bleaching

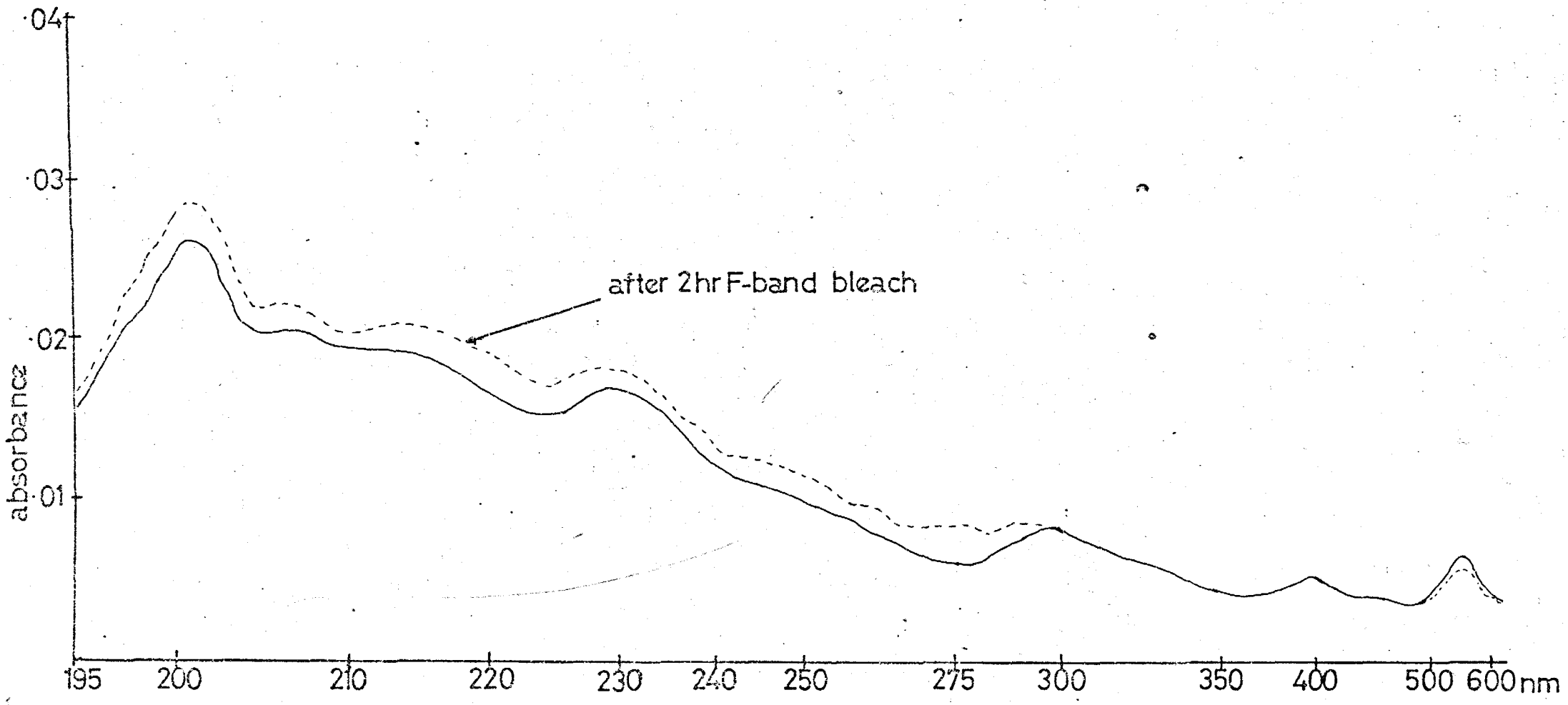

Fig. 6.3(i) Typical absorption spectrum 200 keV stage I G48

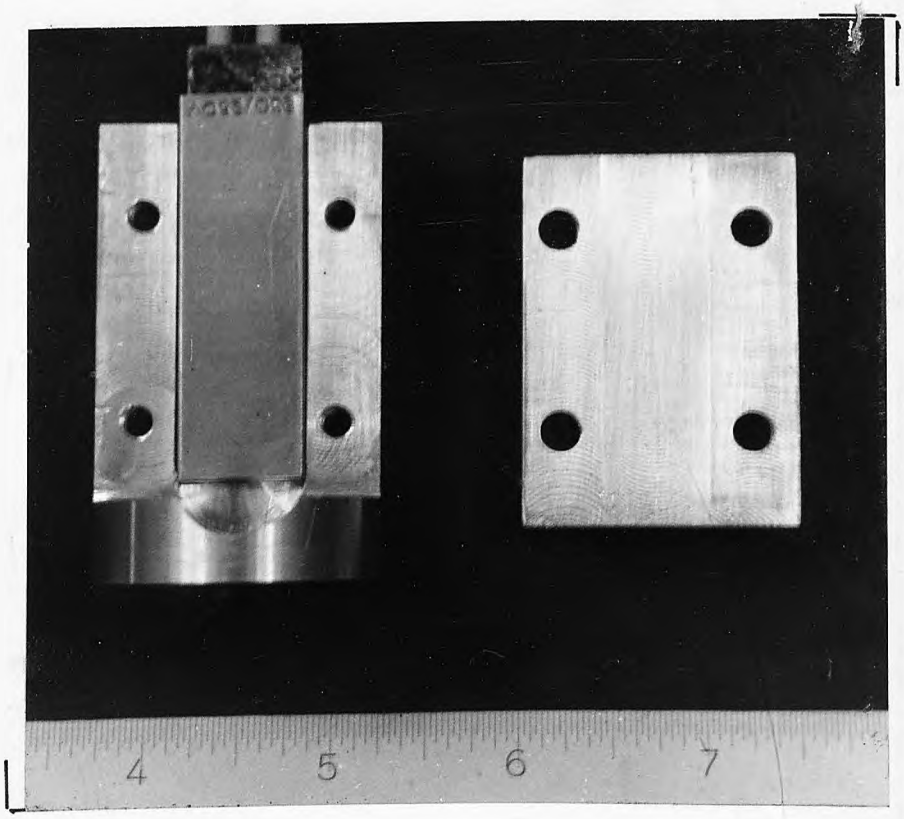

Fig. 6 4(i) Thermode construction

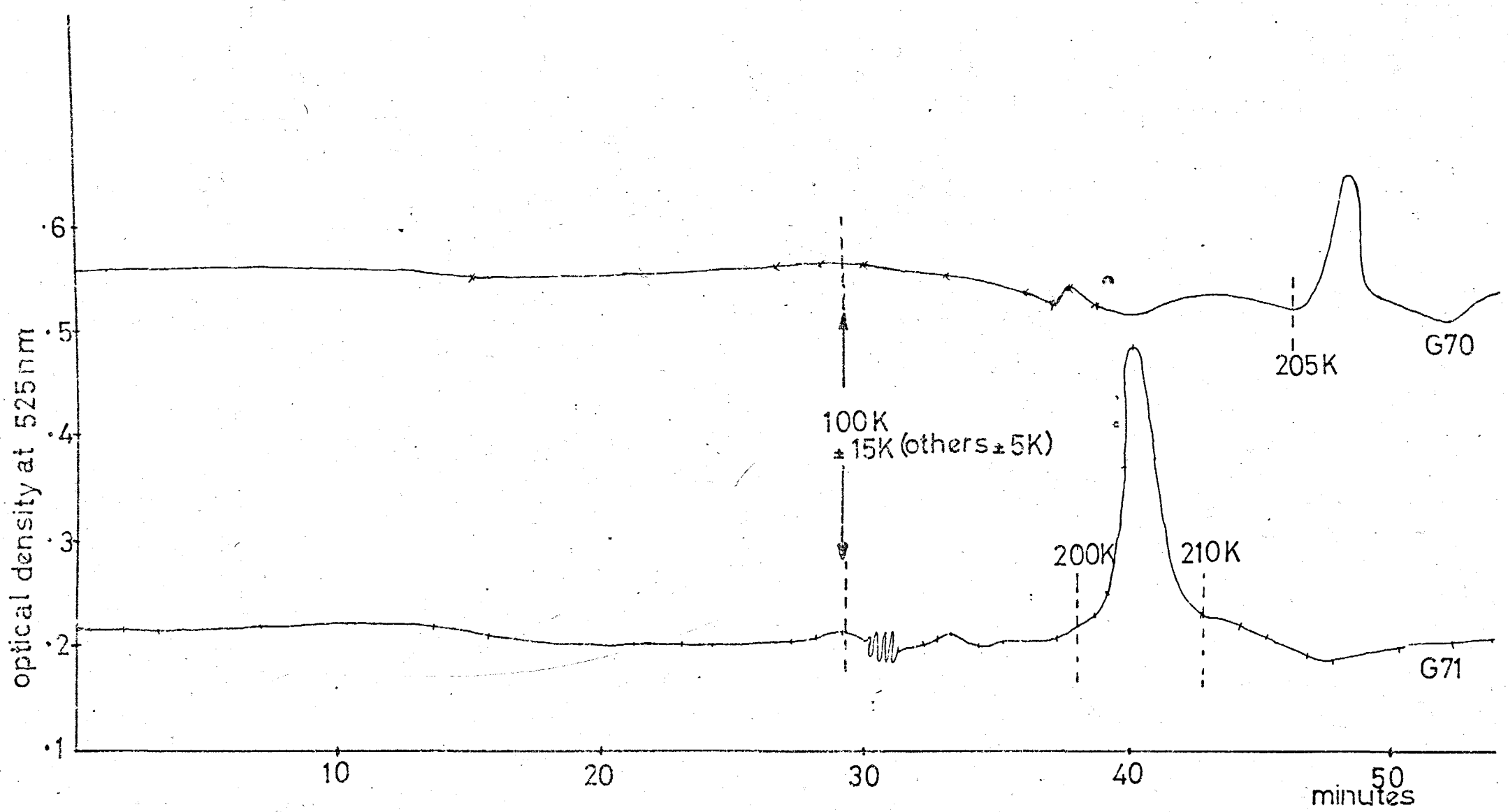

Fig. 6 4(ii) Thermal annealing of F centres in NaBr

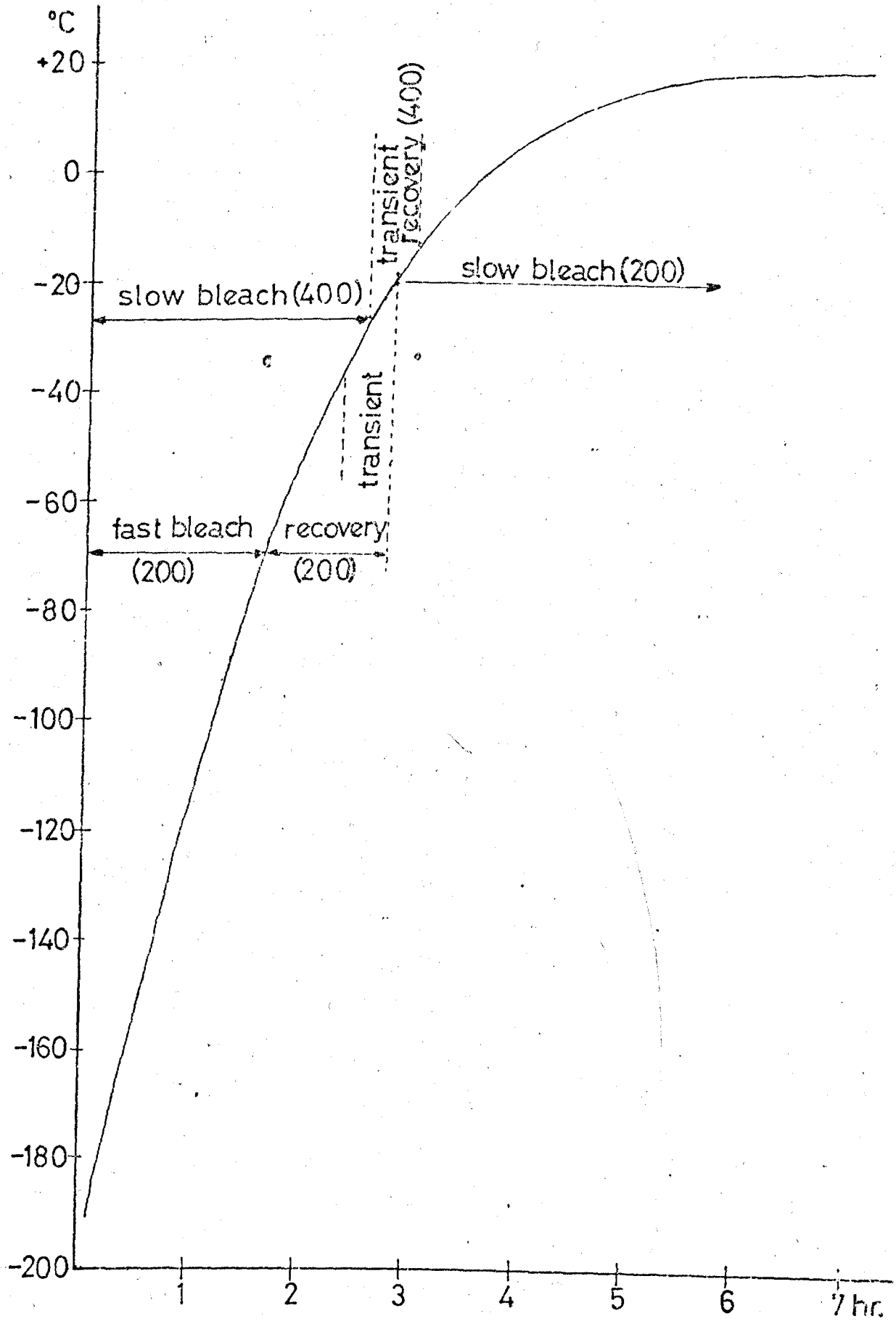

Fig 6 4 (iii) Slow thermal annealing of 200 & 400 keV F centres

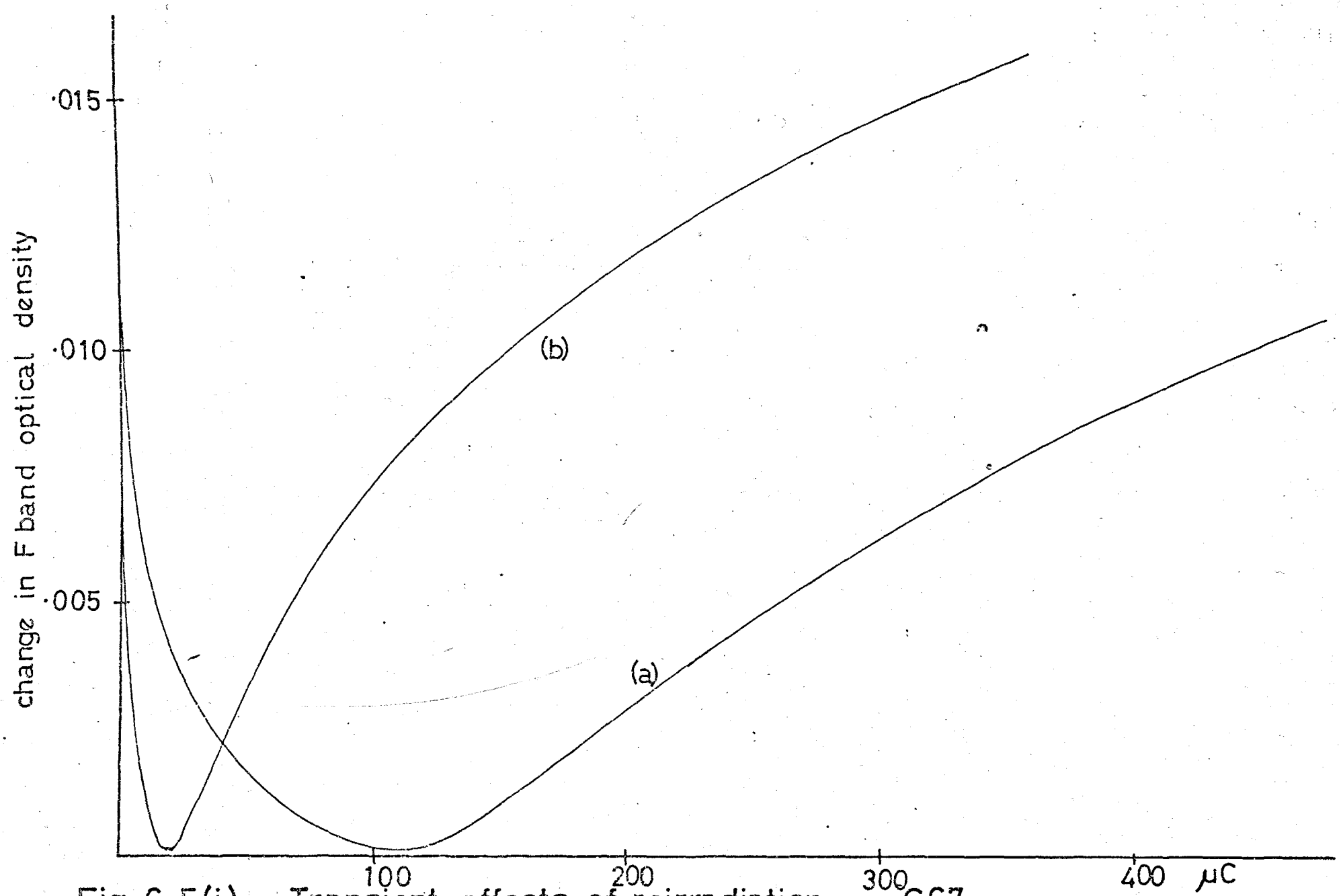

Fig. 6 5(i) Transient effects of reirradiation G67

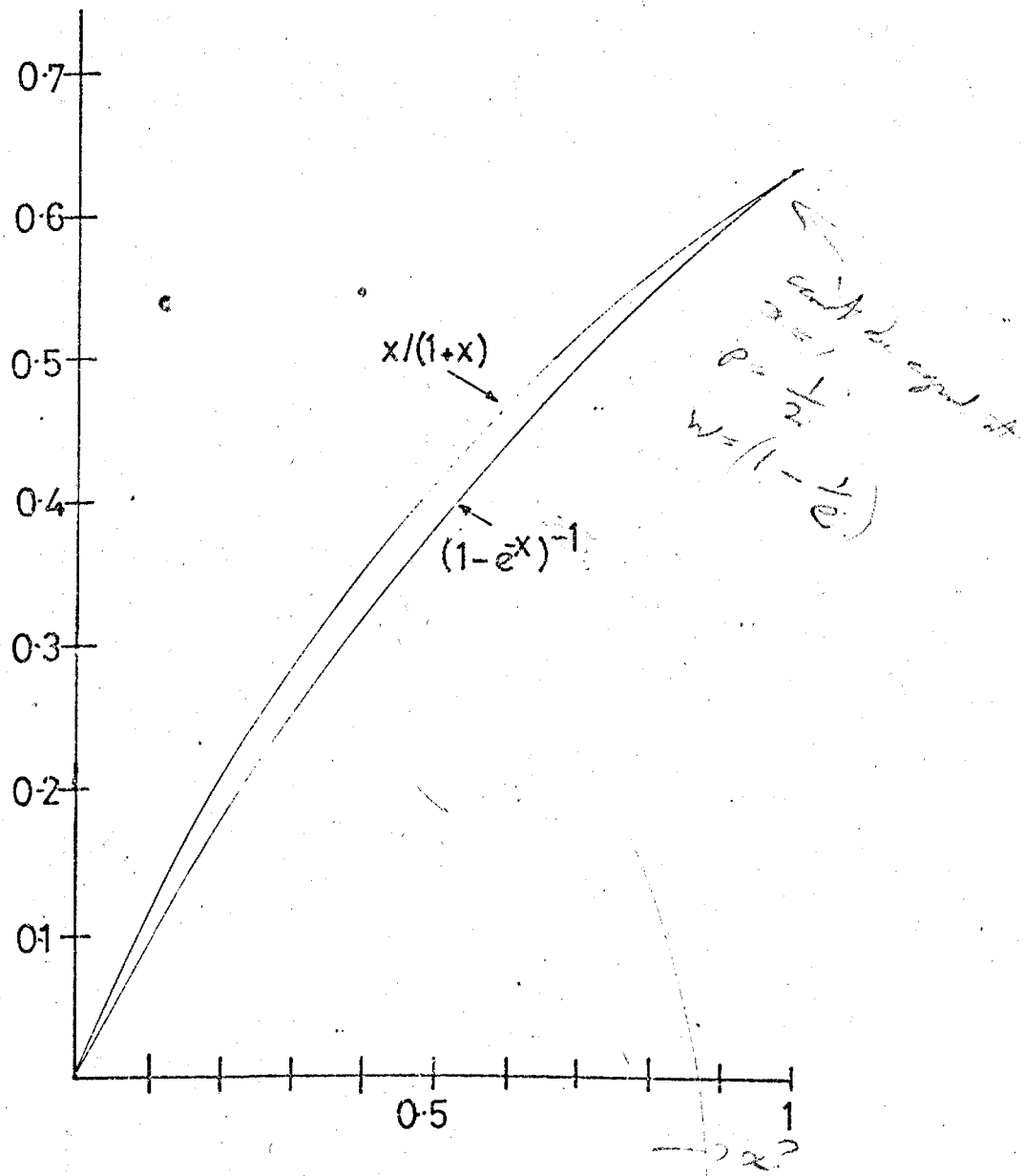

Fig 7 2 (i) Normalised P and W curves

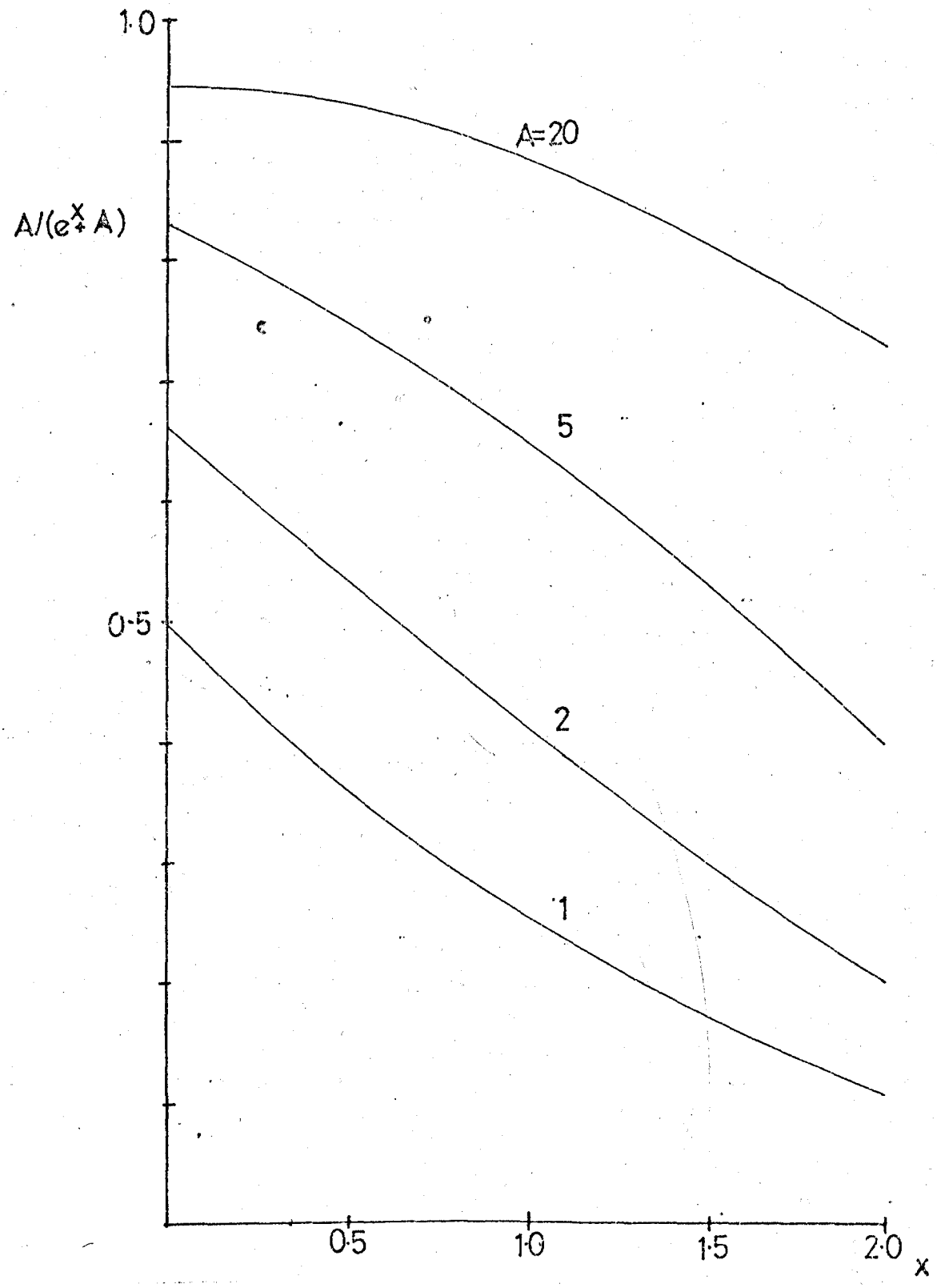

Fig 7 2(ii) Equivalent spatial variation of modified Pooley equation

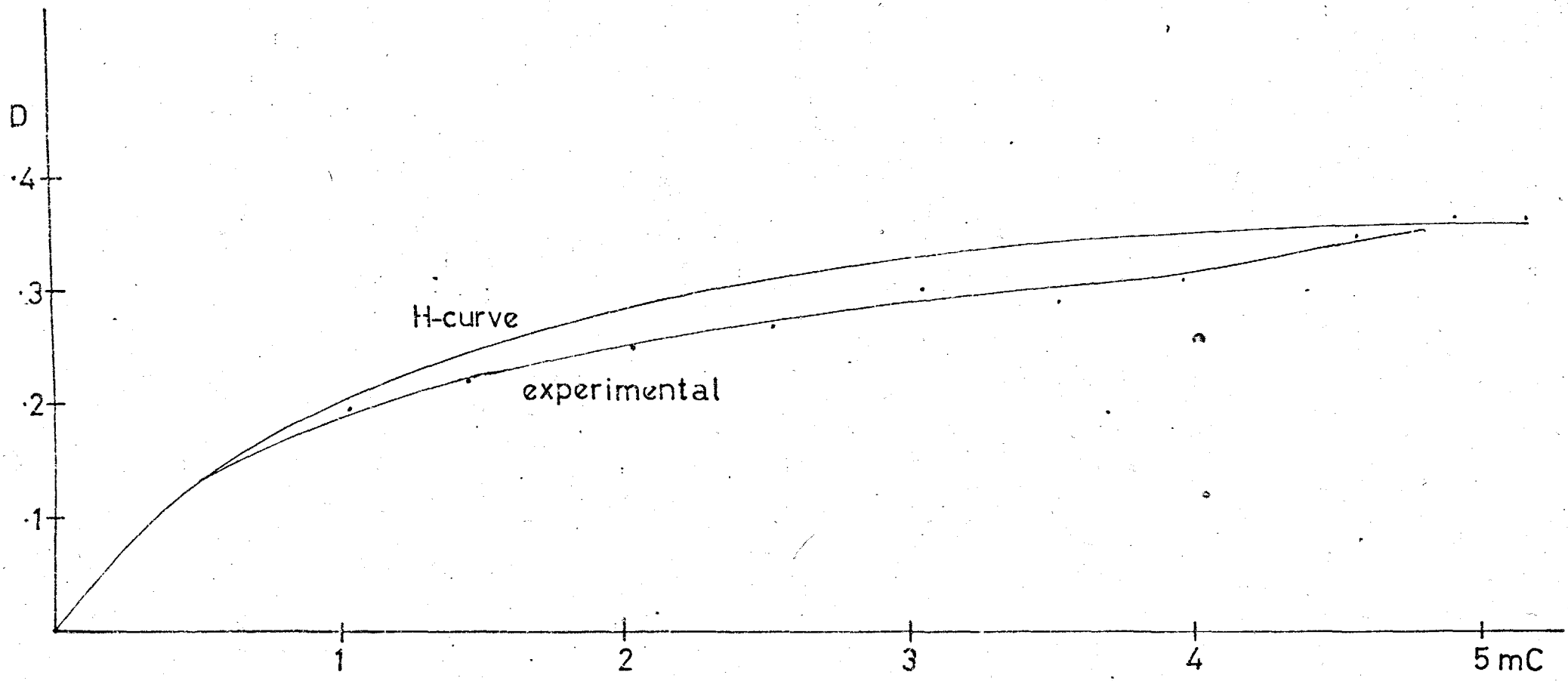

Fig. 7 2 (iii) Typical comparison between experiment and computed Herrmann-Pinard curve

G8

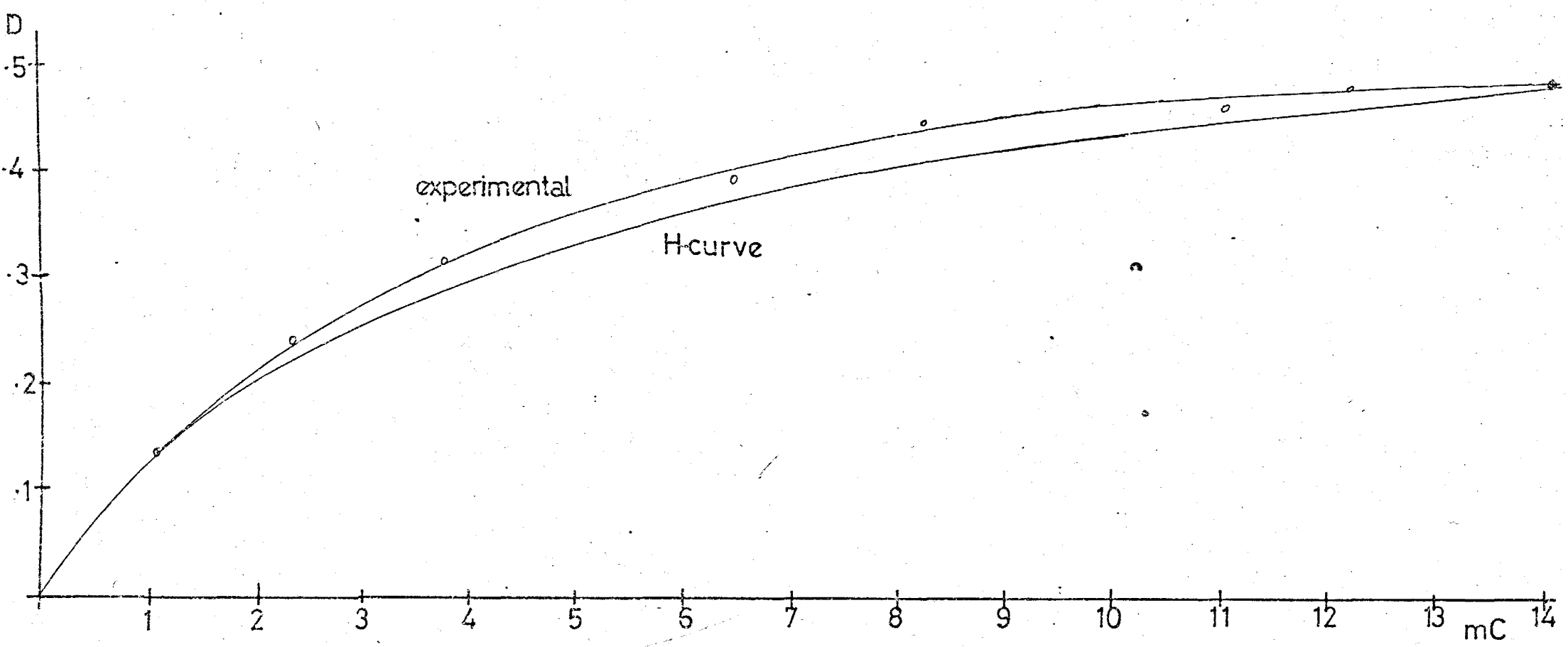

Fig. 7 2(iv) Typical comparison between experiment and computed Herrmann-Pinard curve

G 69

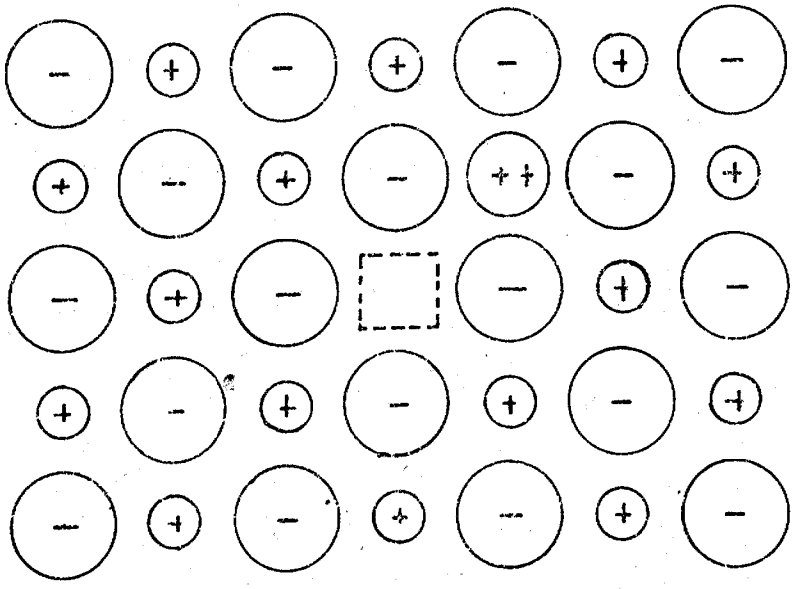

DIVALENT - VACANCY COMPLEX

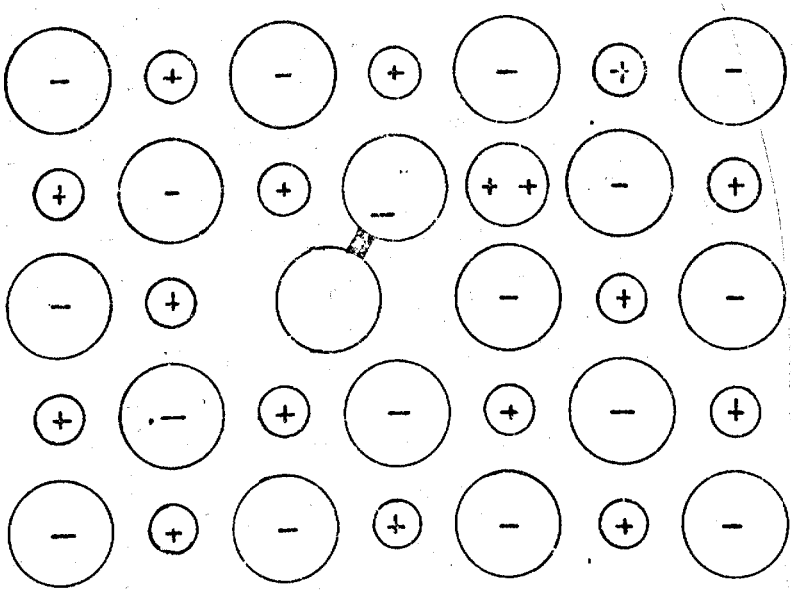

Br_2^--DIVALENT - VACANCY COMPLEX

Fig. 7.3(i) The Hayes-Nichols centre

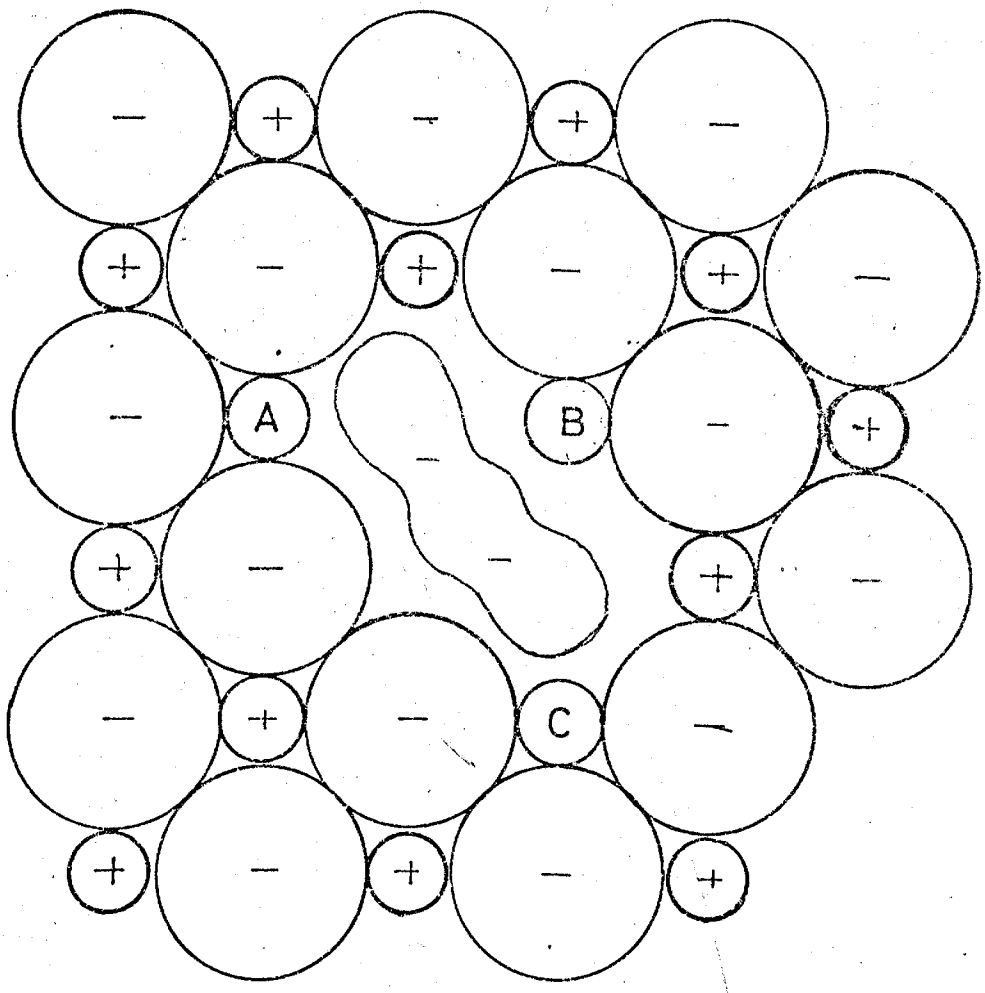

Fig. 7.3.(ii) Possible stabilised intermediate

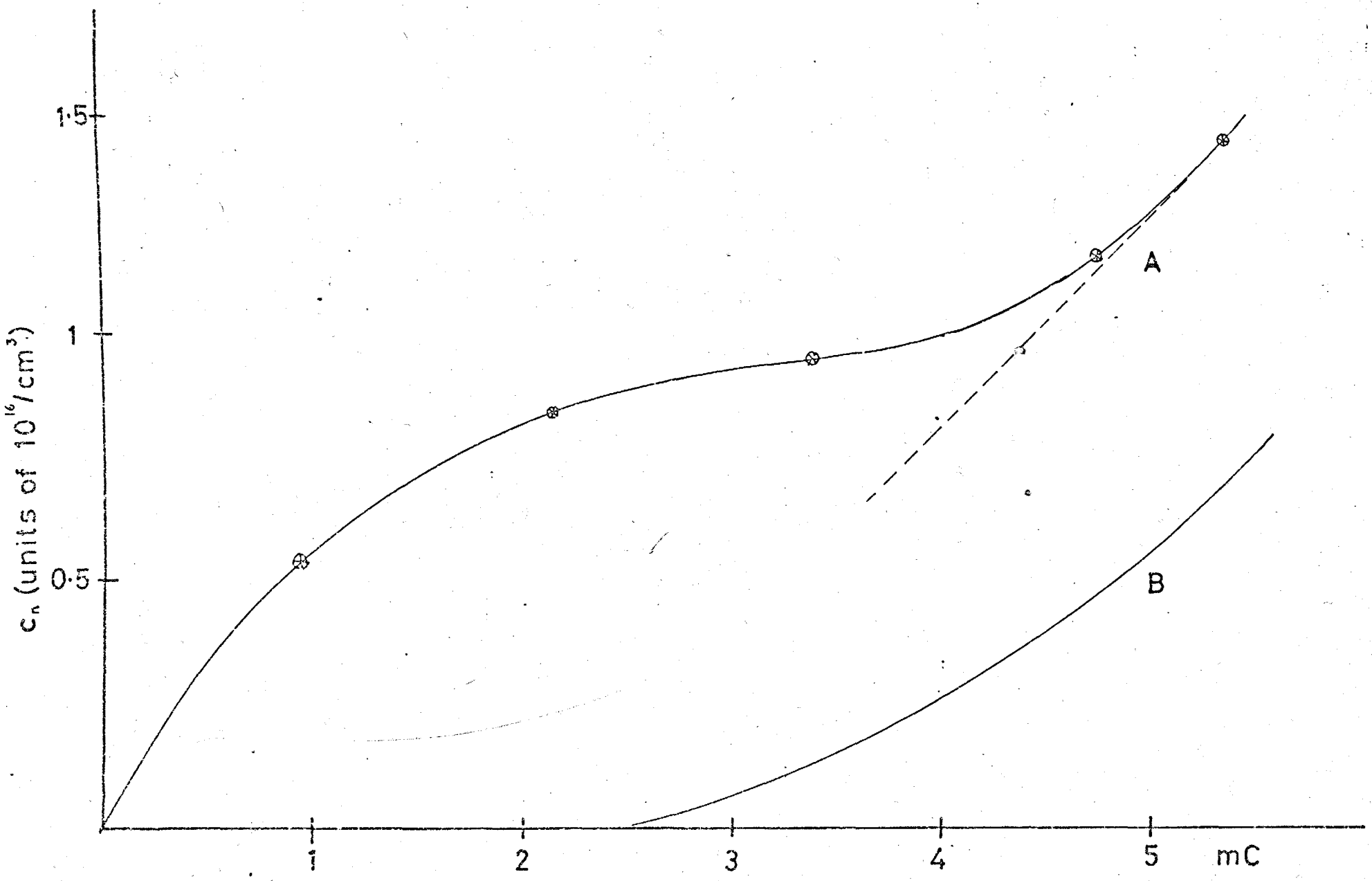

Fig. 7.4(i) F centre concentration vs. dose G63 and calculation

APPENDIX

Published Work

The subsequent papers have been submitted for publication. Their appearance has been delayed by current industrial disputes.

APPENDIX

Published Work

The subsequent papers have been submitted for publication. Their appearance has been delayed by current industrial disputes.

A simple integrator for charged-particle beam dosimetry.

A. M. Calverd

School of Physics, University of Warwick, Coventry, Warwickshire.

Abstract. A current integrator, utilising a current-to-voltage converter and a low-inertia motor, is described. Circuit values permitting resolution of microcoulomb doses to better than ±2.5% over a wide range of input flux are given. The device is inexpensive and reliable.

Submitted to Journal of Physics E

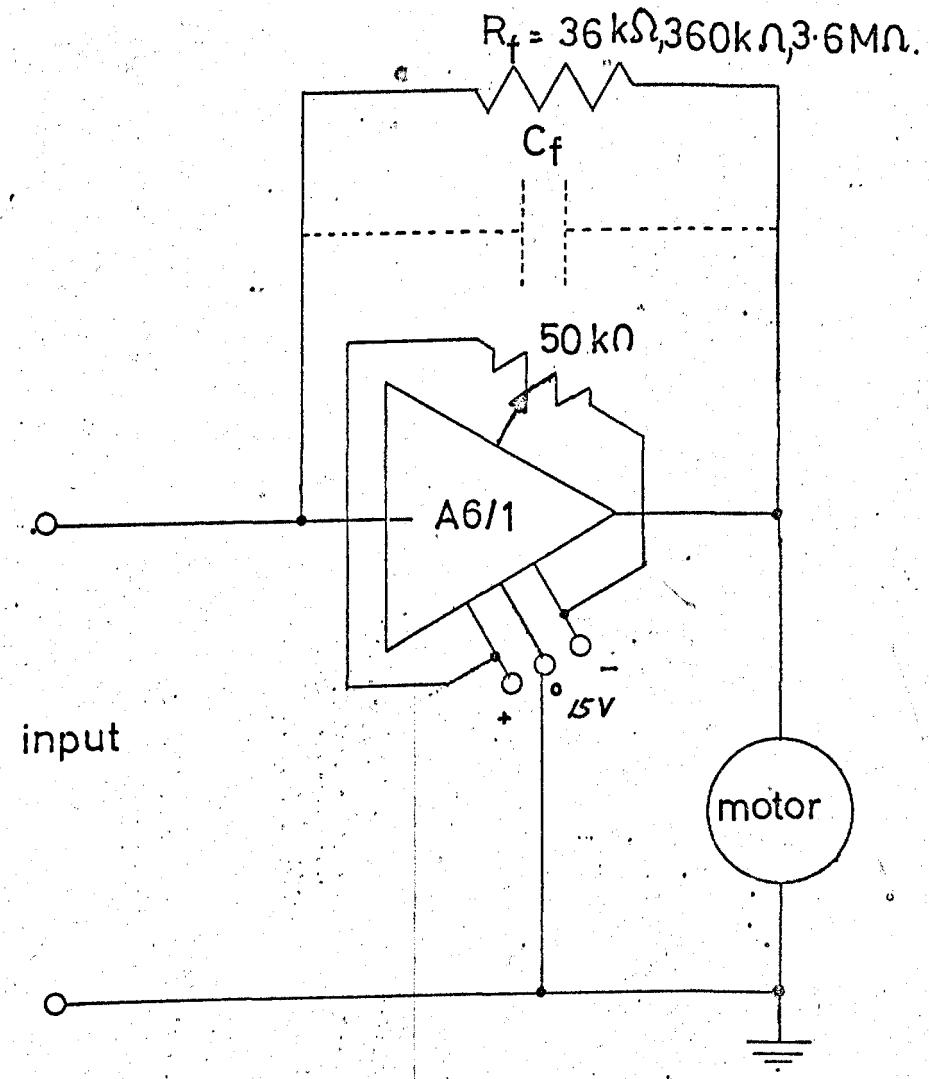
R_f = 36 kΩ, 360 kΩ, 3·6 MΩ.
C_f
50 kΩ
A6/1
+
0
15V
−
input
motor

A simple electron beam switching pulse generator for small accelerators.

A.M.Calverd
School of Physics, University of Warwick, Coventry.*

Abstract A simple circuit is described for producing 700V square pulses with a p.r.r. variable between 0.1 and 400 Hz and complete coverage of duty cycle. Single-shot and continuous operation are available and the system has been found suitable for beam pulsing in a small (400keV) electron accelerator.

* Present address: Division of Radiation Science, National Physical Laboratory, Teddington, Middlesex, U.K.

Submitted to Nuclear Instruments and Methods

The principle of the instrument described here is as follows: a variable frequency asymptotic sawtooth waveform is fed into a Schmitt trigger with a fixed hysteresis and an effectively variable trigger level. The output from this element consists of a variable duty-cycle train of pulses at the p.r.f. of the original sawtooth. This pulse train is used to switch a power output stage from saturation to cutoff and thus produces flat-topped square waves at the full supply voltage.

In the circuit shown, V1 is a highly asymmetric multivibrator which will free-run if S2 is closed. The cycle time is almost exactly 2.2 R_t seconds (R_t in megohms) in this mode. The waveform at V1 cathodes is a positive - going asymptote. Opening S2 puts the circuit into the "single shot" mode and positive spikes applied via the 1000pF capacitor initiate single pulses of length $\sim$ 0.25 R_t. Closing S1 locks the system "on".

The V1 cathode waveform is tapped off into the Schmitt trigger V2 andthe setting of the 25kΩ potentiometer determines the mark/space ratio of the 100V square wave at $V2a_2$, which has a risetime of $<$10μs. The maximum positive excursion of the Schmitt output is to $\sim$0V and consequently feeding the pulse train to V3 grid produces 700V square pulses at V3 anode with rise and fall times $<$100μs.

The instrument was designed to pulse the beam of a 400keV Van de Graaff electron accelerator. This machine was provided with electrostatic deflection plates operating at up to ±2kV for beam steering purposes. The pulse generator was driven from an isolated power supply, so a simple series connection of the output points shown here permitted the pulse to be added to the d.c. level applied to the deflection plates on one or other axis. The electrom beam was focussed on a small aperture in the beam tube beyond the deflection system, and the 25kΩ potentiometer in the output divider chain was adjusted to allow the beam to pass through the aperture with V3 conducting; the system thus switched the beam "on" during the "on" phases of the Schmitt trigger and deflected the electron beam away from the aperture with the Schmitt "off" or in the event of a failure of V3 or the power supplies. With a 1mm aperture about 50cm from the deflection plates provided with the accelerator (H.V.E.C. AS400) the beam pulse shape was close to the V3 conduction cycle shape.

The instrument functioned reliably during three years' use and generated pulses with durations between 10s and 2.5 ms with the appropriate values of R_t. No componenet values are critical and all resistors (except V3 anode load) were 20% ½W types.

The instrument was developed as part of a research project supported by the Central Electricity Generating Board and the Science Research Council, at the University of Warwick. The project was under the general supervision of Dr. M.R.Tubbs. I wish to thank the C.E.G.B. for a maintenance award.

Caption: Circuit diagram of the pulse generator.

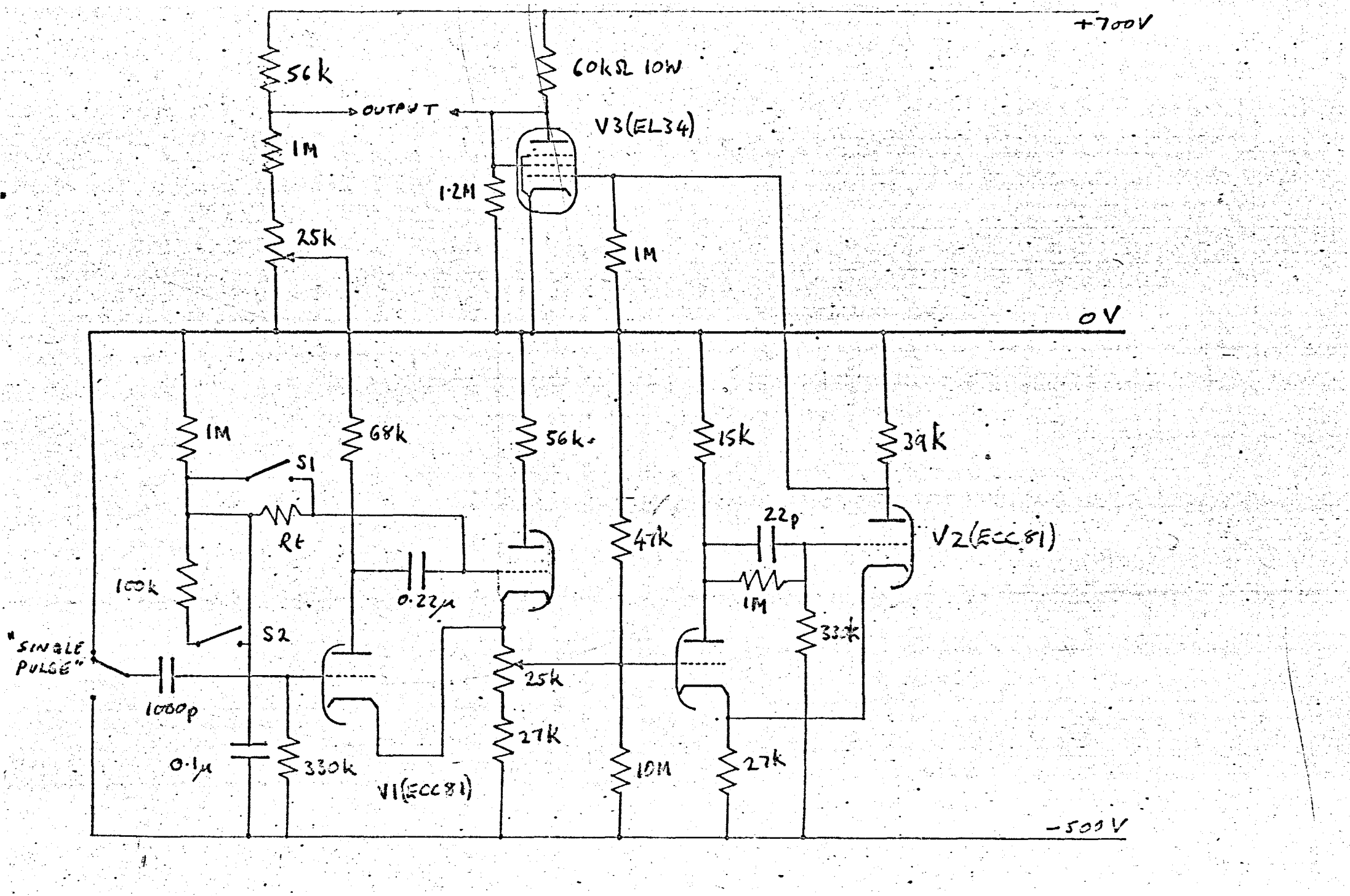
+700V
56k
60kΩ 10W
OUTPUT
V3(EL34)
1M
1·2M
25k
1M
0V
1M
68k
56k
15k
39k
S1
Rt
22p
V2(ECC81)
47k
100k
0·22μ
1M
S2
33k
"SINGLE PULSE"
25k
1000p
27k
0·1μ
330k
V1(ECC81)
10M
27k
-500V

Colour Centres in Electron Irradiated Sodium Bromide

by A.M. Calverd and M.R. Tubbs
School of Physics, University of Warwick, Coventry. CV4 7AL, U.K.

A relatively small amount of research has been carried out on colour centres in sodium bromide since this material is very hygroscopic and is difficult to colour using ionizing radiations. Indeed, experiments on the coloration of alkali halides by X-rays at 4.2°K have shown (1) that, while an F-centre is created for every 10^3eV absorbed in KCl and KBr, the corresponding figure for NaBr is nearly 10^6eV/F-centre. It is thus very difficult to generate high concentrations of colour centres in NaBr by X-irradiation at dose rates of typically 10^{14} to 10^{15}keV/cm^3/sec. As part of a programme of research on colour centre saturation phenomena, we have studied the production of colour centres in NaBr using fast electron irradiation at dose rates of 10^{17} to 10^{20}keV/cm^3/sec.

We have studied the growth of the F band in NaBr single crystals irradiated with 100-500keV electrons from a Van de Graaf electron accelerator. Single crystals of NaBr were obtained from the Harshaw Chemical Co. (H) and from British Drug Houses Ltd., (BDH) and were irradiated at both liquid nitrogen temperature (LNT) and room temperature (RT). Atmospheric moisture markedly affects the colorability of NaBr and saturation F-centre concentrations for specimens cleaved in air were some two to three times larger than those for specimens handled in a dry atmosphere. The experiments described below were all carried out on specimens that were cleaved and mounted in a cryostat in a dry box that was purged with dry nitrogen gas until the water content was less than 10^{-2}p.p.m. Electron irradiations were carried out in vacuo and optical absorption spectra were recorded in situ with a modified Zeiss PMQII spectrophotometer.

Fig. 1 shows the growth of the F-centre concentration in Harshaw NaBr as a function of electron dose at RT (dotted lines) and LNT (full lines) for 400 and 200keV electrons. The growth curve for BDH material (400kV, LNT) is included for comparison. The F-centre concentrations were calculated from Smakula's formula using an oscillator strength of 0.5 and measured electron penetration depths. All the growth curves show a marked tendency towards saturation after doses of ~~[illegible]~~ 3×10^{20} keV cm^{-3} Coulombs with the possible exception of the Harshaw specimen at RT, 400kV. The saturation ~~F-centre concentration for the BDH specimen irradiated with 400kV electrons at LNT is larger than that for the Harshaw specimen.~~

This is almost certainly due to the effects of divalent Calcium impurity (20ppm in BDH, 2ppm in H) since Ca^{++} enhances the colorability of NaCl at LNT and RT (1). The saturation F-centre concentration for Harshaw material irradiated at RT with 200kV electrons is at least ten times larger than that for material irradiated at LNT. This observation may indicate that a large concentration of α-centres (negative ion vacancies) are generated at LNT.

Optical absorption measurements of NaBr at LNT after irradiation show only two strong absorption bands - the F band at 525nm and a strong band at 199-200nm. This band is not the U-band (210nm in NaBr) and appears to be identical to a band seen at 196-199nm in additively coloured and X-irradiated samples (2) where it was labelled the β-band. In fig. 2 we summarize the behaviour of this band and the F-band during colouring and bleaching cycles. The optical density after a short initial irradiation is noted as 1 (at 199nm) and 1^1 (at 525nm) and after an extended bleach with F-light the F-band absorbance is reduced (2^1) while that at 199nm increases (2). This anti-correlation is consistent with the 199nm band being the α-band. A short electron irradiation then reduces the α-band (due ~~to~~ since electrons are ~~being~~ trapped at vacancies to form F-centres) but further irradiation leads to growth of both the α and F-bands (3, 3^1). A second exposure to F-light again produces a reduction of optical density in the F-band (4^1) but an increase at the α-band (4). If the 199nm band is the α-band, the separation between the first exciton peak (at 6·68ev (3)) and the α-band is ~0·45eV whereas it would be 0·92eV if the α-band is placed at ~215nm (2). The separations for KBr and KI are 0·67 and 0·60eV respectively and this suggests that the α-band might appear near 205nm in NaBr.

The oscillator strength of the α-band in NaBr has not been measured but, assuming it is close to that for KBr, our results suggest that twice as many α-centres as F-centres are produced at LNT; this compares with an α/F ratio between 5 and 9 for KBr at 5^oK (4). The saturation concentration of negative ion vacancies produced by 200keV electrons at RT is thus some three times larger than that for LNT. This is partly a result of impurity enhancement at RT but also suggests that interstitials are mobile at LNT but do not form stable aggregates as readily as at RT. The F-centre growth curve for H material (200kV) saturates at an F-centre concentration of 1-2 x $10^{18}/cm^3$ or ~10^{-4} of the available anions. The mechanism of saturation is presumably that of interstitial-vacancy recombination occuring in the 'forbidden - volume' surrounding an F-centre at high concentrations (5).

We wish to thank the Central Electricity Generating Board and the Science Research Council for generous research grants in support of this work. One of us (AMC) wishes to thank the C.E.G.B. for a maintenance award for the period 1967-70.

References

1. Rabin, H and Klick, C.C., Phys. Rev. 117, 1005, 1960.
2. Jacobs, P.W.M. and Krishna Menon, A., Phys. Stat. Sol. 35, K143-5, 1969.
3. Eby, J.E., Teegarden, K.J., and Dutton, D.B., Phys. Rev. 116, 1099-1105, 1959.
4. Ritz, V.H., Phys. Rev., 142, 505-13, 1966.
5. Fooley, D., Brit. J. Appl. Phys., 17, 855-861, 1966.

Captions for Figures

FIG. 1. F-centre growth curves for NaBr irradiated with 200 and 400keV electrons at room temperature (RT) and liquid nitrogen temperature (LNT).

FIG. 2. Behaviour of the F-band and an absorption band at 199nm during two colour/bleach cycles.

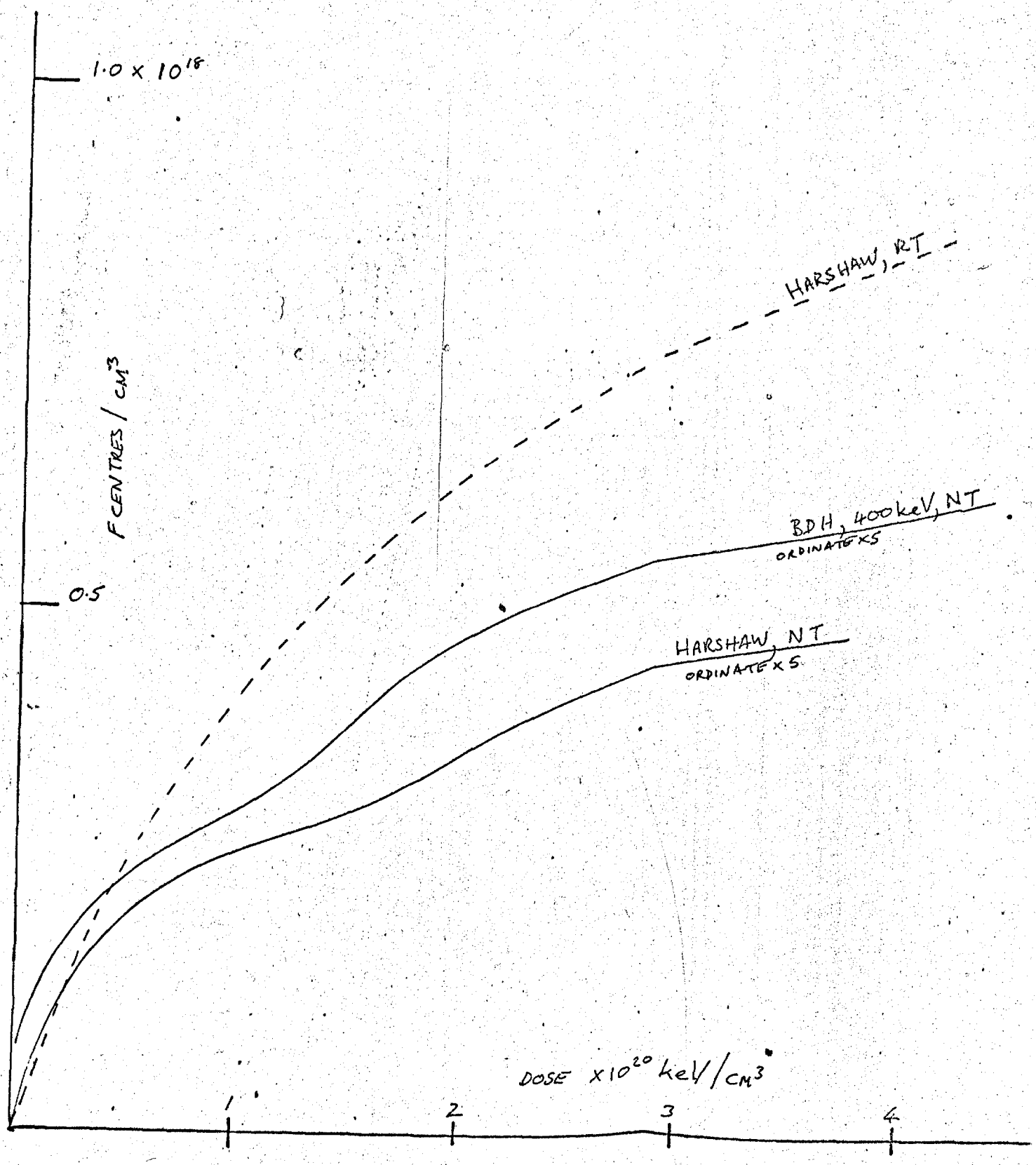

FIG. 1 – SKETCH ONLY.
DIAGRAM IN PREPARATION

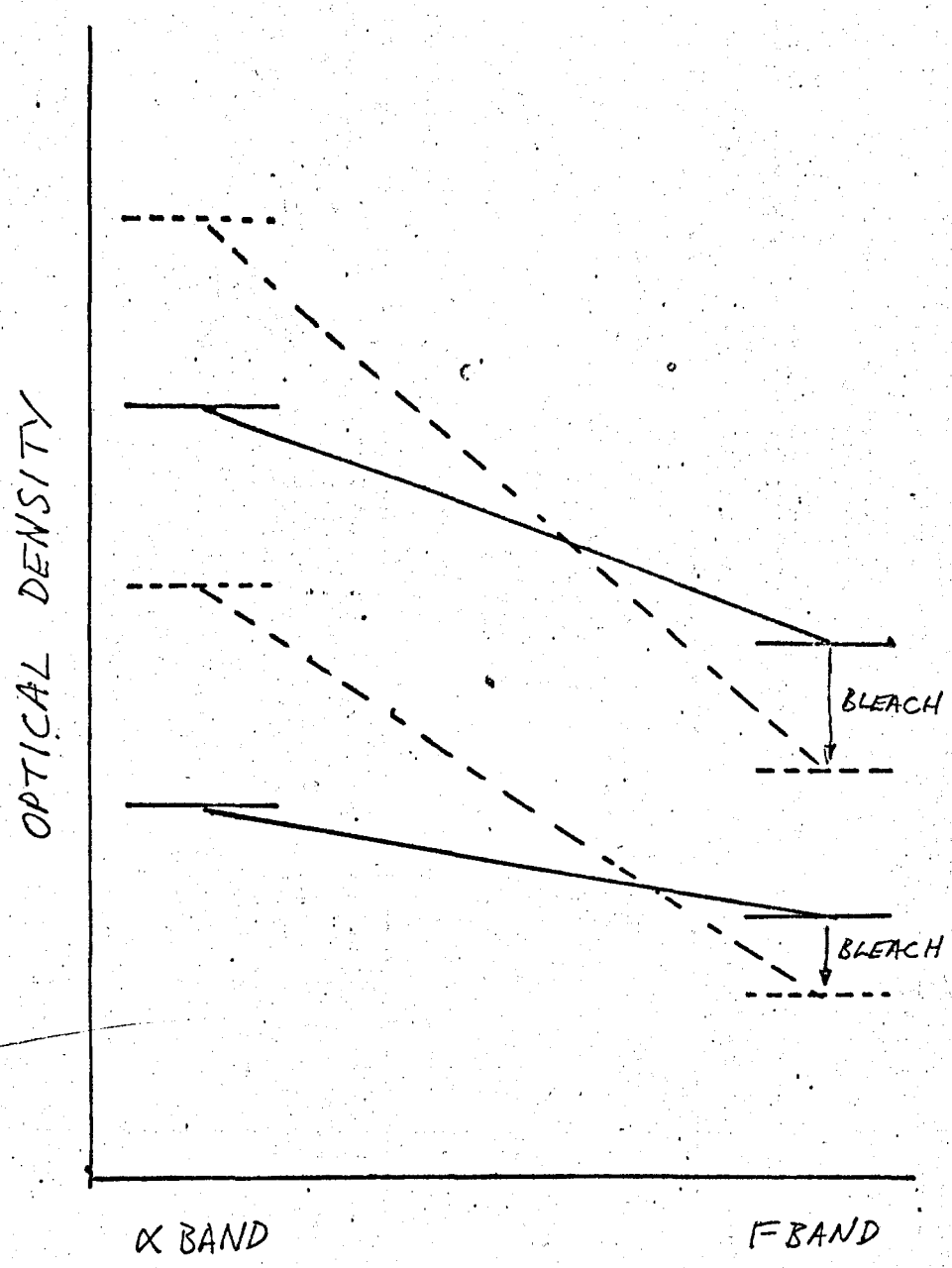

FIG. 2 — SKETCH ONLY
DIAGRAM IN PREPARATION.